Investigations on inorganic-organic hybrid nanomaterials from boehmite [AlOOH] gels for multifunctional applications

By

Shuhailath K.A.
10CC14J39009

A thesis submitted to the
Academy of Scientific and Innovative Research
for the award of the degree of
DOCTOR OF PHILOSOPHY
in
SCIENCE

Under the supervision of
Dr. S. ANANTHAKUMAR

CSIR-National Institute for Interdisciplinary Science and Technology (CSIR-NIIST), Thiruvananthapuram-695 019

Academy of Scientific and Innovative Research
AcSIR Headquarters, CSIR-HRDC Campus Sector 19,
Kamla Nehru Nagar,
Ghaziabad, U.P. - 201 002, India

June 2021

I dedicate this thesis to my family for their
constant support and unconditional love.
I love you all dearly……

COUNCIL OF SCIENTIFIC & INDUSTRIAL RESEARCH
NATIONAL INSTITUTE FOR INTERDISCIPLINARY SCIENCE AND TECHNOLOGY (CSIR-NIIST)
Industrial Estate P.O., Pappanamcode,
Thiruvananthapuram - 695 019, Kerala, INDIA
www.niist.res.in

Dr. S. Ananthakumar
Senior Principal Scientist
Functional Materials Section
Materials Science and Technology Division

Off: 0471-2515289
Mob: 09497271547
Fax: +91-471-2491712
E-mail: ananthakumar70@gmail.com

CERTIFICATE

This is to certify that the work incorporated in this Ph.D. thesis entitled *"Investigations on Inorganic-Organic Hybrid Nanomaterials from Boehmite [AlOOH] Gels for Multifunctional Applications",* submitted by Mrs. **Shuhailath K.A.** (10CC14J39009) to the Academy of Scientific and Innovative Research (AcSIR) in fulfillment of the requirements for the award of the Degree of Doctor of Philosophy in Science, embodies original research work carried-out by the student. We, further certify that this work has not been submitted to any other University or Institution in part or full or the award of any degree or diploma. Research material obtained from other sources and used in this research work has been duly acknowledged in the thesis, Images, Illustrations, figures, table etc., used in the thesis from other sources, have also been duly citied and acknowledged.

Shuhailath 29/06/2021

29/6/21

Shuhailath K.A.

Dr. S. Ananthakumar
(Thesis Supervisor)

STATEMENTS OF ACADEMIC INTEGRITY

I Shuhailath K.A., a Ph.D. student of the Academy of Scientific and Innovative Research (AcSIR) with Registration No. 10CC14J39009 hereby undertake that, the thesis entitled **"Investigations on Inorganic-Organic Hybrid Nanomaterials from Boehmite [AlOOH] Gels for Multifunctional Applications "** has been prepared by me and that the document reports original work carried out by me and is free of any plagiarism in compliance with the UGC Regulations on *" Promotion of Academic Integrity and Prevention of Plagiarism in Higher Educational Institutions (2018)"* and the CSIR Guidelines for *"Ethics in Research and in Governance*.

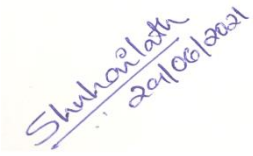

June 29th 2021 **Shuhailath K. A.**

Thiruvananthapuram.

It is hereby certified that the work done by the student, under my / our supervision, is plagiarism-free in accordance with the UGC Regulations on "Promotion of Academic Integrity and Prevention of Plagiarism in Higher Educational Institutions (2018)" and the CSIR Guidelines for "Ethics in Research and in Governances (2020)".

29.06.2021 **Dr. S. Ananthakumar**

Thiruvananthapuram

DECLARATION

I, **Shuhailath K. A**., bearing AcSIR Registration No. 10CC14J39009 declare: that my thesis entitled, "**Investigations on Inorganic-Organic Hybrid Nanomaterials from Boehmite [AlOOH] Gels for Multifunctional Applications**" is plagiarism free in accordance with the UGC Regulations on *"Promotion of Academic Integrity and Prevention of Plagiarism in Higher Educational Institutions (2018)"* and the **CSIR** Guidelines for *"Ethics in Research and in Governance (2020)*".

I would be solely held responsible if any plagiarised content in my thesis is detected, which is violative of the UGC regulations 2018.

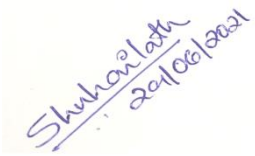

June 29th 2021 Shuhailath K. A.

Thiruvananthapuram

ACKNOWLEDGEMENTS

I sincerely appreciate the almighty God for His graces, strength, sustenance and above all, His faithfulness and love from the beginning of my academic life up to this doctoral level. His benevolence has made me excel and succeed in all my academic pursuits.

Undertaking this "PhD" has been a truly life-changing experience for me and it would not have been accomplished without the help of a countless number of people.

I would like to express my deepest gratitude to my Mentor, ***Dr. S. Ananthakumar****, whose sincerity and encouragement I will never forget. Dr. Ananthakumar has been an inspiration as I hurtled through the path of this Ph.D programme. He is a man of vocabulary and his writing skills are, undoubtedly, a force to be reckoned with.*

I am grateful to ***Dr. A. Ajayaghosh, "****Director of CSIR-NIIST", Dr. Suresh Das and Dr. Gangan Prathap, former directors of the institute for providing necessary facilities & infrastructure. I express* my *sincere gratitude to* ***Dr. Savithri S., "****Head of the division" and former HoD's for their help rendered during the course of this work. I gratefully acknowledge the funding received towards* my *PhD from the Council of Scientific* & *Industrial Research (CSIR) JRF fellowship.*

I very much appreciate ***Dr. V. Karunakaran****, Dr. Suresh C.H.****,*** *Dr. Luxmi Varma and Dr. Mangalam S. Nair, present* & *former co-ordinators of AcSIR for their helpful contributions. At the same time, I also thank all other Doctoral Committee Members:* ***Dr. U.S. Hareesh, Dr. T.P.D. Rajan*** *and* ***Dr. Rajeev K. Sukumaran*** *for their supervision and insightful comments during the course of this study.*

I extend my thanks and gratitude to Dr. K.G.K. Warrier(Retd.), Dr. Saju Pillai, Dr. S Shukla, Dr. K.G Nishanth and Dr. N. Balagopal, from the functional material section for their critical suggestions and advice during my tenure there I would also like to express my thanks to all the other scientists from the MSTD for their help and support.

I also wish to thank ***Mr. Joshy George*** *who provided me with encouragement and patience throughout the duration of CSIR-800 societal programme; his generosity made this study possible.*

I wish to express my sincere thanks to all the administrative ***and technical staff*** *at CSIR-NIIST for their assistance and support. Many thanks to "Mr. Peer Mohammad, Mr. Kiran Mohan, Mr. Harish Raj, Mr. Amal Raj, Mr.* M. *R. Chandran, Mr. Prithvi Raj, Mr. Vibhu, Mr. Shammas, Mr. Adarsh, Ms. Bhavya, Ms. Anjali, Mr. Pratheesh, Ms. Sowmya" and all of whom gave me time and were generous in offering instrumental analysis.*

I'm extremely grateful to ***Mr. Chandrakanth*** *whose support cannot be overestimated. He was there to help me out with the SEM analysis and mental support even with his busy schedule.*

I also express my heartfelt gratitude to ***Dr. S Nishanth Kumar****, from Agro-Processing and Natural products division of CSIR-NIIST, for his sincere help and strong support in carrying out various biological studies.*

I am grateful and I thank all those anonymous Reviewers and editors of the journals who gave critical as well productive comments to my Research Publication.

It is not enough saying thanks and regards to my "Seniors and Colleagues", but for now, that is the least I can do for them. I would like to thank Dr. Linsha V, Dr. Babitha K.B, Dr, Mahesh K.V, Dr. Jeen Maria, Dr.Vaishakh S.S., Dr. Viji, Dr.Sheemol N., Dr. Minju N., Mr. Balanand, Mr. Sujith, Mr. Dhaneesh, Mr. Vishnu, Mr.Vishnu K, Mr. Akhil Das, Mr Shibin, and Mr.Gautham who all have been of great support by working together and having positive discussions and having a memorable time there at CSIR-NIIST.

Apart from my Colleagues, I would like to thank some of my juniors. I like to thank Mr. Muthu, Ms. Angitha T, Ms. Ragi, Mr. Mithran, and Mr. Nithun who was there to help me out during my most struggling period. "Big Thanks to you, Guys!".

I express my heartfelt thanks to Master's project students Mr. Irfan Ali, Ms. Arunima, and Ms. Nivedya, for their friendship, help, and useful discussions. Their assistance during the presented work is gratefully acknowledged.

I would like to extend a huge, warm thanks to my roommates Mrs. Sijla, Dr. Jerin K Pancrecious, Dr. Molji C., Ms. Sajitha Surendran and Mrs. Nimisha G. Nair. I also thank all

my friends in NIIST for their help and cooperation. I would like to mention some of them here, Dr. Deepthi, Dr Salfeena, Dr. Athira.

People here are genuinely nice and want to help you out and I'm glad to have interacted with many. If I have forgotten anyone, I apologize.

I take this opportunity to thank Geetha aunty and Sukumaran Uncle, our house owners, for their love, support, generous care and the homely feeling at Trivandrum.

I express a deep sense of thanks and gratitude to my family for their continuous and unparalleled love, help and support. I thank ***Ummi*** *(Mrs. Ramla Aboo) &* ***Vappi*** *(Mr. Aboo K.B) for their endless love and letting me find my own way. It was their love that raised me up again when I got weary. I always knew that you believed in me and wanted the best for me. I love them* so *much, and I would not have made it this far without them. I thank My brother (Mr. Hazrath Aboo) who has encouraged and helped me mentally and my Sister(Rahmath Safeer) and my brother in law (Mr.Safeer) to whom I could speak most freely. I love you all very much.*

I would like to express my *gratitude to* my ***In-laws*** *Vappa(Mr. Sadique K.K) & Umma(Mrs. Suleikha Sadique) for their motivational and emotional support. They were there staying with me and helping me out during my most stressful time.*

My dream to complete my PhD was so tiring, that at some point I was not confident if I could finish it on time, It would've been impossible without the help of my beloved husband, (Fahad Moideen K.S.) and my son (Zahran Fahad), Without you people, it's hard to imagine how I would survive. My pregnancy had made a delay in finishing the programme, but now looking at him helps me relieve all the stress I have, And finally my husband, who had faith in me and my *intellect even when I felt like falling off the hill because I didn't have faith in myself. These past several years have not been an easy ride, both academically and personally. I truly thank him for being patient, confident and supportive. I feel blessed to have him and our baby who has hopped on to this ride in the final phase and made it more joyous and reminded us to be more mindful in our lives.*

Shuhailath K. A.

CONTENTS

Chapter-1

Introduction: Inorganic-Organic Hybrid Materials: Overview & Recent Advances 1-52

SOL GEL INORGANIC HYBRID MATERIALS: - An Overview

1.1 Hybrid Materials 3

1.2 Classification of Hybrid Materials 6

1.2.1 Class I Hybrid Architecture 6

1.2.2 Class II Hybrid Systems 7

1.3 Synthetic Strategies for Hybrid Materials 7

1.4 Sol-Gel Processing of Inorganic-Organic Hybrids 10

1.5 Sol-Gel Route: Precursors to Gel Formation 10

1.5.1 Precursors 10

1.5.2. Sol 11

1.5.3 Gel 12

1.5.3.1 Gelation 12

1.6 Governing Mechanism in Sol-Gel Transition 13

1.7. Gel based Hybrid Materials based on Drying Techniques 16

1.7.1 Xerogels 18

1.7.2. Aerogels 18

1.7.3. Cryogels 20

1.7.4. Ambigels 21

1.8 Boehmite Hybrids *Via* Sol-Gel Chemistry 22

1.8.1 Aluminium Isopropoxide (AIP) 22

1.8.2 Boehmite 22

1.8.2.1 Preparation 23

1.8.2.2. Structure and Properties of Boehmite 23

1.8.2.2.1. Boehmite :- Structural features 24

1.9 Applications of Boehmite-Organic Hybrids 25

1.9.1 Boehmite as Substrates for Adsorption 26

1.9.2. Boehmite as a Support for Photocatalysts 28

1.9.3. Water Disinfection 30

1.9.4. Boehmite as Superhydrophobic Material 31

1.9.5. Electrochemical Sensor 33

1.9.6. Flame Retardancy 35

1.10. Scope of the Present Thesis 37

1.11 Objective and outlook of the present work 38

1.12 References 40

Chapter-2 53-88

Nano Ceria Decorated Boehmite Gel Hybrids as Photo-catalytic antimicrobial Adsorbents

2.1. Abstract 55

2.2. Introduction 56

2.3 Experimental Section 59

2.3.1 Materials 59

2.3.2. Sol-gel synthesis of boehmite sol (AIP-sol) 59

2.3.3. Preparation of AlOOH/PEI hybrid and CeO_2@AlOOH/PEI hybrid nanocomposite gels and monoliths 60

2.3.4. Characterizations 61

2.3.5 Application study for removal of lignin from aqueous sample 62

2.3.5.1. Adsorption studies 62

2.3.5.2. Photoactivity Studies 63

2.3.5.3. Application study for removal of organic dye from aqueous sample 63

2.3.5.4. Bacterial resistance test 64

2.3.5.4.1. Antibacterial assay by disc diffusion method 64

2.3.5.4.2. Test bacterial culture preparation 64

2.4. Results and Discussion 65

2.4.1. Structural and chemical analysis ofsynthesized hybrid nanocomposite 65

2.4.2. Microstructural analysis of synthesized hybrid nanocomposites 68

2.4.3. Textural features and surface charge of synthesized hybrid nanocomposites 70

2.4.4. Lignin adsorption and photocatalytic degradation studies 71

2.4.4.1. Adsorption studies 71

2.4.4.2. Photocatalytic Degradation Studies 77

2.4.4.3. Removal of organic dyes from environmental aqueous samples 80

2.4.4.4. Antibacterial Activity of the proposed materials 81

2.5 Conclusions 84

2.6 References 85

Chapter-3 89-121

Natural CNSL Oil Crosslinked Boehmite (AlOOH) Hybrids: A New Effective Green-Electrode Design for Sensing Neurotransmitter Dopamine

3.1. Abstract 91

3.2. Introduction 91

3.3 Experimental Section 95

3.3.1 Materials 95

3.3.2. Preparation of boehmite-CNSL hybrid 95

3.3.3. Fabrication of the inorganic-organic hybrid electrode (PFAC/GCE) 95

3.3.4. Real sample preparation 96

3.3.5 Characterization 96

3.3.5.1. Electrochemical characterization 97

3.4. Results and discussion 97

3.4.1. Electrochemical activities of unmodified and PFAC modified GCE 105

3.5 Conclusions 116

3.6 References 117

Chapter-4 123-150

Design of A New Superhydrophobic Boehmite Gel Hybrid and Fabrication of Textile Membranes for Oil-Water Separation

4.1. Abstract 123

4.2. Introduction 123

4.3 Experimental Section 129

4.3.1 Materials 129

4.3.2. Processing of boehmite-CNSL hybrid 129

4.3.3. Fabrication of sperhydrophobic textile membranes 130

4.3.4. Self-Cleaning Test 131

4.3.5 Membrane Durability 131

4.3.6 Oil- Water Separation Test 132

4.3.7. Characterizations 133

4.4. Results and Discussion 133

4.4.1. Structural Characteristics of PWCA Coated Textile 135

4.4.2. Morphological Analysis 136

4.4.3. Surface Wettability 138

4.4.4. Self-Cleaning Property 140

4.4.5. Mechanical Durability 141

4.4.6. The Chemical Stability 141

4.4.7. Oil-Water Separation Capability 142

4.5. Conclusions 147

4.6. References 147

Chapter-5 151-176

Boehmite/Chitosan Hybrid Aerogel:- Study on Thermal Insulation and Flame Retardant Properties

5.1. Abstract 153

5.2. Introduction 153

5.3. Experimental Section 157

5.3.1 Materials 157

5.3.2. Preparation of chitosan aerogel 157

5.3.3. Preparation of cross linked boehmite/chitosan hybrid aerogel 157

5.3.4. Characterizations 158

5.3.5. Heat Insulation and Fire Resistance Analysis 159

5.4. Results and Discussion 159

5.4.1. Structural Characteristics of CHAL Hybrid Aerogel 161

54.2. Textural Analysis 164

5.4.3. Thermal stability of CHAL hybrid aerogel 166

5.4.4. Morphological Analysis 168

5.4.5. Flame test for fire protection applications 170

5.5 Conclusions 173

5.6 References 174

Chapter-6 177-184

Conclusions, Contributions, and Future Direction

6.1. Research Summary 179

6.2. Contributions 181

6.2.1 Boehmite Based Hybrid Photocatalytic Sorbent (CeO_2@AlOOH/PEI) 181

6.2.2. Natural CNSL Oil -Boehmite Hybrid [PFAC] Green-Electrode as Dopamine Sensor 182

6.2.3. CNSL Resin Modified Superhydrophobic Boehmite Gel Hybrids (PWCA) for Oil- Water Separation 182

6.2.4 Boehmite/Chitosan Hybrid Aerogel(CHAL) on Thermal Insulation and Flame Retardant Applications 183

6.3. Recommendations and Future Directions 184

Abstract of the Thesis 185

List of Publications 187

List of conference proceedings 189

Attachment of the photocopy of the publication

Preface

Interdisciplinary science and wet-chemistry methods bring together inorganic and organic active molecules in a single hybrid material to mark their combined beneficial properties. They open up new vistas of quality research in materials chemistry. Recently research was focused more on the design of sol-gel hybrid systems due to their versatile multifunctional characteristics. Boehmite gel is a layered, inorganic/polymeric 3D material that offers promising new hybrid-architectures. Such hybrids find applications as functional and protective coatings, catalysis, sensors and membranes. In this thesis, different kinds of inorganic-organic hybrid materials are designed out of sol-gel derived boehmite. The entire thesis is centered around a thematic concept on '***Inorganic-Organic Hybrid Nanomaterials from Boehmite [AlOOH] Gels***' for functional applications. Macroscopic shaping of boehmite hybrids and the transformation of these hybrids into porous gel architectures with tailoring functionality has been successfully accomplished. In addition to this the beneficial properties of the developed boehmite hybrids was validated for the potential functional applications. The content of this thesis have been presented in six chapters.

Chapter 1 deliberates the general introduction on inorganic-organic hybrid materials, and sol-gel synthesis of hybrid gels to porous structures. The chapter describes the comprehensive literature survey on the evolution of sol-gel chemistry and its growth towards hybrid gels. This chapter also highlights advantages of boehmite hybrids in different fields of science and technology. The specific objectives and outlook of the present work are also outlined in the introductory chapter.

Chapter 2 devotes to the preparation of photoactive, antimicrobial multifunctional hybrid, CeO_2@AlOOH/PEI as a promising catalytic-sorbent. Sol-gel

assisted nano-casting was explored for the synthesis of CeO_2@AlOOH/PEI. This hybrid catalytic-sorbent showed enhanced adsorption and photocatalytic degradation performance for the treatment of industrial waste water contaminated with lignin and organic dye. The antibacterial property was studied against both gram positive and gram negative bacteria. The pronounced interfacial properties of the prepared catalytic sorbent, promotes itself as a promising functional material for diversified applications of adsorption, photodegradation, and antimicrobial activity.

Chapter 3 describes the synthesis of electrochemically active hybrid sensor designed from boehmite gel and natural organic resin, CNSL (PFAC). The prepared hybrid sensor showed electrochemical detecting ability to the neurotransmitter dopamine. The PFAC hybrid sensor displays a higher electro catalytic activity toward DA oxidation with a wider linear detection range of 50 μM to 450 μM and a lower detection limit of 23×10^{-9} m. Furthermore, the developed sensor demonstrated favorable selectivity, operational stability, and reproducibility. Here the PFAC hybrid was also used for the real sample analysis and interference studies, which demonstrates that the proposed modified electrode is a promising candidate in the pharmaceutical and medical fields.

Chapter 4, reports on the formulation of hybrid coating suspension from organic CNSL oil, inorganic boehmite, and organic paraffin wax [PWCA]. This hybrid material showed superhydrohobicity and resistance to water impact. The PWCA hybrid was applied on cotton textile to obtain superhydrophobic flexible membrane assembly with a water contact angle of 160^o. Stability of the as prepared superhydrophobic cotton textile is systematically studied under harsh chemical condition and also with knife scratching test. Furthermore, the coated textiles demonstrated excellent self-cleaning ability and could be used to selectively separate various kinds of oil-water mixture

including crude oil-water mixture. More interestingly, the hybrid coated fabric can recover its super liquid-repellent property after drying at 120 °C in an oven, even after immersing in water for a week. The above mentioned fascinating properties indicated that the PWAC coated textiles a promising candidate for oil-water separation in real world application.

Chapter 5 deals with the fabrication of fire-resistance and low thermal conducting chitosan/boehmite hybrid aerogel (CHAL) via freeze-drying. Importantly, the aerogel exhibited excellent flame retardancy and self-extinguished in the vertical burning test. This work provides a facile, environmentally-friendly, and cost-effective approach to fabricating multifunctional fire-safe, low-density aerogel that has promising applications as green packing material.

Finally, the major conclusion, summary, and the future perspective of the present thesis work are summarized in **chapter 6**.

CHAPTER – 1

Introduction: Inorganic-Organic Hybrid Materials: Overview & Recent Advances

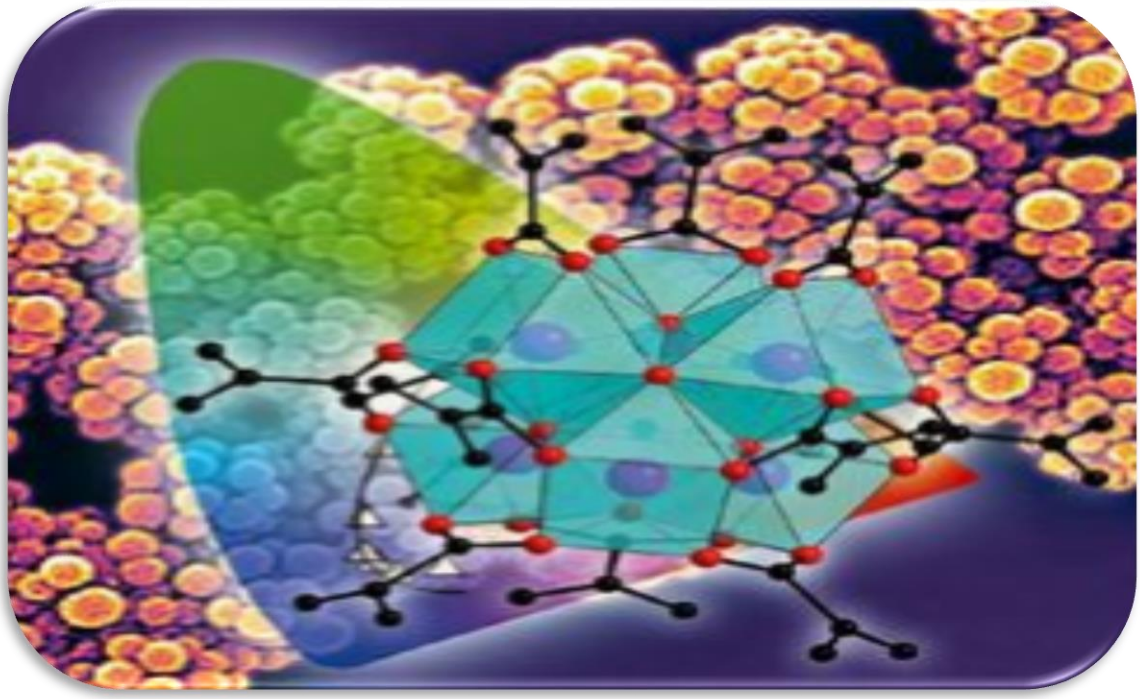

https://www.wiley.com

This thesis mainly focuses on the fabrication of inorganic-organic hybrid materials from boehmite gels for multifunctional applications. Therefore, in this introductory chapter, basic knowledge on hybrid materials, classification of hybrid materials, synthetic strategies for hybrid materials with special reference to sol-gel chemistry, and the pathway involved in the transformation of gels into inorganic-organic hybrids have been described. In addition, a brief literature review on the prior-art on hybrid materials for functional applications has been provided. With this as a background, the main objective of the work and the scope of the thesis are presented at the end.

SOL GEL INORGANIC HYBRID MATERIALS: - An Overview

1.1 Hybrid Materials

The concept of hybridization has existed in nature since the beginning of life on the earth. The mother nature made hybrid architectures by combining inorganic and organic building blocks that appropriately distributed on the *(macro)molecular or nanoscale,* where the inorganic part provides thermo-mechanical stability and an overall physical structure to the natural objects while the organic moiety delivers strong bonding to the inorganic building blocks. Bones, teeth, shells, marine sponges, and diatoms are typical examples of the natural bio-hybrids.[1] Some of the examples of naturally occurring inorganic-organic hybrid material are given in **Table 1.1**.Mostly, Natural bio-hybrid materials contain organic, polymer matrix systems reinforced with inorganic deposits. The scientific excellence in biological hybrids is the accurate blending of inorganic-organic molecules formed at ambient temperatures, an aqueous environment, a neutral pH where a plethora of complex geometries results. Mimicking such structures is the current topic of research interest for the rapidly growing industrial needs.[2, 3]

Commonly, the synthetic hybrid materials require two constituents; one is the matrix and another is reinforcement. Inorganic materials in hybrid systems play several roles: apart from enhancing the mechanical strength and thermal stability, it provides modulating the refractive index, giving an accessible and interconnected porous network for increasing the surface area, sensing ability and catalytic efficiency, or contributing specific magnetic, electronic, redox, electrochemical or chemical properties.[4-13] Organic components greatly extend the range of matrices available to synthetic chemists. Organic materials can offer opportunities to modify the bio to chemical functionality enabling the hybrids to form flexible films and fibres, for

obtaining various geometric structures, to control the porosity features as well as connectivity with inter-particle surface functional groups, for an extend to adjust the balance between hydrophilic/hydrophobic characteristics.

Table 1.1. Examples of naturally occurring inorganic-organic hybrid materials

Inorganic-organic Hybrid material	Inorganic constituent	Organic Constituent
Coccoliths	Calcium carbonate	Protien
Shellfish shells	Calcium carbonate	Chitin
Venus sponge	Silica	Protien
Ivory, bones	Calcium phosphate	Collagen
Teeth of bone-skeletal animals	Hydroxyapatite	Collagen
Diatoms	Silica	Polysaccharide
Radiolaria	Silica	Protien
Brittlestar's lens	Calcium carbonate	Protien
Magnetotactic bacteria	Iron oxide	protien
Ferritin	Iron	Protien
Kidney stone	Calcium oxalate	Uric acid
Teeth of certain molluscs	Calcium carbonate	Chitin

In the last decades, man-made hybrid materials were developed on a large scale with a lot of realized economic applications. The tremendous increase in the scientific publications and patent applications from the year 2005 until the year 2016 is shown in **Fig. 1.1.** explain the essentiality and demand of the hybrid architectures.[14] Due to the possibility of tailored properties via hybridization and also to achieve multifunctional properties, the research community seriously considered this innovative field for continuous investigations.[15, 16] However, the mandate is to make materials in affordable ways.

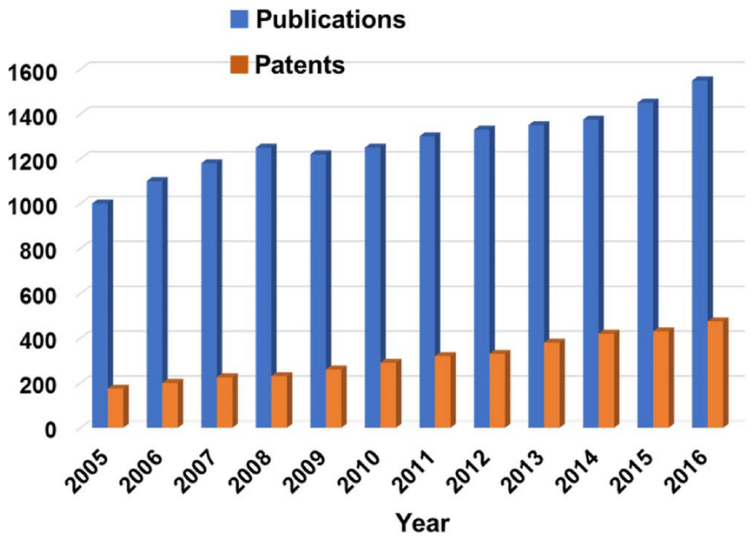

Fig. 1.2. The number of scientific publications and patents on hybrid materials research

Scratch resistant coating technology via hybrid approach is one example in which the inorganic-organic hybrid formulation is easily made by the modification of affordable nanomaterials with a simple surface treatment that can form hybrid films or top-coats to finally obtain better scratch resistance.[17-19] Based on the molecular or nanoscale dimensions of the inorganic building blocks, light scattering in homogeneous matrix material is well-controlled and optically transparent nanocomposite hybrids suitable for optical applications are successfully produced. [20-22] In some cases phase separation of organic and inorganic components is used for the formation of porous materials. [23,24] Smart materials were also fabricated by modification of the composition on the molecular scale and demonstrated for applications such as adsorbents, catalysts, optical devices, sensors, membranes, enzyme immobilization media, electronic and magnetic devices, flame retardants and biomaterial coating. [25, 26] The following section briefly explains the classification of hybrid functional materials widely reported in the literature.

1.2. Classification of Hybrid Materials

Functional hybrid materials are not just a physical combination. They are the molecular level nanocomposites, with at least one component, either the inorganic or the organic constituting part, with a characteristic length on the nanometer size (a few Å to several tens of manometers).[27] The sum of the all properties of the hybrid materials are not the outcome of the properties of individual contributions of their components, but also from the strong synergy created by a hybrid interface.[28, 29] The carefully tailored inorganic/organic interface, including the pattern of distribution, types of physical interactions, the surface energy, and the existence of labile bonds gives the desired properties. Owing to their large importance, various functional hybrid materials can be categorized into two main families depending on the nature of the interface combining the organic components and inorganic materials.[27]

1.2.1. Class I hybrid architectures

It is concerned with hybrid systems in which organic and inorganic components interact via weak bonds such as Van der Waals, electrostatic, or hydrogen bonds. The class I hybrid compounds present a number of intriguing features, such as the material's ease of synthesis, the avoidance of hetero functional metal-organic precursors, and, when desired, the simple removal of the organic phase to easily create functional architectures by self-assembly. The combination of inorganic clusters or particles with organic polymers which lack a strong (e.g. covalent) interaction between the components is one example of such class I hybrid material. If an inorganic and an organic network formed by interpenetrating each other without strong chemical interactions, so called interpenetrating networks, for example, if a sol–gel material is formed in presence of an organic polymer or vice versa. Both materials belonged to class I hybrids.

1.2.2. Class II hybrid systems

Class II hybrid materials are materials in which the components are linked by covalent or ionic-covalent strong chemical bonds. In fact, various hybrid materials comprised both types of interfaces, strong and weak, but due to the importance of the presence of strong chemical bonds on the final hybrid material properties, these types of hybrid are classified as class II. However, we are currently witnessing an increase in the development of hybrid materials of class II.

The presence of covalent chemical bonds between organic and inorganic mineral components has several advantages:

the potential to create entirely novel materials from functionalized alkoxide,

ii) phase separation minimization and iii) better definition of the inorganic-organic interface. Such precise control can result in a better understanding of the material and the relationship between microstructure and properties, as well as easier adjustmet of the hydrophilic-hydrophobic balance, etc. The effective grafting of organic functionality to the inorganic network avoids disadvantages of Class I hybrid compounds. That is the possibility of organic components escaping while the material is in use, such as in sensors or catalysts.

1.3. Synthetic Strategies for Hybrid Materials

There are several synthetic strategies available for the fabrication and formation of hybrid materials, irrespective of the type of hybrid interface formed. [29-32] The reaction route (**Fig.1.2.a**.) is corresponds to soft chemistry-based routes such as conventional sol-gel chemistry, as well as hydro- and solvothermal synthesis, in which molecular precursors like alkoxides, metal salts in the presence of complexing polyfunctional precursors, and organofunctional precursors are used. Hydrolysis of organically

modified metal alkoxides or metal halides condensed with or without metallic alkoxides yields hybrid networks through conventional sol-gel pathways. These materials are typically amorphous with polydisperse size distributions.

Path B (**Fig.1.2.b**.) clearly demonstrates the hybridization of well-defined nanobuilding blocks [NBB] through self-assembly, or intercalation and dispersion, simply intercalation.[32-34] These NBB are precisely tuned objects such as clusters or nanoparticles (metal oxides, metals and alloys, chalcogenides), core/shell nanoparticle composite, or nano-sheets of lamellar compounds (clays, double hydroxides, and lamellar chalcogenides, etc.). Prefabricated nano-objects quite often exhibit reduced reactivity when compared to molecular precursors; the inorganic component is monodispersed or the nanometer scale, allowing the development of well-defined structures which facilitate characterization and control over the quality of final material.

Path C (**Fig. 1.2.c.**) makes use of the self-assembly features of amphiphilic molecules and polymers to produce supramolecular templates that can be used to control the texture and morphology of the final growing solid or gel phase.[34, 35] Over the last decade, a new field has emerged that corresponds to the templated synthesis (with surfactants) of mesoporous hybrids using bridged silsesquioxanes precursors. This process results in a new class of periodically organised mesoporous hybrid silica containing organic functionality within the walls.

Literature evidence strongly indicates the construction of hierarchically structured hybrid materials that are integrated in real devices follows integrative synthesis pathways where chemistry and physics based processing are strongly coupled. The combination of above mentioned procedures in paths A, B, and C allow fabricating hierarchically organized materials with regards to structure and functions.

Generally, inorganic-organic hybrid materials are reported via sol-gel, solvo thermal, hydro thermal methods etc. Among them, the sol-gel method is the most promising method for producing inorganic-organic hybrids. Because it is a low-temperature solution process for producing ceramics, hence organic component decomposition can be significantly reduced.[36, 37] In the 1950's, the term "sol-gel science" was coined to describe the art of manufacturing materials by preparing a sol, gelation of the sol, and removing the solvent.[38] In fact, sol-gel technology has been used since the first experiment with colloidal materials. The sol-gel method was initially developed by mineralogists for the preparation of homogeneous powders to be used in phase equilibria, chemists for the production of nuclear fuel pellets, and ceramists for the preparation of advanced ceramic materials. [38]

This thesis work is pertaining to the sol gel processing of inorganic-organic nano hybrids. The following section briefly describes the various stages involved in the typical sol gel process.

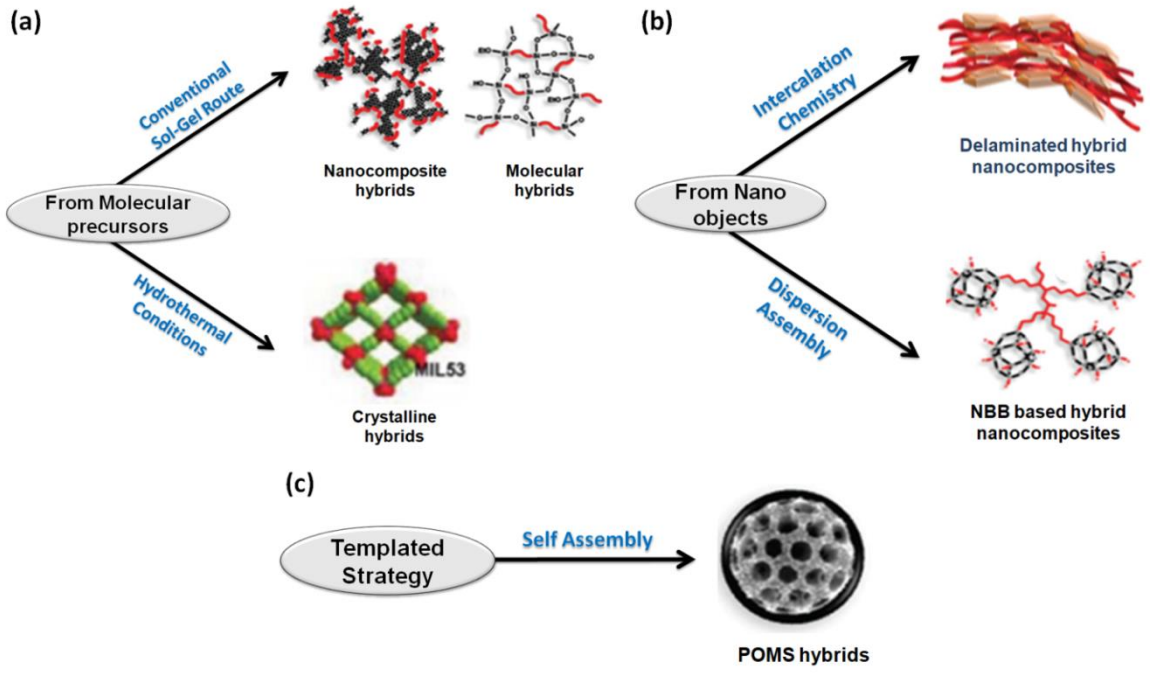

Fig.1.2. The synthetic pathways for the preparation of hybrid materials

1.4. Sol-Gel Processing of Inorganic-Organic Hybrids

The first metal alkoxide gel was prepared from SiCl4 by Ebelmen in the 19th century, who discovered the formation of Si-alkoxide to gel when exposed to air.[39] It was later discovered that atmospheric moisture caused the Si-alkoxide to hydrolyze, which then condensed to form the gel network. The term 'sol-gel' was coined by Graham in 1864, during his work on silica sol.[40] Since then, the sol-gel method has been extensively researched and fine-tuned for the low temperatures preparation of metal-oxide gels. In general, the sol-gel method entails the evolution of inorganic networks through colloidal suspension (sol) formation and gelation of the sol to form a network in a continuous liquid phase (gel). The detailed science involved in sol-gel processing has been reviewed in numerous books and journal publications. [41-43] Simply put, the sol-gel process is the "***formation of an oxide gel network via poly condensation reactions of a molecular precursor in a liquid at low temperature***".

In its early stages, the process was mainly used to develop highly pure and homogeneous inorganic materials such as glasses and ceramics obtained from inorganic metal-oxide gels. Eblemen reported the first inorganic gel, silica gel, derived from silicon-alkoxide, in 1846.[39] Cossa created the first alumina gel in the year 1870.[42] Since then, different types of inorganic gels have been developed, and sol-gel chemistry has made tremendous progress in the development of inorganic metal-oxide gels.[42, 44]

1.5. Sol-Gel Route: Precursors to Gel Formation

1.5.1. Precursors

The major precursors of the sol-gel process consisted of metal or semimetal elements surrounded by various reactive ligands. The important requirements for the selection of sol-gel precursor are: (1) It must be soluble in the reaction medium, and (2) it must be

reactive enough to contribute to gel formation.[45] Metal alkoxide M(OR)z are the most commonly used precursors in sol-gel research, where M=Si, Ti, Zr, Al, Sn, and Ce, OR is an alkoxy group, and Z is the metal's valence or oxidation state. The majority of metal-alkoxide-based sol-gel precursors involve early p-block elements (Al or Si) or early transition group metals (Ti or Zr). When compared to Si alkoxide precursors, metal alkoxides of Al, Ti, or Zr are very reactive towards water due to their low electronegativity and higher Lewis acidity.[46] Likewise, the size and nature of the hydrolyzable alkoxy group (OR) attached to M affect the precursor's solubility and reactivity. In general, the larger alkyl group (R) is more soluble in organic solvents and possesses slower hydrolyzability. Although sol-gel chemistry begins with the hydrolysis and condensation of metal alkoxide precursors, it can also take place between hydrated metal species like salts, oxides, hydroxides, complexes, acrylates, and amines.

1.5.2. Sol

A stable colloidal suspension of solid particles within the liquid medium is termed as sol.[47] The IUPAC defined a colloidal suspension as ***"the molecules or poly molecular particles dispersed in a medium have at least in one direction a dimension roughly between 1-1000 nm".***[42] In this context, sol encompasses a broader range of systems, including inorganic particles, polymeric, and real macromolecules, such as biopolymeric particles formed by solvation and ionic cross-linking. The particles within a sol are small enough to suspend indefinitely because of Brownian motion. Compared with the solvent phase, there is only a small amount of the dispersed phase present, as a result long-range forces, such as gravitation are negligible, while short range forces like Van-der Waals interactions and surface charges dominate in the colloidal system. Electrostatic forces are the major cause of stabilization of the sol as per the Stern model. The adsorption of charged species such as OH- or H+ on the surface (depending on the pH)

results in the formation of an electrical double layer at the liquid-solid interface. As a result, a repulsive interaction with other colloidal particles occurs, which inhibits aggregation to larger particles or destabilisation of the sol.

1.5.3. Gel

The sol-gel reaction results in the formation of two types of gels: one produced by the condensation of colloidal particles (1-1000 nm) or cluster growth, and the other by the cross-linking of polymeric molecules. As in colloidal pathway, nanoparticles with size less than one micrometre are synthesised, which are found to be dispersed in the solvent and are referred to as colloidal sol. Then, these discrete colloidal particles cross-link with one another using hydrogen bonding or electrostatic attraction to form a three-dimensional (3 D) gel network. The transformation of a sol to a gel is defined as the gelation process, and the gels obtained are known as '***colloidal gels***.'[48] Metal salts such as chlorides, nitrates, and sulphates are commonly used to make colloidal gels. In this case, the gel formation mechanism is induced by the electrolytic and steric effects of the colloidal sol particles. As a result, these gels are also referred to as ***'corpuscular gels***.'

In contrast, chemical reactions are the driving force behind gelation in polymeric gels. Without the intermediate formation of individual particles, linear polymeric chains are formed. When this happens, highly branched 3D gel suspensions are formed, which are referred to as '***polymeric gels***'.[48] Metal-alkoxides are the most commonly used precursors for the formation of polymeric gels.

1.5.3.1 Gelation

Gelation refers to the phase transition from "sol to gel". By passing through a transition point known as the ***gel point***, a sol can be transformed into a gel (colloidal or polymeric gel). At this point, sol abruptly transforms from a viscous liquid to a solid phase known

as gel. The chemical reaction that causes gelation usually continues beyond the gelation point, ensuring frequent changes in the structure and properties of the gel.

1.6. Governing Mechanism in Sol-Gel Transition

The sol-gel reaction involves two fundamental chemical reactions: the hydrolysis of the alkoxide precursors to introduce a reactive hydroxyl group on the metal and their condensation to form metal oxide gels.[42, 45, 49] The following equations depict the major steps involved in the sol-gel process when metal-alkoxide is used as the precursor:

$$M\text{-}OR + H_2O \longrightarrow M\text{-}OH + HO\text{-}R \text{---Hydrolysis} \quad (1.1)$$

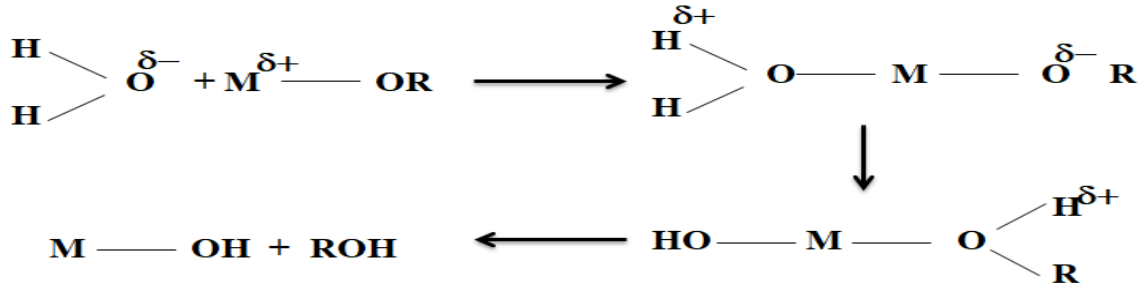

(1.2)

Where, M and R denote metal and alkyl groups respectively. The hydrolysis and condensation reactions are primarily responsible for the sol to gel transition. The metal-alkoxide's alkoxy group reacts with water to form a hydroxyl group, a process known as 'hydrolysis.' As shown in the equation, the hydrolysis reaction involves a nucleophilic attack of the oxygen present in the H_2O molecule on the central atom M, followed by a proton transfer from H_2O to the alkoxy group –OR and the removal of the alcohol molecule (ROH) from the system. Hydrolysis commonly occurs in the presence of either an acid or a base catalyst. Acids protonate negatively charged alkoxide groups, whereas alkaline environments generate strong nucleophiles through deprotonation of hydroxo ligands.[42] The rate of reaction of hydrolysis is also determined by the choice of

precursors used, because the steric factors of the alkyl group vary depending on the type of groups present in the precursor. The larger the alkyl group, the more crowded the nucleus M and thus the slower the rate of hydrolysis. In addition, the longer the chain, the weaker the inductive effects on the central atom and the slower the substitution reaction.

In addition to the hydrolysis reaction, two other reactions can occur: the reverse reaction, also known as re-esterification, and transesterification, in which an alcohol molecule replaces an alkoxide group to produce another alcohol molecule.

$$\text{M-OR+R'OH} \longleftrightarrow \text{M-OR'+HO-R} \longrightarrow \text{Re-esterification (reverse reaction)} \quad (1.3)$$

The condensation process starts when some hydrolyzed molecules begin to form in the solution and continues along with the hydrolysis process depending on the amount of water and catalyst in the solution. The condensation reaction forms a metal-oxygen-metal (M-O-M) bridge and can lead to two distinct reactions, as shown in the equation. Different metal atoms are linked together by an oxygen atom through an alcoxolation reaction between a hydroxyl group and an alkoxy group or an oxolation reaction between two separated hydroxyl groups.

$$\text{M-OR+HO-M} \longrightarrow \text{M-O-M+HO-R} \longrightarrow \text{Condensation alcoxolation} \quad (1.4)$$

$$\text{M-OH+HO-M} \longrightarrow \text{M-O-M+H}_2\text{O} \longrightarrow \text{Condensation oxolation} \quad (1.5)$$

As a result, a stabilised dispersion of metal-oxide sol covered with an active group such as hydroxyl is formed in the solvent. Then, these are cross-linked by the condensation of surface active groups, resulting in the formation of metal-oxide gels. Process parameters such as pH, precursor concentrations, temperature, type of solvent and catalyst, and so on can have a significant impact on the final gel properties. These

fundamental studies have been thoroughly investigated by various researchers.[50-52] In a typical sol-gel reaction, the hydrolysis and polycondensation steps followed by ageing and drying process occur, and the gel network is firmly formed within the gel matrix, resulting in a stiff sol-gel structure. Hence, the sol-gel process can be summarised as follows:

(a) Preparation of the sol from hydrolysis and partial condensation of precursors such as alkoxide or metal salt.

(b) Formation of the gel *via* poly condensation to form metal-oxo-metal or metal-hydroxy-metal bonds.

(c) Syneresis, also known as ageing, is the process by which condensation continues within the gel network, often shrinking it and causing solvent expulsion.

(d) Drying the gel either to produce a dense xerogel *via* porous network collapse, or a cryogel *via* freeze drying, or an aerogel *via* supercritical drying.

(e) Exclusion of surface M-OH groups by calcining at high temperatures up to 800 °C or above.

Nowadays, the sol-gel process is a well-known method for producing gel-based advanced functional materials. Starting from a reactant precursor solution, the solid state can be easily reached at low temperatures via this versatile route. This feature greatly expands the potential for developing new materials with hybrid architectures. It also facilitates the creation of ultra-fine or spherical powders, fibres, dense monoliths, aerogels, thin films, and a wide range of nanostructured materials, as shown schematically in **Fig. 1.3.** Thus, the versatility of sol-gel nanotechnology enables to control the material properties required for functional applications.

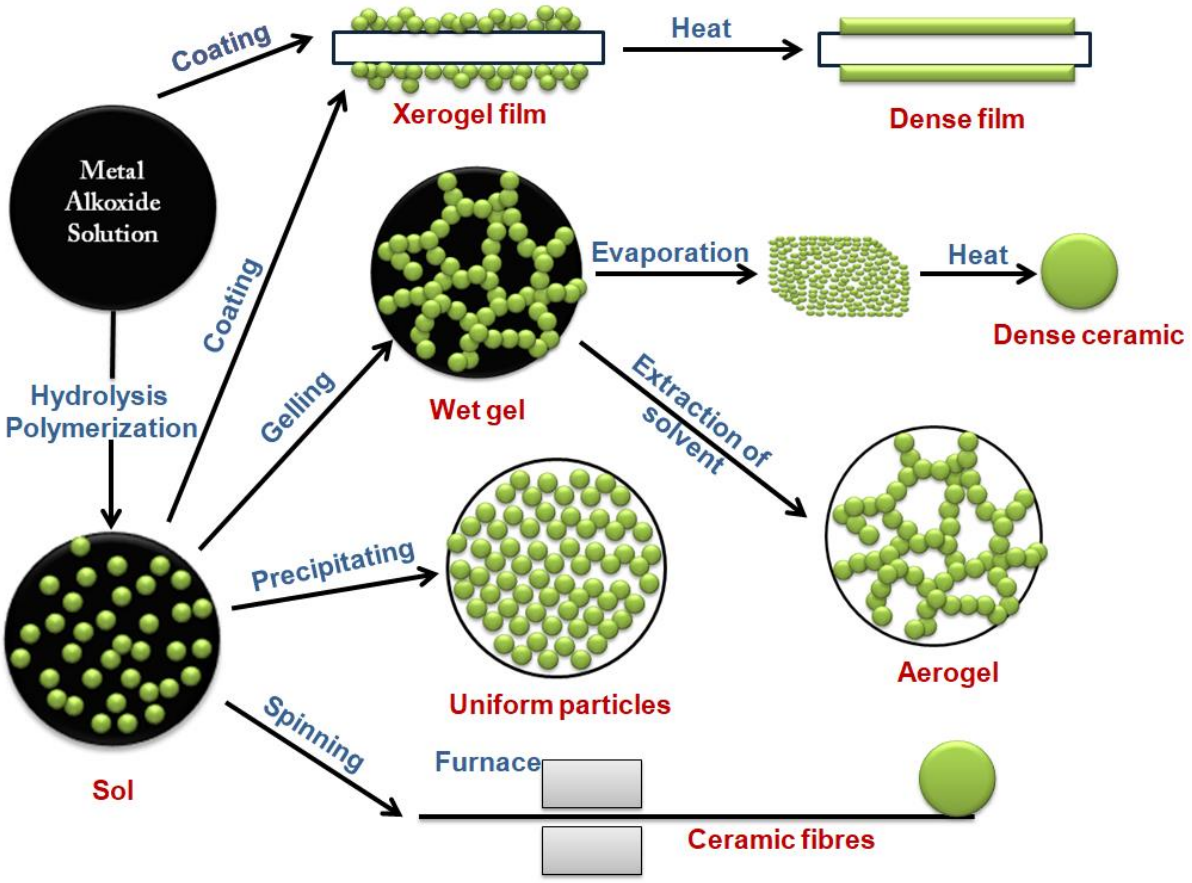

Fig. 1.3. Different types of functional materials obtained via sol-gel synthesis

1.7 Gel based Hybrid Materials based on Drying Techniques

Xerogels, aerogels, cryogels, and ambigels are the classic gel porous materials derived from the sol-gel process. Since, the thesis is focused on porous gel derived hybrid materials, a more detailed account of it is described in this section.

A typical flow diagram of the sol-gel process does not complete with gelation. The wet gel can be aged in its mother liquor or in the solvent after gelation. The period of time between the formation of a gel and its drying is referred to as ageing. During the ageing process, a gel does not become inert; it continues to hydrolyze and condense.[53] It can also go through syneresis, solvent expulsion due to gel shrinkage, and coarsening. Dissolution and re-precipitation of particles can occur during this process, influencing both the chemical and structural properties of the gel after its initial formation. After

that, the gel is dried to remove the solvent. The drying of the gel is an important step in the preparation of gel porous material. Capillary pressure and shrinkage of the gels are the two parameters governing the drying process. It is driven by the capillary pressure, Pc according to the equation 1.6.

$$P_c = 2\gamma \cos\theta / r_p \quad (1.6)$$

Where, γ is the surface tension of the pore liquid, and r_p is the pore radius, which is represented by the equation 1.7.

$$r_p = 2V_p / S_p \quad (1.7)$$

Where, V_p and S_p are pore volume and surface area, respectively. Capillary tension can reach 100-200 MPa during drying; resulting in shrinkage and cracking.[54] A detailed description of the porous gels produced after drying under different conditions is given below.

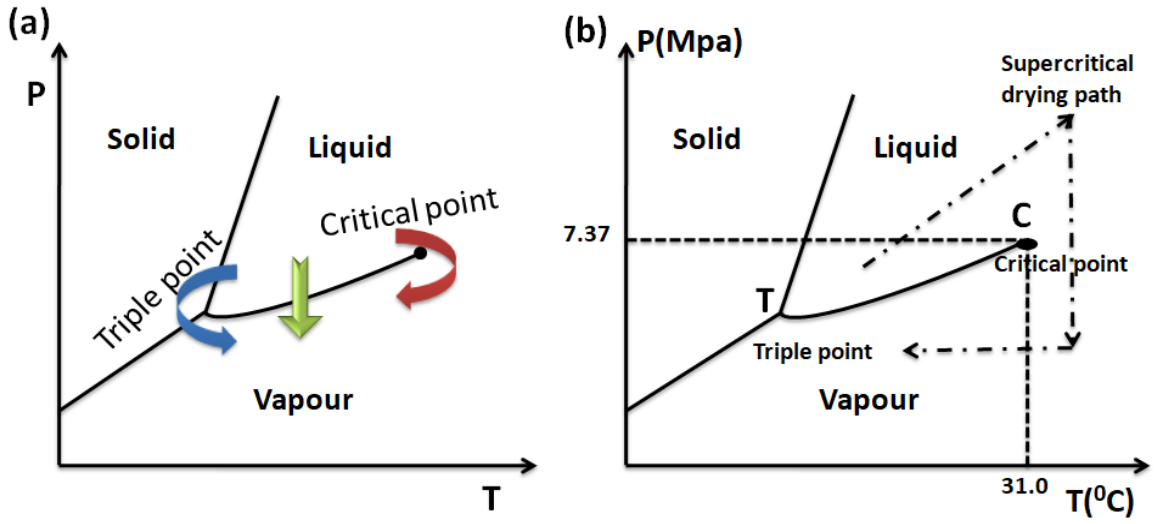

Fig. 1. 4. (a) A typical phase diagram, the boundary between gas and liquid runs from the triple point to the critical point. Evaporative drying is the green arrow, while supercritical drying is the red arrow and freeze drying is the blue. (b) Example of a possible supercritical drying path in the pressure(p)-temperature (T) phase diagram of CO_2[59]

1.7.1. Xerogels

The traditional evaporative drying process provides a significant capillary pressure associated with the liquid vapour interface within a pore, causing the gel network to shrink dramatically. Thus obtained gel is known as Xerogel. In **Fig. 1.4. a.**, a green arrow represents a typical phase diagram for evaporative drying. The differential capillary pressure employed during evaporative drying can also cause the porous network of varying pore size distribution to collapse. Hence, the surface area and pore volume of xerogels are frequently low. Xerogel usually retains less porosity (15- 50 %), and surface area (10-300 m^2g^{-1}), along with very small pore size (1- 10 nm).To reduce capillary stresses, surfactants can be added to the liquid. It was reported that shrinkage of an alkoxide-derived gel is reduced by surfactants, though it is not necessarily eliminated.[55]Although, the addition of "drying control chemical additives'' (DCCA) including such oxalic acid, glycerol, formamide, dimethyl formamide, and tetramethylammonium hydroxide can lower the capillary stress and substantially shrink the gel network.[56-58] The main reason for this drying behaviour is that the addition of DCCA creates a uniform pore size distribution, which in turn reduces differential drying shrinkage.

1.7.2. Aerogels

One convenient approach to reduce pore collapse is to remove the liquid from the pores above the critical temperature (Tc) and pressure (Pc) of the solvent, especially by supercritical drying (SCD).[42,59] When supercritical conditions are applied, there is no separation between the liquid and vapour phases, and the densities become equal. As a result, there is no liquid-vapor interface at this point, and thus no capillary pressure. A typical phase diagram for SCD drying is represented by a red arrow in **Fig.1.4. a.** This method of drying prevents the formation of a liquid-vapor meniscus, which recedes

during the emptying of wet gel pores. The resulting dried gel is known as an aerogel, and it has pore volume comparable to that of the wet gel.[59] SCD is composed of three major steps.

(i) The wet gel is placed in an autoclave, which gradually raises the temperature. As a result, the pressure rises. The pressure and temperature are both increased until they exceed the critical temperature, Tc, and critical pressure, Pc, of the liquid entrapped in the pores within the gel. When the desired temperature and pressure are reached, the conditions are maintained for a specified period of time.

(ii) After that, the fluid is expelled at a constant temperature, causing a pressure drop.

(iii) When the vessel reaches ambient pressure, it is cooled to room temperature, yielding solid aerogels.

Depending on the fluid that impregnates the wet gel, the critical conditions are quite different. There are two types of SCD: High Temperature Supercritical Drying (HTSCD) in alcohol and Low Temperature Supercritical Drying (LTCD) in CO_2. In HTSCD process, a kind of poorly controlled ageing process occurs when the temperature and pressure increases used to reach the desired supercritical conditions. As a result, thus obtained materials are generally hydrophobic and stable when exposed to moisture. On the other hand, the LTSCD method does not facilitates such processes and produces more hydrophilic solids. **Fig.1.4.b.** depicts a possible supercritical drying path in the phase diagram of CO_2 , where the pressure and temperature are increased in such a way that the phase boundary is not crossed; once the critical point is reached, the solvent is ejected at constant temperature ($>T_c$).

Steven Kistler first developed silica aerogels in the early 1930s. [60] Thereafter, a wide range of inorganic metal-oxide aerogels including such as alumina, titania,

zirconia, and many others were produced.[61-63] Non-oxidic aerogels such as chalcogenides, as well as organic aerogels such as carbon and polymeric aerogels, have recently been developed.[64-66] Surprisingly, as of 2013, graphene aerogels were recorded as the world's lightest material. [67]

In general, the aerogel preparation process consists of three major steps:

(i) Solution -sol transition, (ii) sol-gel transition (gelation), and (iii) gel-aerogel transition (drying). All three steps have the potential to influence the microstructure of the aerogel and thus its properties and applications.

1.7.3 Cryogels

The freeze drying method is another way to avoid the presence of a liquid-vapor interface. This method involves freezing the liquid in the gel and thereafter drying it by sublimation.[68] The blue arrow in **Fig.1.4.a.** shows a typical freeze drying phase diagram. A liquid-vapour meniscus formation is prevented in this case. Thus obtained materials are known as cryogels. Although its surface area and mesopore volume are smaller than those of aerogels, they are still significant.[42, 59] unfortunately, freeze-drying does not allow for the preparation of monolithic gels. The reason for this is that the growing crystals repel the gel network, pushing it out of the way until it reaches its breaking point. This phenomenon enables gels to be used as hosts for crystal growth: the gel is so effectively expelled that crystals nucleated in the pore liquid are not contaminated with the gel phase; the crystals can grow up to a few millimetres in size before the strain is so great that macroscopic fractures appear in the gel. Nonetheless, the gel network may be damaged by the nucleation and growth of solvent crystals, which produce very large pores. A rapid freeze method known as flash freezing has been developed to mitigate this event. It is also critical that the solvent has a low expansion coefficient and a high sublimation pressure.

1.7.4. Ambigels

Supercritical drying is recognized as an expensive method that impedes aerogel commercialization. As a result, ambient pressure drying (APD) or subcritical drying of gels is gaining popularity. This approach is thought to be a promising solution for lowering the cost of aerogel production to an economical scale. Because the gels are dried under ambient conditions; the dried gels are referred to as ambigels. APD encompasses a "solvent exchange process and chemical modification of the gel's inner surface." Capillary forces produced during APD or subcritical drying can be lowered by adjusting the contact angle between the solvent/vapour interface and the pore wall. This implies a deliberate modification of the gel's inner surface through the silylation to strengthen the network and by exchange of the pore solvent to reduce capillary force.

The pore solvent is first exchanged with a water-free solvent in the APD method. Subsequently, the reaction with silylating agents was performed to strengthen the network.[69,70] The most commonly used silylating agents are vinyl trimethoxy silane (VTMS), Propyltrimethoxysilane (PTMS), Propyltriethoxysilane (PTES), TRimethyl methoxy silane (TMMS), Methyl triethoxysilane (MTES), Hexamethyldisilazane (HDMZ), and Hexamethyldisiloxane (HDMZO).[71-76] Finally, prior to the drying step, again solvent exchange is performed with a low surface tension solvent, such that drying can carry out at ambient conditions.

The materials dried by freeze-drying (cryogels) and ambient pressure drying or subcritical drying (ambigels)methods, are also termed as aerogels or aerogel like materials Even so, such an extension can be stated only if it can be demonstrated that the pores occupy a very high percentage of a sample volume, e.g., more than 90%, despite the fact that no official definition exists.

1.8 Boehmite Hybrids *via* Sol-Gel Chemistry

In this thesis work ***boehmite***, a mono hydroxy aluminium oxide [AlOOH] based hybrid system was considered for the systematic investigation. Hence a brief account of the synthesis of boehmite hybrids is given in the following section. The Boehmite hybrid was carried out of aluminium isopropoxide as a sol-gel precursor.

1.8.1. Aluminium isopropoxide (AIP)

AIP is a commonly used aluminium-alkoxide precursor for the preparation of boehmite sol. The chemical formula of AIP is $Al(O\text{-}i\text{-}Pr)_3$, where, i-Pr is the isopropyl group($CH(CH_3)_2$).It is a white powder with molecular mass 204.25 g mol^{-1}.Hydrolyzed boehmite sol is the starting precursor for the preparation of boehmite gel derived inorganic-organic hybrids. A brief introduction of boehmite is given below.

1.8.2 Boehmite (AlOOH)

Boehmite is an aluminium oxy-hydroxide with varying water contents. It is classified as partially dehydrated aluminium hydroxides, $Al(OH)_3$. Boehmite is the traditional precursor of transition aluminas. Its name is derived from the German chemist J.Böhm. Alumina with a large surface area is extremely important as adsorbents and catalysts in a wide range of chemical processes. This is primarily due to their favourable properties and acid–base characteristics, which vary depending on the crystal structure and surface hydration/hydroxylation of boehmite.[77] Because the final structure of the industrially relevant -Al_2O_3 and –it is controlled by that of boehmite, a great deal of research and development is being done to synthesize boehmite nanoparticles of various morphologies and shapes.[78,79] This development is consistent with the growing trend of using nano-scaled metal oxides to create inorganic-organic hybrids with novel properties. Since the primary crystallite size of boehmite can be as small as 4.5 nm, it can have a very high specific surface area (>300 m^2 /g). As a result, boehmite is an

excellent inorganic moiety for creating inorganic-organic hybrids with organic polymers. However, the particle size of boehmite dispersed in aqueous media is 4 to 10 times that of its primary crystallite size.

1.8.2.1. Preparation

Boehmite can be produced in various ways. The various types of preparation processes produce a variety of shapes, morphologies, and surface properties. The following are some examples of common methods:

- Solid state decomposition of (mineral) gibbsite, $Al(OH)_3$.[80] This method is also termed as controlled calcinations.
- Precipitation of acidic or basic aluminium salt solutions in an aqueous solution. The corresponding aluminium salt solution is neutralised and aged during this "hydrothermal transformation.[81] ''Different sol–gel procedures usually start from aluminum alcoholates. [82] This route of synthesis is represented by eq. (1.8.)

$$Al(O\text{-}C_3H_7)_3\ (s) + (n+2)\ H_2O\ (l) + HNO_3\ (aq) \longrightarrow AlOOH.nH_2O\ (l) + C_3H_7OH\ (g) \qquad (1.8)$$

A drying step is involved in the sol–gel synthesis that results in solid boehmite. Aside from the drying techniques discussed in section 1.7, industrial spray drying and spray pyrolysis are also used.

1.8.2.2. Structure and properties of boehmite

It is now accepted that -AlO(OH) has an orthorhombic unit cell.[82-84] Boehmite has a double layer of oxygen octahedrons with a central Al atom in its crystal structure. Accordingly, in a distorted AlO6 octahedron, Al is surrounded by six oxygen atoms.[84]

The oxygen on the side is bonded to the hydrolyzed groups of the neighbouring layer of octahedrons via H-bond.[83] **Fig. 1.5**. represents a three dimensional (3D) projection of the crystalline structure of Boehmite.

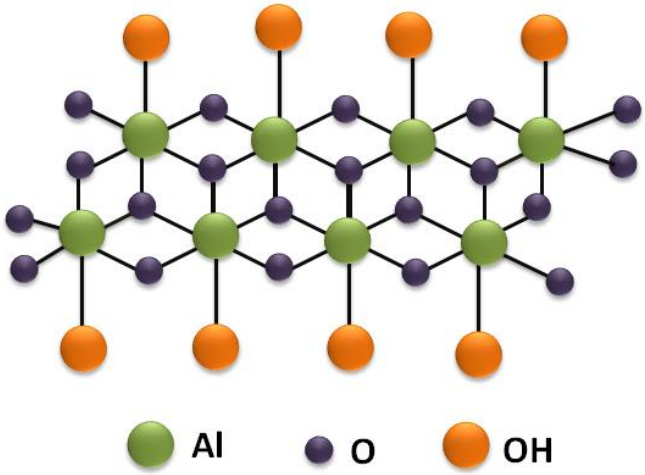

Fig. 1.5. Crystal structure of boehmite

1.8.2.2.1. Boehmite :- Structural features

The various boehmite preparation methods provide numerous opportunities to tailor the shape and surface characteristics (specific surface area, pore volume, pore structure) of boehmite nanoparticles with particulate dimensions in the nanometer range, at least in one direction. Boehmite can be made into needle-like structures in one dimension (1D), such as nanorods, nanotubes, and whiskers.[85-87] 2D sheets were also created, both with and without additional porosity.[88] Many commercially available boehmite manufactured by Sasol (trade names: Dispersal, Dispal) have 1D needle or 2D flake-like shapes.

Three-dimensional (3D) morphologies such as flower-like, urchin-like, flake assembly, multiscale hierarchical, and various mesoporous structures can also be produced.[89-91] The latter boehmite could have BET-specific surface areas greater than 300 m^2/g. They can function as catalysts, catalyst supports, and adsorbents.[91] The majority of the morphology control methods mentioned above employ various types of surfactants as morphology inducing agents or chelating additives. In contrast to template-free synthesis methods, this approach is commonly referred to as a template-directed approach. The morphology control strategy led to the development of new

preparation procedures such as chemical vapour deposition, thermal decomposition of organic complexes, the combination of hydro- and solvothermal methods, and so on.[90] Size dispersion characteristics of boehmite in aqueous (slightly acidified) solutions are even published by some manufacturers. This fact prompted the development of water-assisted(WA) (mediated) boehmite incorporation in polymers.[92] Surface hydroxyl groups may also act as "anchoring" sites for surface modification, according to **Fig. 1.5.** The physical properties of boehmite are summarized in **Table1.2**.

Table 1.2. Physical properties of boehmite

Parameters	Values
Colour	White
Molecular mass	59.99
Density	3.04 g/cc
Specific gravity	3.0-3.1
Mohs hardness	3
Refractive index	1.644-1.668
Tenacity	Brittle
Diaphaneity	Translucent

1.9. Applications of Boehmite-Organic Hybrids

According to a review of the literature, boehmite-based inorganic organic hybrid materials can be used for a variety of functional applications. The various application studies conducted with boehmite-based hybrid materials are summarised in **Fig. 1.6**. However, boehmite based inorganic-organic hybrid materials are widely used for protective coating and membrane filtration applications.[93, 94] In this present thesis work inorganic-organic hybrid materials derived from boehmite gels are explored for applications like adsorption and photodegradation, antibacterial agent, sensor, oil-water

separation filters, and fire retardant material. The preceding sections provide an overview of previous research on these applications.

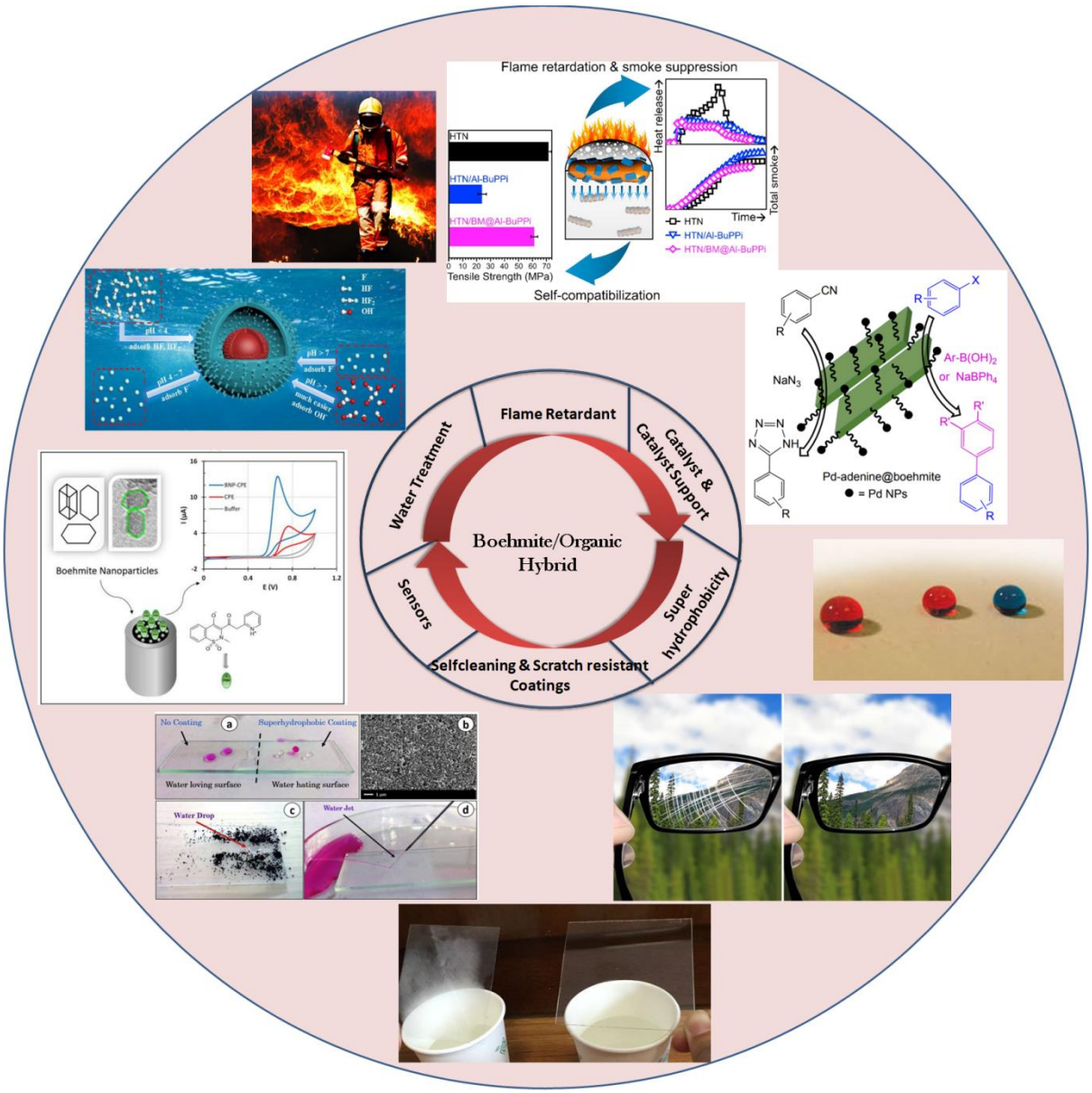

Fig. 1.6. Applications of boehmite hybrids

1.9.1. Boehmite as substrates for adsorption

Adsorption was indeed defined as ***"the process by which molecules, atoms, or ions in a gas or liquid diffuse to the surface of a solid and are held there by weak intermolecular forces.***" The solid material is referred to as the '***adsorbent***,' and the solute that is adsorbed is referred to as the '***adsorbate***.'[95] Du Bois-Reymond proposed

the term adsorption, but Kayser was the first to use it in the literature.[96] Adsorption is widely regarded as a highly effective water treatment technology that produces high-quality treated water. Adsorption is a surface phenomenon defined as an increase in the concentration of any element at the surface or interface between two constituents.[96] An active material used for purification should be able to reduce the pollutant's contamination level to the standard limit before it is discharged into the environment. Adsorption was typically good for inorganic oxides with a rich porous structure and special surface properties qualifications in the field of water treatment. Various sorbents, such as clay, silica gel, alumina, polymeric materials, carbon materials, and others, were used to decontaminate polluted water.

Because of their outstanding physicochemical properties for water treatment, Al-based nanostructures containing aluminium oxide, aluminium hydroxide, and aluminum oxyhydroxide have received a lot of attention.[97, 98] Boehmite has been investigated for the removal of heavy metals and organic pollutants in water and in sewage treatment.[99] Because of the high number of surface -OH groups, boehmite is prone to interacting with foreign molecules and/or heavy metal ions, making it an important adsorbent material.[99] A boehmite-based inorganic-organic hybrid system has also recently been reported. Luo et al. used a Boehmite/PVA hybrid free standing film for chromium adsorption in 2016.[100] The hybrid film had a chromium adsorption capacity of 36.41 mg/g. Rajamani et al. investigated the adsorption of heavy metal ions by boehmite/chitosan hybrid desiccant and discovered that the optimum percentages for Cd(II), Pb(II), and Hg(II) ions were 99.54, 98.84, and 67.58, respectively.[101] The adsorption capacity increased with pH, contact time, and adsorbent dose but decreased with initial concentration. The focus of this thesis is on a boehmite-organic hybrid gel system for organic pollutant, lignin, from the pulp and paper industry.

1.9.2 Boehmite as a support for photocatalysts

Photocatalysis is a type of advanced oxidation process (AOP) that results in the complete and non-selective destruction of organic contaminants.[102] Heterogeneous photocatalysis has recently received a lot of attention for wastewater treatment because it can mineralize persistent pollutants under mild conditions using semiconductor materials. The photocatalytic activity of semiconducting metal oxides such as CeO_2, ZnO, TiO_2, SnO_2, MoO_3, and others has been extensively studied, and the photoactivity mechanism is well understood. Creating hybrid nanocomposite oxide semiconductors is a new field of interest.

CeO_2 is a metal oxide semiconductor that is gaining a lot of attention as a photocatalyst for photocatalytic degradation of various pollutants. CeO_2 has a band gap that varies from 2.6 to 3.4 eV depending on the preparation method.[103] The photoactivity of CeO_2 is governed by defects such as oxygen vacancies and oxygen interstitials, as well as the generation of hydrogen peroxide, superoxide, and hydroxyl radicals on the CeO_2 surface. When CeO_2 is excited by UV light with an energy greater than the material's band gap energy, excitons are formed, which are electrons in the conduction band (CB) and holes in the valence band (VB).[104, 105] The electron-hole pairs thus formed are responsible for the degradation of the adsorbed contaminants at the CeO_2 semiconductor surface by initiating a series of chemical reactions as described in Equations 1.6.-1.10.[104] The generated holes may react with the surface-adsorbed OH- ions, resulting in the formation of OH free radicals. The $^{\bullet}OH$ free radicals can also be formed by the reaction of dissolved oxygen (O_2) with the generated electrons and protons, which results in the formation of hydrogen peroxide (H_2O_2) as an intermediate product, which is then decomposed to the OH free radical by releasing the $^{\bullet}OH$- ion into the aqueous solution. The formation of these active species reduces the rate of electron-

hole recombination and allows for more time to deal with organic pollutants. The photocatalytic mechanism is depicted graphically in **Fig 1.7**.

$$\text{Catalyst} + h\nu \rightarrow e_{CB}^{-} + h_{VB}^{+} \quad (1.8)$$

$$e_{CB}^{-} + O_2 \rightarrow O^{-2} \quad (1.9)$$

$$O^{-2} + e_{CB}^{-} + 2H^{+} \rightarrow \bullet OH + OH^{-} \quad (1.10)$$

$$h_{VB}^{+} + H_2O \rightarrow H^{+} + \bullet OH \quad (1.11)$$

$$\text{Organic Pollutants} \bullet OH \rightarrow \text{Degradation Products } (CO_2, H_2O, \text{etc}) \quad (1.12)$$

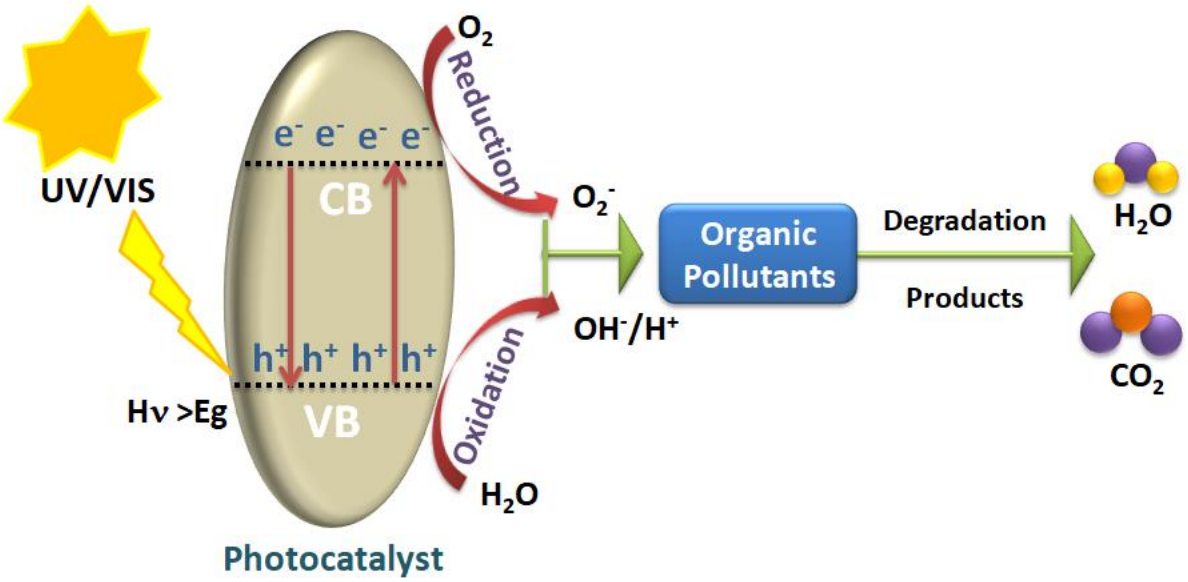

Fig. 1.7. General photocatalytic mechanism of a semiconductor metal oxide

Despite the fact that CeO_2 has unique photocatalytic activity and UV absorption, its optical properties can be improved. One of the methods for improving performance entails combining a semiconductor with metal oxide supporting materials.[106] Based on previous research by Shi et al., Larimi and Khorasheh, and Sun et al., aluminium oxide has a very high surface area, high thermal conductivity, and promising chemical and physical stabilities.[107-109] Boehmite, has been the most important precursor or intermediary for the synthesis of alumina materials. Because of the abundance of surface hydroxyl groups (OH), it is expected that boehmite will interact with foreign molecules

such as pollutant molecules via the formation of hydrogen bonds, which will facilitate the adsorption process and improve the degradation of the absorbed molecule.[99] The photogeneration of reactive oxygen species (ROS) in aqueous solution was investigated using an alginate-boehmite-riboflavin hybrid hydrogel system.[110] Mendoza-Damián et al. reported the co-precipitation synthesis of a photocatalytic AlOOH/SnO_2 system for the degradation of phenol under UV light.[111] Based on a review of the literature, it appears that the combination of AlOOH and CeO_2 based hybrid systems can function as a photocatalyst. The goal of this thesis is to develop mesoporous CeO_2@AlOOH-based hybrid systems with a reasonable surface area because such dual functional materials could potentially offer desirable pollutant adsorption as well as simultaneous degradation.

1.9.3. Water Disinfection

Water disinfection is an important area of materials science. Access to safe drinking water at an affordable price has become increasingly difficult in recent years.[112] Antibacterial materials can be used to safely disinfect water bodies.[113] Locally, antibacterial compounds either kill or slow the growth of bacteria. Organic antibacterial agents are less stable and, as a result, are not recommended for use in water disinfection. With the advent of nanotechnology, stable inorganic antibacterial/antimicrobial agents were created. Previous research has shown that metal oxide nanomaterials (e.g., TiO_2, SiO_2, ZnO, MgO, CaO, CuO, Al_2O_3, Ag_2O, and CeO_2) have good antimicrobial activity.[114, 115] Factors such as photocatalytic bacterial disruption and reactive oxygen species (ROS) play critical roles in killing bacteria in water bodies with nanoCeO_2. [116] In the presence of light, the production of reactive oxygen species (ROS) on the surface of CeO_2 nanoparticles causes oxidative stresses in bacterial cells, eventually leading to cell death.[117] **Fig. 1.8.** depicts a possible

antibacterial mechanism provided by semiconducting metal oxide photocatalytic nanoparticles.[118] According to a literature review, the combination of CeO_2 with boehmite-based hybrid nanostructures ideally kills bacteria through both photoactive catalytic activity and direct interaction.

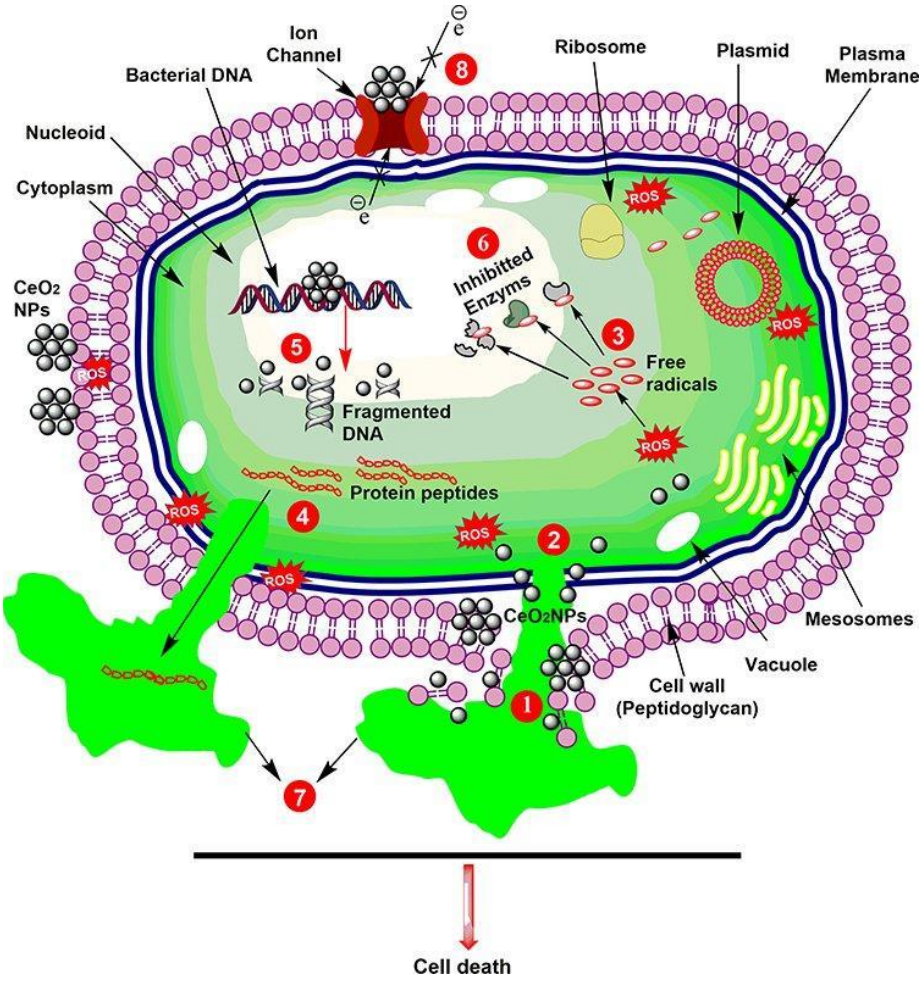

Fig. 1.8. Depiction of the general mechanism of action of CeO_2 nanoparticles on a bacterial cell and its components[118]

1.9.4. Boehmite as superhydrophobic hybrid materials

Superhydrophobicity can be imparted to a surface by chemically/physically modifying the hierarchical surface roughness and topography of low energy surfaces and/or coating the surface with a superhydrophobic component.[119] It is possible to accomplish this by modifying the surface geometry followed by a change in surface energy, or vice versa; the two steps can also be performed concurrently.[120] Superhydrophobic surfaces

have been successfully created on a variety of substrates including metal, paper, textile, wood, and various polymers, ceramics, and composites. Superhydrophobic surfaces must be extremely resistant to harsh environments and conditions.

Table 1.3. Applications of superhydrophobic inorganic- organic boehmite hybrids

Materials	Methods	Contact Angle	Application	Reference
AlOOH/APTES/Oleic acid/PAN	Sonochemical/ Dipcoating	152	Oil/Water Separation	123
AlOOH/Stearic acid	Hydrothermal	167.5	Metal corrosion protection	127
AlOOH/GPTMS/PFOTES	Sol-gel	150	Metal corrosion protection	128
AlOOH/FAS	Powder hydrolysis	155	NA	129
AlOOH/FAS	Sol-gel	150	Antireflective	130

Various superhydrophobic materials, such as TiO_2, cellulose, polymer membrane, silica, ZnO, zeolite, hydrogel, graphene oxide, Al_2O_3, boehmite, and others, have been developed to date for oil-water separation via appropriate surface energy as well as the construction of hierarchical rough surfaces.[121-123] In fact, many superhydrophobic inorganic surfaces have been successfully manufactured, with micro/nano hierarchical architectures typically used to create appropriate roughness. Boehmite is a good candidate material among them due to its non-toxicity, low cost, chemical inertness, high mechanical thermal stability, and easily controlled morphology. Until now, various superhydrophobic boehmite coatings have been fabricated on various substrates with varying hierarchical structures.[124-126] Zhang et al., for example, created a superhydrophobic boehmite membrane on austenitic stainless steels by immersing a boehmite gel film in boiling water (Contact angle (CA) 152°).[124] A simple two-phase thermal method was used to fabricate a superhydrophobic boehmite film from anodic

alumina oxide (AAO) surface with a copper catalyst, yielding a water CA of 152.8°.[125] In addition, Wang et al prepared a superhydrophobic γ- boehmite nanosheets film on a glass substrate by hydrothermal method and the water CA reached 160°±3°.[126] Based on the literature review, it is clear that boehmite is a viable candidate for a strong superhydrophobic material. Boehmite-based inorganic-organic hybrid superhydrophobic materials for oil-water separation, on the other hand, are rarely reported. **Table 1.3.** summarizes some of the literature on boehmite hybrids as superhydrophobic materials.

1.9.5. Electrochemical sensor

A chemical sensor is a device that converts chemical information into an analytically useful signal, ranging from the concentration of a specific sample component to total composition analysis.[131] Chemical sensors are typically made up of two basic components that are linked in series: a chemical (molecular) recognition system (receptor) and a physico-chemical transducer.[132] In the category of chemical sensing methods, electrochemical sensors are very popular. It has a quick response time, a high sensitivity, and in-situ real-time detection.[133] Cyclic voltammetry (CV) has received a lot of attention among voltammetry techniques because it can be used to understand electrode processes and redox mechanisms.[132]The principal stages in the operation of an electrochemical sensor are provided in the **Fig. 1.9.**

Electrochemical sensors are classified as enzyme-based or non-enzymatic. Because of their numerous advantages, enzyme-based sensors are becoming increasingly popular. The main disadvantages of enzymatic sensors are lack of chemical and heat stability (due to the intrinsic nature of enzymes), loss of activity (easily denatured during immobilization process), intolerance to extreme acidic and basic conditions, deactivation by toxic chemicals and humidity, expensive in terms of enzyme

cost, need for specific storage conditions, and time consuming protocols.[134] Non-enzymatic sensor research is becoming increasingly important in order to overcome these constraints.[135] The benefits of enzyme free sensors include: no special storage requirements, the ability to perform under ambient conditions, stability towards temperature, pH, humidity, and toxic chemicals, etc., simplicity, high sensitivity, unique selectivity, reproducibility, cost effectiveness, and so on.[134] Instead of enzymes, the atoms on the surface of modified electrodes act as electrocatalysts in non-enzymatic sensors. Pesticides are the main concern in research on electrochemical sensors to examine food adulteration. Medical diagnosis is another important application of chemical sensors.

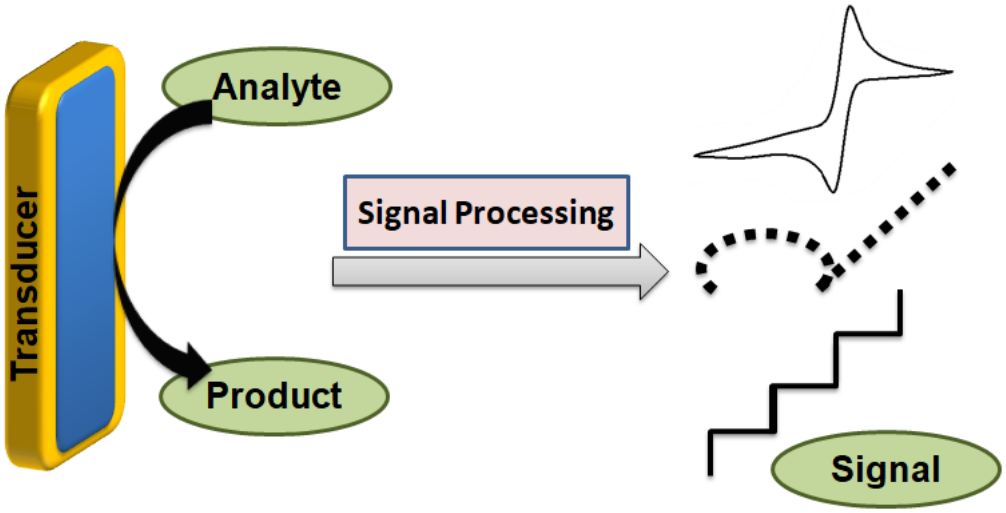

Fig.1.9. Schematic illustration of the working principle of an electrochemical sensor

Non-enzymatic dopamine detection is based on direct electro oxidation of dopamine on catalytic surfaces such as metal or metal oxides. Precious metals such as Pt, Au, and Pd have been used in the direct electro oxidation of dopamine. The risk of chloride poisoning has been observed in Pt and Au-based sensors. At low pH, Ni electrodes become unstable.[134] These precious metal-based sensors frequently exhibit slow kinetics, poor operational stability, a lack of selectivity, and a low antitoxic

ability.[136] Ions can pass through nanostructured substrates with nanopores because they have large surface affinity areas. Nanostructured substrates have been used for biosensing in a variety of applications due to their ability to integrate electrochemical impedance spectroscopy. Because of their established fabrication processes, nano-ordered structures, dramatically large surface areas, easy surface modifications, high surface reaction rate, and intensified output signals, nanoporous alumina have become a hot research area. [137] Nanoporous alumina has numerous applications, including DNA detection, lipid membrane-based biosensors, food borne pathogen biosensing, and virus and cancer cell detection.[137]Similarly, boehmite, an oxy hydroxide form of alumina with a higher surface area than its bulk compound, can provide a higher adsorption capacity, which can be very useful for improving analyte accumulation at the electrode surface in the case of modified electrode preparation. According to recent reports, boehmite modified system is a promising support material for electrochemical analyte detection.[138-140] However, there is no information on the use of a boehmite-based inorganic organic hybrid material as an electrochemical sensor.

1.9.6. Flame retardancy

To prevent or delay the spread of fire, flame retardants are frequently added to other materials. Flame retardant demand in the global industrial sector has surpassed two million tonnes per year. The residential building materials contribute significantly to this requirement. Given the annual increase in building-related energy consumption, the development of energy-saving green residential building materials, designs, and methods is of strategic importance to the world. As a result, it is necessary to reduce the possibility of accidents caused by fire and smoke generated during thermal and electrical shock.

Flame retardants are classified into four types: halogenated, metal hydroxides, phosphorus and nitrogen-based, and intumescent products. Although halogen-based flame retardants are very effective, they emit toxic smoke when burned, so they are outlawed in many countries. Phosphorus and nitrogen-based polymers are also effective, but they reduce the polymer's thermal and mechanical stability.[141, 142] Organic polymer aerogels, such as resorcinol-formaldehyde, are sometimes derived from expensive and toxic materials, whereas inorganic aerogels have poor mechanical properties.[143, 144] As a result, inorganic-biopolymer-based aerogels derived from low-cost precursors have received a lot of attention in recent years. Biopolymers such as cellulose, pectin, silk fibroin, chitin, chitosan, and others have been used to make inorganic organic hybrid aerogels for thermal insulation and fire retardant applications.[145, 146] Similarly, silica, clay, graphene, carbon-based materials, and alumina oxides and hydroxides are used to create inorganic organic hybrid aerogels.[144, 146]

Due to its demonstrated properties such as heat resistance, non-volatile, non-toxic, environmentally friendly, and inexpensive nature, inorganic boehmite is one of the most widely used inorganic flame retardant agent and reinforcing filler for plastics, adsorbent, precursor of catalysis, and ceramics. Boehmite has a layered structure that is similar to other layered structures such as montmorillonite, fluorohectorite, and hydrotalcite. It has the potential to build up surface layers during burning to act as a barrier to mass and heat transfer while also improving char forming properties.[147] **Table 1.4.** shows the boehmite hybrids used for flame retardant and thermal insulation applications. Chitosan (CS) is also a promising substitute for traditional flame retardants because it contains a high concentration of hydroxyl and amino groups, resulting in an aerogel with excellent charring and thermal insulation properties.[148] Furthermore, when exposed to a flame, CS can form a more tightly bound bond with

inorganic substrates such as boehmite, resulting in a compact char layer that protects the aerogel from burning. Furthermore, when compressed, biopolymer aerogels, such as CS aerogel, exhibit more plastically deformable and less brittle behaviour than pure inorganic aerogels, resulting in better compression performance.[148] Boehmite and chitosan are good candidates for making inorganic-organic hybrid flame retardant aerogels.

Table 1.4. Studies on boehmite hybrid system in fire retardant and thermal insulation application

Materials	Synthetic Methods	Properties	Reference
AlOOH/PC/ABS/PTFE	Dispersion-Coagulation	Flame retardancy	149
AlOOH/GPTMS/PET	Sol-Gel	Flame retardancy/ Textile coating	150
AlOOH/PUF	Dispersion	Flame retardancy/ Li-Fe battery	151
AlOOH/PVA/EPS	Dispersion/Dipcoating	Flame retardancy	152
AlOOH/PES	Meltcompounding	Thermal Insulation	153
AlOOH/Cellulose aerogel	Sol-Gel	Thermal Insulation	154

1.10. Scope of the Present Thesis

The remarkable properties of boehmite put forward endless possibilities for the design and synthesis of hybrid functional materials for advanced applications. In the area of boehmite based hybrid materials, the scientific research works are mostly published on functional coatings for automobile fields mainly scratch and corrosion resistant coatings. The demand for longer product life, higher quality, and efficiency have put new challenges on the synthesis and processing approaches of boehmite hybrid materials. Industrial production of technologically important hybrid materials demands low-cost, abundantly available natural raw materials with minimal environmental impact for the mass production. This includes effective utilization of the Natural Organics and replaces

toxic materials. Some major scientific gaps that can be identified in this area are outlined below:

- Lots of research is confined in the direction of preparation of boehmite with different morphology and shape. Boehmite based Inorganic-Organic hybrid materials other than the area of membranes for the treatment of a wide variety of environmental pollutants is not well documented.
- Boehmite based hybrid architectures as catalysts for the various organic reactions, sensors, and sorbents are not extensively studied by scientists and researchers.
- Cashew nut shell liquid (CNSL), an agro industrial waste widely recommended as corrosion inhibitors, is a promising natural resin for hybrid architectures. Utilization of CNSL for inorganic-organic hybrids is not widely reported.
- In particular no literature evidence on the studies related to hybrid design of boehmite with CNSL based natural organic resin.
- Electrochemical sensor applications of boehmite based inorganic-organic hybrid materials are very limited.

Systematic research can bridge the gap in the area of boehmite based hybrid materials. Based on the relevant information on the boehmite hybrids, the entire thesis work focuses on the synthesis of inorganic-organic hybrid materials from boehmite gels for functional applications.

1.11. Objectives and Outlook of the Present Work

The main objective of the thesis is ***"Design and Development of Boehmite [AlOOH] based Hybrid Nanomaterials for Functional Applications".*** The distinctive objectives are as follows:

- **Develop Boehmite Gel Hybrids and study the material as Adsorbent, Photocatalyst, and Antimicrobial Agent**

  Boehmite, Polyethyleneimine[PEI], and nano ceria will be exploited for the synthesis of hybrid photocatalytic sorbent for the treatment of highly concentrated lignin (considered as pollutant in pulp and paper industry and biofuel industry) polluted water. Poly ethylene imine is selected due to its inherent adsorption affinity towards anionic pollutants and their mixtures. Nano ceria is chosen because of its photoactivity and antibacterial property which will be an additional advantage to the Boehmite/PEI hybrid. CeO_2@Boehmite/PEI hybrid system will be explored for the adsorption and photodegradation of lignin and also antimicrobial agent against Gram positive and Gram negative bacteria.

- **Design a New CNSL Resin-Boehmite Gel Hybrid and develop Electrochemical Biosensor for Neurotransmitter Dopamine**

  Next milestone is to use boehmite as an electrode for electrochemical sensors. Here, the major challenging question is how a non-conducting boehmite acts as an electrode. For that a hybrid material will be synthesized out of boehmite and cashew nut shell liquid (CNSL). Hydroxyl rich boehmite and CNSL will attract the dopamine and facilitate the electron transfer mechanism. This hybrid system will be further explored for the electrochemical detection of dopamine.

- **Fabricate Super hydrophobic Boehmite Gel hybrid and Study the material for oil-Water Separation towards Crude oil and other Organic Solvents**

  To achieve the third objective of the thesis work, boehmite is hybridised with CNSL and then with paraffin wax to obtain super hydrophobic coating formulation. Then the super hydrophobic hybrid suspension will coat on the textile and will be analyzed for the oil water separation of light oil and heavy oil including crude oil.Durability of the super

hydrophobic substrate is the major concern of oil-water separation process. This challenge will also be addressed in this work.

- **Processing of Boehmite Hybrid Aerogels and Study the Thermal Insulation and Flame Retardant properties**

  Boehmite has the excellent fire retardant property and is extensively used as a promising material that could endow polymer materials with excellent flame retardancy. As a final attempt boehmite will be used for the synthesis of hybrid aerogels for thermal insulation and fire retardant application. Biopolymer chitosan will be explored for the fabrication of hybrid aerogel and freeze drying technique will be utilized. Chitosan is selected because; it is a promising substitute for traditional flame retardant because it contains plenty of hydroxyl groups and amino groups, which endows aerogel with excellent charring capability and thermal insulation.

All the above objectives are in fact very much new to the field of Boehmite based functional hybrids. The scientific contributions made in this PhD work is an additional exploratory research to bring out the beneficial properties of boehmite based hybrids other than the well-established thermo-mechanical coating applications.

1.12. References

1. Mann, S.; Biomineralization: Principles and concepts in Bioinorganic materials chemistry *Oxford University press, **2001**.*

2. Sarikaya, M.; Furlong, C.E.; Staley, J.T. Nanodesigning and properties of biological composites, *Am. Soc. Mech. Eng. **1994**, 28, 47-48.*

3. Tampieri, A.; Sandri, M.; Landi, E.; Pressato, D.; Francioli, S.;Quarto, R.; Martin, I. Design of graded bio-mimetic osteochondral composite scaffolds*", Biomater. **2008,**29(26),3539-3546.*

4. Rogers, M.; Small, A.; Amos, T.; Johnson, A.; Sterner, L. A new flame retardant additive for polymeric composites. *InternationalSAMPE Symposium and Exhibition Proceedings **2006**,51- 7.*

5. Zhang, Y.; Vassilopoulos, A.P.; Keller, T. Stiffness degradation and fatigue life prediction of adhesively-bonded joints for fiber reinforced polymer composites*. Int. J. Fatigue **2008**, 30(10-11), 1813-1820.*

6. Meric, G.; Ruyter, I.E. Bond strength between a silica glass fiber-reinforced composite and artificial polymer teeth*. ActaOdontol. Scand."**2007**-65(5)-306-312.*

7. Hufenbach, W.; Weimann, C.; Richter, H.; Langkamp, A.;Behnisch, T. Development of textile reinforced CMC lightweight modules for high performance automotive damping systems*. Keram. Z. **2007**-59(5),342-344.*

8. Costacurta, S.; Malfatti, L.; Falcaro, P.; Innocenzi, P. Photocurable silica hybrid organic-inorganic films for photonic applications*. J.Sol-Gel Sci. Technol. **2007**,44(1), 59-64.*

9. Kim, H.K.; Kang, S.J.; Choi, S.K.; Min, Y.H.; Yoon, C.S. Highly efficient organic/inorganic hybrid nonlinear optics materials via sol-gel process, synthesis, optical properties, and photo bleaching for channel waveguides. *Chem. Mater. **1999**-11(3)-779-788.*

10. Singh, V.; Pandey, S.; Singh, S.K.; Sanghi, R. Sol-gel polycondensation of tetraethoxysilane in ethanol in presence of vinyl modified guar gum: synthesis of novel nanocomposite adsorbent materials, *J. Sol-Gel Sci. Technol. **2008**, 47, 58-67.*

11. Yang, H.; Zhu, Y. Glucose biosensor based on nano-SiO2 and unprotected Pt nanoclusters. *Biosens. Bioelectron. **2007**-22(12),2989-2993.*

12. Fang, Z.; Wang, S.; Zhao, L.; Dong, B.; Xu, Z.; Ren, J.; Yang,Q. Novel organic-inorganic hybrid fluorescent material as a selective chemosensor and adsorbent for Pb2+ ion. *Mater. Lett.* 2008, 62(10-11), 1514-1517.

13. Nam, S.E.; Kim, S.O.; Kang, Y.; Lee, J.W.; Lee, K.H. Preparation of Nafion/sulfonated poly(phenyl silsesquioxane)nanocomposite as high temperature proton exchange membranes . *J. Membr. Sci.* 2008, 322(2), 466-474.

14. (Source: SciFinder Scholar: https://scifinder-n.cas.org).

15. Owens G. J.; Singh, R. K.; Foroutan, F.; Alqaysi, M.; Han, C.M.; Mahapatra, C.; Kim, H.W.; and Knowles J. C. Sol-Gel based materials for biomedical applications. *Prog. Mater. Sci.**2016*** 77,1.

16. McCarthy J. R.; and Weissleder R. Multifunctional magnetic nanoparticles for targeted imaging and therapy. *Adv. Drug Deliv. Rev.,**2008 60**, 1241.*

17. Groenewolt M.; Highly Scratch resistant coating for automotive applications. *Progr. Org. Coat., **2008**, **61**, 106.*

18. Amerio, E.; Fabbri, P.; Malucelli, G.; Messori, M.;Sangermano, M.; and Taurino R. Scratch resistance of nano-silica reinforced acrylic coatings. *Prog. Org. Coat.*, **2008,** 62, 129.

19. Wu, L. Y. L.; Chwa, E.; Chen, Z.; and Zeng, X. T. A study towards improving mechanical properties of sol–gel coatings for polycarbonate. *Thin Solid Films, **2008**, 516, 1056*.

20. Nagayama S. and Ochiai,B. Zinc-bis(allydithiocarbamate) for highly refractive and flexible materials via the tool ene reaction *Polym. J.* ***2016*** *48, 1059.*

21. B. Ochiai and H. Konta, One-Pot Synthesis of Organic-Sulfur-Zinc Hybrid Materials via Polycondensation of a Zinc Salt and Thiols Generated in Situ from Cyclic Dithiocarbonates. *Molecules,****2015*** *20, 15049.*

22. Ochiai B. and Konta, H. Organic sulfur-zinc-hybrid nano particle for optical application synthesized via polycondensation of trithiol and Zn(OAc2)*Nanoscale. Res. Lett.,****2013***, ***8***, 373. Matteis, F. D.; Prosposito, P.; Sarcinelli, F.;Casalboni, M.; Pizzoferrato, R.A.; Furlani,M. V.; Russo, A.; Vannucci, and Varasi M. Organic-Inorganic Hybrid Functional Materials: AnIntegrated Platform for Applied Technologies. *J. Non-Cryst. Solids,* ***1999****, 245, 15.*

23. Ng, E. P. and Mintova, S. Nanoporous materials with enhanced hydrophobicity and high water sorption capacity. *Microporous Mesoporous Mater* ***2008,*** *114, 1.*

24. Xu L.; and Lee, H. K. Preparation, characterization and analytical application of a hybrid organic-inorganic silica based monolith*"Journal of Chromatography A,* ***2008****-1195, 78.*

25. Zhu, H.T.; Du, J.; Lu, Y.; Su, F.; & Li, Y.G. Immobilization of enzymes on an organic-inorganic hybrid Network consisting of Dawson-type polyoxotungstate and zinc(II)-biimidazole complex moiety. *New Journal of Chemistry* ***2019****, 43, 146-153.*

26. Meng, L., Watson II, B. W., & Qin, Y. Hybrid Conjugated Polymer/Magnetic Nanoparticle Composite Nanofibers through Cooperative Non-Covalent Interactions. Nanoscale Advances*. Department of Chemistry & Chemical Biology, University of New Mexico,* ***2020*** *MSC03 2060*

27. Judeinstein, P. and Sanchez, C. Hybrid organic–inorganic materials: a land of multidisciplinarity *J. Mater. Chem.* ***1996-6****,-511*

28. Sanchez, C.; Soler-Illia, G. J. A. A.;Ribot, F. and Grosso, D. Design of functional nano-structured materials through the use of controlled hybrid organic–inorganic interfaces. *Comptes Rendus Chimie* ***2003****, 6, 1131*

29. Sanchez, C.; Soler-Illia, G. J. A. A.;Ribot, F.; Lalot, T.; Mayer, C. R and Cabuil, V. Designed Hybrid Organic–Inorganic Nanocomposites from Functional Nanobuilding Blocks**.***Chem. Mater.* ***2001****-13, 3061.*

30. Soler-Illia, G. J. A. A.; Sanchez, C.; Lebeau, B. and Patarin, J. Chemical Strategies To Design Textured Materials: from Microporous and Mesoporous Oxides to Nanonetworks and Hierarchical Structures*. Chem. Rev.*, ***2002***,102,4093.

31. Ozin, G. A. Periodic Mesoporous Organosilicas (PMOs): Nanostructured Organic-Inorganic Hybrid Materials*. Chem. Commun.,* ***2000****-419.*

32. D. J. Tranchemontagne, J. L. Mendoza-Cortes, M. O'Keeffe, and O. M. Yaghi, Secondary building units, nets and bonding in the chemistry of metal–organic frameworks. *Chem. Soc. Rev.*, ***2009***, *38,* 1257.

33. Warren, S. C.; Messina, L. C.; Slaughter, L. S.; Kamperman, M.; Zhou, Q.; Gruner, S. M.; DiSalvo, F. J.; and Wiesner, U. Ordered Mesoporous Materials from *Science, **2008**-320, 1748.*

34. Nicole, L.; Rozes, L.; and Sanchez, C. Integrative Approaches to Hybrid Multifunctional Materials: From Multidisciplinary Research to Applied Technologies. *Adv. Mater., **2010**-2, 3208*

35. Kresge, C. T.; Leonowicz, M. E.; Roth, W. J.; Vartuli, J. C.; and Beck, J. S. Ordered mesoporous molecular sieves synthesized by a liquid-crystal template mechanism. *Nature,**1992**-359, 710.*

36. Tiwari, I.; Mahanwar, P.A. Polyacrylate/silica hybrid materials: A step towards multifunctional properties. *J. Dispers. Sci. Technol. **2019**, 40, 925–957.*

37. Coan, T.; Barroso, G.S.; Machado, R.A.F.; de Souza, F.S.; Spinelli, A.; Mothz, G. A novel organic-inorganic PMMA/polysilazane hybrid polymer for corrosion protection. *Prog. Org. Coat. **2015**, 89, 220–230.*

38. Bergna.; Horacio E. Colloid Chemistry of silica: An Overview in Bergna, Horacio E.The Colloid Chemistry of Silica *Advances in Chemistry Series, American Chemical Society, Washington DC **1994**-40-41,234.*

39. Ebelmen. Untersuchungen uber die Verbindungen der Borsäure and Kieselsaure mit Aether. *Justus Liebigs Annalen der Chemie **1846**, 57, 319.*

40. Graham T. On the properties of silicic acid and other analogous colloidal substances. *Journal of the Chemical Society **1864**,17, 318.*

41. Patrick. W.A Silica Gel and process of making the same. *1919, US patents: Patent No.1297724,.*

42. Brinker C.J; Scherer G.W. Sol-Gel Science: The physics and chemistry of sol-gel processing. *Academic press: London, **1990.***

43. Prakash S.S; Brinker C.J;Hurd A.J; Rao S.M. Silica Aerogel Films Prepared at ambient pressure by using Surface Derivatization to Induce Reversible drying Shrinkage. *Nature **1995**-374, 439*

44. Pierre A.C. Introduction to Sol-Gel Processing. *Kluwer: Boston, ISBN : 1988,978-0-7923-8121.*

45. Schmidt H.K; Geiter E; Mennig M;Krug H;Becker C; Winkler R.P. The sol-gel process for nano-technologies: New nanocomposites with interesting optical and mechanical properties. *Journal of Sol-gel Science and Technology **1988** 13 397.*

46. Wang D; Bierwagen G.R, Sol-Gel coatings on metals for corrosion protection. *Progress in Organic Coatings* ***2009****-64-327.*

47. Shaw D.J, Introduction to Colloid and surface Chemistry. *Butterworth-Heinemann: Oxford,* ***1992****.*

48. Zelinski B.J.J; Uhlmann, D.R. Gel Technology in ceramics *J.Phys.Chem.Solids* ***1984****-45-1069.*

49. Livage J; Sanchez C. Sol-Gel chemistry *Journal of Non-Crystalline solids* ***1992****-11-145.*

50. Mukerjee S.P, Sol-gel processes in glass science and technology *Journal of Non-Crystalline solids* ***1980-****42-477.*

51. Saka M; Ueda R, Formation of metallic nanowires by utilizing eletro migration. *Journal of Materials Research* ***2005****,20,2712.*

52. Ulku S; Balkose D; Balatacboglu H, Effect of Preparation pH on pore Structure of Silica-Gels' *Colloid and Polymer Science* ***1993****,271,709*.

53. Scherer G.W. Aging and drying of gels. *Journal of Non-Crystalline Solids* ***1988****,77,100.*

54. Scherer G.W; Smith D.M, Cavitation during drying of a gel. *Journal of Non-Crystalline Solids* ***1995****,189,197.*

55. Zarzycki J;Prassas M;Phalippou J, Synthesis of glasses from gels: the problem of monolithic gels. *Journal of Materials Science* ***1982****,17,3371.*

56. Chan J.B; Jonas J. Effect of various amide additives on the tetramethoxysilane sol-gel process. *Journal of Non-Crystalline Solids* ***1990****,79,126.*

57. Chen H; Rucknstein E, A new type of hydrous titanium oxide adsorbent. *Journal of Colloid and Interface Science* ***1991****,145,581.*

58. Roger C; Hampden-Smith M.J. Formation of porous metal oxides via sol-gel type hydrolysis of metal alkoxide complexes modified with organic templates. *Journal of Materials Chemistry* ***1992****,2,1111.*

59. Pierre A.C; Pajonk G.M, Chemistry of aerogels and their applications. *Chemical Reviews* ***2002****,102,4243.*

60. Kistler S.S, Coherent Expanded Aerogels and Jellies. *Nature* ***1931****,127,741.*

61. Baumann T.F; Gash A.E; Chinn S.C; Sawvel A.M; Maxwell R.S; Satcher J.H. Synthesis of High-Surface-Area Alumina Aerogels without the use of Alkoxide Precursors. *Chemistry of Materials* ***2005****,17,395.*

62. Husing N; Schubert U, Aerogels airy materials: Chemistry, structure, and properties *Angewandte Chemie-International Edition* ***1988****,37,23.*

63. Chervin C.N; Clapsaddle B.J; Chiu H.W; Gash A.E; Satcher J.H; Kauzlarich S.M, Aerogel synthesis of yttria-stabilized zirconia by a Non-Alkoxide sol-gel route. *Chemistry of Materials* ***2005****,17,3345.*

64. Bag S; Trikalitis P.N; Chupas P.J; Armates G.S; Kanatzidis M.G. Porous Semiconducting Gels and Aerogels from Chalcogenide Clusters. *Science **2007**,317,490.*

65. Pekala R.W. Organic aerogels from the polycondensation of resorcinol with formaldehyde. *Journal of Material Science **1989**,24,3221.*

66. Tan C; Fung B.M; Newman J.K; Vu C. Organic aerogels with very high impact strength. *Advanced materials **2001**,13,644.*

67. Zaho Y; Hu.C ; Hu. Y; Cheng H; Shi G; Qu.L. A versatile ultralight, nitrogen doped graphene framework. *Angewandte Chemie **2012**,124,11533.*

68. Husing N; Schubert U, Aerogels airy materials: Chemistry, structure, and properties. *Angewandte Chemie-International Edition **1988**,37,23.*

69. Bangi U.K.H; Rao A.V; Rao A.P, A new route of preparation of sodium silicate-based hydrophobic silica aerogels via ambient-pressure drying. *Science and Technology of Advanced Materials **2008**.*

70. Rao A.V; Hedge N.D; Hirashima H. Absorption and desorption of organic liquids in elastic superhydrophobic silica aerogels. *Journal of Colloid and interface science **2007**,305,124.*

71. Hedge N.D; Hirashima H; Rao A.V, Two step sol-gel processing of TEOS based hydrophobic silica aerogels using trimethylethoxysilane as a co-precursor. *Journal of porous materials **2007**,14,165.*

72. Rao A.V; Kalesh R.R. Comparative studies of the physical and hydrophobic properties of TEOS based silica aerogels using different co-precursors. *Science and Technology of Advanced Materials **2003**,4,509.*

73. Rao A.V; Pajonk G.M. Effect of methyltrimethoxysilane as co-precursor on the optical properties of silica aerogels. *Journal of Non-Crystalline Solids **2001**,285,202.*

74. Rao A.V; G.M Pajonk; D. Haranath. Synthesis of hydrophobic aerogels for transparent window insulation applications. *Materials science and technology **2001**,17,343.*

75. Wagh P.B; Begag R; Pajonk G.M; Rao A.V; Haranath D, Comparison of some physical properties of silica aerogel monoliths synthesized by different precursors. *Material Chemistry and Physics **1999**,57,214.*

76. Wagh P.B; Rao A.V; Haranath D, Influence of molar ratios of precursor, solvent and water on physical properties of citric acid catalyzed TEOS silica aerogels. *Materials Chemistry and Physics **1998**,53,41.*

77. Zhang, Z.; Pinnavaia, T. J. J. Mesostructured γ-Al_2O_3 with a Lathlike Framework Morphology. *Am. Chem. Soc. **2002**, 124,12294*.

78. Bokhimi, X.; Toledo Antonio, J. A.; Guzman Castillo, M.L.; Hernandez Beltran, F. J. Relationship between Crystallite Size and Bond Lengths in Boehmite. *Solid State Chem. **2001**, 159,32*.

79. Wilson, S. J. J. The dehydration of boehmite, γ-AlOOH, to γ-Al_2O_3" *Solid State Chem.* ***1979****, 30, 247*.

80. Candela, L.; Perlmutter D. D; Kinetics of boehmite formation by thermal decomposition of gibbsite. *Ind. Eng. Chem. Res.* ***1992****,31, 694*.

81. Mishra, D.; Anand, S.; Panda, R. K.; Das, R. P; Hydrothermal preparation and characterization of boehmites. *Mater. Lett.****2000****, 42, 38*.

82. Nguefack, M.; Popa, A. F.; Rossignol, S.; Kappenstein, C. Preparation of alumina through a sol–gel process. Synthesis, characterization, thermal evolution and model of intermediate boehmite. *Phys. Chem. Chem. Phys.* ***2003****, 5, 4279*.

83. Fankhanel, J.; Silbernagl, D.; Ghasem Zadeh Khorasani, M.;Daum, B.; Kempe, A.; Sturm, H.; Rolfes, R. J; Mechanical Properties of Boehmite Evaluated by Atomic Force Microscopy Experiments and Molecular Dynamic Finite Element Simulations. *Nanomater.****2016****-13.*

84. Br€uhne, S.; Gottlieb, S.; Assmus, W.; Alig, E.; Schmidt, M.U. Atomic Structure Analysis of Nanocrystalline Boehmite AlO(OH). *Cryst. Growth Des.* ***2008****, 8, 489*.

85. Buining, P. A.; Padma Manoharan, C.; Philipse, A. P.; Lekkerkerker, H. N. W. Preparation of (non-)aqueous dispersions of colloidal boehmite needles. *Chem. Eng. Sci.* ***1993****, 48, 411.*

86. Kuang, D.; Fang, Y.; Liu, H.; Frommen, C.; Fenske, D; Fabrication of boehmite AlOOH and γ-Al_2O_3 nanotubes *via* a soft solution route. *J. Material Chem.* ***2003****, 13, 660.*

87. Yu, Z.Q.; Wang, C.X.; Gu, X.T.; Li,C; Photoluminescent properties of boehmite whisker prepared by sol-gel process. *J. Lumin.* ***2004****,106, 153.*

88. Liu, S. L.; Chen, C. Y.; Liu, Q. P.; Zhuo, Y. W.; Yuan, D.; Dai, Z. H.; Bao, Vertically aligned γ-AlOOH nanosheets on Al foils as flexible and reusable substrates for NH_3 adsorption. *J. C. RSC Adv.* ***2015****, 5, 71728*.

89. Tang, Z.; Liang, J. L.; Li, X. H.; Li, J. F.; Guo, H. L.; Liu, Y. Q.; Liu, C. G. Synthesis of flower-like Boehmite (γ-AlOOH) via a one-step ionic liquid-assisted hydrothermal route. *J. Solid State Chem.* ***2013****, 202, 305.*

90. Song, X. L.; Yang, P.; Jia, C. C.; Chen, L.; Matras-Postolek. Monodispersed hierarchical γ-AlOOH/$Fe(OH)_3$ micro/nanoflowers for efficient removal of heavy metal ions from water.*K. RSC Adv.* ***2015****, 5, 33155*.

91. Yang, F.; Wang, Q.; Yan, J.; Fang, J.; Zhao, J.; Shen, W. Preparation of High Pore Volume Pseudoboehmite Doped with Transition Metal Ions through Direct Precipitation Method. *Ind. Eng. Chem. Res.* ***2012****, 51, 15386.*

92. Karger-Kocsis, J.; Kmetty, _A.; Lendvai, L.; Drakopoulos, S.;Barany, Water-Assisted Production of Thermoplastic Nanocomposites. *T. Materials* ***2015****, 8, 72*.

93. Seok, S. I., Kim, J. H., Choi, K. H., & Hwang, Y. Y. Preparation of corrosion protective coatings on galvanized iron from aqueous inorganic–organic hybrid sols by sol–gel method. *Surface and Coatings Technology,* **2006**, *20(11), 3468–3472.*

94. Hota, G.; Kumar, B.R.; Ng, W.J; *et al.* Fabrication and characterization of a boehmite nanoparticle impregnated electrospun fiber membrane for removal of metal ions. *J Mater Sci **2008**, 43,212–217*

95. Seader, J. D.; Henley, E. J.; Roper, D. K. Separation Process Principles Chemical and Biochemical Operations. *Third.; John Wiley & Sons, **2011**.*

96. Dabrowski, A. Adsorption - from Theory to Practice. *Adv. Colloid Interface Sci.* **2001**, *93*, 135–224.

97. Ge, J.R.; Deng, K.J.; Cai, W.Q.; Yu, J.G.; Liu, X.Q.;Zhou, J.B. Effect of structure directing agents on facile hydrothermal preparation of hierarchical γ-Al2O3 and their adsorption performance toward Cr(VI) and CO2. *J. Colloid Interf. Sci. **2013,**401,34- 39*.

98. Kumar, E.; Bhatnagar, A.; Hogland, W.; Marques, M.; Sillanpää, M. Interaction of anionic pollutants with Al-based adsorbents in aqueous media-a review. *Chem. Eng. J. **2014** ,241,443-456.*

99. Dubey, S. P., Dwivedi, A. D., Sillanpää, M., Lee, H., Kwon, Y.-N., & Lee, C. Adsorption of As(V) by boehmite and alumina of different morphologies prepared under hydrothermal conditions. *Chemosphere, **2017**, 169, 99–106.*

100. Luo, L.; Cai, W.; Zhou, J.; & Li, Y. Facile synthesis of boehmite/PVA composite membrane with enhanced adsorption performance towards Cr(VI). *Journal of Hazardous Materials, **2016**, 318, 452–459.*

101. Rajamani, M.; & Rajendrakumar, K. Chitosan-boehmite desiccant composite as a promising adsorbent towards heavy metal removal. *Journal of Environmental Management, **2019**,244, 257–264.*

102. Rashid J.; Barakat M. A.; Salah N.; Habib S. S.; "Ag/ZnO nanoparticles thin films as visible light photocatalyst. *RSC Advances, **2014**, 4, 56892-56899.*

103. Sharma, D.; Sastsangi, V.R.; Shrivastav, R.; Waghmare, U.V.; Dass, S. Understanding the photoelectrochemical properties of nanostructured CeO2 /CuO2 heterojunction photoanode for efficient photoelectrochemical water splitting. *Int. J. Hydrog. Energy **2016**, 41, 18339–18350*.

104. Khan,M.E.; Khan,M.M.; Cho,M.H. Ce3+-ion, surface oxygen vacancy, and visible light-induced photocatalytic dye degradation and photocapacitive performance of CeO2 -graphene nanostructures. *Sci. Rep. **2017**, 7, 5928.*

105. Wang, J.; Han, A.; Jaenicke, S.; Chuah, G.-K. Advances in sorbents and photocatalytic materials for water remediation. In New and Future Developments in Catalysis—Catalysis

for Remediation and Environmental Concerns; *Suib, S.L. Ed; Elsevier: Amsterdam, The Netherlands,* ***2013****-127–153.*

106. Zheng, Y.; Liu, J.; Cheng, B.; You,W.; Ho,W.; Tang, H. "Hierarchical porous Al2O3ZnO core-shell microfibers with excellent adsorption anity for Congo red molecule." *Appl. Surf. Sci.* ***2019****, 473, 251–260.*

107. Larimi, A.; Khorasheh, F. Renewable hydrogen production by ethylene glycol steam reforming over Al2O3 supported Ni-Pt bimetallic nano-catalysts. *Renew. Energy* ***2018****, 128, 188–199.*

108. Shi, D.; Wang, H.; Kovarik, L.; Gao, F.; Wan, C.; Hu, J.Z.; Wang, Y. WOx supported on -Al2O3 with di_erentmorphologies as model catalysts for alkanol dehydration. *J. Catal.* ***2018****, 363, 1–8.*

109. Sun, J.; Wang, Y.; Zou, H.; Guo, X.; Wang, Z. Ni catalysts supported on nanosheet and nanoplate -Al2O3 for carbon dioxide methanation. *J. Energy Chem.* ***2019****, 29, 3–7.*

110. Carolina V.; Waiman. A; , Jose Natera B; Walter, A.; Massad,B.; Graciela, P.; Zanini, A. Novel hybrid materials based on alginate-boehmite-riboflavin for photogeneration of reactive oxygen species in aqueous media. Potential environmental implications. *Dyes and Pigments,****2020,*** *177, 108281*

111. Mendoza-Damián, G.; Tzompantzi, F.; Pérez-Hernández, R.; Gómez, R.; & Hernández-Gordillo. Photocatalytic properties of boehmite–SnO 2 composites for the degradation of phenol. *Catalysis Today****,2016****-266, 82–89.*

112. Zeng X.; Wang G.; Liu Y.; Zhang X.; Graphene-based antimicrobial nanomaterials: rational design and applications for water disinfection and microbial control. *Environmental Science: Nano,* ***2017****, 4, 2248-2266.*

113. Gao N.; Chen Y.; Jiang J.; AgFe2O3-GO Nanocomposites Prepared by a Phase Transfer Method with Long-Term Antibacterial Property. *ACS Applied Materials and Interfaces,* ***2013****, 5, 11307-11314.*

114. Raghupathi K. R.; Koodali R. T.; Manna A. C.; Size-Dependent Bacterial Growth Inhibition and Mechanism of Antibacterial Activity of Zinc Oxide Nanoparticles *Langmuir,* ***2011****, 27, 4020-4028.*

115. Liu J.; Rojas-Andrade M. D; Chata G.; Peng Y.; Roseman G.; Lu J. E.; Millhauser G. L.; Saltikov C.; Chen S. Photo-enhanced antibacterial activity of ZnO/graphene quantum dot nanocomposites *Nanoscale,* ***2018****,,10****,*** *158-166 .*

116. Sharma, G.; Prema, D.; Venkata Prasanna, K. S.; Prakash, J.; Sahabuddin, S.; & Devanan; Venkatasubbu, G. Photo induced antibacterial activity of CeO2/GO against wound pathogens. *Arabian Journal of Chemistry* ***2020.***

117. Reddy Yadav, L. S., Lingaraju, K., Daruka Prasad, B., Kavitha, C., Banuprakash, G., & Nagaraju, G. "Synthesis of CeO2 nanoparticles: Photocatalytic and antibacterial activities." *The European Physical Journal Plus, **2017**,132-5.*

118. Kumar K.M.; Mahendhiran M.; Diaz M.C.; et al. Green synthesis of Ce3+ rich CeO2 nanoparticles and its antimicrobialstudies." *MaterLett. **2018**,214,15–19./J.Matlet.**2017**,11-097*

119. Ma M. and Hill R. M. Superhydrophobic Surfaces. *Curr. Opin. Colloid Interface Sci., **2006**,11 193–202.*

120. Erbil H. Y.; Demirel,A. L.; Avci, Y. and Mert, O. Transformation of a Simple Plastic into Superhydrophobic Surface. *Science, **2003**,299,1377–1380.*

121. Yong Liu, Meng Xia, Lili Wu, Shenxin Pan, Yuhong Zhang, Ben Qiao He, and Peixin. Physically Cross-Linked Double-Network Hydrogel for High-Performance Oil–Water Separation Mesh. *Industrial & Engineering Chemistry Research **2019** 58 (47), 21649-21658*

122. Latthe, S. S.; Sutar, R.; Shinde, T.; Pawar, S.; Khot, T.; Bhosale, A.; Liu, S. Superhydrophobic Leaf Mesh Decorated with SiO2 Nanoparticle–Polystyrene Nanocomposite for Oil–Water Separation. *ACS Appl. Nano Mater. **2019,**22-799–805.*

123. Zhang, M.;Wu, Z.; Meng, F.; & Lin, H. . Facile preparation of grass-like hierarchical structured γ-AlOOH coated stainless steel mesh with superhydrophobic and superoleophilic for highly efficient oil-water separation. *Separation and Purification Technology **2019**,212,347-354.*

124. Zhang, X.; Honkanen, M.; Järn, M;, Peltonen, J.; Pore, V.; Levänen, E.; & Mäntylä, T. Thermal stability of the structural features in the superhydrophobic boehmite films on austenitic stainless steels. *Applied Surface Science, **2008**-254(16), 5129–5133.*

125. Tang, K.; Yu, J.; Zhao, Y.; Liu, Y.; Wang, X.; & Xu, R. Fabrication of super-hydrophobic and super-oleophilic boehmite membranes from anodic alumina oxide film via a two-phase thermal approach. *Journal of Materials Chemistry,**2006**-18*

126. Wang, Z.; Tian, Y.; Fan, H.; Gong, J.; Yang, S.; Ma, J.; & Xu, J. Facile seed-assisted hydrothermal fabrication of γ-AlOOH nanoflake films with superhydrophobicity. *New Journal of Chemistry, **2014**-38(3)-1321.*

127. Milošev I;Bakarič T; Zanna S; Seyeux A; Rodič P; Poberžnik M; Marcus P; Electrochemical, Surface-Analytical, and Computational DFT Study of Alkaline Etched Aluminum Modified by Carboxylic Acids for Corrosion Protection and Hydrophobicity. *Journal of The Electrochemical Society, **2019**, 166(11), C3131–C3146.*

128. Kesmez, Ömer. Hydrophobic, organic–inorganic hybrid sol–gel coatings containing boehmite nanoparticles for metal corrosion protection. *Chemical Papers.* **2019**,*74. 10.1007/s11696-019-00931-6.*

129. Kocjan, A.; Dakskobler, A.; & Kosmac, T. Superhydrophobic Nanostructured Boehmite Coatings Prepared by AlN Powder Hydrolysis.*International Journal of Applied Ceramic Technology, **2010**-8(4), 848–853.*

130. Zhang, X.; & Levänen, E.; & Mäntylä, Tapio. Superhydrophobic Antireflective Boehmite Film Made by Sol-Gel Technique on Glass. *Department of Materials Science, Tampere University of Technology.*

131. Thevenot D. R.; Toth K.; Durst R.; Wilson G. S. Electrochemical biosensors: recommended definitions and classification *Pure Applied Chemistry, **1999**, 71, 2333-2348.*

132. Li Y.; Xu J;, Sun C.; Chemical Sensors and Biosensors for the Detection of Melamine. *RSC Advances, **2015**, 5, 1125-1147.*

133. Cai R.;Rao W.; Zhang Z.; Longa F.; Yina Y. An imprinted electrochemical sensor for bisphenol A determination based on electrodeposition of a graphene and Ag nanoparticle modified carbon electrode. *Analytical Methods, **2014**, 6, 1590-1597.*

134. Zhu H.; Li L.; Zhou W.; Shaode Z.; Chen X.; Advances in non-enzymatic glucose sensors based on metal oxides. *Journal Materials Chemistry B, **2016**, 4, 7333-7349.*

135. Zhao Y.; Fan L.; Hong B.; Ren J.; Zhanga M.; Queb Q.; Jib J. Nonenzymatic detection of glucose using three-dimensional PtNinanoclusters electrodeposited on the multiwalled carbon nanotubes. *Sensors and Actuators B, **2016**, 231, 800-810.*

136. Dhara K.; Stanley J.; Ramachandran T.; Nair B. G.; Satheesh Babu T. G. Cupric Oxide Modified Screen Printed Electrode for the Nonenzymatic Glucose Sensing. *Journal of Nanoscience and Nanotechnology, **2016**, 16, 8772-8778.*

137. Li J.; Sun W.; Wang X.; Duan H.; Wang Y.; Sun Y.; Ding C.; Luo C Ultra-sensitive film sensor based on Al2O3–Au nanoparticles supported on PDDA-functionalized graphene for the determination of acetaminophen. *Anal Bioanal Chem **2016**-408-5567–5576.*

138. Ghalkhani, M.; & Salehi, M. Electrochemical sensor based on multi-walled carbon nanotubes–boehmite nanoparticle composite modified electrode. *Journal of Materials Science, **2017**,52(20), 12390–12400.*

139. Gholivand, M. B.; Malekzadeh, G.; & Derakhshan, A. A. Boehmite nanoparticle modified carbon paste electrode for determination of piroxicam. *Sensors and Actuators B: Chemical, **2014**,201-378–386.*

140. Zhao, C.; Zhang, H.; & Zheng, J. A non-enzymatic electrochemical hydrogen peroxide sensor based on Ag decorated boehmite nanotubes/reduced graphene oxide nanocomposites. *Journal of Electroanalytical Chemistry, **2017**-784-(55–61)*

141. Camino, G.; Costa, L; Performance and mechanisms of fire retardants in polymers A Review. *Polym. Degrad. Stabil.**1988**,20 (3), 271-294.*

142. Wang, X.;Two-Dimensional Inorganic Nanomaterials: A Solution to Flame Retardant Polymers. *Nano Adv.**2016,**1 (1), 1-16.*

143. Yu, Z.L.; Yang, N.; Apostolopoulou-Kalkavoura, V.; Qin, B.; Ma, Z.Y.; Xing, W.Y.; Qiao, C.; Bergström, L.; Antonietti, M.; Yu, S.H. Fire-retardant and thermally insulating phenolic-silica aerogels. *Angew. Chem. Int. Ed. **2018**,130-4628–4632.*

144.Huang, P.; Fan, M. Development of facture free clay-based aerogel. *Formulation and architectural mechanisms. Composites, Part B **2016**, 91, 169–175.*

145. Maleki, H., Montes, S., Hayati-Roodbari, N., Putz, F., & Huesing, N. Compressible, Thermally Insulating, and Fire Retardant Aerogels through Self-Assembling Silk Fibroin Biopolymers Inside a Silica Structure" *An Approach towards 3D Printing of Aerogels. ACS Applied Materials & Interfaces, **2018**-10(26), 22718–22730.*

146. Chen, J.; Xie, H.; Lai, X.; Li, H.; Gao, J.; & Zeng, X. An ultrasensitive fire-warning chitosan/montmorillonite/carbon nanotube composite aerogel with high fire-resistance. *Chemical Engineering Journal,* **2020**-*125729.*

147. Yuan, B.; Zhang, J.; Yu, J.; Song, R.; Mi, Q.; He, J.; Zhang, J. Transparent and flame retardant cellulose/aluminum hydroxide nanocomposite aerogels. *Sci. China Chem. **2016**, 59, 1–7.*

148. Zhao, S.; Malfait, W.J.; Guerrero-Alburquerque, N.; Koebel, M.M.; Nyström, G. Biopolymer aerogels and foams: chemistry, properties, and applications. *Angew.Chem. Int. Ed. 2018,57,7580–7608.*

149. Pawlowski, K. H.;, & Schartel, B. Flame retardancy mechanisms of aryl phosphates in combination with boehmite in bisphenol A polycarbonate/acrylonitrile–butadiene–styrene blends. *Polymer Degradation and Stability, **2008**,93(3), 657–667.*

150. Guido, E.; Alongi, J.; Colleoni, C.; Di Blasio, A.; Carosio, F.; Verelst, M.; Rosace, G. Thermal stability and flame retardancy of polyester fabrics sol–gel treated in the presence of boehmite nanoparticles. *Polymer Degradation and Stability, **2013**-98(9),1609–1616.*

151. Huang, P.-H.; Chang, S.J.; Li, C.C.; & Chen, C.A. Boehmite-based Microcapsules as Flame-retardants for Lithium-ion Batteries.*Electrochimica Acta, **2017**-228, 597–603.*

152. Hamdani-Devarennes, S.; El Hage, R.; Dumazert, L.; Sonnier, R.; Ferry, L.; Lopez-Cuesta, J.M.; & Bert, C. Water-based flame retardant coating using nano-boehmite for expanded polystyrene (EPS) foam. *Progress in Organic Coatings, **2016**,99, 32–46.*

153. Monti, M.; & Camino, G. Thermal and combustion behavior of polyethersulfone-boehmite nanocomposites. *Polymer Degradation and Stability, **2013**,98(9), 1838–1846.*

154. Fan, B.;Chen, S.; Yao, Q.; Sun, Q.; & Jin, C. Fabrication of Cellulose Nanofiber/AlOOH Aerogel for Flame Retardant and Thermal Insulation. *Materials, **2017**-10(3), 311.*

CHAPTER – 2

Nano Ceria Decorated Boehmite Gel Hybrids as Photo-catalytic Antimicrobial Adsorbents

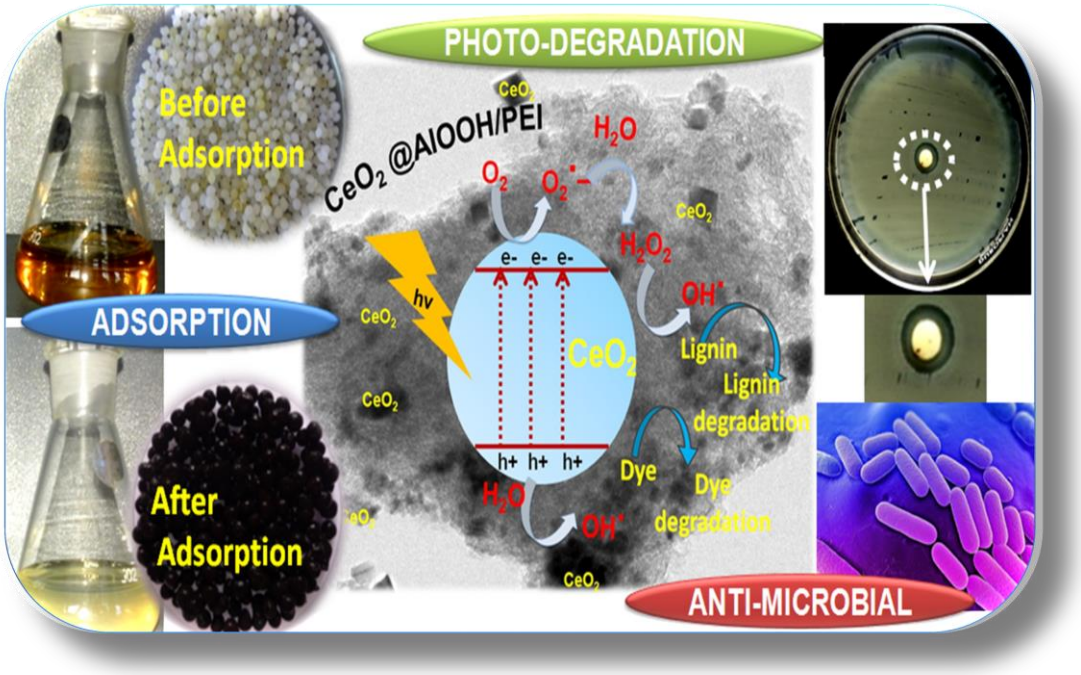

This chapter has been adapted from following publication

Shuhailath, K. A.; Linsha , V.; Nishanth Kumar, S.; Babitha, K. B.; Peer Mohamed, A.; Ananthakumar, S. https://doi.org/10.1039/C6RA07836B 2

2.1. Abstract

In this study amine functionalized, mesoporous monohydroxy aluminium oxide (boehmite) (AlOOH/PEI) hybrid is prepared and further catalytically engineered with nano-CeO_2 to make a multifunctional photoactive and antimicrobial catalytic-sorbent (CeO_2@AlOOH/PEI). This hybrid catalyst is explored for the treatment of industrial waste water contaminated with lignin and organic dye. Structural and physico-chemical properties of this catalytic-sorbent were characterized using powder XRD, FT-IR, SEM, TEM, N_2 sorption analysis, TGA and zeta-potential measurements. Efficiency of both AlOOH/PEI hybrid and CeO_2@AlOOH/PEI hybrid nanocomposite for the lignin adsorption was first examined with respect to various adsorption parameters and subsequently the adsorption kinetics was verified with standard Lagergren pseudo-first-order and pseudo-second-order mathematical models. The results revealed that the adsorption kinetics follows pseudo-second-order model. A comparative study was also done with other known conventional sorbents and the preparedCeO_2@AlOOH/PEI catalytic sorbent shows a better adsorption capacity towards lignin. Photodegradation of lignin and methyl orange dye using CeO_2@AlOOH/PEI hybrid nanocomposite was also investigated under sunlight and UV irradiation. More than 85% of both the pollutant degraded within the time interval of 100 min. Above all, the antibacterial property of CeO_2@AlOOH/PEI sorbent was also studied against both gram positive and gram negative bacteria and showed efficient antimicrobial activity against the tested bacteria. An eco-friendly, self-regenerative, sustainable CeO_2@AlOOH/PEI catalytic sorbent is designed and validated for the recovery of water resources from the lignin and dye contaminated industrial effluent.

2.2. Introduction

Adsorption and photodegradation are two highly connected, simple processes for the effective recovery of reusable water from industrial waste stream. Many known conventional sorbents and catalysts are not high enough to perform simultaneously both functions in a solo material. Nanostructured hybrid materials exhibiting multiple functions such as selective adsorption to hazardous pollutants, photocatalytic degradation of toxic elements, thermo-chemical stability, and resistance against microbial attack, have great potential as advanced functional material. Design and development of such catalytically engineered high surface area, mesoporous hybrid adsorbents possessing self-regeneration capability to regain its catalytic efficiency by simple photoirradiation became extremely essential for the sustainable waste water treatment technologies.

Paper mills, bio-fuel production plants and textile dye units require such catalytic sorbents for the treatment of voluminous industrial effluents. Processed water from these industries are usually contaminated with intensely coloured lignin and organic dyes.[1-3] Over 10000 different dyes has been used by textile industry with an annual consumption of 7 x 10^5 tons and ultimately gushed into the natural water bodies.[3,4] A paper mill typically discharges 8700 gallons of lignin contaminated water per ton of paper produced.[5] It causes severe environmental pollution not only to the land mass fertility but also to the aquatic systems, and also increases the COD and BOD of the water bodies.[5, 6]Despite of all these downsides; lignin an aromatic biopolymer is composed of phenyl propanoid units such as p-coumaryl alcohol, coniferyl alcohol and sinapyl alcohol linked through a variety of C-C bonds and ether linkages.[7] These lignin derivatives have good industrial values and hence the removal of lignin in a safe manner is also considered to be a great concern in such industries.[8]

For several years, wastewater treatment is being carried out via adsorption, coagulation, flotation, oxidation, biosorption, biodegradation, UV photodecomposition and ultrafiltration, but these methods are not cost-effective.[9, 10] Adsorption is considered to be one of the most promising methods for effluent treatment due to its high efficiency, low cost and easy handling.[10,11] Several studies have been reported on adsorption of lignin using activated carbon from xylo-oligosaccharides, pre-hydrolysis kraft and waste water from mechanical pulping.[12-14] Similarly, photocatalytic methods also found to be a better technology for the decomposition of toxic wastes. The main advantage seen here is the complete degradation of organic pollutants to carbon dioxide and water.[15-17] For this purpose, use of nanostructured semiconducting TiO_2, CeO_2, ZnO, Fe_2O_3 photocatalytic metal oxides are being explored.[15] Rare studies were reported for photocatalytic degradation of lignin. Kobayakawa et al. studied the complete mineralization of lignin using TiO_2 as photocatalyst.[18] Ohnishi et al. reported noble metal loaded $TiO_2$and demonstrated extreme competence in decolourization of lignin effluent.[19]

However, in recent years integrated adsorption and degradation are emerging as a more efficient and simplest technology for waste water treatment. Hence, engineered hybrid catalytic-sorption technologies using catalytically modified carbon, mesoporous silica and alumina, as well as bio-polymeric catalytic-sorbents are recently explored.[20-22]Such synergetic effect was reported using powdered TiO_2 and activated carbon (AC) in the sorption and catalytic degradation of organic pollutants.[22] Cordero et al. studied the associative effects between TiO_2 and AC during the photodegradation of 4-Chlorophenol using various kinds of AC.[23]

In this work, a catalytic-sorbent material CeO_2@AlOOH/PEI hybrid nanocomposite was designed out of inorganic and organic functional moieties having

competent adsorptive and photocatalytic functions for single-stage cleaning technologies. Boehmite (AlOOH), a layered inorganic oxy hydroxide form of alumina is a thermally stable, inert medium, used as solid industrial inorganic adsorbent for the removal of toxic pollutants from effluents.[24-25] Sol-gel is a technique recognized for synthesizing porous metal-oxides with controlled pore architecture. Hence, the surface characteristics of sol-gel synthesised AlOOH was tailored by introducing organic polyethylene imine (PEI) functionality to further enhance the adsorption capacity. Additionally, CeO_2 is decorated over AlOOH/PEI hybrid gels to obtain CeO_2@AlOOH/PEI hybrid nanocomposite framework. $CeO_2$is an n-type semiconductor, with a band gap of 2.9- 3.2 eV, well known for non-toxicity, high thermal stability and recognized as a visible light driven photocatalyst.[26] Monolithic macro beads of CeO_2@AlOOH/PEI porous supports were fabricated via sol-gel granulation technique, so that it can be easily packed in a reactor for the continuous operation. Effective performance of the CeO_2@AlOOH/PEI catalytic sorbent was then studied primarily for lignin adsorption as well as a model methyl orange dye with respect to various adsorption parameters and the results are discussed. The photocatalytic degradation of lignin and dye were also studied in presence of UV and sunlight to recover the water from contaminated source. Additionally, we have also analysed the adsorption efficiency of the material using lignin contaminated effluent received from the local paper mill.

We have also explored the antibacterial ability of the proposed material. Nowadays, the need for functional materials with antimicrobial property in water treatment is more investigated. The designing of a material which can act as an adsorbent, photocatalyst and antimicrobial agent is still considered to be a challenge task. The antibacterial property of proposed hybrid material was assessed using Gram-

negative *E. coli*, *K. pneumoniae* and Gram-positive *S. aureus* as model organisms and the results are discussed.

2.3. Experimental Section

2.3.1. Materials

All chemicals and reagents used were of analytical grade. Aluminium isopropoxide (AIP, purity >98%), alkali kraft lignin, branched-polyethylene imine (PEI, MW ~ 25000) and cerium dioxide (CeO_2,nanopowder, < 25 nm particle size) were purchased from Sigma Aldrich and Methyl Orange (MO) from SD fine chemicals was used as model anionic organic dye. Black liquor, a paper mill effluent, was kindly supplied by the company Hindustan Newsprint Limited, Kerala, India. *Staphylococcus aureus* MTCC 902 (*S. aureus*), *Escherichia coli* MTCC 2622 (*E. coli*) and *Klebsiella pneumonia* MTCC 109 (*K. pneumoniae*) were used as test bacterial pathogens for antimicrobial studies. All the test microorganisms were purchased from Microbial Type Culture collection Centre, IMTECH, Chandigarh, India. The test bacteria were maintained on nutrient agar slants.

2.3.2. Sol-gel synthesis of boehmite sol (AIP-sol)

A stable boehmite sol (AIP-sol) was prepared by the well known Yoldas process, involving the hydrolysis and condensation of AIP.[27] The alkoxide precursor, AIP was first hydrolysed in 1000 mL distilled water at 80-85^{o}C, and after stirring for 1 h, the hydrolysed product, was peptized with 1 M HNO_3 until the pH become 3. The peptized AIP sol was then refluxed overnight at 90-95 ^{o}C. The resultant sol was gravimetrically estimated for the boehmite (AlOOH) content. The AlOOH concentration in the resultant AIP sol was 0.0675 g mL^{-1}.

2.3.3. Preparation of AlOOH/PEI hybrid and CeO_2@AlOOH/PEI hybrid nanocomposite gels and monoliths

In a typical process, 1 M AIP sol (50 mL) containing 3.37 g of AlOOH content was mixed with 1.5g of PEI, and stirred for 2 h. A rapid coagulation occurred and the sol transformed into stiff gel. The gel was treated further with 1 M HNO_3 to control the pH in the range 2 to 3. At this stage, the thick gel collapsed and resulted in flowable gel mass to obtain AlOOH/PEI hybrid gel. For the preparation of catalytically engineered CeO_2@AlOOH/PEI hybrid nanocomposite gel, the same experiment was repeated as mentioned above. To the AlOOH/PEI hybrid gel, 0.8 g nano-$CeO_2$was mechanically blended. The gel mixture was stirred for 3-5 h to obtain a well homogeneous CeO_2@AlOOH/PEI hybrid nanocomposite gel. The chemical interaction of AlOOH with PEI and CeO_2 modified AlOOH/PEI gels is illustrated in the **Fig.2.1**.

The gels obtained were then moulded into cylindrical and spherical monolithic structures. The gel was aged in ammonia in cylindrical vials to obtain cylindrical monoliths. The gel was subjected to spherical granulation process by an injector into the ammonia bath maintained at pH = 8.5, prepared with a top-layer out of paraffin oil. The acidified gel when dropped in ammonia bath, undergo immediate gelation and self-assembled to highly uniform, spherical shape wet gel beads. The wet gel samples were evaporative dried in hot air oven to obtain xerogels samples.

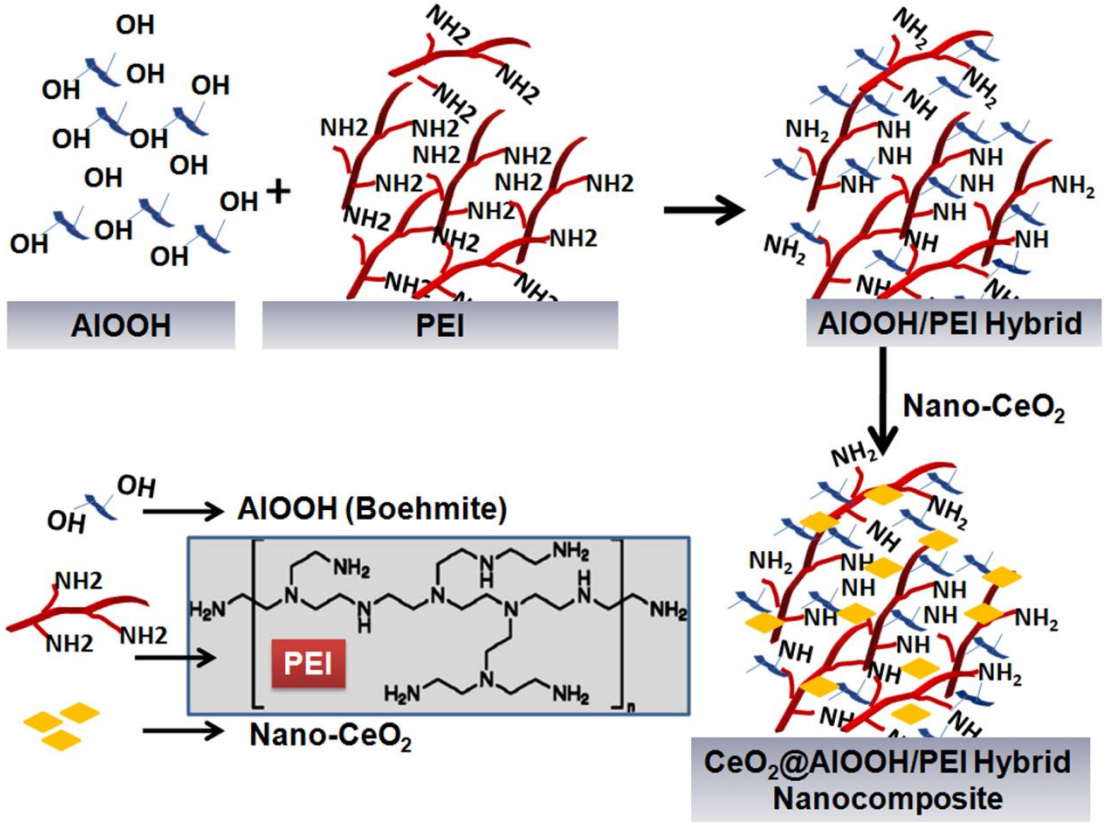

Fig.2.1. Simplified scheme of synthetic steps involved in the formation of AlOOH/PEI hybrid and CeO_2@AlOOH/PEI hybrid nanocomposite

2.3.4. Characterization

X-ray diffraction (XRD) patterns of the samples were obtained with a Philips X'pert Pro X-ray diffractometer in the 2θ range 10-80° using Cu Kα radiation (λ = 1.54178 Å)under a voltage of 40 kV and current of 40 mA. Fourier Transform Infrared (FTIR) analysis was performed using Shimadzu IR Prestige-21 spectrophotometer to understand the chemical interaction in the hybrid system. A standard KBr pellet technique was employed and the chemical structure of the hybrid was analysed in the wavelength range of 4000-400 cm^{-1}through transmission method. The thermal decomposition of AlOOH/PEI and CeO_2@AlOOH/PEI was investigated by Shimadzu TG-50 Thermo Gravimetric Analyser (TGA), between the temperature range 100-1000^oC at a constant heat flow of 10^oC min^{-1} in air atmosphere. The bulk micro-structural characteristics of the hybrid monoliths were examined using JEOL 5600 SL Scanning Electron Microscope

(SEM). The morphological features of the hybrids were ascertained further by Tecnai G2, FEI Transmission Electron Microscope (TEM) operated at an accelerating voltage of 300 kV. The surface charge analysis was carried out using 3000H Malvern Zetasizer Instrument. Surface area and porosity nature was studied by standard N_2 adsorption technique using Micromeritics Gemini 2375 surface area analyzer after degassing the samples at 200^{o}C for 2 h. Brunauer-Emmett-Teller (BET) model was utilized to calculate the specific surface areas. A desorption isotherm was used to determine the pore-size distribution using the Barrett-Joyner-Halenda (BJH) model. Shimadzu UV 240 IPC UV/Vis spectrophotometer was used to determine the concentration of lignin and organic dye MO in aqueous solution. The characteristics peaks at wavelengths 280 and 464 nm, was considered for the analysis of lignin and MO, respectively.

2.3.5. Application study for removal of lignin from aqueous sample

2.3.5.1. Adsorption studies

Adsorption capacities of AlOOH/PEI and CeO_2@AlOOH/PEI sorbents towards kraft lignin were investigated by batch experiment at room temperature. For the adsorption experiments, lignin stock solution was prepared with 10g lignin in 1L distilled water. From this stock solution, different concentrations of lignin solution (500, 1000, 2000, 2500, 3000, 4000, 6000, 8000 mg L^{-1}) were prepared. In a typical batch experiment, 0.5 g of sample was added to 25 mL of lignin solution. For analyzing the adsorption efficiency, 1 mL of the lignin solution was withdrawn from the bulk at definite time intervals. After centrifugation (8000 rpm, 10 min at room temperature), the concentration of the lignin in solution was determined by UV/Vis spectrophotometer and the amount of lignin adsorbed was calculated using equations (2.1. and 2.2):

$$\% \text{ Adsorption} = (C_0 - C_e)/C_0 \times 100 \quad (2.1)$$

$$Q_e = (C_o - C_e) \times V / m \quad (2.2)$$

where Q_e(mg g^{-1}) is the amount of lignin adsorbed, C_o (mg L^{-1}) is the initial lignin concentration, C_e(mg L^{-1}) is the lignin concentration at equilibrium, V (mL) is the volume of lignin solution, and m(g) is the amount of adsorbent added. The effect of pH and temperature on lignin adsorption process was studied over pH range 1 to 12 and temperature 30, 35, 45, 55 and 65 °C. The pH of the lignin solution was adjusted using 0.1M NaOH and 0.1M HNO_3. The rate of adsorption of lignin was studied at different time intervals that were as long as 700 min using different initial concentrations as mentioned above at pH 5 and 30°C.

2.3.5.2. Photoactivity studies

Photocatalytic activity of the as prepared samples was evaluated by the photodecomposition of kraft lignin with the illumination of sunlight and UV. 0.5 g of the catalytic material was stirred with 75 mL of lignin (4000 mg L^{-1}). Prior to any irradiation, the reactant solutions were magnetically stirred in the dark for 30 min to establish adsorption/desorption equilibrium between lignin and the catalyst surface. Later, the samples were exposed to UV/sunlight irradiation. About 5 mL of sample was collected at different time intervals and centrifuged for separating the residue. Degradation of lignin was analysed by the decrease in the absorption peak at λ_{max} 280 nm for lignin with the aid of UV/Vis spectrophotometer. The percentage of lignin degradation was calculated using the equation (3):

$$\% \text{ Degradation} = (C/C_0) \times 100 \quad (2.3)$$

where C_0 is the initial concentration and C is the concentration of the lignin at time t.

2.3.5.3. Application study for removal of organic dye from aqueous sample

Batch adsorption experiments were carried out by adding 0.5 g of the samples to 25 mL of 25 mg $L^{-1}$of organic dye MO in aqueous solution. The mixture was shaken vigorously at 30℃ for different lengths of time. The supernatant was then collected, centrifuged

(8000 rpm, 10 min at room temperature) and was assayed in a spectrophotometer. The amount of adsorbed MO was calculated from the absorbance measured at 464 nm before and after adsorption. Similarly, photodegradation studies were also conducted by illumination with UV and sunlight. The percentage adsorption and degradation were calculated as mentioned above.

2.3.5.4. Bacterial resistance test

2.3.5.4.1. Antibacterial assay by disc diffusion method

The antibacterial activity of the test samples was determined by the disc diffusion method against the test bacteria on Muller–Hinton agar, according to the Clinical and Laboratory Standards Institute (CLSI). The media plates (MHA) were streaked with bacteria 2-3 times by rotating the plate at 60ºC angles for each streak to ensure the homogeneous distribution of the inoculums. After inoculation, discs (10 mm Hi-Media) loaded with 100 µg mL^{-1} of the test samples were placed on the bacteria-seeded plates using sterile forceps. The plates were then incubated at 37ºC for 24 h. The inhibition zone around the discs was measured and recorded. Ciprofloxacin (Hi-Media) was used as the positive controls to compare the efficacy of the test samples. The assays were carried out in duplicates.

2.3.5.4.2. Test bacterial culture preparation

All the three bacterial strains were streaked onto nutrient agar plates. The plates were incubated at 37°C for 24 h and further maintained at 4°C. A single isolated colony of each culture was inoculated in nutrient broth and incubated at 37°C for 18 h until the stationary growth phase was reached. After incubation, the cells were harvested by centrifugation at 10,000 rpm for 10 min, washed twice in sterile phosphate buffered solution and finally resuspended in phosphate buffered solution.CeO_2@AlOOH/PEI catalytic sorbents were then added into the bacterial suspension and then incubated for 1h.

2.4. Results and Discussion

2.4.1. Structural and chemical analysis of synthesized hybrid nanocomposite

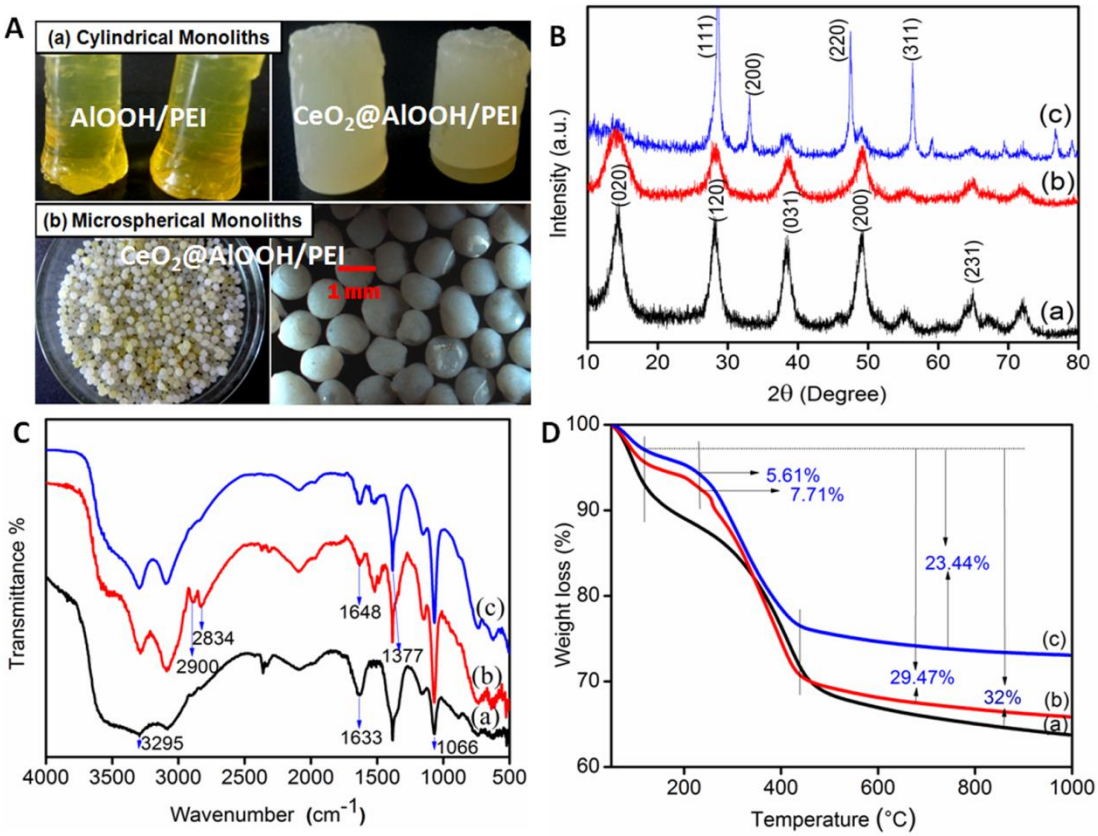

Fig.2. 2. (A) Optical images (B) powder XRD patterns (C)FTIR spectra and (D) TGA analysis of the synthesised material, in all the graphs (a) pure AlOOH (black line) (b) AlOOH/PEI (red line) and (c) CeO_2@AlOOH/PEI (blue line)

Fig.2.2.A. shows the optical micrograph of monolithic structures fabricated from the functionally engineered AlOOH/PEI and CeO_2@AlOOH/PEI hybrid nanocomposite xerogels. Monolithic structures especially spherical shape for functional porous materials is more preferable in the case of specific adsorbent/catalytic support used in fluidized bed for separation and purification processes. This is because spheres can be uniformly suspended with higher packing density, can reduce breakage loss by collision and lower pressure drop. Herein, the as-prepared granules have a size of around 2-3 mm in diameter, which shrinks to 1 mm in diameter during drying which is suitable for use as an adsorbent/catalytic support. We have carried out all the further characterization and studies of this microspherical monolithic supports.

The powder XRD of the sol-gel AlOOH, and its hybrids AlOOH/PEI and CeO_2@AlOOH/PEI are shown in **Fig.2.2.B.** In the XRD pattern of the obtained boehmite (curve a), the diffraction peaksat 2θ values 14.2°, 27.8°, 38.3°, 49.1° and 64.1° can be indexed for the Bragg reflection planes (020), (120), (031), (200), and (231) of orthorhombic boehmite crystals. These peaks are found to be closely matching with the standard reported for the AlOOH crystals (JCPDS card 21–1307).[28] Upon hybridization of organic moiety PEI and immobilization of nano-CeO_2, the crystalline peaks notably changed. In AlOOH/PEI system (curve b), the peak width is broadened and the intensity is decreased indicating the bulk effect of amine moieties. In comparison to the XRD patterns of AlOOH/PEI, CeO_2 decorated AlOOH/PEI hybrid nanocomposite (curve c), peaks correspond to nano crystalline CeO_2 is seen at 2θ = 28.6°, 33.1°, 47.5° and 56.3° which are attributed to the presence of (111), (200), (220), and (311) planes, respectively (JCPDS card 34-0394).[29] These pattern clearly, suggesting that the nano-CeO_2 is well distributed in the AlOOH/PEI hybrid gel network forming a nanocomposite hybrid system.

The hybrid nature of the catalytically activated AlOOH/PEI sorbent was also confirmed by FT-IR analysis. In **Fig. 2.2.C**, the FTIR spectra show the characteristic feature of AlOOH hybrid functionally modified with PEI and nano-CeO_2. The chemical interaction of the reactive functional groups in PEI with inorganic AlOOH to form AlOOH/PEI and CeO_2@ AlOOH/PEI hybrid nanocomposites is clearly understood from the respective characteristic FTIR bands. Alkoxide derived sol-gel AlOOH (curve a) exhibits the characteristic band for Al-O-Al stretching vibration at 1066cm^{-1}.[30] The peaks at 3295, 1633, 1162 cm^{-1}can be assigned to stretching, bending mode of adsorbed water and deformation mode of –OH group, respectively. The hybrid formation was well confirmed by the presence of symmetric and asymmetric stretching vibration of

functional groups C-H (-CH_2-), associated to the PEI organic component, at 2900-2834 cm^{-1} and the existence of N-H bending at 1633 cm^{-1} (curve b).Similarly, Stretching vibration of N-Hand C=N were also observed at 3295 $cm^{-1}$and 1648 cm^{-1}respectively. While, in nano-CeO_2 decorated hybrid catalyst (curve c), the appearance of absorption band between 500-750 cm^{-1} is attributed to the characteristic stretching vibration mode of Ce-O. A vibration band at 1377 cm^{-1} appeared in CeO_2@AlOOH/PEI due to the presence of vibration overtone of surface hydroxyl group of nano-CeO_2.

Thermal stability of hybrid nanocomposite was assessed by TGA and the corresponding thermogram is shown in **Fig.2.2.D.** The thermal decomposition patterns of AlOOH/PEI and CeO_2@AlOOH/PEI hybrids with unmodified AlOOH in the temperature range 50 to1000^oC. All the three systems exhibit two stage weight losses; one at 100 and 450^oC and another between 450 to 1000^oC. It can be summarized that the first stage weight loss can be attributed to the dehydration of adsorbed water molecules in the hydrolysed AlOOH. Decomposition of sol-gel AlOOH is well documented and the dehydroxylation is recorded at temperatures 250 to 400 ^oC. The weight loss at 450^oC is credited to the dehydroxylation of hydroxyl group in the phase transition from AlOOH to γAl_2O_3. The mass loss is comparatively low for hybrid AlOOH/PEI (5.1%) and hybrid nanocomposite CeO_2@AlOOH/PEI (3.5%) than single phase parent AlOOH (9.4%). AlOOH having a structure of double layers of octahedra exposes oxygen atom by crystallite surface.[31] These oxygen atoms can readily react with hydroxyl and hydrogen ions of water molecules. Hence more number of water molecules can be adsorbed on the surface of AlOOH. In the case of AlOOH/PEI and CeO_2@AlOOH/PEI, these surface oxygen atoms are not available because of the cross linking with highly reactive amino (-NH_2) group present in the PEI polymer. The thermogram shows additional weight loss due to polymer degradation at temperatures

250-300 ^{o}C in AlOOH/PEI and CeO_2@AlOOH/PEI. The parent AlOOH exhibits a steep weight loss of 32% in the entire temperature range whereas AlOOH/PEI and CeO_2@AlOOH/PEI show a gradual total weight loss of 29.4 and 23.4 %, respectively. The change in slope of the weight loss curves indicates better thermal stability in AlOOH/PEI and CeO_2@AlOOH/PEI.

2.4.2. Microstructural analysis of synthesized hybrid nanocomposite

Fig.2.3. depicts the SEM microstructures of bulk AlOOH/PEI and CeO_2@AlOOH/PEI granules. In case of AlOOH/PEI hybrid **Fig. 2.3.a** and **2.3.b**, the surface texture is very homogeneous and it appears that the hybrid gel spheres have random assemblage during wet gel granulation and the polymeric PEI has played definite role as structure directing macromolecule. A sign of thermal-stress during drying is noticed. Overall the image confirms the clustering of boehmite nanolamellar during gelling and retained the agglomerated structure during drying. Structurally modified AlOOH/PEI hybrid has porous texture. **Fig. 2.3.c.** and **2.3.d.** represent the SEM images of nano-CeO_2 modified AlOOH/PEI hybrid. The surface texture clearly indicates that nano-CeO_2 particles are uniformly distributed in the hybrid gel matrix.

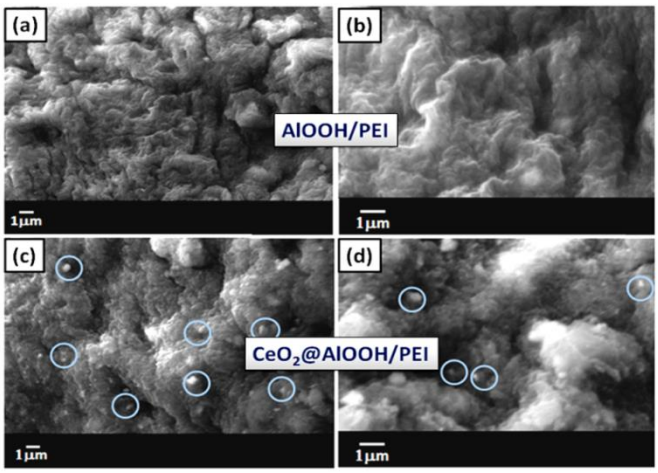

Fig.2.3. SEM images of (a) and (b) AlOOH/PEI (c) and (d) CeO_2@AlOOH/PEI at magnifications of 10 KX and 20 KX, respectively.

The microstructure also reveals the relatively smooth surface and ordered gel assembly with minimal drying stress. The nanolamellar AlOOH particle and also the distribution of PEI and nano-CeO_2 in boehmite hybrid are further confirmed by the TEM images. The dispersion of pure AlOOH deposited on Cu-grid clearly shows the nano-dimensional, lamellar type AlOOH crystallites (**Fig. 2.4.a.**). In hybrid AlOOH/PEI (**Fig. 2.4.b.** and **2.4.c.**) homogeneous distribution of lamellar boehmite crystallites on PEI polymer is observed. The TEM images (**Fig.2.4.d.**) for pure CeO_2 shows nano-octahedron type morphology. Hence, in the bulk CeO_2@AlOOH/PEI hybrid nanocomposite, the presence of uniformly distributed nanoparticulate octahedron CeO_2 is very well observed in AlOOH/PEI network. The SEM and TEM images also confirmed the hybrid gel mass is porous and catalytically modified which can be better exploited for the adsorption and photodegradation of organic contaminants.

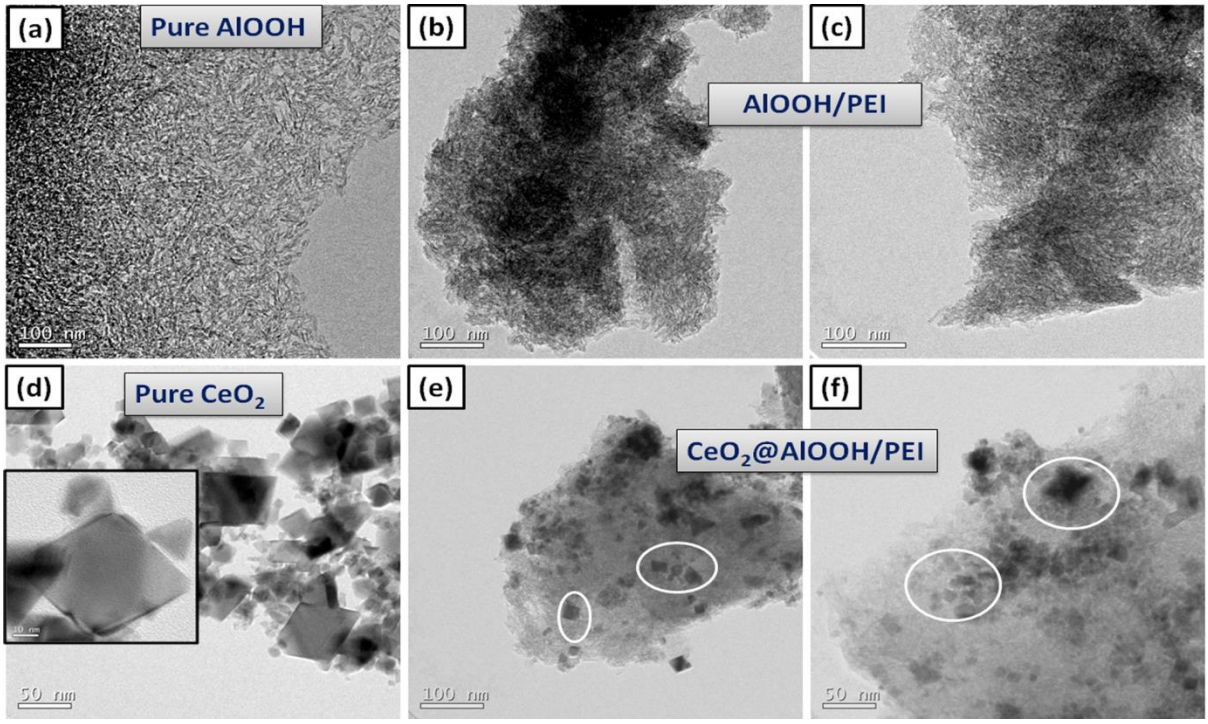

Fig.2.4. TEM micrographs (a) pure AlOOH, (b and c) AlOOH/PEI (d) pure $CeO_2$and (e and f) CeO_2@AlOOH/PEI

2.4.3. Textural features and surface charge of synthesized hybrid nanocomposites

Surface area and the functional groups on the surface of the adsorbents are the two crucial factors influencing the adsorption process. The bulk surface area and associated pore feature of the catalytically modified AlOOH sorbent is analysed through N_2 sorption analysis. **Fig.2.5.a.** shows the N_2 adsorption/desorption isotherm of parent AlOOH, AlOOH/PEI and CeO_2@AlOOH/PEI. All the three samples display a typical Type IV isotherm with steep hysteresis loop in the relative pressure range of 0.45 - 0.95, which suggests that the hybrids have mesoporous structures. The mesoporous AlOOH has high specific surface area of 311 $m^2 g^{-1}$ and an average pore diameter of 4.8 nm. In aminated and nano-CeO_2 modified hybrids, the BET surface area are slightly decreased to 260 and 215 $m^2 g^{-1}$ respectively implying that the organic functional group and catalytic nano-CeO_2 trap in the mesopores considerably. **Table 2.1.** summarizes the BET surface area and pore feature evaluated for the boehmite and hybrids. Moreover, the pore size distribution (**Fig.2.5.b.**) shows of AlOOH/PEI and CeO_2@AlOOH/PEI exhibits higher pore diameter 6.5 and 5.6 nm, respectively than the parent AlOOH (4.8 nm). Therefore, the higher surface area and porosity of the hybrid material can provide more active sites to improve its adsorption capability.

The susceptibility of the prepared samples towards adsorption can also be evaluated through the zeta potential measurements. This is measured to examine the surface charge of synthesised material at different pH ranges. The results are presented in **Fig.2.5.c.** The isoelectric point (IEP) of AlOOH/PEI and CeO_2@AlOOH/PEI hybrid were found to be 9.8 and 5.5, respectively indicating the adsorbents will be positively charged below this pH values and hence adsorption of anionic pollutant became more prominent.

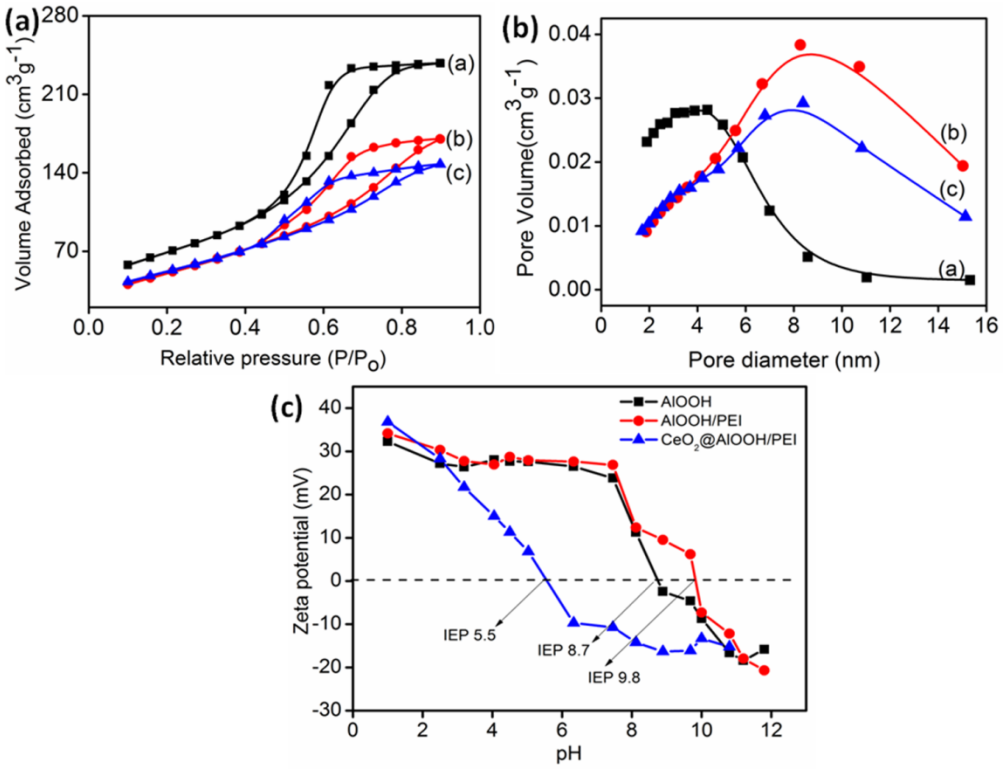

Fig.2.5. (a)Nitrogen adsorption and desorption isotherms and (b) Pore-size distribution curve (c) Zeta potential analysis of pure AlOOH, AlOOH/PEI and CeO_2@AlOOH/PEI as a function of pH

Table 2.1.Pore textural parameters of the synthesized hybrid gels

Samples	BET/Langmuir Surface area[a] (m^2g^{-1})	Mesopore volume (cm^3g^{-1})	Total pore volume[b] (cm^3g^{-1})	Pore diameter[c] (nm)
AlOOH	311/512	0.3009	0.3256	4.8
AlOOH/PEI	260/430	0.2863	0.4675	6.5
CeO_2@AlOOH/PEI	215/356	0.2833	0.2933	5.6

[a] Surface area calculated from nitrogen adsorption isotherms using the BET equation, [b] Pore volume calculated from nitrogen adsorption at p/p0 = 0.9, [c] Determined using the BJH model of the nitrogen adsorption curve.

2.4.4. Lignin adsorption and photocatalytic degradation studies

2.4.4.1. Adsorption studies

Lignin adsorption studies were conducted in batch process. Effect of very relevant influential factors such as concentration, contact time, pH and temperature was systematically studied. The initial lignin concentration is an important driving force to

overcome the mass transfer resistance of the lignin from the aqueous to the solid phase. The uptake of lignin by AlOOH/PEI and CeO_2@AlOOH/PEI hybrid sorbents were first determined with the initial lignin concentration in the range (5-100) x 10^2 mg L^{-1}at pH 5 (**Fig. 2.6.a.**). A pronounced increase in the lignin adsorption capacity by AlOOH/PEI and CeO_2@AlOOH/PEI hybrid is seen with increasing lignin concentration. The maximum adsorption capacity estimated for AlOOH/PEI and CeO_2@AlOOH/PEI hybrids is 66.31 mg g^{-1} and 97.53 mg g^{-1} respectively at the initial concentration of 4000 mg L^{-1}. Similarly, % lignin removal for both the hybrid systems initially increased at lower concentration and then decreased with increasing concentration. This is because at higher lignin concentrations, the increased number of adsorbate ion can interact with the available binding site of the adsorbent and facilitate faster uptake of lignin. Hence, for the further studies a fixed initial concentration of 4000 mg L^{-1} was used.

For water treatment technology, a perfect adsorbent should possess faster uptake of pollutants and reach equilibrium in shorter time. **Fig. 2.5.b.** shows the effect of contact time on the adsorption efficiency of lignin using AlOOH/PEI and CeO_2@AlOOH/PEI by altering the time of contact from 0-150 min. It was observed that uptake of lignin increases with increase in contact time and the equilibrium adsorption was reached within 30 min for both the sorbents.

The solution pH is another critical factor affecting the adsorption process. pH of the solution directly alters the solution chemistry and chemical interaction with the binding sites of the adsorbent surface. The adsorption of lignin onto the hybrid sorbents was assessed at pH values in the range 1-12 (**Fig. 2.6.c.**). The hybrids show a strong dependence of pH on the adsorption capacity of the lignin. As the pH of lignin solution increases from 1 to 5, the adsorption capacity of the hybrid sorbent increased due to the positively charged sorbent surface. Maximum adsorption of lignin by hybrid is seen at

pH 5. Under acidic pH, the protonation of imine and amine functional groups present in the hybrid adsorbent occurs.[32] Thus, a strong electrostatic force of attraction between protonated adsorbent and negatively charged lignin can lead to better adsorption (**Fig. 2.9.**). When the pH increases above 5, the lignin adsorption tendency gradually declined. At this pH ranges, probably deprotonation of surface amino groups occurs and results in electrostatic repulsion with lesser uptake of lignin. Also, AlOOH/PEI shows maximum adsorption in broad range of pH when compared to CeO_2@AlOOH/PEI, probably due to the variation in the IEP (AlOOH/PEI - 9.8 and CeO_2@AlOOH/PEI - 5.5). Hence, sorption kinetic and photodegradation studies were carried out at a fixed pH 5.

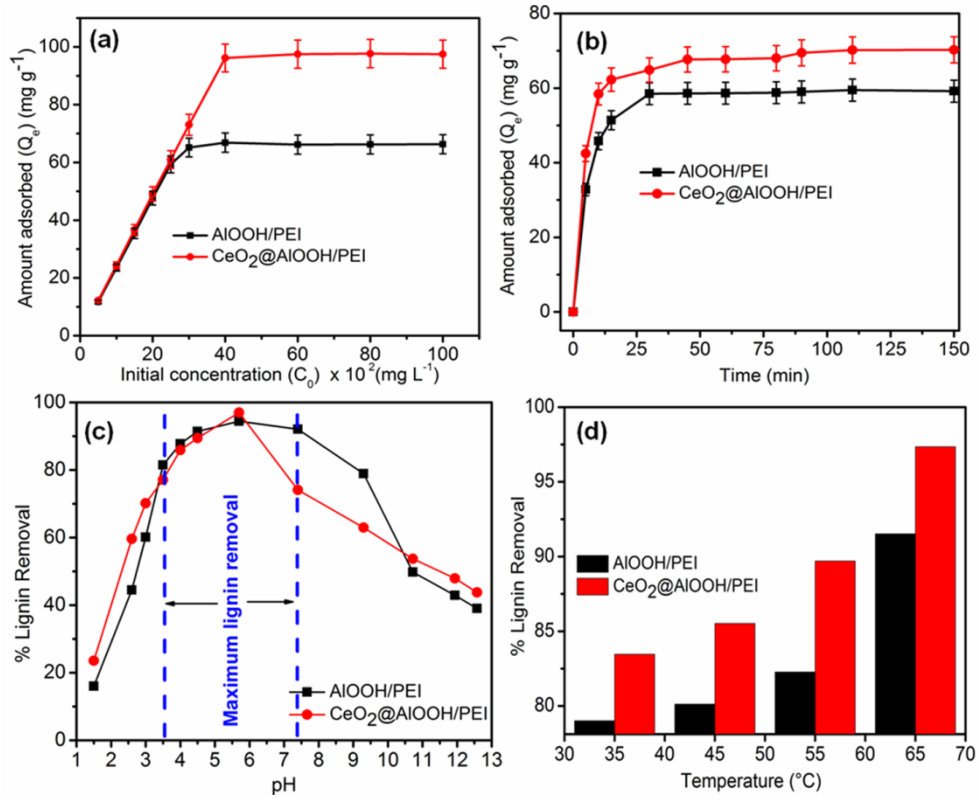

Fig. 2.6. Effect of (a) initial concentration (b) contact time (c) lignin solution pH, and (d) temperature on amount of lignin adsorbed by AlOOH/PEI and CeO_2@AlOOH/PEI hybrid sorbent

In addition to pH, the temperature effect is also studied for the lignin adsorption between temperature range 35 to 65 ^oC and the results are shown in **Fig. 2.6.d.** It was found that, in both the adsorbents the lignin uptake increases with increasing

temperature. It is renowned that increase in temperature decreases the solution viscosity.[33] In such case it can enhances the mobility of lignin molecules and provides adequate energy to facilitate the interaction between lignin molecules and sorption sites at the surface of sorbents.

It is observed from **Fig. 2.7.a.** and **2.7.b.**, the adsorption proceed quickly in the initial stage of reaction and then becomes slow until the sorption process nearly reach equilibrium. The initial rapid adsorption of lignin by AlOOH/PEI and CeO_2@AlOOH/PEI is due to the presence of large number of adsorption sites (amine and imine group present in the polymer PEI) on hybrid and nanocomposite. The subsequent slow step is attributed to the limited active adsorption sites on the surface of the adsorbent.[34]Lignin adsorbed on the surface would further hinder the diffusion of other lignin resulting in a long time to reach equilibrium. Based on the data obtained from experimental runs, pseudo-first-order model and pseudo-second-order model were used to simulate the kinetics adsorption of lignin on to both the AlOOH/PEI shown in **Fig.2.7.(c and d)** and CeO_2@AlOOH/PEI shown in **Fig.2.7.** (**e and f**).The used kinetic model equations are given below:

Pseudo-first-order: $\log (q_e - q_t) = \log q_e - (k_1/2.303)\, t$ (2.4)

Pseudo-second-order: $t/q_t = (1/k_2 q_e^2) + (1/q_e)\, t$ (2.5)

Where q_e and q_t are the amounts of lignin adsorbed on the adsorbents (mg g^{-1}) at equilibrium and at time t (min), respectively. k_1 (min^{-1}) and k_2 (g $mg^{-1}min^{-1}$) are the rate constants of the pseudo-first-order and pseudo-second-order adsorption, respectively. Kinetic data modelling was performed by a linear regression analysis and the results are shown in **Table 2.2**.

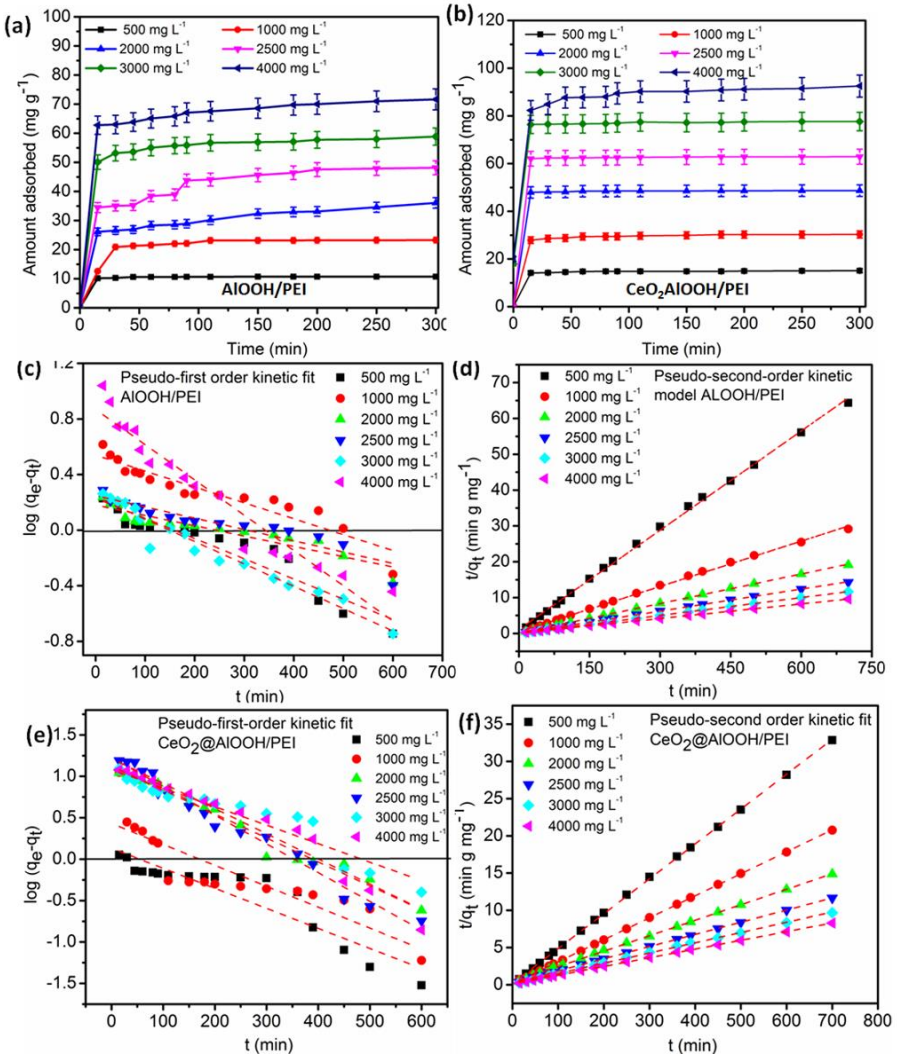

Fig.2.7.Adsorption kinetics study of (a) AlOOH/PEI and (b) CeO_2@AlOOH/PEI with lignin conc. 500-4000 mg L^{-1}, equilibration time t = 600 min (graph shown only up to 300 min), kinetic model fit for pseudo-first-order and pseudo-second-order adsorption(c and d) AlOOH/PEI and (e and f)CeO_2@AlOOH/PEI

The kinetic plot shows that the lignin adsorption process on AlOOH/PEI and CeO_2@AlOOH/PEI were found to fit better with pseudo-second-order with a high correlation coefficient (R^2=0.999) than pseudo- first-order (R^2=0.97). The best correlation of pseudo-second-order model with the experimental data reveals that the rate limiting step in adsorption process is controlled by chemisorption, which is a monolayer adsorption. [35] The rate of adsorption is one of the most important parameter in the kinetic study. From the **Table 2.2.**, it is evident that the values of k_2 decreases

with increasing concentration. This may be due to the fact that, at higher concentration of lignin solution, lower is the possibility of lignin to get attached to the active site of the adsorbent surface.

Table 2.2. Kinetic parameters of lignin adsorption on AlOOH/PEI and CeO_2@AlOOH/PEI

	AlOOH/PEI			CeO_2@AlOOH/PEI		
Kinetic models	Co (mg L^{-1})	K [a] x 10^{-2}	R^2	Co (mg L^{-1})	K [a] x 10^{-2}	R^2
Pseudo-first-order	500	0.3339	0.8981	500	0.4606	0.8441
	1000	0.2625	0.8797	1000	0.4606	0.7544
	2000	0.1711	0.8624	2000	0.4606	0.9767
	2500	0.1871	0.8650	2500	06909	0.9787
	3000	0.3707	0.9519	3000	04606	0.9044
	4000	0.5849	0.9368	4000	0.6909	0.9478
Pseudo-second order	500	0.7871	0.9985	500	0.2483	0.9998
	1000	0.4063	0.9985	1000	0.8423	0.9999
	2000	0.8905	0.9997	2000	0.1239	0.9994
	2500	0.7701	0.9998	2500	0.1246	0.9997
	3000	0.9526	0.9999	3000	0.1176	0.9993
	4000	1.4330	0.9999	4000	0.1018	0.9997

[a] Pseudo-first- order kinetic model K= k_1 (min^{-1}) and Pseudo-second-order kinetic model K=k_2 (g mg^{-1} min^{-1})

Compared to PEI cross linked AlOOH hybrid, the nano-CeO_2 modified hybrid display enhanced adsorption. From the adsorption data it is understood that the most probable mechanism controlling the lignin adsorption is as follows; surface of the hybrid adsorbent possess large number of amino (-NH_2) group which get protonated. Thus the adsorption of anionic organic pollutant takes place by electrostatic interaction with protonated amino group on the surface (**Fig. 2.9.a.**). In addition to the -NH_2 group, AlOOH nanoparticles have large number of surface hydroxyl group that may also uptake

anionic pollutants by hydrogen bonding and van der Waals interaction (**Fig. 2.9.a.**). Hence, a complete decolorization of lignin was observed within the adsorption equilibrium (**Fig. 2.9.b.**). The adsorption capacity of the prepared sorbents was compared with the known conventional sorbents and results are summarized in **Table 2.3.** It demonstrates that CeO_2@AlOOH/PEI hybrid sorbent possess remarkable adsorption capacity than some of the known conventional sorbents.

Table 2. 3. Comparison of results obtained in this study with other adsorbents

Adsorbents	Adsorption parameters		Adsorption capacity ($mg\ g^{-1}$)
	pH	Temperature (^{o} C)	
Bentonite	5	30	25.54
n-Silica	5	30	27.51
Zeolite	5	30	27.93
AlOOH/PEI	5	30	66.31
CeO_2@AlOOH/PEI	5	30	97.53

2.4.4.2. Photocatalytic Degradation Studies

The photocatalytic activity of the developed material towards lignin under sunlight and UV irradiation after the dark adsorption is shown in **Fig.2.8.** It can be seen from the **Fig.2.8.(a and c)**, the photodegradation of lignin using AlOOH, AlOOH/PEI was negligible under both the sunlight and UV than that of CeO_2@AlOOH/PEI. For the photodecomposition of lignin, adsorption efficiency of the catalyst plays a key role, since photocatalytic reaction generally occurs at the surface of catalyst than in the bulk. Lower the value of C/C_0 denotes higher degree of photoactivity, where, C_0 and C are the initial concentration and the original concentration of lignin at different irradiation time, respectively. To quantitatively assess the photocatalytic efficiency of the catalyst, kinetic data of these reactions fit the apparent first order rate equation,

$$\ln(C_0/C) = k \times t \qquad (2.6)$$

where C_0 and C are the concentrations of lignin at the time t = 0 and t respectively; k is the rate constant. After 100 minutes of irradiation 98 and 96 % of lignin was degraded with CeO_2@AlOOH/PEI under UV and sunlight, respectively with decay rate constant of k=0.038 (UV) and k=0.003 min^{-1} (sunlight).

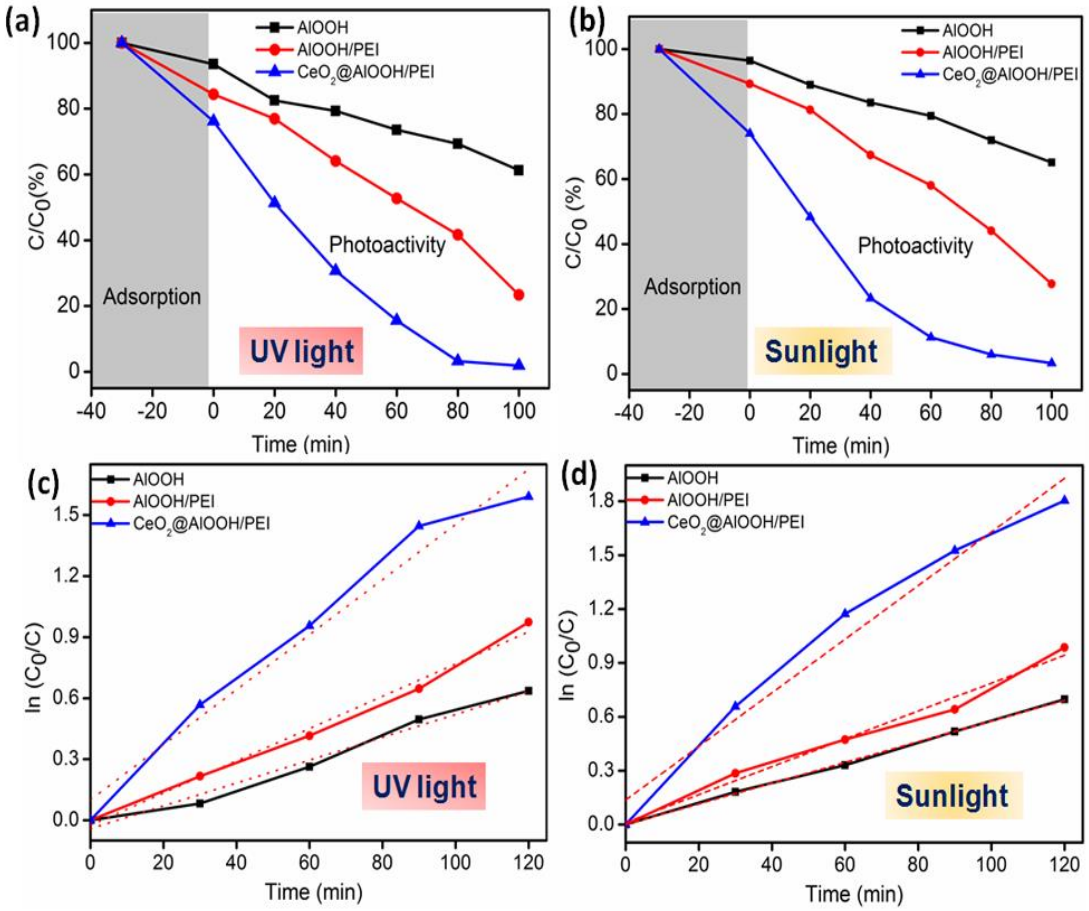

Fig.2.8. Photocatalytic degradation and corresponding regression curves of ln (C_0/C) versus irradiation time of lignin on AlOOH, AlOOH/PEI and CeO_2@AlOOH/PEI under sunlight (and b) and UV (c and d), respectively

Mechanism of the degradation of lignin under both the UV and sunlight includes the absorption of photon by semiconductor oxide (nano-CeO_2) and generate electron-hole pair.[36] This is pictorially represented in **Fig. 2.9.c**. The dissolved oxygen in the lignin solution captured the electron ejected from the valence band to form super oxide radical anion ($^{\bullet}O2^-$) and hydrogen peroxide (H_2O_2). These intermediates are capable of

producing strong oxidizing agent such as hydroxyl radical (•OH) which can degrade the pollutants. The photodegradation process described detail by the following equations.

$CeO_2 + h\mu \rightarrow e^- + h^+$ (2.7)

$O_2 + e^- \rightarrow O_2^{\bullet-}$ (2.8)

$H_2O + h^+ \rightarrow {}^\bullet OH$ (2.9)

$O_2^{\bullet-} + H+ \rightarrow {}^\bullet OOH$ (2.10)

$^\bullet OOH + O_2^{\bullet-} + H^+ \rightarrow O_2 + H_2O_2$ (2.11)

$H_2O_2 + O_2^{\bullet-} \rightarrow {}^\bullet OH + OH^- + O_2$ (2.12)

Organic pollutant + ($^\bullet OH$, $^\bullet O_2^-$, and / or O_2) → degraded products (2.13)

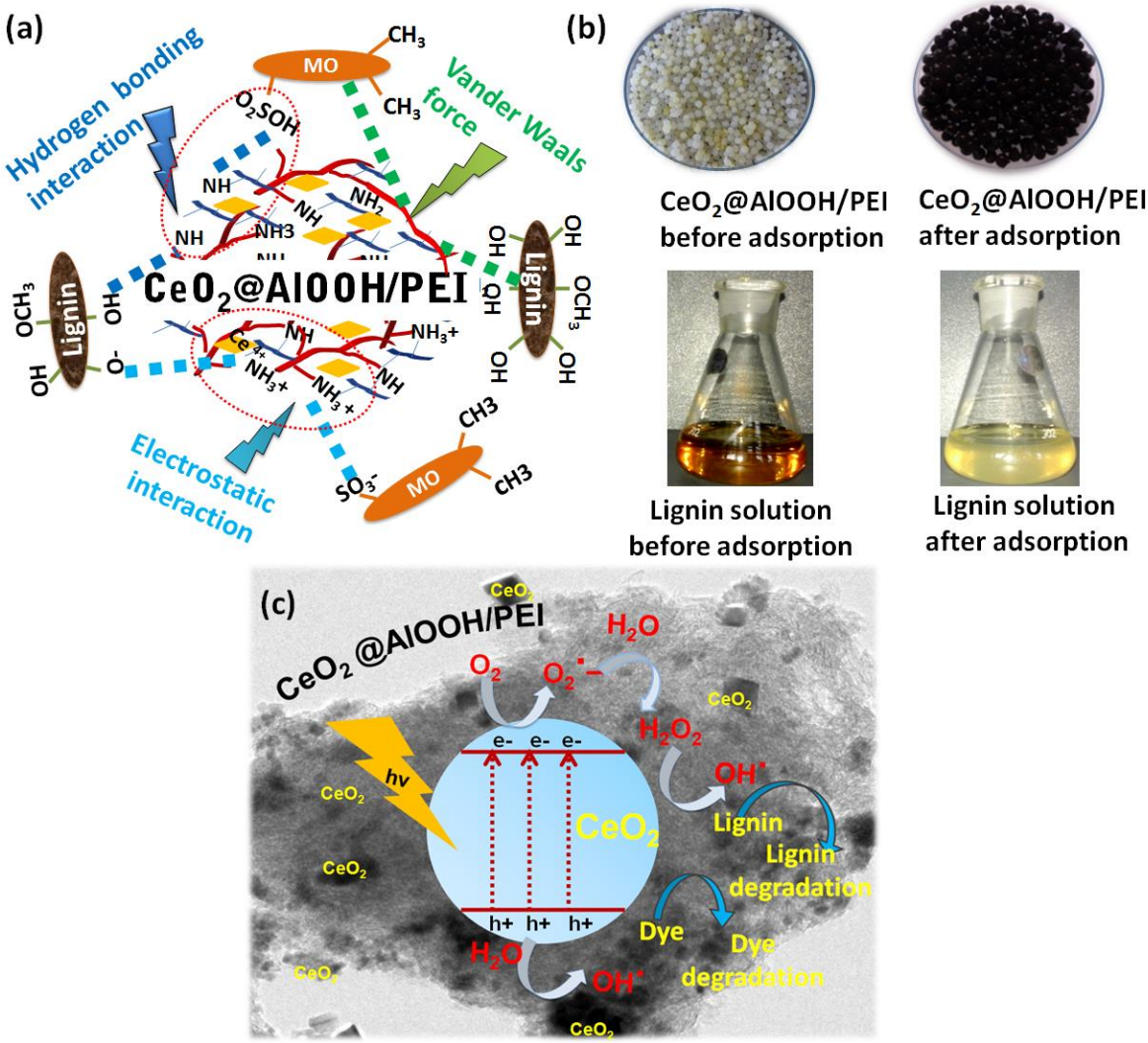

Fig. 2.9. Schematic illustration (a) of the possible interaction between CeO_2@AlOOH/PEI hybrid nanocomposite sorbent with lignin and MO dye molecule (b) photograph of CeO_2@AlOOH/PEI and lignin solution before and after adsorption (c) proposed mechanism for photocatalytic degradation of the organic pollutants under light irradiation

2.4.4.3. Removal of organic dyes from environmental aqueous samples

MO, a typical anionic dye was selected as a model dye pollutant for the adsorption performance of the proposed material. **Fig. 2.10.** (**a and b**) showed the removal percentage (%) for MO after different lengths of time. As expected, the removal efficiency of CeO_2@AlOOH/PEI hybrid nanocomposite material for MO was 95 % within 30-40 min, which was superior to that of the original materials remarkably for AlOOH and AlOOH/PEI 34 % and 67 % respectively. This phenomenon can be explained by electrostatic interaction between the positively charged sorbent and negatively charged MO molecule as described earlier.

The evaluation of photocatalytic activity of the prepared sample was also carried out using MO. **Fig. 2.10.** (**c and d**) illustrates the photocatalytic activity of the catalytic sorbent under both the sunlight and UV light irradiation. It was noticed that about 90 % of MO was degraded within 120 min under UV and 85% degradation under sunlight with CeO_2@AlOOH/PEI. In contrast photocatalytic activity of AlOOH and AlOOH/PEI were extremely lower than that of CeO_2@AlOOH/PEI, which indicates that removal has only occurred due to adsorption. The kinetics of the photodegradation of MO was assessed using the first order reaction. The apparent rate constant K_{app} determined for CeO_2@AlOOH/PEI was 0.57 and 0.72 min^{-1} under sunlight and UV, respectively.

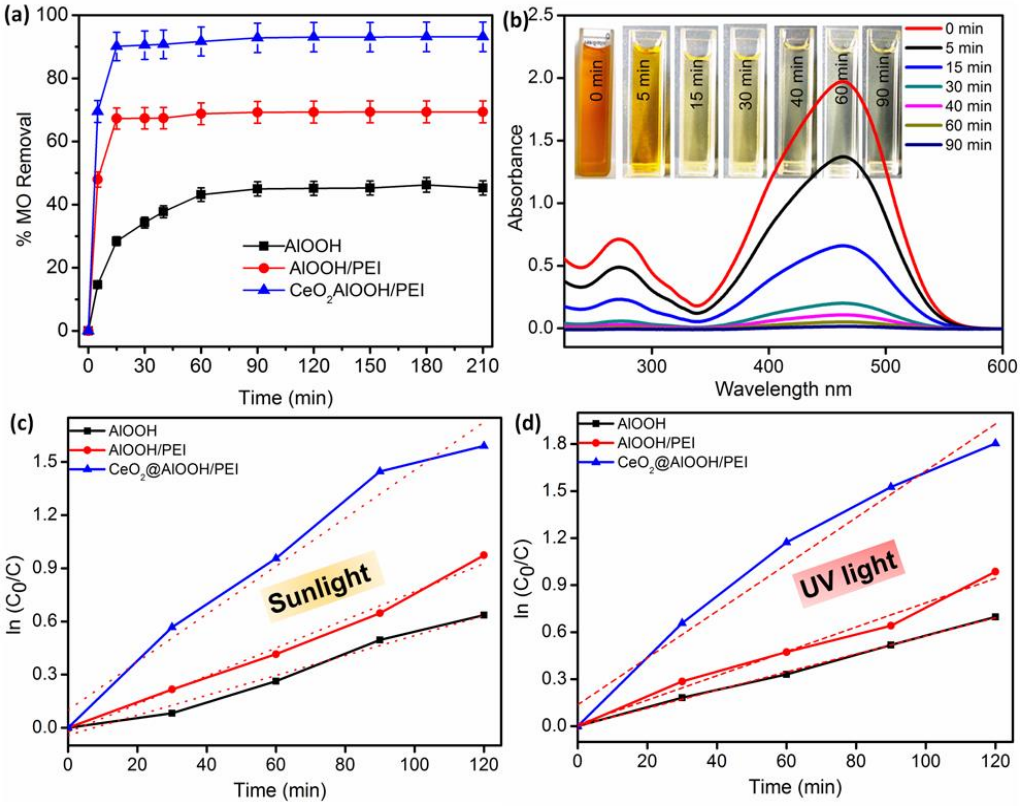

Fig. 2.10. (a and b) Adsorption curves of MO from aqueous solution at various time intervals (c and d) regression curves of ln(C_0/C) versus irradiation time of MO on AlOOH, AlOOH/PEI and CeO2@AlOOH/PEI under sunlight and UV

2.4.4.4. Antibacterial Activity of the proposed materials

The antibacterial property of the prepared hybrid material was assessed using Gram-negative (*E. coli*, *K. Pneumonia*) and Gram-positive (*S. Aureusas*) bacteria as a model microorganisms by the disc diffusion method. These bacteria were selected for the investigation of antibacterial efficacy, because they are usually associated with water distribution systems which cause infections. **Fig.2.11.** shows the results obtained for disc diffusion assay of AlOOH, AlOOH/PEI and CeO_2@AlOOH/PEI. We observed that both aminated and CeO_2 decorated hybrid system shows the clear zone of inhibition around the samples after 24 h of incubation when compared to pure AlOOH. Among the three tested bacteria, *K. Pneumonia* shows larger zone of inhibition of around 13 mm radius and *E. coli*and *S. aureus*have comparatively smaller zone of inhibition of 10 and 11 mm radius, respectively (**Fig. 2.11.**).

From the earlier reports, it was observed that quaternary ammonium compounds causes lysis of the bacterial cell walls by binding with cell components and further causes the seepage of cytoplasm.[37] Similarly, PEI was demonstrated to have a broad spectrum of antimicrobial activity against large number of Gram-positive and Gram-negative bacteria.[37, 38] A strong antibacterial effect against all tested bacteria was observed in PEI modified AlOOH hybrid material. The acidified AlOOH/PEI gel results in the formation of quaternary ammonium in the gel framework, which strongly interacts with bacterial cell walls and disrupts negatively charged bacterial cell membrane.

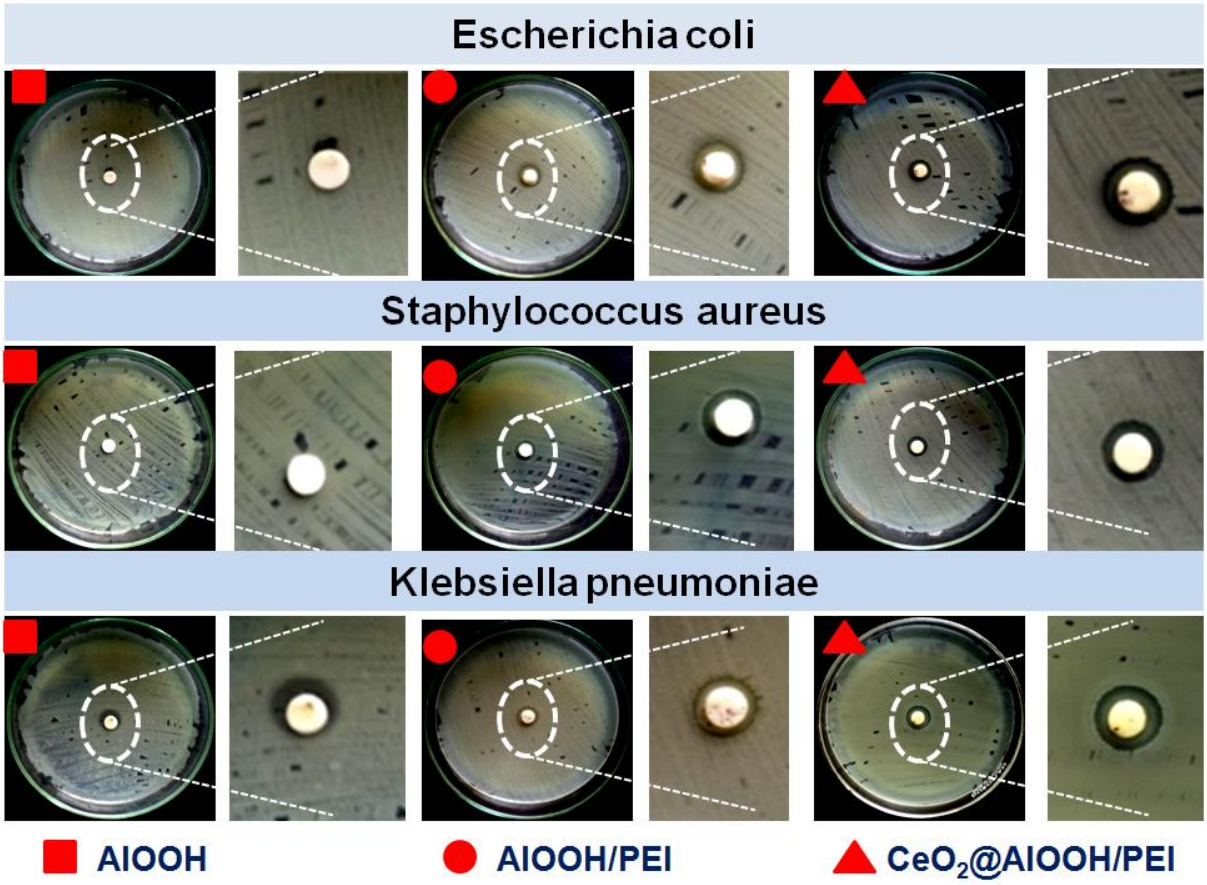

Fig. 2.11.Photographs of the antibacterial test of ■AlOOH, ●AlOOH/PEI and ▲CeO_2@AlOOH/PEI against Gram-negative *Escherichia coli*, *Klebsiella pneumoniae* and Gram-positive *Staphylococcus aureus*as model microorganisms

Furthermore, CeO_2 itself has antibacterial effect. The formation of oxygen species and reactive oxide species (ROS) in CeO_2 can be utilized for the bacterial toxicity effect.[39] The most prominent ROS responsible for the bactericidal effect are hydroxyl,

super-oxide radicals and H_2O_2 formation.[39,40] When bacteria come in contact with CeO_2, it interrupts the transport of electron, protein oxidation and also causes the membrane potential collapse. Hence, the coupled oxidation by the dissolved oxygen binding to the surface of CeO_2, production of ROS from H_2O_2, and basic exciton formation through the semiconducting nature are the major reason for efficient antibacterial activity exhibited by the developed hybrid material.

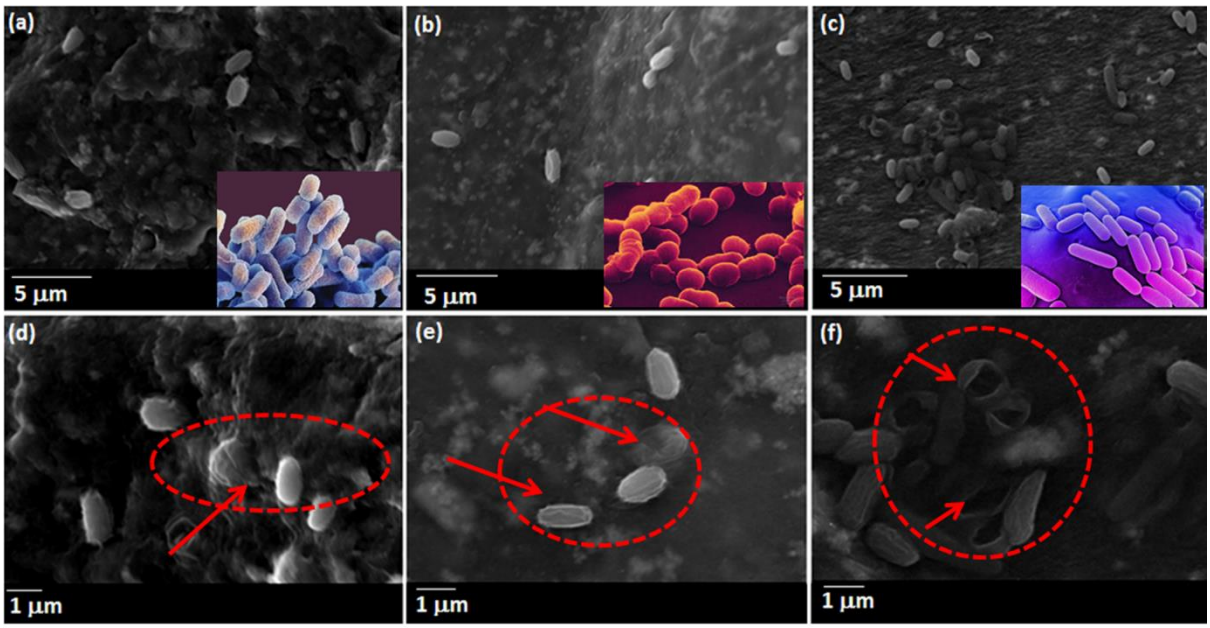

Fig. 2.12. SEM images CeO_2@AlOOH/PEI hybrid material after 10 minutes incubation with(a) *S. aureus*(b) *E. Coli* (c) *K.pneumoniae*. Optical images of the used bacteria for the experiment are shown in the inset corresponding SEM images. High magnification images showing the disruption of cell walls of the bacteria (d) *S. aureus* (e) *E. coli* (f) *K. pneumonia* as a result of antibacterial efficiency of the material

Antibacterial activity of CeO_2@AlOOH/PEI against *E. coli*, *K. Pneumonia* and *S. aureus* was further investigated using SEM microscopy. The CeO_2@AlOOH/PEI porous microbead was incubated with bacterial solution at room temperature for 1 h. It was found that large number of bacteria was attached and killed all through the time of contact with the bacterial solution (**Fig. 2.12.**). Slow disruption of bacterial cell wall was also clearly noticed form SEM (**Fig. 2.12.** d-f). Among the three tested bacteria, larger number of *K. pneumoniae* is adhered on the surface of the hybrid sorbent when

compared to other two test bacteria. Probably the reason for this is *K. pneumonia* cell surface consist of filaments with thin hair-like extension, as a result large number of it get adhered on the material surface. Hence, all these results indicates that it a promising material in removal of bacterial pathogens from water.

2.5. Conclusions

In summary, a novel multifunctional photocatalytic-sorbentCeO_2@AlOOH/PEI was developedby simple sol-gel synthesis route for adsorption and degradation of organic pollutants and micro-organisms. The monolithic photocatalytic sorbent can be designed in any dimension and shape to facilitate the separation from the treated waste water.The detailed investigation of the adsorption behaviour of the Photocatalytic sorbent revealed that the adsorption performance was mainly dominated by electrostatic, hydrogen bonding and Vander Waals interaction between the surface of the sorbent and the organic pollutants. The adsorption efficiency of CeO_2@AlOOH/PEI towards lignin and MO is about 95%and 98% respectively within the time interval of 30 min. The maximum adsorption capacity of the sorbent CeO_2@AlOOH/PEI towards lignin was 97 mgg^{-1}. We also found that the pseudo-second-order equation (R^2=0.99) gave the better correlation for the adsorption kinetics of lignin than the pseudo-first-order equation (R^2=0.97). The excellent Photocatalytic activity of CeO_2@AlOOH/PEI was found to retain under both sunlight and UV for lignin and MO. About 98% of lignin and 89 % of MO can be decomposed within the time interval of 100 and 120min with UV light irradiation.Also, more than 85% of both lignin and MO degraded under sunlight with an irradiation time of 100 min.The prepared hybrid AlOOH/PEI and hybrid

nanocomposite CeO_2@AlOOH/PEI shows the better adsorption and excellent antibacterial efficiency towards both gram positive and gram negative bacteria.

2.6. References

1. Zhao, S. P.; Zhou, F.; Li, L. Y.; Cao, M. J.; Zuo, D. Y.; Liu, H. T. Removal of anionic dyes from aqueous solutions by adsorption of chitosan-based semi-IPN hydrogel composites. *Composites Part B* **2012**, *43*, 1570-1578.
2. Amaral, F. M.; Kato, M. T.; Florencio, L.; Gavazza, S. Color, matter and sulfate removal from textile effluents by anaerobic and aerobic processes. *Bioresour. Technol.* **2014**, *163*, 364-369.
3. Colin, A. L.; Johannes, H.; Peter, C.; Michael, C. Photocatalytic active coatings for lignin degradation in a continuous packed bed reactor. *Int. J. Photoenergy* **2014**, doi.org/10.1155/2014/502326.
4. Zhang, S. X.; Zhang, Y. Y.; Bi, G. M.; Liu, J. S.; Wang, Z. G.; Xu,Q.; Xu, H.; Li, X. Y. Mussel-inspired polydopamine biopolymer decorated with magnetic nanoparticles for multiple pollutants removal. *J. Hazard. Mater.* **2014**, *270,* 27-34.
5. Andrew, D.; Lucian, A. L. Titanium Dioxide Catalyzed Photodegradation of Lignin in Industrial Effluents. *Ind. Eng. Chem. Res.* **2004**, *43,* 7996-8000.
6. Zulfikar, M. A.; Mariske, E. D.; Samitha, D. D. Adsorption of lignosulfonate compounds using powdered eggshell. *Songklanakarin J. Sci. Technol.* **2012**, *34,* 309-316.
7. John, D. N.; Bryan, S. M.; Corey, R. J. S. A Photochemical Strategy for Lignin degradation at room temperature. *J. Am. Chem. Soc.* **2014**, *136,* 1218-1221.
8. Dhrubojyoti, D. L.; Melvin, P. T.; Xiao wen, C.; Gregory, L. H.; Bin, Y. Noble-metal catalyzed hydro deoxygenation of biomass-derived lignin to aromatic hydrocarbons. *Green Chem.* **2014**, *16,*897–910.
9. Shi, B.; Li, G.; Wang, D.; Feng, C.; Tang, H. Removal of direct dyes by coagulation: The performance of preformed polymeric aluminum species. *J. Hazard. Mater.* **2007**, *143,* 567-574.
10. Chen, B.; Zhu, Z.; Liu, S.; Hong, J.; Ma, J.; Qiu, Y.; Chen, J. Facile hydrothermal synthesis of nanostructured hollow iron-cerium alkoxides and their superior arsenic adsorption performance. *ACS Appl. Mater. Interfaces* **2014**, 6, 14016-14025.
11. Zhu, X. D.; Liu, Y. C.; Zhou, C.; Zhang, S. C.; Chen, J. M. Novel and high-performance magnetic carbon composite prepared from waste hydrochar for dye removal. *ACS Sustainable Chem. Eng.* **2014**, *2,* 969-977.
12. Daniel, M.; Debora, N.; Anna, M.; Vanessa, T. F.; Vanessa, F. Removal of Lignin and Associated Impurities from Xylo-oligosaccharides by Activated Carbon Adsorption. *Ind. Eng. Chem. Res.* **2006**, *45,* 2294-2302.

13. Jenny, S. G.; Herbert, S. Regeneration of Spent Activated Charcoals Used for Lignin Removal from Pre hydrolysis-Kraft Pre hydrolyzates. *Ind. Eng. Chem. Res.* **2012**, *51,* 8624-8630.
14. Kerstin, I. A.; Marie, E.; Magnus, N. Removal of Lignin from Wastewater Generated by Mechanical Pulping Using Activated Charcoal and Fly Ash: Adsorption Kinetics. *Ind. Eng. Chem. Res.* **2011**, *50,* 7733–7739.
15. Zhao, D.; Chen, C.; Wang, Y.; Ma, W.; Zhao, J.; Rajh, T.; Zang, L. Enhanced Photocatalytic Degradation of Dye Pollutants under Visible Irradiation on Al(III)-Modified TiO_2: Structure, Interaction, and Interfacial Electron Transfer. *Environ. Sci. Technol.* **2008**, *42,* 308–314.
16. Amit, K.; Gaurav, S.; Naushad, M.; Pardeep, S.; Susheel, K. Polyacrylamide/$Ni_{0.02}ZnO_{0.98}$ Nanocomposite with High Solar Light Photocatalytic Activity and Efficient Adsorption Capacity for Toxic Dye Removal. *Ind. Eng. Chem. Res.* **2014**, *53,* 15549-15560.
17. Wang, Q.; Chen, C.; Zhao, D.; Ma, W.; Zhao, J. Change of Adsorption Modes of Dyes on Fluorinated TiO_2 and Its Effect on Photocatalytic Degradation of Dyes under Visible Irradiation. *Langmuir* **2008,** *24,* 7338-7345.
18. Kobayakawa, K.; Sato, Y.; Nakamura, S.; Fujishima, A. Photodecomposition of kraft lignin catalized by titanium dioxide. *Bull. Chem. Soc. Jpn.* **1989**, *62,* 3433-3436.
19. Ohnishi, H.; Matsumura, M.; Tsubomura, H.; Iwasaki, M. Bleaching of lignin solution by a photocatalyzed reaction on semiconductor photocatalysts. *Ind. Eng.Chem. Res.* **1989**, *28,* 719-724.
20. Amaresh, C. P.; Parida, K. M.; Binita, N. Enhanced photocatalytic and adsorptive degradation of organic dyes by mesoporous Cu/Al_2O_3–MCM-41: intra-particle mesoporosity, electron transfer and OH radical generation under visible light. *Dalton Trans.* **2011**, *40,* 7348–7356.
21. Farzana, M. H.; Meenakshi, S. Synergistic Effect of Chitosan and Titanium Dioxide on the Removal of Toxic Dyes by the Photodegradation Technique. *Ind. Eng. Chem. Res.* **2014**, *53,* 55-63.
22. Katie, B.; Yael ,D.; Isam, S. Synergetic effect between photocatalytic degradation and adsorption processes on the removal of phenolic compounds from olive mill wastewater. *water Res.* **2012**, *46,* 789-798.
23. Cordero, T.; Chovelon, J. -M.; Duchamp, C.; Ferronato, C.; Matos, J. Surface nano-aggregation and photocatalytic activity of TiO_2 on H-type activated carbons. *Applied Catalysis B: Environmental* **2007**, 73, 227-235.
24. Anthony, R. A.; Warwick, R.; Philip, C. A.; Nafty, V.; Peter, C. J.; Leone, S.; Daniel, N.; Jennifer, M. P. Functionalised pseudo-boehmite nanoparticles as an excellent adsorbent material for anionic dyes. *J. Mater. Chem.* **2008**, *18,* 2466–2474.
25. Linsha, V.; Suchithra, P.S.; Mohamed, A. P.; Ananthakumar, S. Amine-grafted alumino-siloxane hybrid porous granular media: A potential sol–gel sorbent for treating hazardous Cr(VI) in aqueous environment. *Chem. Eng. J.* **2013**, *220*, 244–253.

26. Tang, Z. –R.; Zhang, Y.; Xu, Y. –J. A facile and high-yield approach to synthesize one-dimensional CeO_2 nanotubes with well-shaped hollow interior as a photocatalyst for degradation of toxic pollutants. *RSC Advances* **2011**, *1,* 1772–1777.
27. Wong, F. L.; Azi, A. A. Development of crack-free alumina sol-gel/poly(vinyl alcohol) membranes for glucose oxidase immobilization, *Asian J. Chem. Eng.* ***2007***, *7,* 61–67.
28. Zhao, Z. -G.; Nagai, N.; Kodaira, T.; Hukuta, Y.; Bando, K.; Takashima, H.; Mizukami, F. Surface treatment- and calcination temperature-dependent adsorption of methyl orange molecules in wastewater on self-standing alumina nanofiber films. *J. Mater. Chem.* ***2011***, *21,* 14984-1498
29. Zhang, N.; Fu, X.; Xu, Y.-J. A facile and green approach to synthesize Pt@CeO_2nanocomposite with tunable core-shell and yolk-shell structure and its application as a visible light photocatalyst. J. Mater. Chem. **2011**, 21, 8152-8158.
30. Ai, Q.; Yang, D.; Zhu, Y.; Jiang, Z. Fabrication of Boehmite/Alginate Hybrid Beads for Efficient Enzyme Immobilization.*Ind. Eng. Chem. Res.* **2013**, *52* , 14898-14905.
31. Taobo, H.; Lan, X.; Shenlin, Z. Different nanostructures of boehmite fabricated by hydrothermal process:effects of pH and anions.*CrystEngCom.***2009**, *11,* 1338–1342.
32. Sana, N.;Katrin, K.;Aleeza, F.; Hatice, D.; Zehra, O.; Eylul, T.; Basit, Y.; Saadia, R.; Tariq, H. R. Design and Fabrication of Branched Polyamine Functionalized Mesoporous Silica: An Efficient Absorbent for Water Remediation. *Appl. Mater. Interfaces* **2014**, *6,* 4408-4417.
33. Xiaoyun, H.; Keith, B. M.; Pavel, N. N.; Dermot, B.; Brett, P.; John, H.T. L. Adsorption and Desorption of Methylene Blue on Porous Carbon Monoliths and Nanocrystalline Cellulose. *ACS Appl. Mater. Interfaces* **2013**, *5,* 8796-8804.
34. Zhang, Y. –X.; Yu, X. –Y.; Jin, Z.; Jia, Y.; Xu, W. –H.; Luo, T.; Zhu, B. –J.; Liu J.-H.; Huang, X.-J. Ultra high adsorption capacity of fried egg jelly fish-like γ-AlOOH(Boehmite)@SiO_2/Fe_3O_4 porous magnetic microspheres for aqueous Pb(II) removal. *J. Mater. Chem.***2011**, *21,* 16550–16557.
35. Liu, L.; Gao,Z. Y.; Su, X. P.; Chen, X.; Jiang, L.; Yao, J. M. Adsorption Removal of Dyes from Single and Binary Solutions Using a Cellulose-based Bioadsorbent. *ACS Sustainable Chem. Eng.* **2015**, *3,* 432-442.
36. Kabra, D.; Song, M. H.; Wenger, B.; Friend, R. H.; Snaith, H. J. High efficiency composite metal oxide-polymer electroluminescent devices: a morphological and material based investigation. *Adv. Mater.* **2008**, *20,* 3447–3452.
37. Kawabata, N.; Nishiguchi, M. Antibacterial activity of soluble pyridinium-type polymers. *Appl. Environ.Microbiol.* **1988**, *54,* 2532–2535.
38. Beyth, N.; Houri-Haddad, Y.; Baraness-Hadar, L.; Yudovin-Farber, I.; Domb, A. J.; Weiss, E. I. Surface antimicrobial activity and biocompatibility of incorporated polyethylenimine nanoparticles. *Biomaterials* **2008**, *29,* 4157–4163.

39. Pelletier, D. A.; Suresh,A. K.; Holton, G. A.; McKeown, C. K.; Wang, W.; Gu, B .; Mortensen, N. P.; Allison, D. P.; Joy, D. C.; Allison, M. R.; Brown, S. D.; Phelps, T. J.; Doktycz, M. J. Effects of Engineered Cerium Oxide Nanoparticles on Bacterial Growth and Viability. *Appl. Environ. Microbiol.* **2010***, 76,* 7981–7989*.*
40. Dumas, E. M. ; Ozenne, V. ; Mielke, R. E.; Nadeau,J. L**.** Toxicity of CdTe quantum dots in bacterial strains. *IEEE Trans. Nanobiosci.* **2009***, 8,* 58–64*.*

CHAPTER – 3

Natural CNSL Oil Crosslinked Boehmite (AlOOH) Hybrids: A New Effective Green-Electrode Design for Sensing Neurotransmitter Dopamine

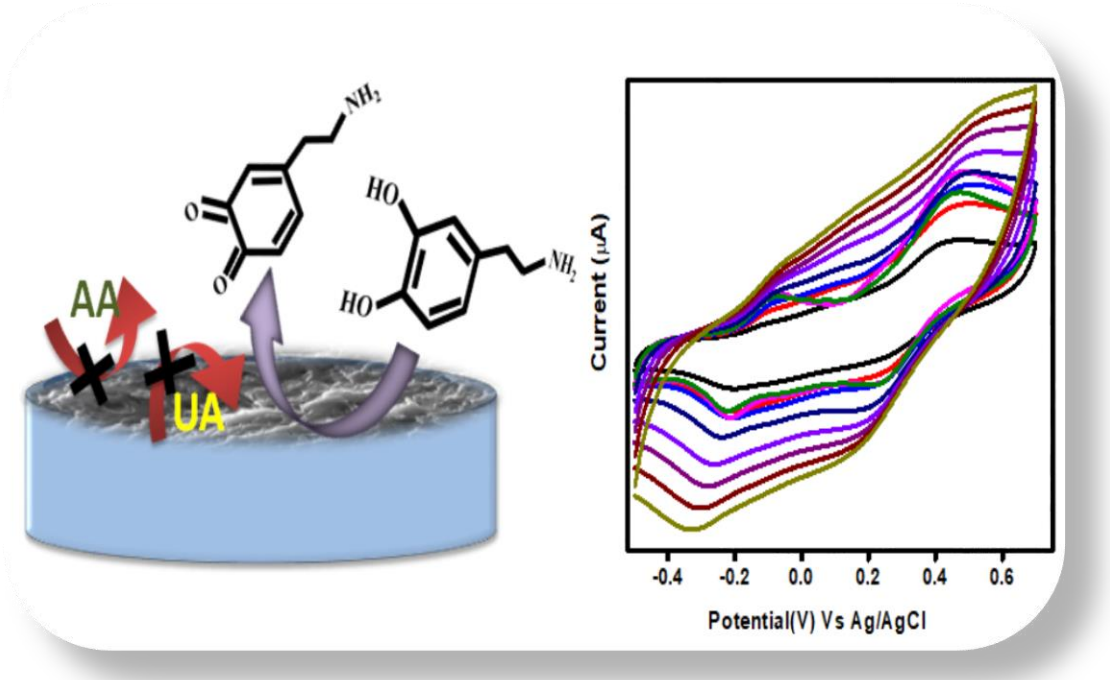

3.1. Abstract

A new inorganic-organic hybrid electrode assembly is designed out of the layered oxyhydroxy alumina (AlOOH) combined with natural plant derived oil, cashew nut shell liquid (CNSL) and reported for the first time for electrochemically detecting dopamine (DA). In this hybrid architecture,the presence of inherent meso/micro porosities in layered AlOOH and its active surface hydroxyl groups favourably generate synergistic effect with polyphenol functional groups in CNSL that promote diffusion of dopamine through $\pi-\pi$ interaction to catalytically oxidize the molecule showing sensitivity with accuracy. The study confirmed that this sensor design displays higher electro-catalytic activity toward DA oxidation with a wider linear detection range of 50 μM to 450 μM and a lower detection limit of 23×10^{-9} m. The efficiency of the sensor electrode was further examined in human blood serum. The results obtained in this study encourage that the designed 'green-electrode' can be used as an electrochemical sensor in the pharmaceutical and medical fields. The electro-catalytic performance and operational efficiency of this new hybrid sensor system was established using electrochemical impedance spectroscopy, cyclic voltammetry, and chronoamperometry tools. The present study is significant and futuristic because the organic electrode from CNSL oil is not only a value addition but also opened a way to fabricate lead and carbon free sensor devices.

3.2. Introduction

Neurotransmitters are endogenous chemicals that act as the messenger for the transmission of nerve impulses. Dopamine (DA) is an important neurotransmitter belonging to the catecholamine family ensuring a pivotal role in inter-neuronal communication.[1-3] Abnormal level of dopamine causes neurological diseases and therefore the concentration of dopamine in blood as well as urine is usually monitored

in the medical diagnostics.[1,4,5] To date, various analytical methods have been deployed for the determination of DA in vivo/vitro; includes high performance liquid chromatography, fluorescence spectrophotometry, capillary electrophoresis, UV-visible spectrophotometry, and enzymatic methods.[6-10] These techniques provide excellent selectivity in the detection of DA. However, due to the fascinating electroactivity of DA, its determination via electrochemical methods is seriously considered.[11- 14]

The sensing ability of the DA sensors highly depends upon their performance toward electro-catalytic oxidation of DA. Conventional bare electrodes have certain limitations to detect DA selectively and accurately due to electrode fouling and degradation of response. Moreover, DA concentration is extremely low in the extracellular fluid of the central nervous system making the detection a great challenge. Another difficulty in accurately monitoring the DA is due to a substantial interference of ascorbic acid that may cause serious misinterpretation of the medical diagnostics data.[15-17] Hence, it is very critical to develop highly efficient EDO catalysts. Surface modification of the electrode with a suitable material has been a strategy employed to obtain greater electrochemical accuracy. In this regard, researchers have screened series of materials ranging from conducting polymers, nanoparticle-polymer, metal, metal oxides, metal complexes, semiconductor nanoparticles, metal-organic frameworks to carbonaceous materials like graphene, carbon nanotubes (CNT), carbon fibre electrode (CFE), and carbon-paste electrode (CPE).[18-20]

Recent reports recommend materials possessing significantly large specific surface area and surface permeability, mesoporous structure can be considered for designing modified electrode assembly. [21-23] In this category, use of layered boehmite, a mono hydroxy aluminium oxide (AlOOH) is recently reported. It is a stable inorganic material preferred as a support for electrochemical sensor because of its chemical

resistance, layered nature, mechanical durability and transparency.[24, 25] More importantly, boehmite due to its surface hydroxyl groups and high surface area offers better chemisorption of analyte molecules. The high adsorption capacity of boehmite nanoparticles enhances the accumulation of analyte at the electrode surface during the fabrication of modified electrodes. The boehmite hydroxyl groups also provide endless possibilities for any functionalization making it a suitable substrate for the designing of hybrid electrochemical sensors.

In this work, new hybrid architecture is designed using oxy-hydroxy alumina, boehmite (AlOOH) and CNSL oil that surprisingly showed enhanced electrochemical response for the detection of dopamine. CNSL is an agro-industrial by-product from the cashew nut industry. Presence of reactive phenolic hydroxyl group and meta substituted unsaturated aliphatic chain in CNSL oil, it is considered to be very promising for the development of synthetic and functional products.[26-29] Earlier works show, CNSL is a feedstock for the production of a wide variety of organic/polymeric materials. The interest is growing to utilize CNSL and its components as green, non-toxic starting material for making of new molecules and products.[30, 31] As on today, CNSL oil finds industrial uses in coatings to obtain anti-fouling, anti-corrosive, and self-curing properties.[32, 33] To the best of our knowledge and also from the literature survey, it is confirmed that there is no reports on the application CNSL oil as such for the fabrication of electrode and electrochemical sensors.

Also, there are not many reports on boehmite for the modification of electrochemical sensors. A very few researchers published the electrochemical behavior of boehmite for electrochemical sensor application. Ganjali et al. studied the voltametric determination of dopamine using a glassy carbon electrode modified with ZnO/Al_2O_3 nanocomposite. [34] Ghalkhani M. et al. reported a design of multiwalled carbon

nanotubes combined with the boehmite nanoparticle, a modified composite electrode, and studied for the electrochemical sensitivity for catecholamines.[25] Wei et al. also used AlOOH@SiO_2/Fe_3O_4 magnetic microspheres for the electrochemical detection of toxic metal ions present in drinking water.[35] The clever combination of inorganic and organic nanomaterials leading to the development of a multifunctional system with enhanced properties may open a new possibility for utilizing hybrid materials as enhanced elements for constructing electrochemical sensing platform with high performance. This is because hybrid materials could provide larger electrochemically active surface areas for the adsorption of analyte and effectively accelerate the electron transfer between electrode and detection molecules, which could lead to a more rapid and sensitive current response. [36]

In this work, nano size boehmite particles were first obtained by the well-known sol-gel process .[37] The sol gel derived boehmite surface was further tailored with organic functional groups such as polyvinyl alcohol (PVA) and CNSL oil in order to increase the surface adsorption capacity. PVA is a water-soluble polymer, offers easy film-forming and notably good permeability characteristics .[38] Large number of OH groups present in PVA and CNSL oil could develop the electrostatic repulsion with the OH group present in the DA, and possibly increases the voltametric response. It is expected to show selective determination of DA even in the presence of ascorbic acid (AA). The synergistic effect of the AlOOH/CNSL oil hybrid assembly was systematically analysed for electrochemically sensing the dopamine. This demonstrative study is reported for the first time.

3.3. Experimental Section

3.3. 1. Materials

All reagents were used as received without any further purification. Aluminium isopropoxide [AIP] (purity ≥ 98%), Dopamine [DA ($C_8H_{11}NO_2$)], Caffeic acid [CA], Uric acid [UA], Ascorbic acid [AA], Glucose, and Blood serum were purchased from Sigma Aldrich. Formaldehyde [HCHO] (37%) was procured from Merck. Polyvinyl alcohol [PVA] (86-89% hydrolysed) was obtained from Alfa Aesar. CNSL oil was kindly supplied by Vijayalaxmi Cashew Company, Kollam, Kerala.

3.3. 2. Preparation of boehmite-CNSL hybrid

Firstly, AlOOH colloid suspension was prepared at pH 3 *via* Yoldas process according to the previous reported work.[37] Nano size boehmite powder was obtained by directly drying the colloid at 70 °C in an oven.10 wt.% PVA solution was prepared by heating PVA granules in distilled water at 80 °C for 4 hrs. In this typical synthesis, 3 mL of formaldehyde was added into 25mL of 10 wt.% PVA solution, followed by vigorous shaking for 30 min and subsequently 1g AlOOH nano powder was added to get the stabilized, homogeneous, boehmite colloid. With this resultant boehmite colloid, 1 g of CNSL oil was ultrasonically blended, resulting in the formation of a brown color, thick homogeneous, viscous hybrid gel. This hybrid gel was further used as a sensor material. All physio-chemical and electro-chemical characterizations were studied out of this hybrid gel. For convenience, this hybrid sensor thus obtained was given a notation as **PFAC** hybrid [*PVA/Formaldehyde/AlOOH and CNSL oil*].

3.3.3. Fabrication of the inorganic-organic hybrid electrode (PFAC/GCE)

Prior to the surface modification of glassy carbon electrode(GCE), it was mechanically polished with a BAS polishing kit assay. Then, the GCE was electrochemically pretreated using cyclic voltammetry (CV) in PBS solution (pH 7) at a potential scan rate (V) of 50

mV s^{-1}between -1.0 V and 1.0 V for 50 no. of cycles (n=50) for attaining the reproducible responses. After the pretreatment, a thin film of PFAC hybrid was coated on the surface of GCE by drop casting 2 µl of PFAC ultrasonically dispersed in ethanol medium. It was allowed to dry in air for 20 min at room temperature and cycling in the optimal potential window from -0.5 V to 1 V against Ag/AgCl. The PFAC hybrid modified GCE was designated as PFAC/GCE. For comparison, different concentrations of PFAC hybrids were fabricated using similar procedure. To prepare Dopamine immobilized electrodes, both the bare GCE and PFAC/GCE were immersed in PBS (pH 7) containing 1 mM Dopamine for 10 min. The immersed electrode was removed and washed with double distilled water to remove the PFAC/GCE surface bound Dopamine and potential cycled in the optimal potential window.

3.3. 4. Real sample preparation

For the Real Sample Analysis, 100 µL of human blood serum was ultrasonically homogenized with 10 ml of PBS at pH 7. The mixture was filtered and appropriately diluted with pH 7 PBS solution (dilution factor 1:5 ratio). 10 ml of the prepared real sample was taken, and DA was added at different concentrations from the real sample stock solution prepared with1 mM DA using a standard addition approach. DA quantification of real samples in the absence and presence of known concentrations of added DA was carried out using chronoamperometry.

3.3.5. Characterization

Rheology studies were conducted using stress-controlled Anton Paar Rheo Viscometer. PVA-Formaldehyde [PF] and PFAC hybrid gel were studied for rheology. X-ray powder diffraction (XRD) patterns of the hybrids were obtained with a Philips X'pert Pro X-ray diffractometer in the 2θ angle 10-80 ^{o}using Cu Kα radiation (λ= 1.54178 A°) under a voltage of 40 kV and current of 40 mA. Fourier transform infrared (FTIR) analysis was

performed using Shimadzu IR Prestige-21 spectrophotometer to understand the chemical interaction in theCNSL-AlOOH hybrids. The chemical interaction of the hybrid was analysed in the wavelengths 4000-400 cm^{-1}through transmittance mode. The thermal decomposition of PF and PFAC hybrids was investigated by Shimadzu TG-50 Thermo Gravimetric Analyser (TGA), between the temperature range of 100-800 °C at a constant heat flow of 10 °C min in the air atmosphere. The bulk micro-structural characteristics of the hybrids were examined using JEOL 5600 SL Scanning Electron Microscope (SEM). The surface chemistry of the prepared hybrids were analyzed using X-ray photoelectron spectroscopy (XPS, PHI 5000 VersaProbe II, ULVAC-PHI Inc., USA) equipped with micro-focused (200 μm, 15 KV) monochromatic Al-Kα X-Ray source (hν = 1486.6 eV). Both survey spectra and narrow scan (high-resolution spectra) were recorded. Survey scans were recorded with an X-ray source power of 50 W and pass energy of 187.85 eV. High-resolution spectra of the major elements were recorded at 46.95 eV pass energy.

3.3.5.1. Electrochemical characterization

Cyclic voltammetry (CV) and Amperometric studies were performed using SP-300 electrochemical workstation from Biologic Instruments Inc., France. Electrochemical impedance spectroscopy (EIS) measurements were performed using ZSimpWin Software. A conventional three electrode system was used for electrochemical detection with glassy carbon electrode (GCE) as the working electrode, a saturated Ag/AgCl as a reference electrode and a Platinum(Pt) wire as the counter electrode.

3.4. Results and Discussion

Sol gel derived, PVA stabilized hydroxy alumina colloid maintained at pH~3 turns to viscous gel when the natural CNSL oil is slowly blended. The possible governing

chemical interaction and mechanism that involved in this new hybrid gel is schematically illustrated in **Fig.3.1**. PVA is a known aqueous polymeric stabilizer having large number of inter and intra molecular hydrogen bonds.[38, 39] Similarly, nanoparticulate boehmite also contains highly reactive surface –OH groups.[40] Therefore, the hydroxy alumina offers strong chemical interactions such as electrostatic attraction and hydrogen bonding with the PVA-formaldehyde (PF) moieties. CNSL, a by-product from cashew industrial processing and one of the richest natural sources of phenolic compounds, such as anacardic acids (60–70 %), cardols (10–20 %), cardanols (3–10 %), 2-methylcardols (2–5 %), and other minor constituents.[41] Direct blending of CNSL oil into the AlOOH-PF (PFA) matrix induces the integration and crosslinking of CNSL through the H-bonding and gradually forms a massive network structure with a great deal of crosslinking and interweaving. **Fig.3.2.** shows the physical state of the different blends of PVA-Formaldehyde [PF], PVA-Formaldehyde-colloidal alumina [PFA], PVA-Formaldehyde - CNSL oil [PFC], and finally the CNSL blended PVA-Formaldehyde-colloidal boehmite [PFAC] hybrid. It can be visually seen that a homogenous chemical interaction followed by slow transformation into a thick bulk gel is successfully formed only in CNSL blended [PFAC] system that indicates the CNSL oil is an organic gelator. Interestingly the transition of flowing colloidal medium into stable gel is a gradual effect and in this study, the stable 3D gel is formed only after 96 hours.

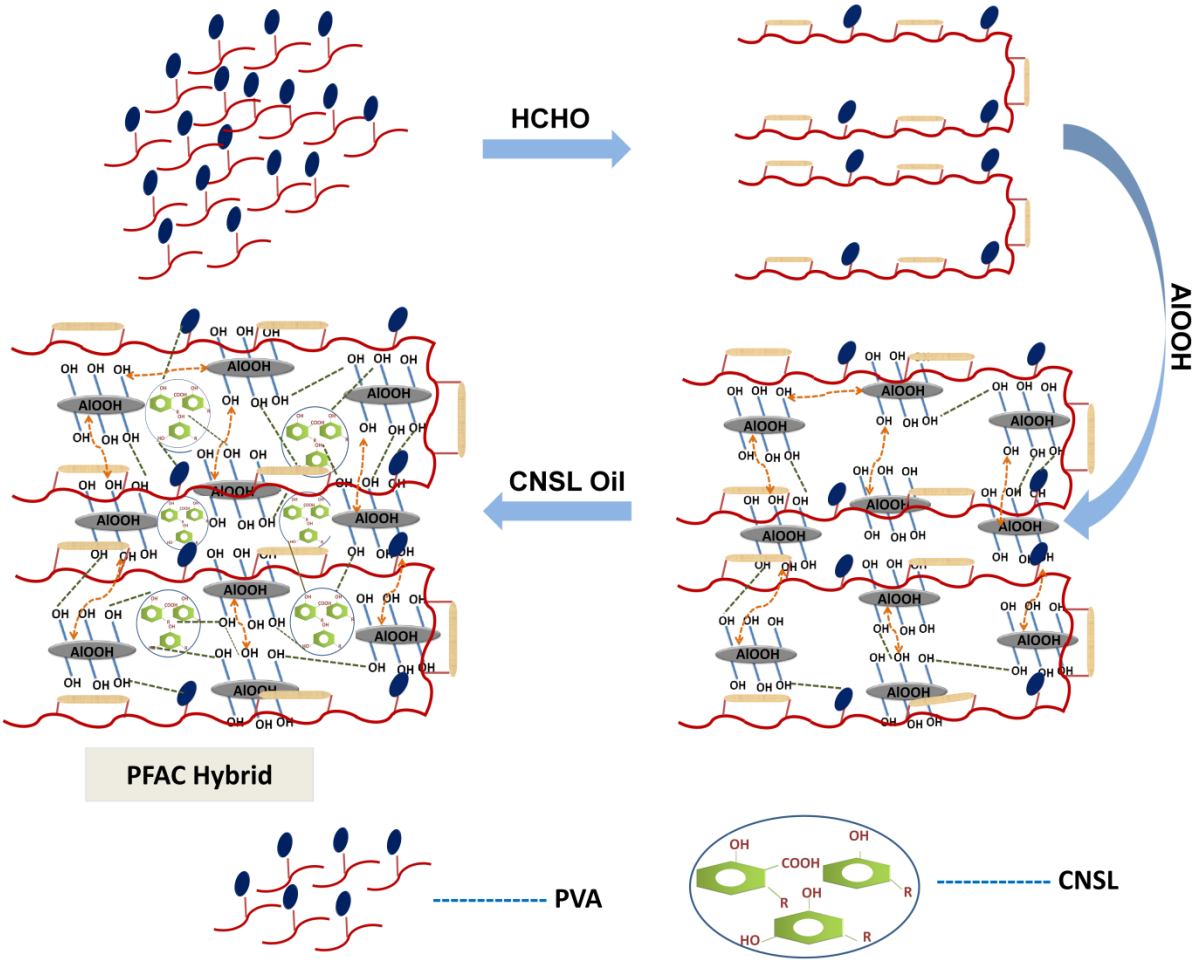

Fig.3.1. Preparation of Hybrid PFAC

The rheology of the pure PF, PFA, PFC, and PFAC hybrid gels were carefully monitored to understand the chemical interaction, cross linking, and gelation properties. **Fig.3.2.(a&b)** shows the viscosity trends at different shear rates. Pure PF and PFA samples showed very low viscosity and no change with increasing shear rate. A negligible increase in the shear stress with respect to shear rate is also seen. The low viscosity data observed with PF, PFA, and PFC confirmed, no significant chemical interaction when the colloidal alumina and CNSL oil is blended independently. However, the viscosity as well as shear stress is completely changed in case of PFAC where the hydroxyl alumina and CNSL oil is blended with PVA-formaldehyde. At low shear rates the viscosity is very high and it is decreasing with increasing shear rates. In

PFAC, the gel shows 'shear thinning' flow behaviour. The PF, PFA, and PFC, either effective chemical interaction or the polymerization to form the hybrid gel. While in PFAC, the gradual decrease in viscosity with shear rates confirm, the applied shear force disintegrates the interconnected hybrid network into single fragments and distributes them uniformly in the medium. It is evident from the viscosity study that the CNSL oil chemically interact with AlOOH-PVA-Formaldehyde through hydrogen bonding and electrostatic interaction that successfully form the PFAC hybrids.

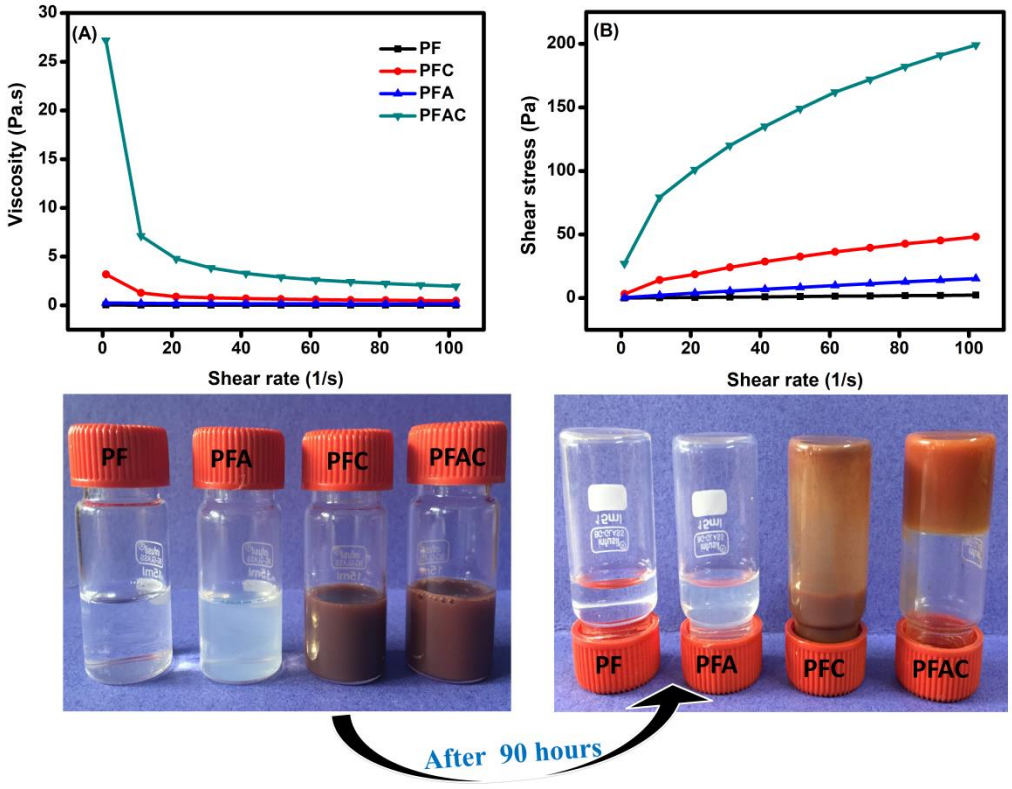

Fig.3.2. Variation of shear rate with (a) viscosity and (b) shear stress, and the photographic images of the hybrids at time 0 sec and after 90 hrs

Fig. 3.3.A. presents the XRD analysis of the films made from PF, PFA, PFC, and PFAC hybrid. In pure PF (**Fig. 3.3.A.(a)**), two broad diffraction peaks at 2θ values 19.6° and 40.8°can be indexed to the Bragg reflection planes (101) and (111) corresponds to crystalline nature of PVA. [42] In the system PFA (**Fig. 3.3.A.(c)**), the broad diffraction

peaks at 2θ values 14.2°, 27.8°, 38.3°, 49.1°, and 64.1° can be indexed to the Bragg reflection planes (020), (120), (031), (200), and (231) of orthorhombic crystalline boehmite.[43] These diffraction peaks are closely matching with the standard pattern reported for the boehmite (JCPDS card 21-1307). In PFC system (**Fig. 3.3.A.(b)**), the corresponding crystalline peak at 2θ =19.6°a notable change is seen. In PFC as well as PFAC hybrids, the peak width is broadened and the intensity decreased indicating the bulk effect of CNSL organic moiety. Comparatively, the less intense and broad peaks present in PFC and PFAC indicates the CNSL oil not only chemically interact but also changes the crystallinity of hydroxyl alumina colloid in the hybrid system.

The chemical interaction is further confirmed by FTIR spectroscopy. The FTIR spectra of pure PVA and formaldehyde (PF), and PF hybridized with CNSL, and boehmite are shown in **Fig.3.3.B.** Several changes in the spectral features were observed when the comparison is made with the FTIR spectra of pure PF with PFAC hybrids. The peak centered at 3307 cm^{-1} assigned to the stretching vibration of hydroxyl groups (-OH) of pure PF was shifted to 3336, 3341, and 3345 cm^{-1} in PFC, PFA, and PFAC systems, which indirectly indicates the specific interaction of CNSL and AlOOH. In addition to this, the C–H stretching of CH_2 which showed absorption at 2928 cm^{-1} both in the case of pure PF and its hybrids. The peak at 1730 cm^{-1}corresponding to C=O stretching of PVA in PF was shifted to lower wave numbers in the hybrid system. [44] The peak at 1434 cm^{-1} corresponds to C–H bending of pure PVA.[44] This peak is shifted to higher wavelength region in hybrid systems. The vibration of CH_2 group was found at 1378 cm^{-1} corresponding to C–H wagging in pure PF and it was shifted to higher wave numbers in the complexed systems. The C–C stretching vibration of PF appearing at 1248 cm^{-1} was shifted to 1239 cm^{-1} in hybrid systems. C–O stretching occurred at 1016 cm^{-1} in PF and it was shifted to 1090 cm^{-1} in

hybrids. This clearly showed that the interaction between the pure PF, CNSL and AlOOH. The vibration peak appearing at 840 cm^{-1} assigned to C–H rocking mode of PF. Also, new peaks at 1066 cm^{-1} which was found in PFA hybrid could be attributed to the Al-O-Al stretching vibration.[45]Hence, from the FTIR analysis, the hybrid formation between PF, CNSL, and AlOOH was confirmed.

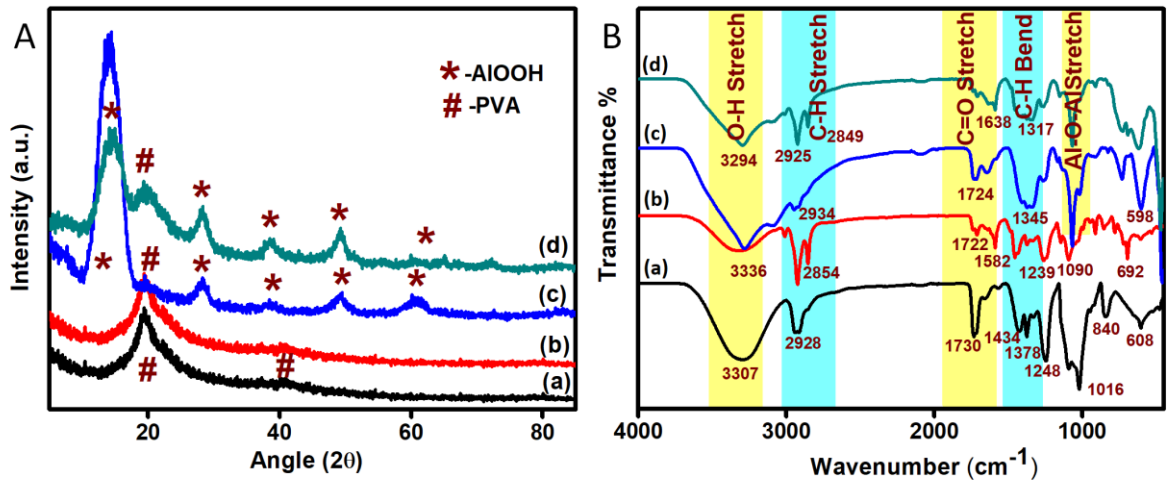

Fig.3.3. A. XRD patterns of pure PF and its hybrid B.FTIR spectra of pure PF and its hybrids

Further, investigation on the reaction of AlOOH with PF and CNSL was carried out using XPS analysis on both boehmite and PFAC hybrid (**Fig.3.4.).**The XPS survey spectra of AlOOH show signals corresponding to O 1s, Al 2s, Al 2p, and low-intensity C 1s (**Fig. 3.4.A.**).The presence of the C 1s signals may be owing to the adsorption of carbon dioxide (CO_2) or the presence of a trace amount of carbonaceous contaminants on the surface of AlOOH nanoparticles and the signal was weak. The XPS wide scan spectrum of PFAC hybrid depicted in **Fig.3.4.B**. The presence of enhanced C 1s signal is an indication of the hybrid nature of the surface of the material, involving PF and CNSL oil. For further study, high-resolution XPS O1 s and Al 2p spectra of AlOOH and PFAC hybrid were analyzed. In **Fig.3.4.C.,**the O 1s binding energy peak of AlOOH showed the two different oxygen species: a binding energy of 530.12 eV is from the crystal structure

(Al-O-Al), and 531.34 from the hydroxyl groups (Al-O-H).[46] Thus, based on the integral area of the peaks, it can be inferred that, more O elements exist in the form of surface hydroxyl group rather than Al-O-Al in the AlOOH structure. These signals were shifted towards binding energy (BE) of 531 & 531.32 eV for the PFAC hybrid sample (**Fig. 3.4.D.).**The Al 2p signal in pristine AlOOH could be deconvoluted into two types of chemical environments with binding energies at 74.88 and 73.81 eV, which are associated with the chemical bonds of Al–O–Al and Al–OH, respectively (**Fig. 3.4.E.).** [47]n the case of PFAC hybrid, only one peakis observed in the deconvoluted Al 2p spectrum at 73.94 eV (**Fig. 3.4.F.)**, which is probably due to the hybrid formation through the free surface Hydroxyl group. The removal of oxygen containing functional groups could ensure the good electrical conductivity of PFAC hybrid, which was formed conductive networks between adjacent AlOOH nanoparticles, PF, and CNSL oil. [48]

The structural morphology of the prepared alumina hybrid coating investigated through SEM analysis. **Fig.3.5.** shows the cross sectional SEM images of the pure PF and the hybrid film. The images(**Fig.3.5. a.**) indicates that the section of the pure PF film has less visible surface roughness with cell boundaries compare to that of the other hybrids. In the case of the surface of the PFA coating, it is comparatively smoother with very little bulging than PFC and PFAC. This is due to the difference in the properties and structure of the component presents in hybrid system, thus, giving unique properties to each of them. Upon hybridization with CNSL (PFC), the surface of film is found to have spherical like network, while in PFAC hybrid showed spherical coral surface framework.

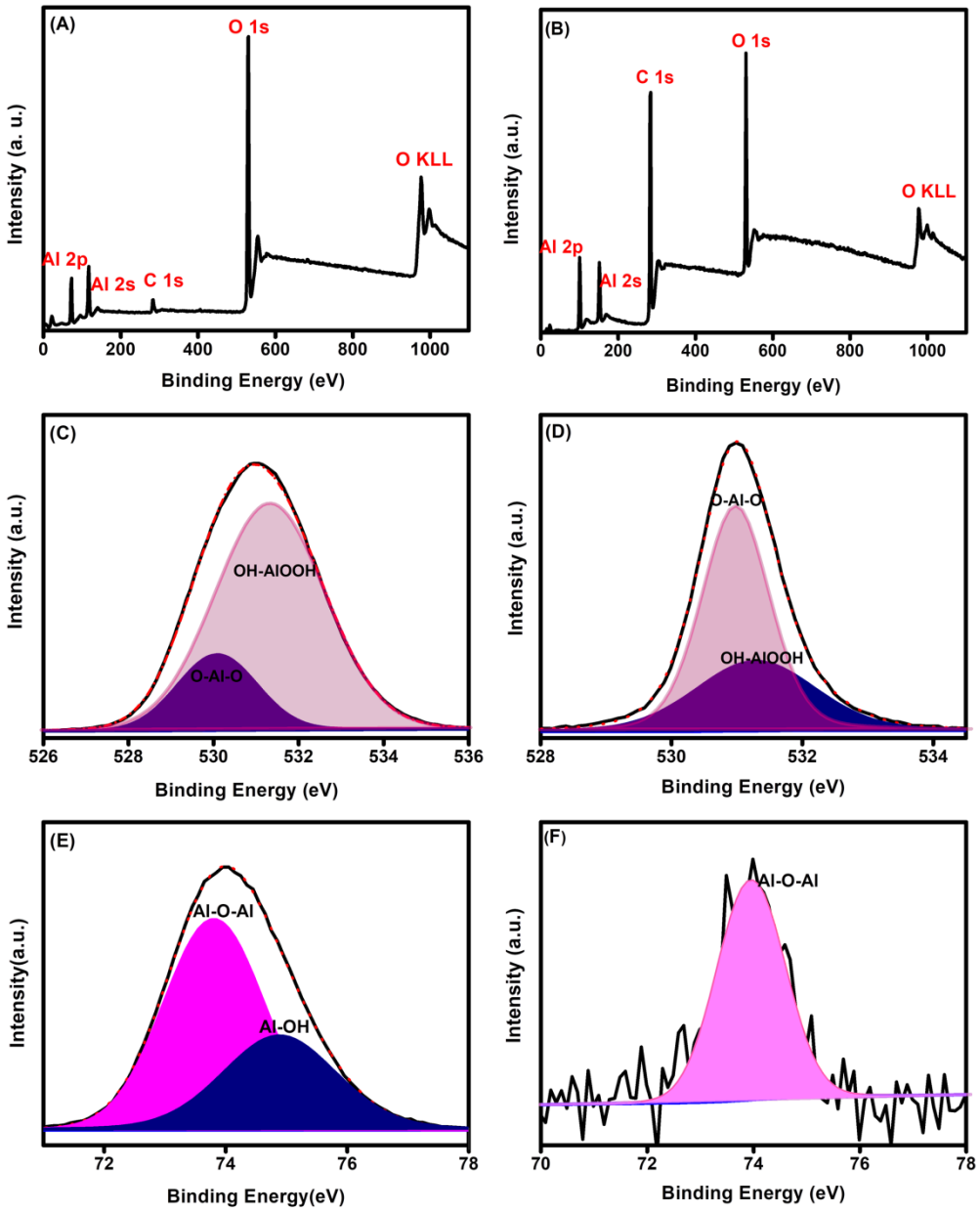

Fig.3.4. XPS spectra of (A) pure AlOOH, (B) PFAC Hybrid, (C) and (D) O1 S Spectra of boehmite and PFAC, and (E) and (F) Al 2p Spectra of boehmite and PFAC

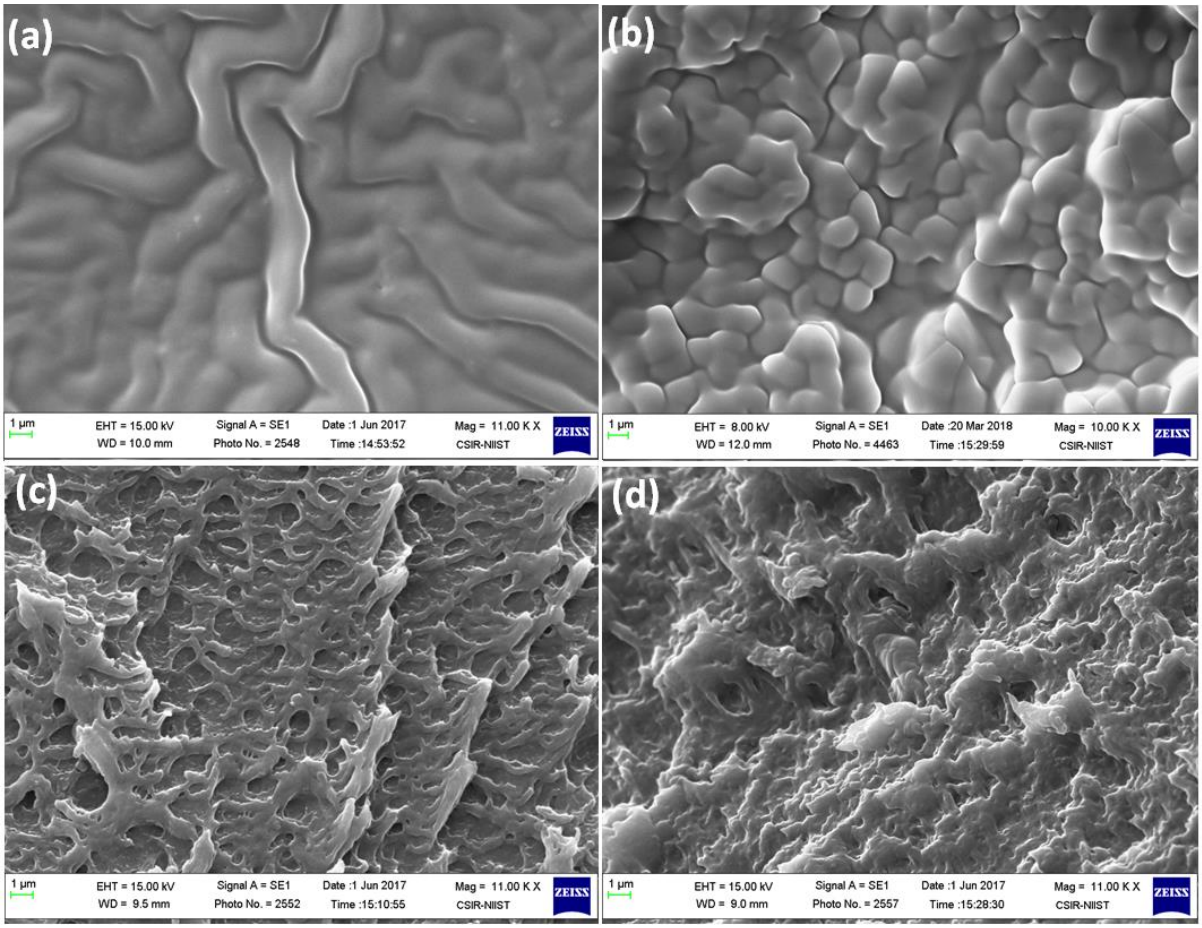

Fig. 3.5. SEM images of (a) pure PF resin, (b) PFC, (c) PFA, and (d) PFAC hybrids

3.4.2. Electrochemical activities of unmodified and PFAC modified GCE

The Electrochemical Impedance Spectroscopy (EIS) is a powerful technique to examine the electron charge transfer properties of unmodified and modified electrodes in 0.1 M KCl containing 2 mM potassium ferricyanide $K_{2/3}$ ($[Fe(CN)_6]^{-3/-4}$) at an applied frequency range from 1 MHz to 0.1 KHz and an amplitude of 10 mV.[49] **Fig.3.6.** shows the Nyquist plot of bare GCE, PF/GCE, PFC/GCE, PFA/GCE, and PFAC/GCE. In a typical Nyquist plot, the semicircle portion represents the electron-transfer resistance (R_{ct}) at higher frequency range while a linear part at lower frequency range corresponds to the diffusion limited process. Randle's-equivalent circuit model was proposed to simulate the experimental data, which comprises of electrolyte resistance (R_s), double layer

capacitance (C_{dl}), charge transfer resistance (R_{ct}) and Warburg impedance (Z_w). As seen in **Fig.3.6**,PFAC/GCE exhibits low charge transfer resistance (R_{ct}) and high conductivity than unmodified GCE. The exhibited R_{ct} value is only 8.046 Ω which is comparatively lower than the other electrodes such as bare GCE (10.47 Ω), PF/GCE (12.3 Ω), PFC/GCE (12.71 Ω), and PFA/GCE (10.37 Ω). These results clearly confirmed that the synergistic effect of inorganic AlOOH particle and organic functional moiety CNSL oil, offer a better electrochemical catalytic behavior, thus resulting in the rapid electron-transfer process on the GCE surface.

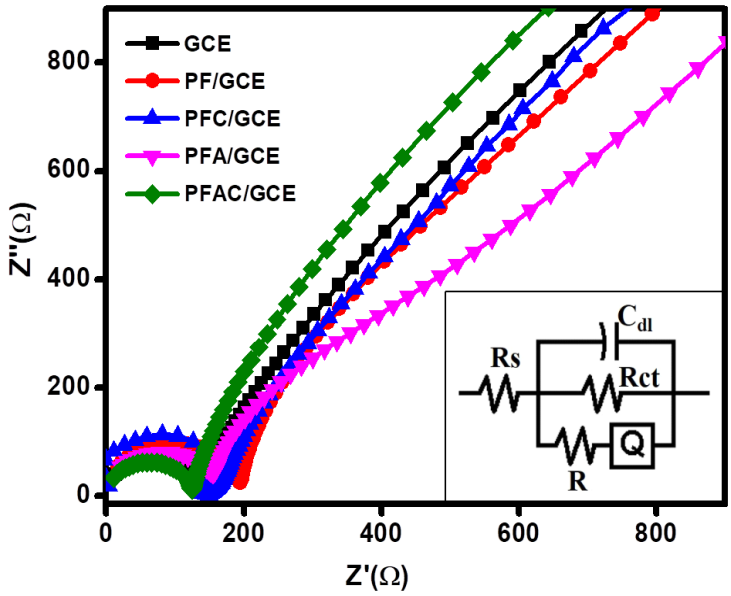

Fig.3.6. EIS spectra of (bare GCE, PF/GCE, PFC/GCE, PFA/GCE and PFAC/GCE in the presence of 2 mM $K_{2/3}[(Fe(CN_6)^{-3/-4}]$ in 0.1 M KCl

Redox couple of ferri-ferro cyanide was selected to study the electrochemical behavior of unmodified and modified electrodes. **Fig.3.7.A.** displays the CV responses of the bare GCE, PF/GCE, PFC/GCE, PFA/GCE, and PFAC/GCE in the presence of 2 mM $K_{2/3}[(Fe(CN)_6]^{-3/-4}$ in 0.1 M KCl at υ=50 mV s-1. The typical quasi-reversible one-electron redox behavior of ferricyanide ions was observed in all the modified

electrodes. Remarkably, PFAC/GCE showed the improved electrochemical response to employed probe in comparison with bare GCE, and other modified electrodes. For a reversible reaction, the peak current ratio must be equal to 1.[50]Furthermore, the calculated apparent standard electrode potential ($E_o' = E_{pa}+E_{pc}/2$) values for bare GCE, PF/GCE, PFC/GCE, PFA/GCE, and PFAC/GCE were found to be 455.9, 476.5, 432.1, 430.8, and 301 mV respectively. Obtained results exhibited the best response, smallest E_o' and the highest peak current value for PFAC modified electrode. These results indicating that the combination of the AlOOH nanoparticle and organic CNSL oil played a key role in the increase in electrostatic attraction of the ferri/ferrocyanide ions toward modified electrode surface and thus providing the conducting bridges for the electron-transfer of $Fe(CN)_6^{-3/4}$. Further, investigated the influence of scan rate on the voltametric response of PFAC/GCE in supporting electrolyte of $[Fe(CN)_6]^{-3/-4}$) by varying the scan rate from 10 to 100 mV s^{-1} as represented in **Fig. 3.7.B**. Obviously, The CV curve was linearly enhanced with increasing scan rate. A linear relationship was obtained between oxidation peak current (I) against the square root of scan rate (v) was found with a correlation coefficient of 0.99(Inset **Fig. 3.7.B**.). In addition to that, the electrochemically active surface area, A_e (cm^2) for a reversible electrochemical process under the diffusive control system (T =25 °C) were calculated using the Randels-Sevcikequation.[51] The obtained A_e values of bare GCE, PF/GCE, PFC/GCE, PFA/GCE, and PFAC/GCE were estimated to be 0.076 cm^2, 0.016 cm^2, 0.082 cm^2, 0.086 cm^2, and 0.124 cm^2. This clearly indicates that the hybrid PFAC typically exhibit enhanced electrochemically active surface area, which is noticeably different from those of the individual constituents. Hence, the above electrochemical studies confirm that the PFAC-modified GCE has exceptional electrocatalytic activity.

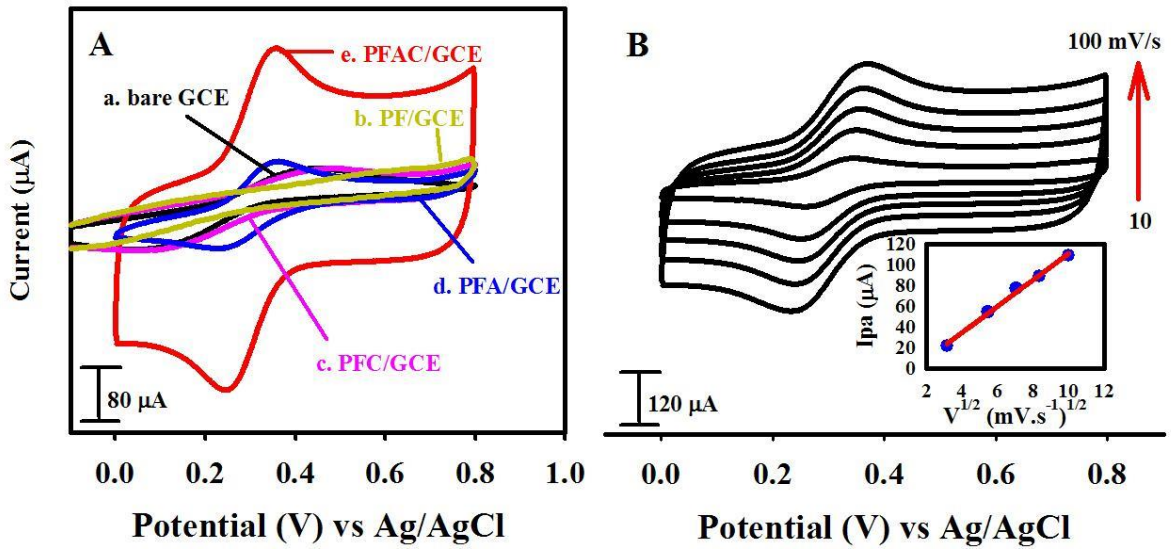

Fig.3.7. (A) CV responses of (a) bare GCE, (b) PF/GCE, (c) PFC/GCE, (d) PFA/GCE, and (e) PFAC/GCE. (B) Effect of various scan rates on PFAC/GCE (inset shows the calibration plots of I_{pa} Vs $\upsilon^{1/2}$) All in the presence of 2 mM $K_{2/3}[(Fe(CN_6)^{-3/-4}]$ complex containing 0.1 M KCl at υ=50 mV $.s^{-1}$

To explore the practical viability of PFAC hybrid, DA was chosen as characteristic probe to investigate their electrochemical behavior. **Fig.3.8.A**. showed the cyclic voltammogram (CV) of bare GCE, PF/GCE, PFC/GCE, PFA/GCE, and PFAC /GCEbetween the potential windowof -0.5 to 0.7 V vs Ag/AgCl in pH 7 PBS solution, containing 500 µM DA. A lower oxidation peak raising from 0.3 V vs Ag/AgCl until 0.45 V was obtained for bare GCE (curve a) with a maximum detection current of 2.87 µA. As we can see, the oxidative current of DA has significantly increased with modified electrodes, PF/GCE, PFC/GCE, PFA/GCE, and PFAC/GCE were found to be 13.78 µA, 25.11 µA, 31.18 µA, and 108.4 µA at 0.58 V, 0.59 V, 0.425 V, and 0.423 V(**Fig.3.8.A.(b-e)**). The PFAC/GCE electrode resulted in large faradaic currents with broad reduction peaks near -0.2 V as shown in **Fig.3.8.A.** This may be due to increased oxygen sites (hydroxyl group) present in the AlOOH and CNSL oil (in PFAC), which helps to improve electrical reduction of DA.[52] Interestingly, a shift in the peak potential towards lower value (0.423 V) was observed for the PFAC/GCE when compared to the other electrodes. This confirms the

faster electron transfer between dopamine and electrode surface due to, the π–π stacking interaction between the DA and CNSL oil. The synergy between hydroxyl rich porous AlOOH and aromatic CNSL oil present in PFAC hybrid, fabricate it a greater electron promoter and a promising supporting electrode material. From the above results, it was anticipated that PFAC hybrid could be an excellent material for electrochemical sensing of Dopamine.

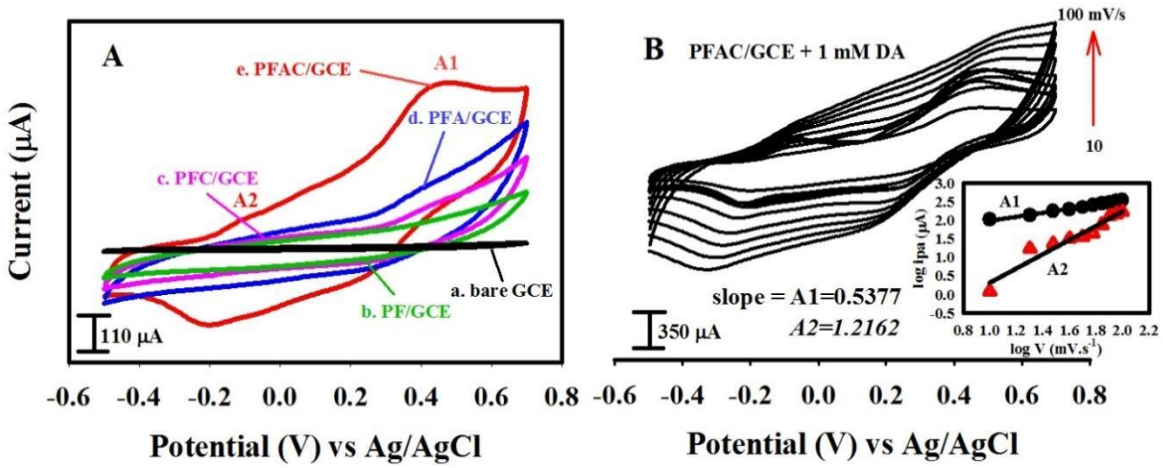

Fig.3.8. CV responses of (A) (a) bare GCE, (b) PF/GCE, (c)PFC/GCE, (d)PFA/GCE and (e) PFAC/GCE in the presence of 1 mM of DA, in 0.1 M PBS solution (pH 7.0) at υ = 50 mV s^{-1} and (B) PFAC/GCE for υ = 10–100 mV s^{-1}, inset is the calibration plot for log υ Vs log I_{pa}

To further scrutinize the mechanism and kinetics of the electron transfer reaction at the electrode, whether it is diffusion or adsorption controlling, the scan rate (v) dependent CV on PFAC/GCE was performed in PBS solution consisting of 300 mM DA in the range of 10–100 mV s^{-1}. It can be observed from the **Fig.3.8.B**, the oxidation and reduction current of DA at the electrode increased with the increment of scan rate, although their peak potential value gradually shifts to more positive and negative directions. The peak potential separation (ΔE_p) becomes higher with increasing scan rate due to the increased irreversibility of the electrode process. [53]Moreover, a good linear relationship between peak currents (log I) and the square root of the scan rate

(log $v^{1/2}$) with a correlation coefficient of 0.52 was also observed(**Fig.3.8.B** (inset)). These results indicating that DA oxidation at PFAC electrode is a typical diffusion-controlled electrocatalytic process.[54]

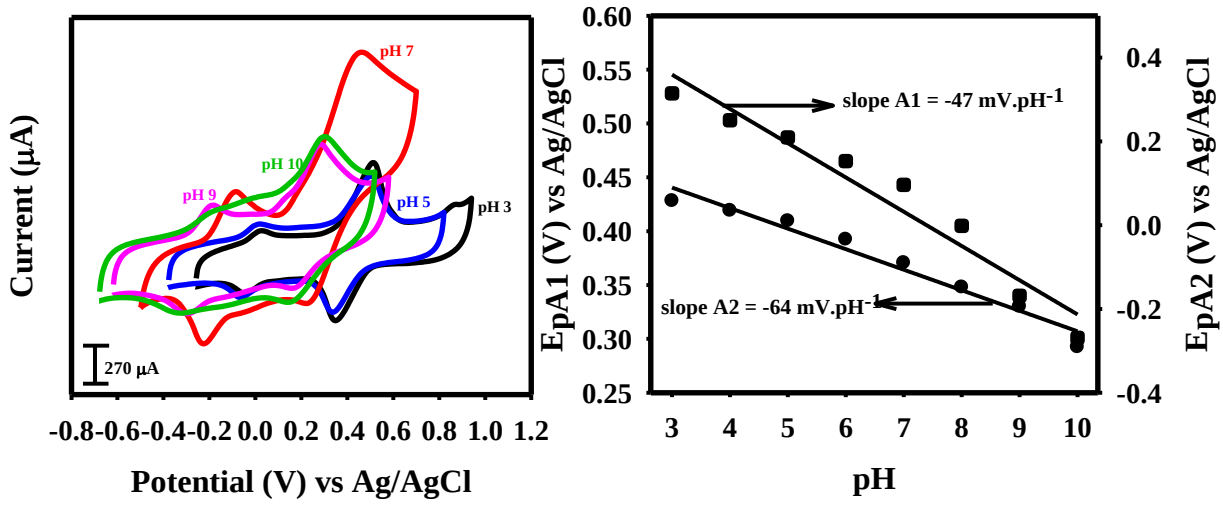

Fig.3.9. (A) Effect of pH on PFAC/GCE for n =1 in 1 mM DA at υ = 50 mV s^{-1}(B) The calibration plot between E_{pa} Vs pH

The pH of the supporting electrolyte solution takes part in determining the electrochemical response of DA. We further examined the effect of pH on the electrochemical response of DA at PFAC/GCE modified electrode in 0.1M PBS containing 300 µM DA in the pH range of 3- 10 at a scan rate of 50 m V/s (**Fig. 3.9.A.**). A well-defined redox couple of DA was obtained for different pH values. From the graph (**Fig. 3.9.A.**), it is clear that the oxidation and reduction peak potentials shifted toward the negative values with the increase of electrolyte pH. Also, the redox peak of DA reaches a maximum at about pH=7, specifies that the DA electrocatalysis at the PFAC/GCE electrode is a pH dependent reaction and pH 7 selected as the ideal condition for the electrochemical detection of DA. **Fig. 3.9.B.** displays the calibration plot of anodic and cathodic peak potential Vs different solution pH. The slope of plots of E_{pa} Vs pH and E_{pc} Vs pH were found to be -47 mV at pH-1 and -64 mV at pH-1, which is close to the

Nernstian value (−59 mV/pH at 25 °C), for electrochemical reactions involving an equal number of protons and electrons. The electrochemical reaction of DA at the PFAC/GCE electrode can be expressed as in **Fig.3.9.** Therefore, we can conclude that PFAC has exceptional electrocatalytic behavior towards the oxidation of DA in 0.1M PBS with a pH of 7, and preferred for the subsequent experiments.

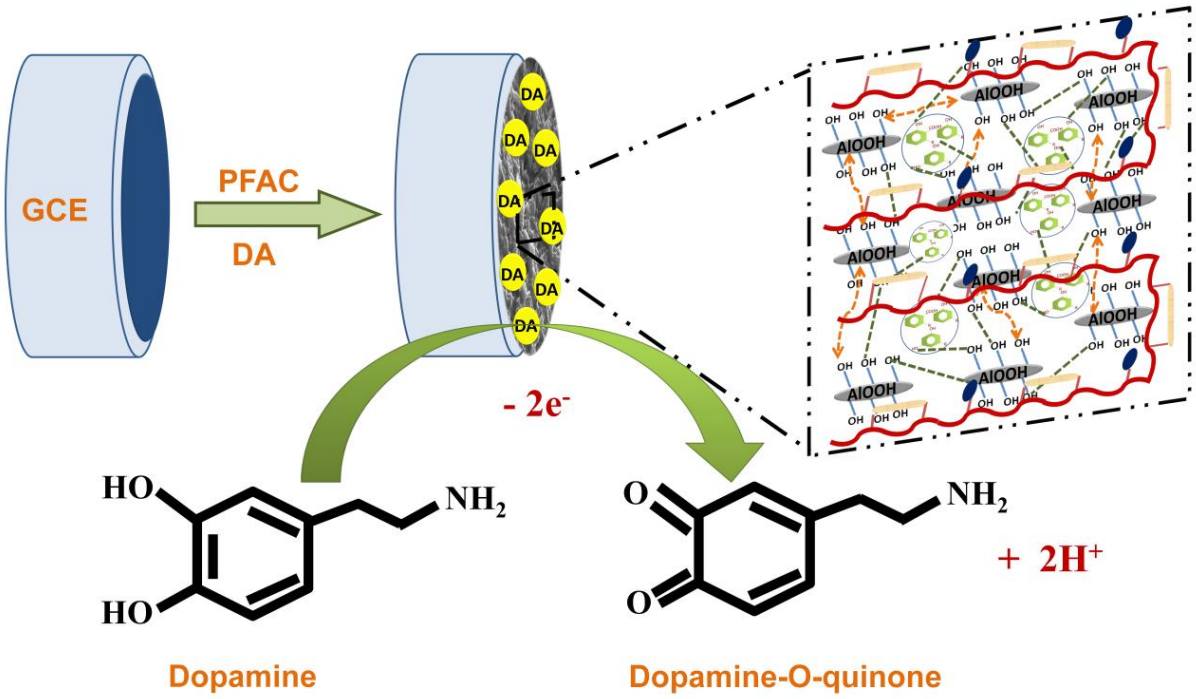

Fig.3.10. Electrochemical oxidation mechanism of dopamine on PFAC/GCE electrode

Repeatability, reproducibility, and stability of thePFAC were also evaluated by determining the redox reaction of DA, in 0.1 M PBS containing 300 μM DA. Repeatability of the results was studied by performing ten replicate cycles withthe same electrode, refreshed after each measurement. The relative standard deviation (RSD) of 0.87% (**Fig.3.11.B.**) was attained, indicating high precision in repeatability of the PFAC/GCE electrode.This level of accuracy is a need for routine quality control analysis.Furthermore, to investigate the reproducibility of the results five independent identical electrodes were fabricated. It was found that the oxidation peak currents of DA did not show any significant change. The remarkable reproducibility for the proposed

electrode was confirmed by obtaining the relative standard deviation (RSD) of 1.18% for the redox currents(**Fig. 3.11.C.**).To evaluate the stability, a series of 500 continuous measurements of the PFAC/GCE electrode response in the experimental condition was performed. As we can see in **Fig. 3.11.A.**, the peak current of the DA is 90% of the initial value, which indicated a good stability of PFAC/GCEelectrode. In addition, the long term stability of the sensor was also explored without regenerating the surface time after time. The response to DA was measured every 5 days after stored at 4 °C and showed satisfied performance as original. These result suggested that the PFAC/GCE sensor exhibited good repeatability, reproducibility and stability. Therefore, the PFAC/GCE displays the potential for detection of DA in environmental samples with favorable characteristics.

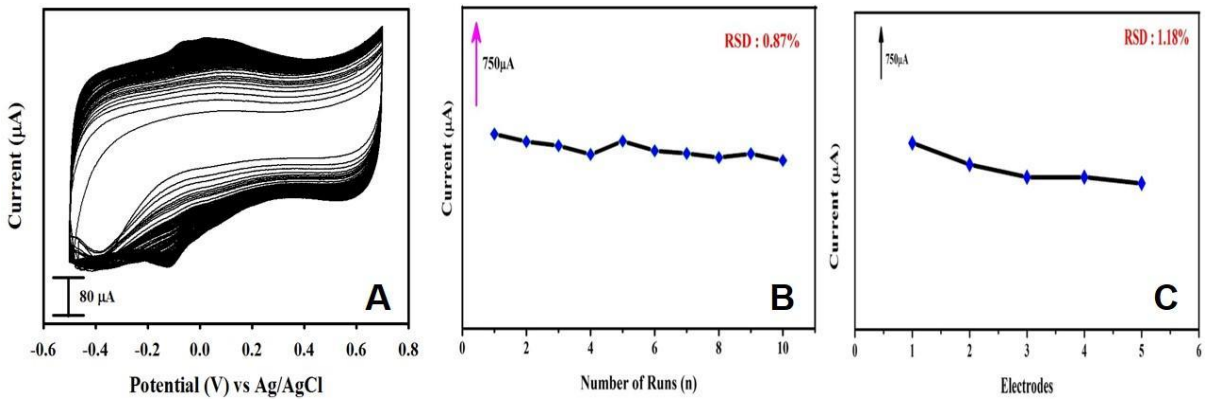

Fig.3.11.(A) CV responses of the same PFAC/GCE under optimal conditions in the blank pH 7 PBS for 500 continuous cycles (B) Current responses of the same PFAC/GCE subjected to CV for 10 cycles per day for 10 days in 500 µM DA under optimal conditions. (C) Current responses of five different PFAC subjected to CV for 10 cycles per electrode in 500 µM DA under optimal conditions

Fig.3.12. displays the amperometric curve for DA oxidation at PFAC/GCE with the successive injection into homogeneously stirred (200 rpm) 0.1M PBS solution at a fixed potential of 0.423. A stable amperometric response could be detected within 400 s after the addition of DA. Then the current response increased linearly with every successive addition of DA from 50 µM to 450 µM (the inset of **Fig.3.12.**) with a correlation

coefficient (R^2) of 0.9937 and sensitivity value is 0.0219 μA/μM. Besides, the limit of detection (LOD) was found to be 23 nM. The linear range of DA detection and the LOD of PFAC/GCE towards DA oxidation were compared with the recent reports and were presented in **Table 3.1**. Compared to the previous reports, our sensor provided higher electrocatalytic performance with a wide linear detection range, low detection limit towards electro-oxidation of DA.

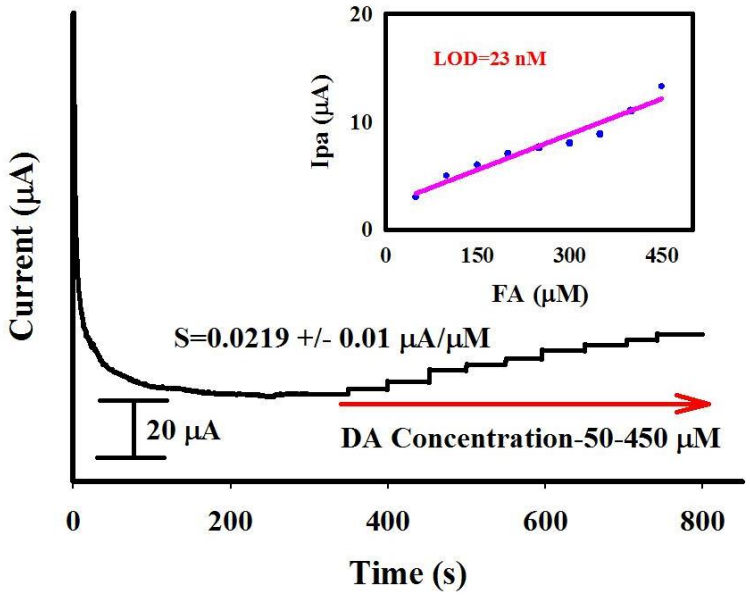

Fig.3.12. Amperometric responses obtained for PFAC/GCE in varying DA concentrations from 50 – 450 μM in 0.1 M PBS (pH 7.0), and the inset illustrates the calibration plots of i–t peak current response Vs DA

In the extracellular fluid of the central nervous system and serum, there also exist other species which are interference for DA detection such as ascorbic acid (AA), uric acid (UA), and glucose. [61]To assess the effect of interference in determining the presence of DA was studied by using the chronoamperometry technique at the operating potential of 5V. **Fig. 3.13.** showed the amperometric responses of the above-mentioned species on the fabricated PFAC electrode in 0.1 MPBS solution. The sequential injection of DA, followed by DA, UA, and GA is conducted at a time interval of

60 s. It can be observed that the electrode was insensitive to those three interference but had a remarkable response to DA.

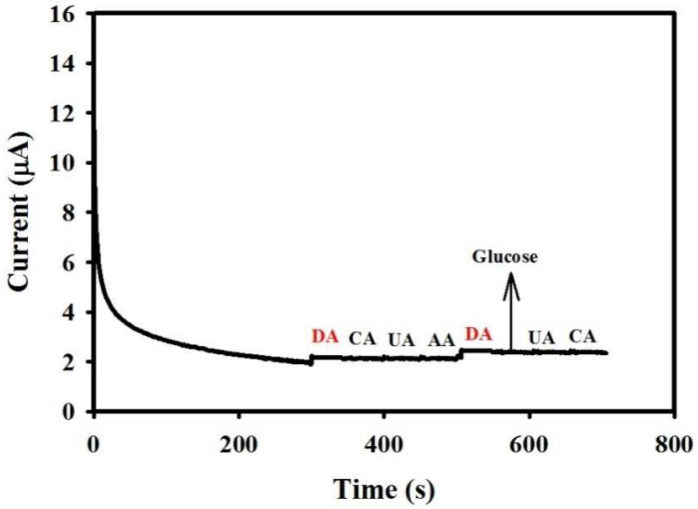

Fig. 3.13. The amperometric responses of PFAC for DA in the presence of potentially chemical interfering compound at 0.423 V under 200 rpm. All in 50 μM concentrations

The excellent selectivity for DA detection probably benefited from the π–π interactions of DA molecules with the aromatic structure of CNSL and presence of the larger number of hydroxyl group of boehmite and CNSL made greater adsorption and diffusion for DA to the surface of the electrode.[61] These results demonstrated the high selectivity and interference tolerance of the PFAC/GCE sensor.

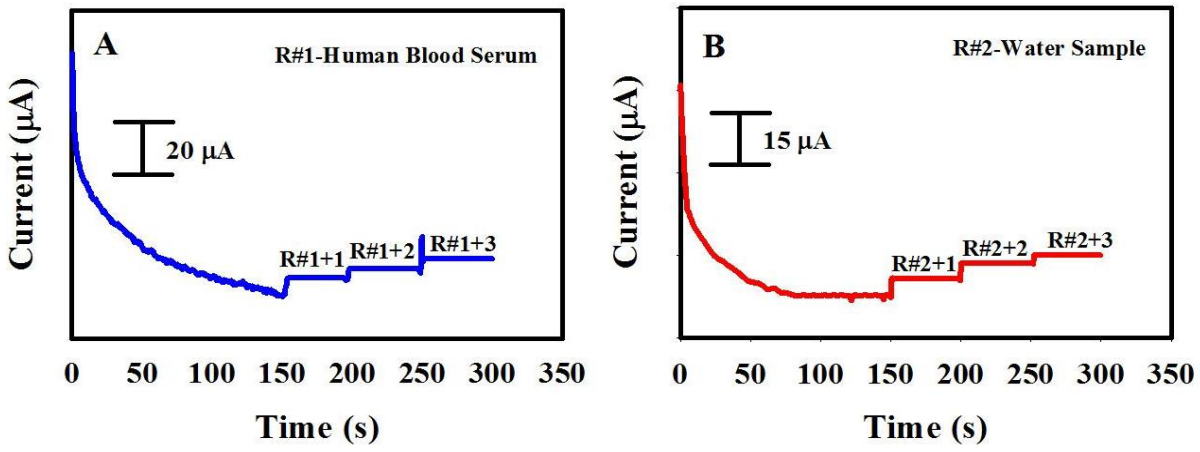

Fig.3.14. Amperometric responses of DA oxidation on PFAC hybrid from (A) Blood serum and (B) water samples at 0.423 V under hydrodynamic condition

Table 3.1.Comparison of the efficiency of some recently modified electrodes used in the electrooxidation of dopamine with the propose modified electrode in this work

Electrode	Technique	Linear range	LOD(pm)	REF
GONRs/PEDOT:PSS	Amperometry	0.05–16.55	0.030	55
PEDOT-LSG	Amperometry	1 - 150	0.33	56
3D rGO/AuPd NP /ITO	Flouresence	0.5 - 135	0.2	57
TGA-MoS_2	Photo sensitivity	0.05 - 20	27	58
AuNPs@MoS_2-NSs/GCE	DPV	5.0-200.0	1.0	59
3D pGO-GNP-pGO- ITO	DPV	0.1 - 30	1.28	52
CAuNE	CV	1–100	5.83	60
PFAC	Amperometry	50-150	0.023	Present Study

For the practical application of the proposed electrode, the detection of dopamine in the real samples such as human blood serum and river water was performed. The standard addition method was used to quantify the amount of DA in the real sample. The recovery of dopamine was studied by spiking blood serum and water with three different concentrations. 100 µL of the real sample was diluted 100 times with 0.1 M PBS and DA spiked at three different concentrations (50, 100, and 150 µM) in three replicates. The **Fig. 3.14.** displays the current response of DA in real samples, while **Table 3.2.** shows the calculated recovery range of sensor signals. As shown in **Table 3.2**, the recovery obtained is varied from 94 % to 97.6 %. The results revealed that the developed sensor has the potential for the quantification of DA in real samples.

Table 3.2. Determination of DA in human blood serum and water samples using PFAC/GCE.

Real Sample	Spiked (μM)	Detected (μM)	Recovery (%)
Human Blood Serum (R1)	10	9.4	94
	20	19.7	98.5
	30	29.3	97.6
Water Sample (R2)	10	8.9	89
	20	18.4	92
	30	28.7	95.6

3.5. Conclusion

In the present work, a new hybrid PFAC/GCE electrode was successfully synthesized by the facile physical blending method and explored for the first time to perform as a catalyst for electrochemical detection of DA. The suggested strategy was unique in its simplicity. The physiochemical studies were employed to examine the morphology and properties of PFAC hybrid. The results showed that the hybrid formation between AlOOH and organic moiety. Besides, the electrochemical measurements illustrate that the strong combination of CNSL oil and inorganic porous AlOOH advantages the ability to improve current, fast electron transfer kinetics and increased electrochemically active surface area. This as-prepared sensor showed wide linearity, very low detection limit, good selectivity and stability, reproducibility, and anti-interference ability towards the detection of DA. The prepared sensor is the most promising candidate for the determination of DA in real samples. More significantly, PFAC hybrid as a new material may possess many mysterious properties waiting to be explored. This work offers a new promising platform for preparing an electrochemical DA sensor with high performance and low cost and can be used in pharmaceutical and clinical application.

3.6. References

1. Li, B. R.; Hsieh, Y. J.; Chen, Y. X.; Chung, Y. T.; Pan, C. Y.;Chen, Y. T. An Ultrasensitive Nanowire-Transistor Biosensor for Detecting Dopamine Release from Living PC12 Cells under Hypoxic Stimulation. *J. Am. Chem. Soc.* ***2013****, 135, 16034–16037.*
2. Freeman, R.; Elbaz, J.; Gill, R.; Zayats, M.; Willner, I. Analysis of Dopamine and Tyrosinase Activity on Ion-Sensitive Field-Effect Transistor (ISFET) Devices. *Chem. – Eur. J.* ***2007****, 13, 7288–7293.*
3. Lin, C. H.; Hsiao, C. Y.; Hung, C. H.; Lo, Y. R.; Lee, C. C.; Su, C.J.; Lin, H. C.; Ko, F. H.; Huang, T.-Y.; Yang, Y.-S. Ultrasensitive detection of dopamine using a polysilicon nanowire field-effect transistor. *Chem. Commun.* ***2008****, 5749–5751.*
4. Feng, X.; Zhang, Y.; Yan, Z.; Chen, N.; Ma, Y.; Liu, X.; Yang, X.;Hou, W. Self-Degradable Template Synthesis of Polyaniline Nanotubes and their High Performance in the Detection of Dopamine. *J.Mater. Chem. A* ***2013****, 1, 9775–9780*
5. Liu, S.; Yu, B.; Zhang, T. Preparation of Crumpled Reduced Graphene Oxide-Poly(p-phenylenediamine) Hybrids for the Detection of Dopamine. *J. Mater. Chem. A* ***2013****, 1, 13314–13320.*
6. Khattar R;Mathur P. 1-(Pyridin-2-ylmethyl)-2-(3-(1-(pyridin-2-ylmethyl)benzimidazol-2-yl)
   propyl) benzimidazole and its copper(II) complex as a new fluorescent sensor for dopamine (4-(2-aminoethyl)benzene-1,2-diol). *Inorg. Chem. Commun.* **2013**,31, 37–43.
7. Syslova, K.; Rambousek, L.; Kuzma, M.; Najmanova, V.;Bubenikova,-Valešova, V.; Šlamberova, R.;Kačer P. Monitoring of dopamine and its metabolites in brain microdialysis: method combining freeze-drying with liquid chromatography-tandem mass spectrometry. *J. Chromatogr. A* ***2011****, 1218,3382–3391.*
8. Bouri, M.; Lerma-Garcia, MJ.; Salghi, R; Zougagh, M.;Rios A. Selective extraction and determination of catecholamines in urine samples by using a dopamine magnetic molecularly imprinted polymer and capillary electrophoresis. *Talanta* ***2012****, 99, 897–903.*
9. Feng, X.; Zhang, Y.;Yan, Z.; Chen, N.; Ma, Y.; Liu, X.; Yang, X.;Hou, W. Self-degradable template synthesis of polyaniline nanotubes and their high performance in the detection of dopamine. *J. Mater. Chem. A* ***2013,*** *1,9775–9780.*
10. El-Beqqali, A.;Kussak, A.; Abdel-Rehim, M.; Determination of dopamine and serotonin inhuman urine samples utilizing microextraction online with liquid chromatography/electrospray tandem mass spectrometry. *J. Sep. Sci.* ***2007****,30*, 421–424.
11. Ge, B.;an Y, Xie Q.; Ma, M.; Yao, S. Preparation of chitosan–dopamine-multiwalled carbon nanotubes nanocomposite for electrocatalytic oxidation and sensitive electroanalysis of NADH. *Sens. Actuators B, Chem.* ***2009***,137, 547–554.
12. Hammami, A.;Sahli, R.; Raouafi, N. Indirect amperometric sensing of dopamine using a redox-switchable naphthoquinone-terminated self-assembled monolayer on gold electrode. *Microchim. Acta* ***2016***, *183*, 1137–1144.
13. Karthik, R.; Chen, S. M.; Elangovan, A.; Muthukrishnan, P.; Shanmugam, R. and B.S,.Lou, Phyto mediated biogenic synthesis of gold nanoparticles using Cerasus serrulata and its utility in detecting hydrazine, microbial activity and DFT studies. *J. Colloid Interface Sci,****2016***, 468, 163–175.

14. Karthik, R.; Sasikumar, R.; Chen, S. M.; Govindasamy, M.; Vinoth Kumar, J. and Muthuraj, V.; Green Synthesis of Platinum NanoparticlesUsing Quercus GlaucaExtract and ItsElectrochemical Oxidation of Hydrazine in Water Samples. *Int. J. Electrochem. Sci.**2016**, 11, 8245 –8255.*
15. Chen, B.; Chen, D.; Li, F.; Lin, X.; Huang, Q. Graphitic porous carbon: efficient synthesis by a combustion method and application as a highly selective biosensor. *J. Mater. Chem. B **2018**, 6, 7684–7691.*
16. Gao, F.; Cai, X.; Wang, X.; Gao, C.; Liu, S.; Gao, F.; Wang, Q. Highly sensitive and selective detection of dopamine in the presence of ascorbic acid at graphene oxide modified electrodes. *Sens. Actuators, B **2013**, 186, 380–387.*
17. Zhang, C.; Ren, J.; Zhou, J.; Cui, M.; Li, N.; Han, B.; Chen, Q. Facile fabrication of a 3,4,9,10-perylene tetracarboxylic acid functionalized graphene-multiwalled carbon nanotube-gold nanoparticle nanocomposite for highly sensitive and selective electrochemical detection of dopamine. *Analyst **2018**, 143, 3075–3084.*
18. Numan, A.; Shahid, M. M.; Omar, F. S.; Ramesh, K. and Ramesh, S. Facile fabrication of cobalt oxide nanograin-decorated reduced graphene oxide composite as an ultrasensitive platform for dopamine detection. *Sens. Actuators, B, **2017**, 238, 1043–1051.*
19. Palanisamy, S.; Thangavelu, K.; Chen ,S. M.; Thirumalraj, B. and Liu, X. H. Preparation and characterization of gold nanoparticles decorated on graphene oxide polydopamine composite: Application for sensitive and low potential detection of catechol.*Sens. Actuators, B, **2016**, 233, 298–306.*
20. Thangavelu, K.; Palanisamy, S.; Chen, S. M.; Velusamy, V.; Chen, T. W and Ramaraj, S. K. Electrochemical Determination of Caffeic Acid in Wine Samples Using Reduced Graphene Oxide/Polydopamine Composite *J. Electrochem. Soc., **2016**, 163, B726–B731.*
21. Melde, B. J.; and Johnson, B. J. Mesoporous, materials in sensing: morphology and functionality at the meso-interface. *Anal. Bioanal. Chem., **2010**, 398, 1565–1573.*
22. Lee, C. H.; Lin, T. S.and Mou, C. Y. Mesoporous materials for encapsulating enzymes. *Nano Today, **2009**, 4, 165–179.*
23. Walcarius, A. and Kuhn, A. Ordered porous thin films in electrochemical analysis. *TrAC, Trends Anal. Chem., **2008**,27, 593–603.*
24. Gao, C.; Yu, X.; Xu Y.; R.X., Liu J.H.; & Huang X.J. AlOOH-Reduced Graphene Oxide Nanocomposites: One-Pot Hydrothermal Synthesis and Their Enhanced Electrochemical Activity for Heavy Metal Ions. *ACS Applied Materials & Interfaces, **2012**, 4(9), 4672–4682.*
25. Ghalkhani, M.; & Salehi, M. Electrochemical sensor based on multi-walled carbon nanotubes–boehmite nanoparticle composite modified electrode. *Journal of Materials Science, **2017**, 52(20), 12390–12400.*
26. Scorzza, C; Nieves J. and Vejar, F. Synthesis and Physicochemical Characterization of Anionic Surfactants Derived from Cashew Nut Shell Oil. *J. Surfact. Deterg., **2010**, 13, 27.*
27. Raju, S. and Kumar, P. Cathodic electrodeposition of self-curable polyepoxide resins based on cardanol. *J. Coat. Technol. Res. **2011**, 8, 563.*
28. Amorati R.; Attanasi O. A.; Favi G.; Menichetti S.; Pedulli G. F. and Viglianisi C. Cathodic electrodeposition of self-curable polyepoxide resins based on cardanol.*Org. Biomol. Chem., **2011**, 9, 1352.*
29. Zhou, Q.; Cho, D. ; Park, W. H.; Song, B. K.; and Kim, H. J. FT-IR studies on the curing behavior of poly cardanol from naturally renewable resources. *J. Appl. Polym. Sci., **2011**, 122,2774.*

30. Attanasi, O. A.; Del Sole, R.; Filippone, P.; Mazzetto, S. E.; Mele, G.; and Vasapollo, G. Synthesis of novel lipophilic porphyrin-cardanol derivatives. *J. Porphyrins Phthalocyanines,* ***2004****,8, 1276.*
31. Oliveira, T. I. S.; Dos Santos; Lomonaco V. N.; Correia D.; Mazetto A. N.; Lima-Neto S. E. & D.E. Gold Electrode Modified with Cu-Porphyrin Derived from Cardanol as Electrochemical Sensor for Nitric Oxide. *Journal of The Electrochemical Society,* ***2013***, *160(8), B113–B118.*
32. Balgude, D.B.; and Sabnis, A.S. CNSL: An environment friendly alternative for the modern coating industry. *J.Coat Technol Res*. 2014, 11(2), 169–183
    Balgude, D.; & Sabnis, A. Investigation of CNSL-Based Hybrid Sol in Conventional Polymeric Material. *Journal of Renewable Materials,* ***2016***, *4(2), 146–157.*
33. Ganjali;Mohammad. Voltammetric Determination of Dopamine Using Glassy Carbon Electrode Modified with ZnO/Al2O3 Nanocomposite. *International Journal of Electrochemical Science.* 2018, *13. 2519-2529. 10.20964/2018.03.11.*
34. Wei,Y.;Yang,R.;Zhang,Y.;Wang,L.;Liu,J.H.&HuangX.J. Highadsorptive γ-AlOOH(boehmite) SiO2/Fe3O4 porous magnetic microspheres for detection of toxic metal ions in drinking water. *Chemical Communications,* ***2011,****47(39), 11062.*
35. Cincotto,F.H.;Canevari,T.C.;Campos,A.M.;Landers,R.;&MachadoS.A. Simultaneous determination of epinephrine and dopamine by electrochemical reduction on the hybrid material SiO2/graphene oxide decorated with Ag nanoparticles. *The Analyst,* ***2014***, *139(18), 4634.*
36. Wong,F.L.; Azi,A. A Development of crack-free alumina sol-gel/poly(vinyl alcohol) membranes for glucose oxidase immobilization, *Asian J. Chem. Eng.* ***2007****, 7,* 61–67*.*
37. El-Shamy,A. G. New free-standing and flexible PVA/Carbon quantum dots (CQDs) nanocomposite films with promising power factor and thermoelectric power applications. *Materials Science in Semiconductor Processing,* ***2019,****100, 245–254.*
38. Laksmono, J. A.; Sudibandriyo, M.; Saputra, A. H.; & Haryono A. Development of porous structured polyvinyl alcohol/zeolite/carbon composites as adsorbent. *IOP Conference Series: Materials Science and Engineering,* ***2017***, *201, 012006.*
39. Ghamari, M.; Imani A.; Williams, J.F. *et al.* Aluminum oxyhydroxide-doped PMMA hybrids powder prepared via facile one-pot method towards copper ion removal from aqueous solution. *Int Nano Lett* ***2019***, 9**,** 317–325.
40. Lomonaco,D.; Mele,G.; & Mazzetto, S.E. Cashew Nutshell Liquid (CNSL): From an Agro-industrial Waste to a Sustainable Alternative to Petrochemical Resources. *Cashew Nut Shell Liquid,* ***2017***, *19–38.*
41. Siva,S.Devi, Selvasekarapandian, S.;Karthikeyan, S.; Vijaya, N.; Kingslin Mary Genova, F.; Sanjeeviraja C. Structural and AC impedance analysis of a blended polymer electrolyte based on *PVA and PAN, Indian J. Sci. Res.****2013*** *2 1e3.*
42. Zhao, Z.G.; Nagai, N.; Kodaira, T.; Hukuta, Y.; Bando, K.; Takashima, H.; Mizukami, F. Surface treatment- and calcination temperature-dependent adsorption of methyl orange molecules in wastewater on self-standing alumina nanofiber films. *J. Mater. Chem.* ***2011****, 21,* 14984-1498.
43. Hamdalla, T. A., & Hanafy, T. A. (). Optical properties studies for PVA/Gd, La, Er or Y chlorides based on structural modification. *Optik - International Journal for Light and Electron Optics,* ***2016***, *127(2), 878–882.*
44. Ai, Q.; Yang, D.; Zhu, Y.; Jiang, Z. Fabrication of Boehmite/Alginate Hybrid Beads for Efficient Enzyme Immobilization.*Ind. Eng. Chem. Res.* **2013**, *52 ,* 14898-14905.

45. Huestis, P., Pearce, C. I., Zhang, X., N'Diaye, A. T., Rosso, K. M., & LaVerne, J. A. . *Radiolytic stability of gibbsite and boehmite with adsorbed water. Journal of Nuclear Materials,* ***2018,*** *501, 224–233.*
46. Sahoo, N. G.; Cheng, H. K. F.; Li, L.; Chan, S. H.; Judeh, Z.;Zhao, Functionalized carbon nanomaterials as nanocarriers for loading and delivery of a poorly water-soluble anticancer drug: a comparative study. *J. Adv. Funct. Mater.* ***2009****, 19, 3962.*
47. Sang Youp Hwang; Cheol-Ho Lee; Hae Ri Lee; Su-Young Son; Sungho Lee; Han-Ik Joh, Porous reduced graphene oxides derived by selective removal and formation of oxygen functional groups and their electrochemical capacitances. *Chemical Engineering Science,Volume 2021, 231,116301,ISSN 0009-2509,*
48. Bagheri H.; Afkhami A.; Khoshsafar H. and Hajian A.Protein capped Cu nanoclusters-SWCNT nanocomposite as a novel candidate of high performance platform for organophosphates enzymeless biosensor. *Biosens. Bioelectron,****2017****, 89, 829–836.*
49. Karikalan, N.; Karthik, R.; Chen, S. M. and Chen H. A. A voltammetric determination of caffeic acid in red wines based on the nitrogen doped carbon modified glassy carbon electrode. *Sci.Rep.,* ***2017****, 7, 45924,*
50. Kokulnathan, T., Joseph Anthuvan, A., Chen, S.-M., Chinnuswamy, V., & Kadirvelu, K. Trace level electrochemical determination of the neurotransmitter dopamine in biological samples based on iron oxide nanoparticle decorated graphene sheets. *Inorganic Chemistry Frontiers,* ***2018****, 5(3), 705–718.*
51. Choo, S.S.; Kang, E.S.; Song, I.; Lee, D.; Choi, J.W., & Kim, T.H. Electrochemical Detection of Dopamine Using 3D Porous Graphene Oxide/Gold Nanoparticle Composites. *Sensors,* ***2017****, 17(4), 861.*
52. Yan, X.; Gu, Y.; Li, C.; Zheng, B.; Li, Y.; Zhang, T.; Zhang, Z.;Yang, M. Morphology-controlled synthesis of Bi2S3 nanorods-reduced graphene oxide composites with high-performance for electrochemical detection of dopamine. *Sens. Actuators, B* ***2018****, 257, 936–943.*
53. Yuan, Q.; Liu, Y.; Ye, C.; Sun, H.; Dai, D.; Wei, Q.; Lai, G.; Wu, T.; Yu, A.; Fu, L.; Chee, K. W. A.; Lin, C.T. Highly stable and regenerative graphene-diamond hybrid electrochemical biosensor for fouling target dopamine detection. *Biosens. Bioelectron.* ***2018****, 111, 117–123.*
54. Su, C.-H.; Sun, C.-L.; & Liao, Y.C. Printed Combinatorial Sensors for Simultaneous Detection of Ascorbic Acid, Uric Acid, Dopamine, and Nitrite. *ACS Omega,* ***2017****, 2(8), 4245–4252.*
55. Xu, G.; Jarjes, Z.A.; Desprez, V.; Kilmartin, P.A.; & Travas-Sejdic,J. Sensitive, selective, disposable electrochemical dopamine sensor based on PEDOT-modified laser scribed graphene. *Biosensors and Bioelectronics,* ***2018****, 107, 184–191.*
56. Hou, Y.; Sheng, K.; Lu, Y.; Ma, C.; Liu, W.; Men, X.; Song, H. Three-dimensional graphene oxide foams loaded with AuPd alloy: a sensitive electrochemical sensor for dopamine. *Microchimica Acta,* ***2018****, 185(8).*
57. Xu, B.; Su, Y.; Li, L.; Liu, R.; & Lv, Y. Thiol-functionalized single-layered MoS 2 nanosheet as a photoluminescence sensing platform via charge transfer for dopamine detection. *Sensors and Actuators B: Chemical,* ***2017****, 246, 380–388.*
58. Chen; Chen, & Hong. Fabrication of Au Nanoparticle-Decorated MoS2 Nanoslices as Efficient Electrocatalysts for Electrochemical Detection of Dopamine. *Catalysts,* ***2019****, 9(8), 653.*

59. Kim, D.S.; Kang, E.S.; Baek, S.; Choo, S.S.; Chung, Y.H.; Lee, D.;Kim, T.H. Electrochemical detection of dopamine using periodic cylindrical gold nanoelectrode arrays. *Scientific Reports,* ***2018***, *8(1).*
60. Huang, Q.; Lin, X.; Tong, L.; & Tong, Q.X.. Graphene Quantum Dots/Multiwalled Carbon Nanotubes Composite-Based Electrochemical Sensor for Detecting Dopamine Release from Living Cells. *ACS Sustainable Chem. Eng.* ***2020***, 8, 3, 1644–1650

CHAPTER – 4

Design of A New Superhydrophobic Boehmite Gel Hybrid and Fabrication of Textile Membranes for Oil-Water Separation

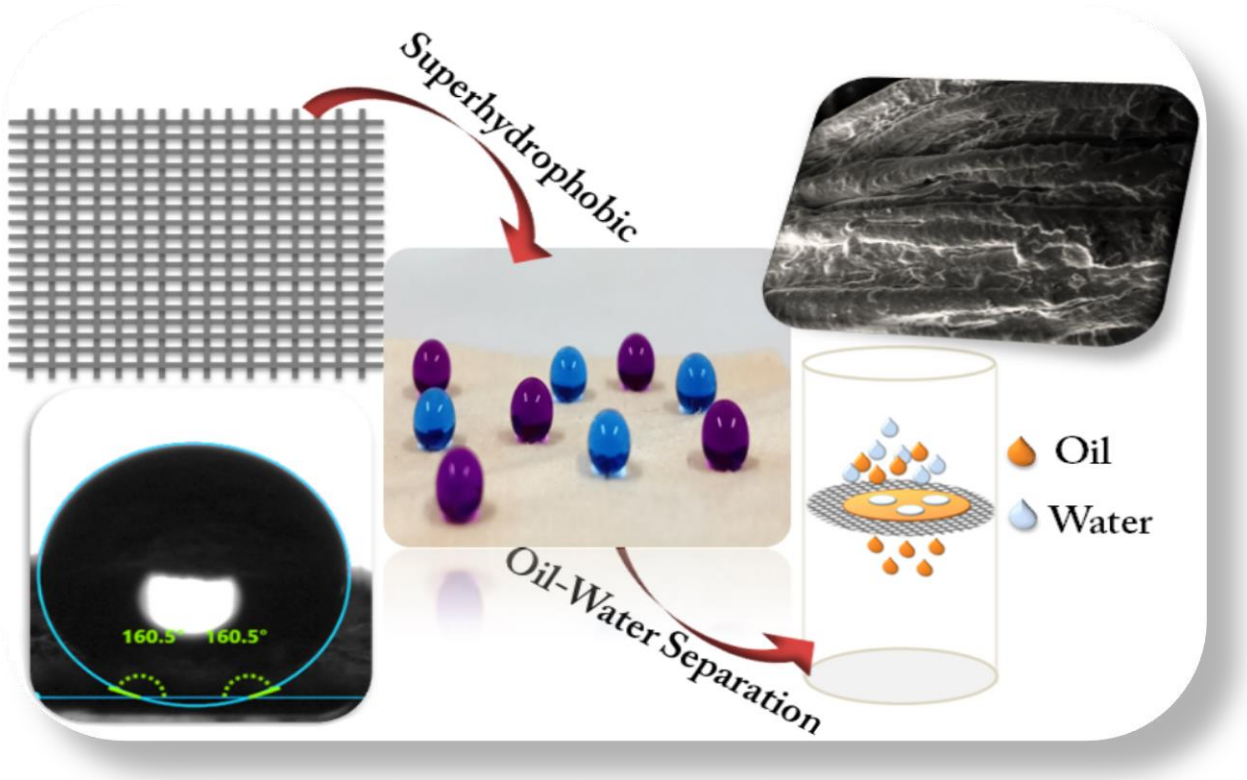

4.1. Abstract

In this chapter, a novel inorganic-organic hybrid system was designed involving a natural organic resin, namely cashew nut shell liquid (CNSL) and sol-gel boehmite. This new boehmite gel hybrid system exhibits superhydrophobic characteristics and the design aspects involved, the chemical modification of boehmite gel with CNSL oil followed by the incorporation of paraffin wax into the CNSL-Boehmite gel system to form a hybrid coating formulation. The hybrid formulation thus obtained was subsequently applied as a coating onto the surface of the textile fabrics. A superhydrophobic textile membrane comprising a nano/micro porous structure was finally achieved as an end product with a maximum contact angle of 1600. This hybrid textile membrane exhibited fast separation of various organic contaminants like hexane, petrol, diesel, chloroform, dichloromethane, and crude oil from oil-water mixtures with separation efficiency greater than 97%. This facile hybrid system lasts for more than 15 separation cycles. The present work demonstrates a promising functional hybrid textile membrane that can be utilized for the treatment of water contaminated with industrial oils as well as the selective removal of oil from the marine spilled. This kind of CNSL-Boehmite gel hybrid is prepared and investigated for the first time and the scientific merits of this new hybrid material architecture are discussed in this chapter.

4.2. Introduction

Appropriate strategies for the treatment of oily wastewater, separation of oil-water from the petroleum refinery zones, marine oil spills, and also from the numerous automobile cleaning centres became very essential for the effective environmental management and maximum oil recovery.[1-4] Over the past two decades, extensive research efforts were made to develop more efficient novel materials to address the

separation of oil from the marine environment.[5-9] Polymer sorbents, activated carbon, and hydrophobic aerogels were found to be practical for such applications.[10-12] Even though they are promising, new hybrid materials are still being investigated for faster and cheaper separation technologies.

Membrane separation is widely studied by researchers for high-performance filtration and such membrane modules were made out of hydrophilic-oleophobic and hydrophobic-oleophilic membrane materials. Hydrogel, polymer membranes, TiO_2, $Cu(OH)_2$, and cellulose have been studied and reported as filtration membranes.[13-17] In one of the reported studies, a metallic- mesh was coated by hydrogels which was found efficient in separating the mixtures of water and light oils, including gasoline and crude oil solely driven by gravity.[18] However, weak environmental adaptability and susceptibility to contamination still remain as few obstacles.

Ever since the first report published by Feng et al., on the superhydrophobic and superoleophilic polytetrafluoroethylene (PTFE) coated mesh for the oil/water separation, work on the fabrication of superhydrophobic membranes, including self-assembly, chemical etching, electrochemical treatment, vapor deposition, plasma treatment and lithography etc., became more popular.[19-22] Nevertheless, there still exist lots of limitations for large-scale fabrication of such functional membranes. The cost involved, tedious methodology, toxic fabrication procedures like fluorochemicals modification, low stability and flexibility in harsh practical environments and poor recyclability were some of the factors identified for the development of hydrophobic membrane systems for any oil-water separation.

Despite these pioneering works, designing less expensive, stable materials for the heavy oil-water mixture separation is still desired. Currently, most of the hydrophobic-oleophilic materials are fabricated by modifying porous substrates, e.g

polyester fabrics, copper and steel grids, which are either unstable in highly acidic/alkaline medium or unable to work for oil-water emulsion separation.[23-25]Therefore, it is a challenge to prepare stable hydrophobic surfaces with high mechanical strength and toughness, chemical stability and high flux using facile and cost-effective methods.

Cotton textile is an affordable, easily available flexible material that offers strong absorption ability. Therefore, we hypothesize that it could be one of the low-cost substrates that can be explored for developing cheaper oil-water separation systems if the textile surface is established with a suitable nano/micro porous structure with appropriate hydrophobic-oleophilic properties.

Inspired by the epicuticular wax on lotus surface, some efforts have been made to render wax with superhydrohobicity through the fabrication of hierarchical structures.[26, 27] Wax is suitable to uphold the required chemistry and morphology for superhydrophobicity, and they are capable of reorganizing on heating to regenerate the surface structure. There are reports confirming either waxes alone or wax-incorporated formulations are ideal to attain superhydrophobicity.

Cai et al. developed a novel fluorine-free, water compatible material system.[28]Polydimethylsiloxane (PDMS) or paraffin wax emulsions where combined with a silica suspension and ultimately applied to polyester fabrics. They successfully rendered the fabrics superhydrophobic with contact angles >145° and roll-off angle lower than 1.5°.Seo et al. produced a superhydrophobic surface with paraffin wax and candle soot.[29] Zeng et al. used paraffin wax to produce superhydrophobic copper foil.[30] They could achieve a contact angle of 152^0 .[30] Zhao et al. fabricated a superhydrophobic polyester textile with easily repairable ability by modifying pristine textile with PDMS

and paraffin wax under 120°C.[31] From all these literature evidences, it is clear that, paraffin wax could produce hydrophobic surface on textile fabrics.

Generally, Cashew nut shell liquid (CNSL) is a product of the cashew processing industry. CNSL contains number of reactive phenolic derivatives (cardanol, cardol, 2-methyl cardol and anacardic acid) with highly hydrophobic aliphatic chains.[32] Prior art literature advocates that the CNSL is mainly used to obtain Resol and Novolac which are routinely used as a thermoset resin for the fabrication of biocomposites.[33-35] CNSL is also recommended for the development of sustainable coatings with many desired properties; flame retardancy, water repellency, anti-bacterial and anti-termite. For example, Huang et al. reported a work in which cardanol based polybenzoxazine and amino-modified silica nanoparticles were combined to develop a superhydrophobic coating (PC-a/SiO_2) on mild steel for anti-corrosion coatings.[36]Bai et al. reported the preparation of superhydrophobic cotton textile by using cardanol based benzoxazine.[37] The potential grafting of cardanol with long side chain on the cellulose fibers of cotton, forming a structure similar to the waxy surface of lotus leaves, offers a simple and green method for the fabrication of cost effective water-repellent coatings.

In this chapter, a hybrid coating suspension from organic CNSL oil, boehmite, and paraffin wax [PWCA] was prepared. This hybrid suspension was used to modifying pristine cotton textile and demonstrated its superhydrophobicity and resistance to water impact. The coated textiles possess excellent self-cleaning ability and could be used to selectively separate various kinds of oil-water mixture including crude oil-water mixture. More interestingly, the fabric can recover its super liquid-repellent property after drying at 120 °C in an oven, even after immersing in water for a week. The studies indicated that the PWCA coated textiles a promising candidate for oil-water separation in real time application.

4.3. Experimental

4.3.1. Materials

Aluminium isopropoxide (AIP, purity >98%) was purchased from Aldrich and used as received condition. Paraffin wax and ethanol were obtained from Merck Specialities Pvt. Ltd. Nitric acid (HNO_3, purity 69-72%), and ethylenediamine tetra acetic acid (EDTA) were obtained from S. D. Fine-Chem. Ltd. Fisher Scientific India supplied hexane, chloroform, and dichloromethane. Crude oil was obtained from Kochi Refinery Ltd., Petrol and diesels were procured from the local suppliers. Analytical grade solvents were used in this work without any further purification. Double distilled water was used for the preparation of boehmite (AlOOH) sol.

4.3.2. Processing of boehmite-CNSL hybrid

Fig. 4.1. is the schematic representation of the experimental steps involved in the fabrication of PWCA coated superhydrophobic textile membranes. The major steps employed are: (i) Refluxing the boehmite [AlOOH] gel powder with CNSL oil in the presence of ethanol solvent (ii) Introducing CNSL modified boehmite gel into the melted paraffin wax (iii) Coating of the pristine textile fabric surface with the AlOOH-CNSL-Wax based hybrid formulation.

The typical preparation of a stable AlOOH sol using the modified Yoldas procedure was already described and provided in Chapter 2/Section 2.2.2.The same was repeated for obtaining boehmite sol. Sol was dried at 70 ℃ in an oven and the obtained boehmite gel powder was used to make PWCA hybrid. For making the hybrid formulation, firstly, AlOOH and CNSL oil were taken in the reflux flask and refluxed with ethanol at 80 ℃ for 4 hrs. The amount of CNSL was varied to obtain the samples with different boehmite:CNSL ratio such as 5:1, 5:1,5: 3, and5:5 in weight basis. The CNSL modified boehmite gel product was washed three times with ethanol and dried at 80 ℃

for 6 h. For the convenience, the obtained product was named as AlOOH@CNSL. It was further treated with paraffin wax. For this, 5g of paraffin wax was heated at 60 ℃ along with slightly excess amount of ethanol to form a homogeneous mixture. With this certain amount of boehmite@CNSL and EDTA as cross linker were added and the mixture was magnetically stirred for 10 minutes. The mixture slowly gets coagulated and converted to thick translucent gel mass. Then the gel mass was cooled to room temperature and finally the wax incorporated CNSL modified boehmite gel hybrid was obtained. For convenience, the hybrid is named as PWCA hybrid.

4.3.3. Fabrication of sperhydrophobic textile membranes

In 20 mL of ethanol, 1 g of PWCA hybrid was dissolved. A 4x4 cm piece of pristine cotton textile procured from the retail showroom was pre-treated by washing ultrasonically in deionized water followed by ethanol. The cleaned textile fabric was soaked in the ethanol-PWCA hybrid mixture for 5 minutes. Finally, the textile was dried at 120°C in an oven for 4 hours to remove the solvent. This procedure produced boehmite-CNSL-Wax modified superhydrophobic cotton textile membranes. The membrane thus obtained was named as PWCA@CT. For the proper evaluation of the scientific roles played by different constituents like wax and AlOOH-CNSL, samples were made with only paraffin wax coatings(PW), and also with different concentration of CNSL oil modified AlOOH-wax hybrid coatings. The coated textile membranes were marked as PW, PWCA1, PWCA3, PWCA5, and PWCA7 respectively.

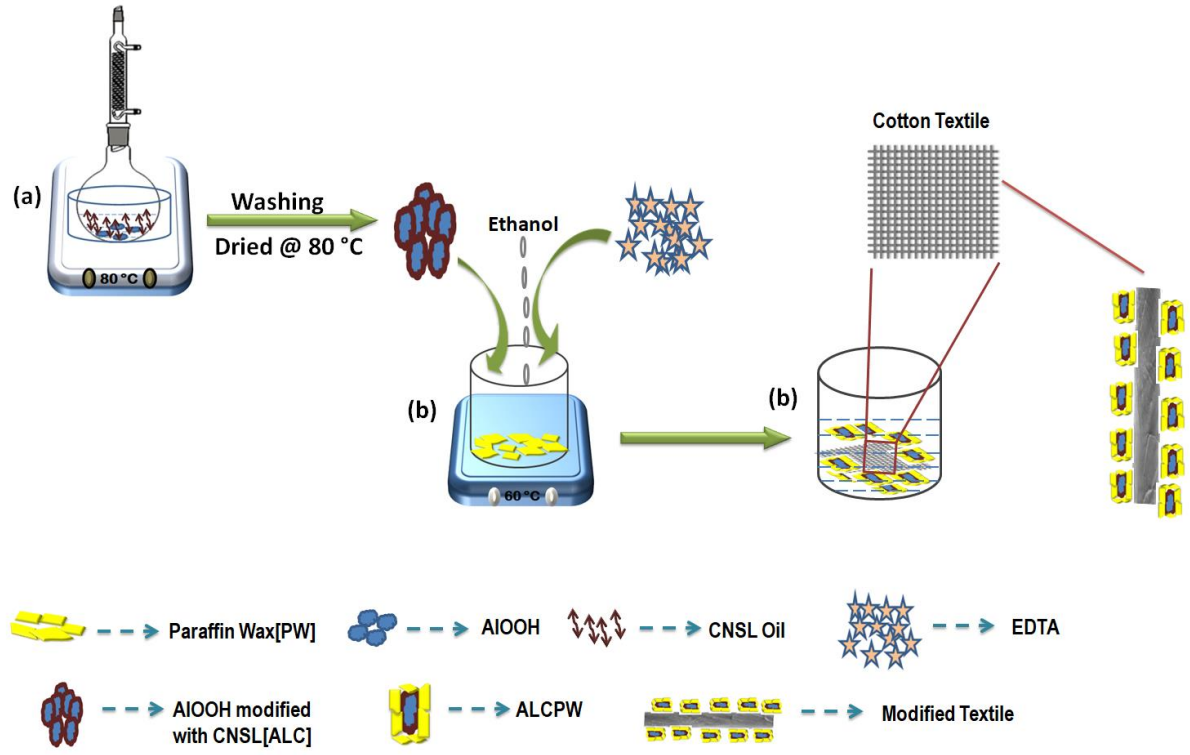

Fig. 4.1. Illustration of synthetic procedures involved in the fabrication of PWCA@CT

4.3.4. Self-Cleaning test

The self-cleaning property of the hybrid coated textile membrane was checked using the freely rolling water droplets. The coated textile membrane was sprinkled with the fine particles of an inorganic pigment. The water droplets were then formed on the surface. Droplets were allowed to roll down by slightly tilting the fabric. The removal of pigment particles by the rolling water droplets was closely monitored with the magnifying lens. The elimination of the pigment particles was clearly seen that indicates the self-cleaning ability of the boehmite-CNSL-Wax modified textile membrane.

4.3.5. Membrane durability

Durability of the prepared hybrid textile membrane was examined by immersing the samples in acidic/alkaline solution. The coated textile membranes were immersed in 1 M HCl, 1 M NaOH, and saturated NaCl solutions for seven days. The samples were then washed with ethanol and dried for 3 hours at 120 °C for CA test. The mechanical

robustness of the hybrid coatings was tested by knife scratching method. The coated, hybrid textile membrane (dimension 4x 4 cm^2) was properly glued on a glass surface and intensive cross-scratches were applied. The scratch marks were then visually noticed for checking the scratch resistance ability.

4.3.6. Oil- Water separation test

Six types of test liquids *hexane, petrol, diesel, dichloromethane, chloroform, and crude oil* were selected for examining the oil-water separation efficiency. The light oils are represented by hexane, petrol, diesel, and crude oil; Dichloromethane, and chloroform represent heavy oil. Oils can be classified as light, medium, heavy, andweathered depending on the viscosity and density values as shown in **Table 4.1.** The physical properties of the selected test liquids are listed in the **Table 4.2.**

Table 4.1. Classification of different types of oil

Oil type	Viscosity range (cP)	Density range (g cm^{-3})
Light	1–10	0.820–0.870
Medium	200–400	0.860–0.930
Heavy	1500–2500	0.930–1.000
Weathered	8000–10000	0.930–1.000

Table 4.2. Physical properties of the selected test liquids used in this study

Test liquid	Viscosity (cP) (20 °C)	Density (g cm^{-3})
Hexane	0.29	0.66
Petrol	6.38	0.80
Diesel	3.61	0.85
Dichloromethane	0.72	1.325
Chloroform	0.53	1.49
Light crude oil (API° = 90)	8.04	0.64

The oil-water (1:1 v/v) mixture was poured into the separator, and the separation process was solely driven by gravity. This process was repeated 15 times to ensure the textile's reusability. After each cycle, the modified textile was rinsed with ethanol and driedat 120^0C.Equation 1 was used to calculate the oil-water separation efficiency.

$$Separation\ Efficiency = \frac{m1}{m0} \times 100\ \% \quad (4.1)$$

Where, m_0 and m_1 represents the initially added oil mass, and finally collected oil mass after oil- water separation respectively.

4.3.7. Characterizations

FTIR spectra were recorded with a resolution of 2 cm^{-1} using a Perkin Elmer FTIR/ATR spectrometer-2. Scanning electron microscope (SEM) images of the pristine and superhydrophobic textile were observed using Zeiss EVO 18 Cryo-SEM operated at an accelerating voltage of 20 kV. Piece of bare as well as hybrid coated textile membranes were directly mounted on the SEM grids and images were acquired. The water repellent property was assessed trough contact angle measurement using a Kruss drop shape analyzer with water as the probe liquid (3 μL) at ambient temperature.

4.4. Results and Discussion

The inorganic nature, thermal stability at elevated temperatures, easy dispersibility and more importantly its unique whiskers morphology and nano laminated layered structure make the boehmite a promising candidate for developing multiporous membranes. Like many other oxides/hydroxides, boehmite does not exhibit any hydrophobic property that limits its use for any oil-water separation applications. In

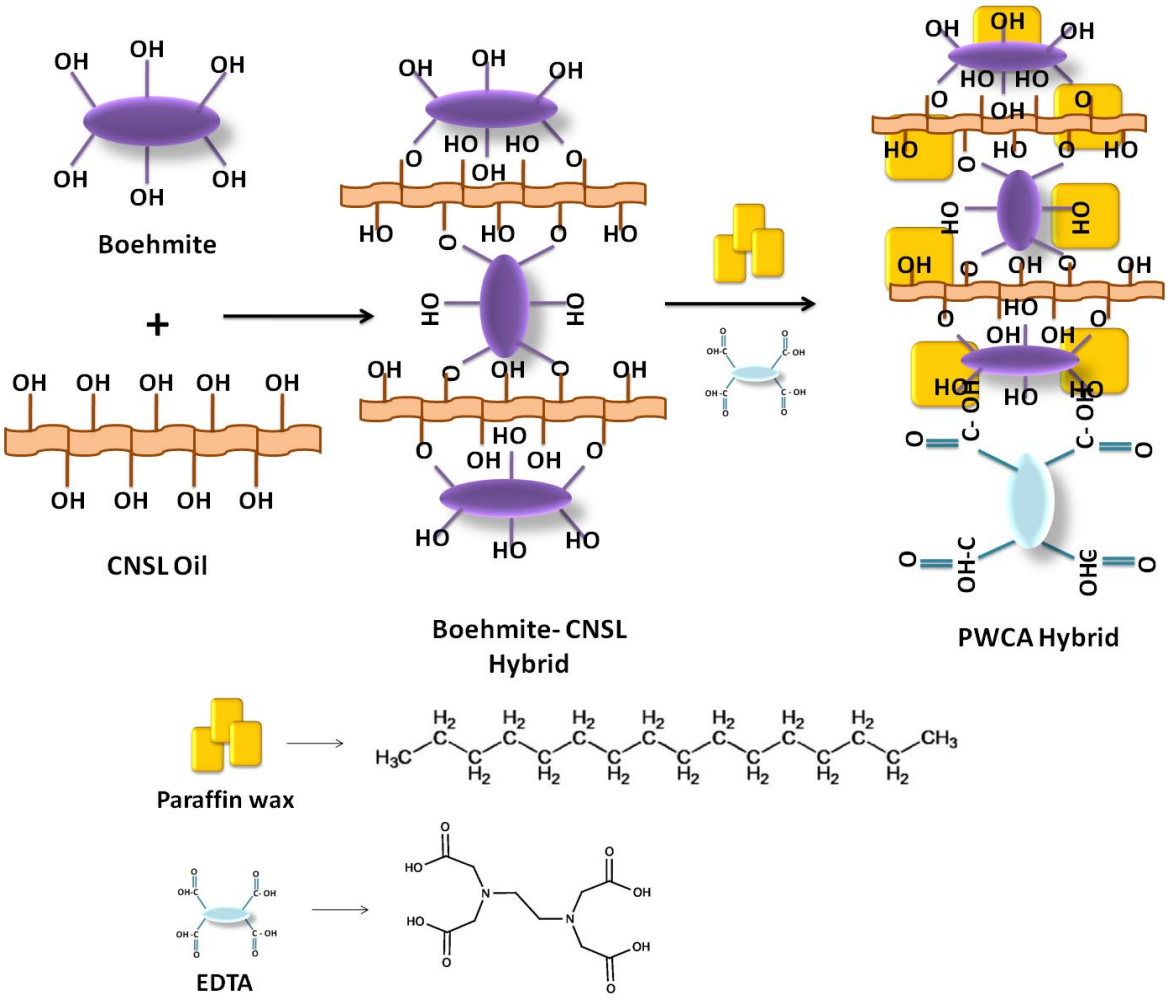

Fig. 4.2. Plausible mechanism of formation of the hybrid PWCA

general, the hydrophobic functionality is derived by introducing appropriate flourochemicals and silane functionality. Other than silanes, use of natural sources like CNSL oil is an alternate. CNSL has attractive thermal stability. Thermogravimety analysis of CNSL oil was studied earlier and it seems the maximum degradation occurs in the temperature range 180 to 300°C. It makes CNSL a competitive functional molecule to expensive silanes. Plausible mechanism of formation of the hybrid PWCA is depicted in **Fig. 4.2.**The incorporation of boehmite into CNSL to develop hybrids, it results in the dispersion of layered boehmite in CNSL medium and also produce chemical interaction between the surface hydroxyl groups with the phenolic moieties present in the CNSL. FTIR study confirms the nature of the chemical interactions of boehmite-CNSL hybrids.

4.4.1. Structural characteristics of PWCA coated textile

FTIR study was conducted on raw paraffin wax, CNSL resin, and the boehmite-CNSL hybrid systems prepared in this study. The prepared textile membranes using different hybrid composition s were also analyzed and the results are presented in **Fig. 4.3.**

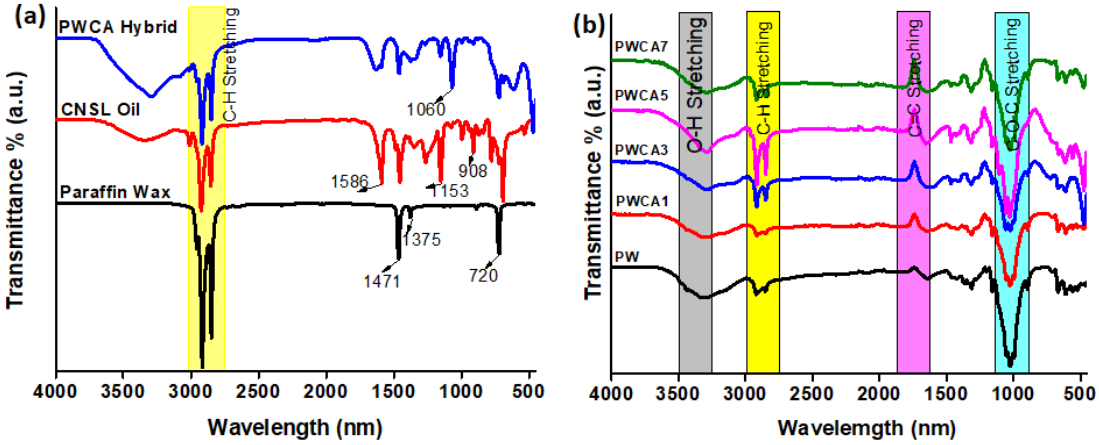

Fig.4.3. FTIR spectra of (a) paraffin wax, CNSL oil, PWCA hybrid (b) Different concentration of CNSL in PWCA hybrid coated textile

Fig. 4.3.a. shows the FTIR spectra recorded for the wax. The peaks of pure paraffin wax at the wavelengths 1471cm^{-1} and 1375 cm^{-1} represents the C- C in plane vibrations, and CH_2 rocking absorption band at 720 cm^{-1} confirms the linear saturated aliphatic structure of the paraffin wax.[38]In the case of CNSL oil, the peaks seen at 3172, 1586, and 1153 cm^{-1} can be referred to the absorption peak correspond to-OH groups, C=C stretching of benzene ring, and C-O stretching vibrations respectively.[39]In all cases(**Fig. 4.3.b.**) the peaks at 2848- 2915 cm^{-1} represents the C-C stretching of hydrocarbon. [38]Besides, the band at 1060 cm^{-1}, 1690 cm^{-1} corresponds to Al-O-Al stretching vibration and absorption peaks of carbonyl bonds in EDTA respectively.[40,41] The absorption peak of the carbonyl group at about 1690 cm^{-1} in EDTA shifted to 1632 cm^{-1} in the spectrum of the PWCA hybrid. These results confirm the formation of hybrid PWCA. **Fig. 4.3.b.** shows the FTIR spectrum of PWCA hybrid suspension with varying

amount of CNSL coated on textile fibres. All the peaks presented in the PWCA hybrid appeared in the textile indicating the surface is firmly covered by hybrid coatings. The FTIR study shows clearly that the CNSL-boehmite and paraffin wax have been incorporated onto the surface of the textile fibres

4.4.2. Morphological analysis

The morphology features of the uncoated bare textile, the textile coated with only paraffin wax, and also with the boehmite-CNSL hybrid formulation were observed at different magnifications and analysed to study the effect of the hybrid coatings to form the membranes. The SEM images convincingly show a homogenous coverage of the wax coating as well as CNSL-boehmite hybrid coatings. The fabric surface shows significant variation on the roughness profile.

Herein, an appropriate multiscale roughness was successfully reached through the hybrid suspension of PWAC on the cotton textile surfaces. The morphology of modified textile membranes was dramatically changed, as shown in **Fig. 4.4. (a- f).** SEM image corresponds to the bare textile surface show poor surface roughness **Fig. 4.4.a. Fig. 4.3.b.** that represents the surface after treating with wax, it is seen that the wax coating enhances the surface smoothness and the fabrics surface is well covered with wax indicating the fabrics are modified firmly for exhibiting hydrophobicity, the inherent nature seen with wax. The smoothness seen in the wax coated fabric seems to change when CNSL-boehmite-wax based hybrid formulation is obtained. Once the textile piece is immobilized with the hybrid formulation, the surface regains its' roughness indicating the hydrophobicity may be higher in hybrid coated textiles **Fig.4.4.c**.

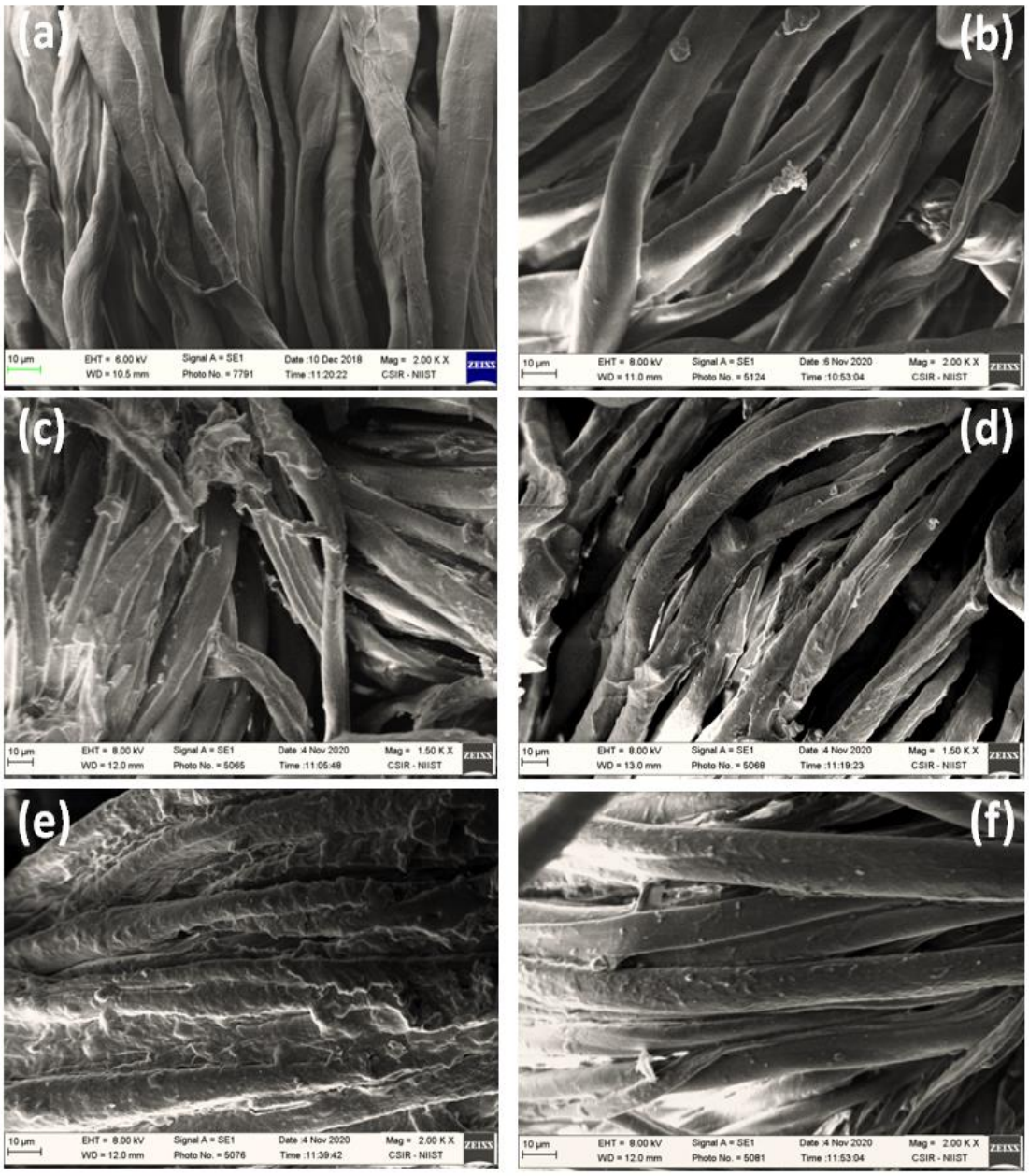

Fig. 4.4.SEM image of (a) pristine cotton textile, (b) PW, (c) PWCA1, (d) PWCA3, (e) PWCA5, and (f) PWCA7 coated textile

The SEM images implying a stronger interaction between the hybrid coating and the textiles. The evolution of micro/nano structures were also seen on through textile fibres **Fig.4.4.(b,c).** When the amount of CNSL is gradually increased, the roughness nature is also increased which is producing more micro-nano scale roughness **Fig. 4.4.(d,e).** SEM images clearly describe the modified textile membrane has a compact

encapsulation of the wax, as well as CNSL-Boehmite hybrid system. The complete encapsulation favours the decrease in the overall size of the inter-fabric voids in the woven textile and produced controlled porosity of the textile membranes.

4.4.3. Surface wettability

The surface contact angle measurements clearly confirm the transformation of hydrophilic textiles to hydrophobic membranes due to hybrid coatings. The progressive increase on the surface hydrophobicity was gradually increased at different stages of surface modifications. When the concentration of CNSL in the hybrid formulation was varied, the textile membrane attained different level of hydrophobicity. The water contact angle (CA) was monitored with respect to the CNSL concentrations. **Fig.4.5.** depicts the variation of water CA as a function of CNSL concentration on hybrid formulation. When the amount of CNSL was increased from zero to a 1: 1 ratio of CNSL/AlOOH, in the hybrid formulation, the CA increased consistently from 139° to 160°. Water contact angle is reduced to 141° due to a further increase in CNSL.

As we all know, the bare cotton textiles readily absorb water indicating it is highly hydrophilic nature. Similar to bare cotton, the un-modified boehmite also exhibit strong affinity to water. However, when the bare textile fabric is coated with paraffin wax, the surface hydrophilicity suddenly changed to hydrophobic as expected and the water contact angle of about 139° is seen in this case. However, to make the textile fabric hydrophobic to super hydrophobic, the wax alone is insufficient. Here, the CNSL-Boehmite shows some advantage. When CNSL-boehmite hybrids were introduced, the contact angle value reaches 160° for the hybrid system PWCA 5, indicating that the participation of wax and CNSL-boehmite hybrid facilitate superhydrophobic surface formation.

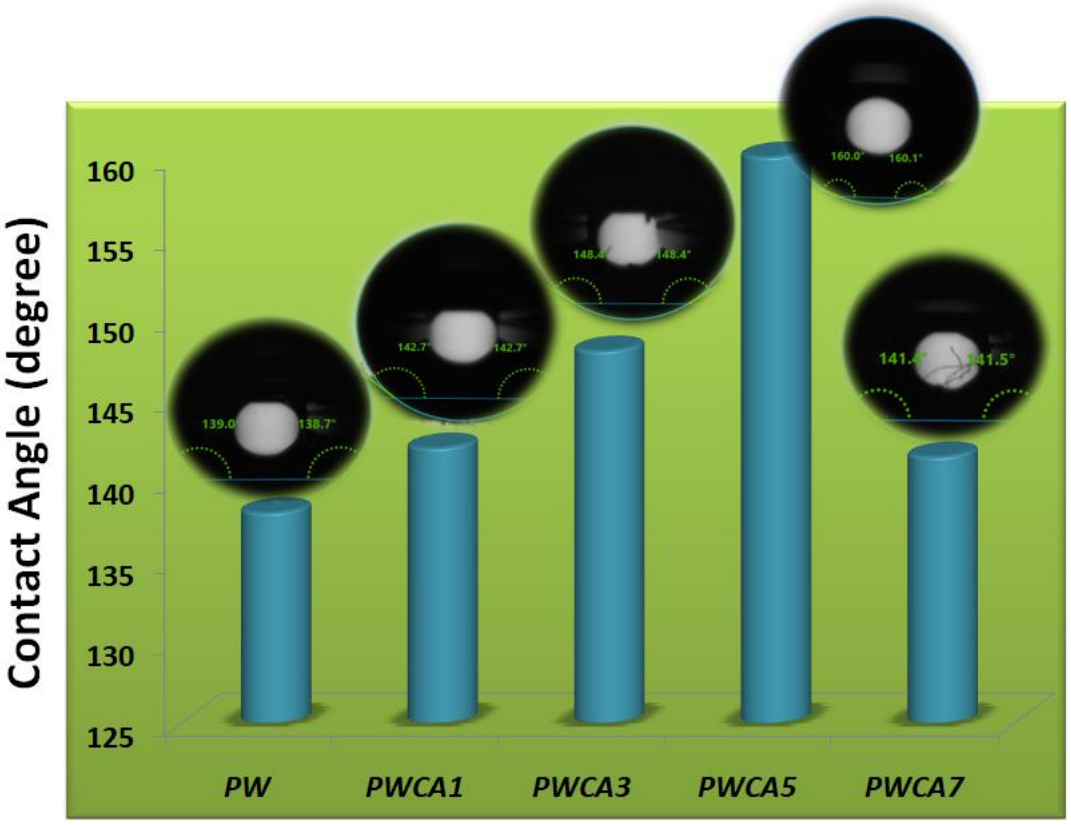

Fig. 4.5. Graph of contact angle as a function of hybrid suspension coated textile

For further experimental verification, the textile membrane denoted as PWCA5 was chosen due to its high contact angle value. Testing with the dyed water droplets was conducted to understand the superhydrophocity of the textile membrane. Dyed water droplets were applied to the coated and uncoated textile membrane surfaces, respectively. Water droplets easily penetrated through bare textiles and the organic dye was absorbed onto the fabrics surfaces **Fig.4.6.a..**The PW and hybrid PWCA5 superhydrophobic coatings demonstrated exceptional repellence to water droplets. The droplets maintained high sphericity on the various sites of the modified textile membranes **Fig.4.6. (b,c).**The PWCA5 hybrid, in particular, offered well reserved spherical nature than the sample PW. In this case, the water droplet freely rolled off, indicating the composite coatings perfectly works for self-cleaning surfaces. In the case

of PWCA hybrid coated textile membrane, the spherical shape of the water droplet was also well maintained for strong acidic as well as strong basic solutions.

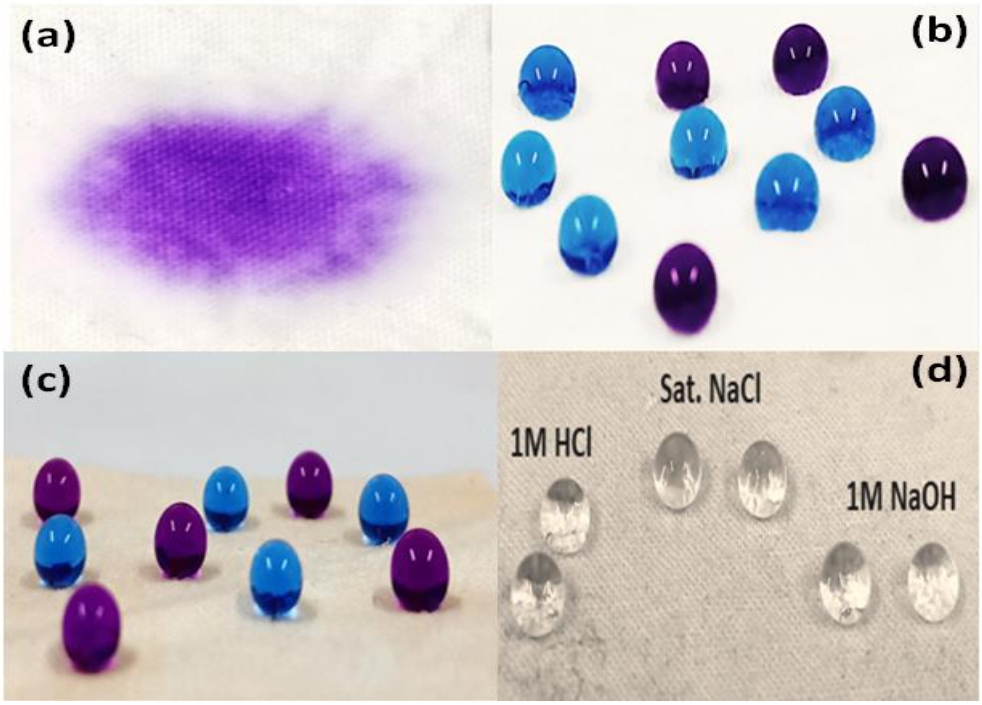

Fig.4.6. Photographic images of dyed water droplets on the surface of (a) bare cotton textile, (b) wax coated-PW, and (c) hybrid coated PWCA5, and (d) PWCA5 coated textile with 1M HCl, 1M NaOH, and Sat. NaCl

4.4.4. Self-Cleaning property

For membranes, self-cleaning is one of the desirable properties expected for any practical uses. Self-cleaning property is generally seen with superhydrophobic surfaces. To establish the advantages of the superhydrophobicity seen with the hybrid sample PWCA 5, the self-cleaning tendency was examined. For that, the hybrid modified textile membrane was firmly fixed on a glass plate to make it free from any wrinkles, and to facilitate free fall rolling an angle of 25^{o} was given by simple tilting. Then the hybrid modified textile membrane was sprinkled with the fine particles of blue color inorganic pigment powder to intentionally contaminate the surface. The blue color pigment particles were selected only to visibly see the rolling of the dust particles. Fig.4.6 shows the different stages of the self-cleaning experiment. When water is allowed to pass

through the hybrid modified superhydrophobic textile membrane, the pigment particle dusts were also rolled off smoothly and rapidly from the membrane surface along with the water without a residual. This study demonstrates the ready self-cleaning as well as water-repelling quality of superhydrophobic textile membrane prepared in this work.

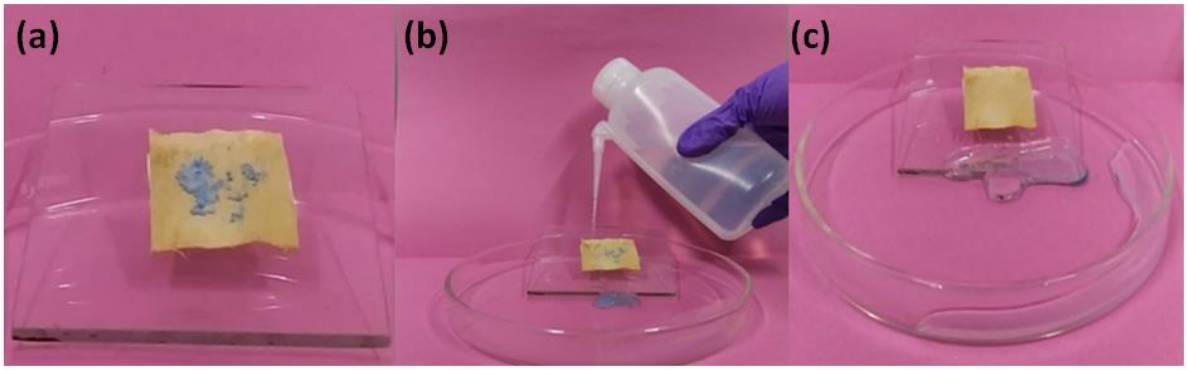

Fig. 4.7. Self cleaning process of PWCA5 hybrid coated textile

4.4.5. Mechanical durability

The durability of superhydrophobic coatings is a crucial factor that limits their widespread application, because mechanical friction can destroy micro- and nanostructures, resulting in the loss of superhydrophobicity. Knife-scratch test was used to assess the mechanical durability of the superhydrophobic coating on the textile **(Supporting Details Provided in the Video).** Intensive scratches were applied on the coated surfaces to imitate the scratch conditions in practical applications, and water droplets were squeezed on the surfaces after knife-scratch. It was noticed that the coating still retained their non-wetting property, regardless of scratches. The contact angle was 158^{o}, indicating that scratching did not induce a significant decrease in the superhydrophobicity on the hybrid coatings.

4.4.6. The chemical stability

In practical applications, coating durability is critical, especially in harsh environments such as acid, alkali, and salt solution. The textile membrane modified with the hybrid PWAC5 was thoroughly tested for the chemical attack using strong acid and alkali

solutions, as well as with saturated NaCl solution. It is seen that the hybrid coating remained stable even after 1 week of immersion in 1 M HCl solution, NaOH solution and saturated NaCl water solution. It was ascertained by monitoring the contact angle before and after immersion test. The resistance towards chemical attack was confirmed from the CA value. The hybrid top-coat still retained the CA value at 160° in 1M HCl solution. Nevertheless, a negligible minute decrease of the CA value is seen in case of Sat. NaCl. and NaOH solution. In these cases the CA value decreased from 160 to 159.5° and 158.3° respectively. The coating was extremely stable, most likely due to the multiple cross-linked networks being bridged by covalent bonds and firmly covered on the textile fibres.

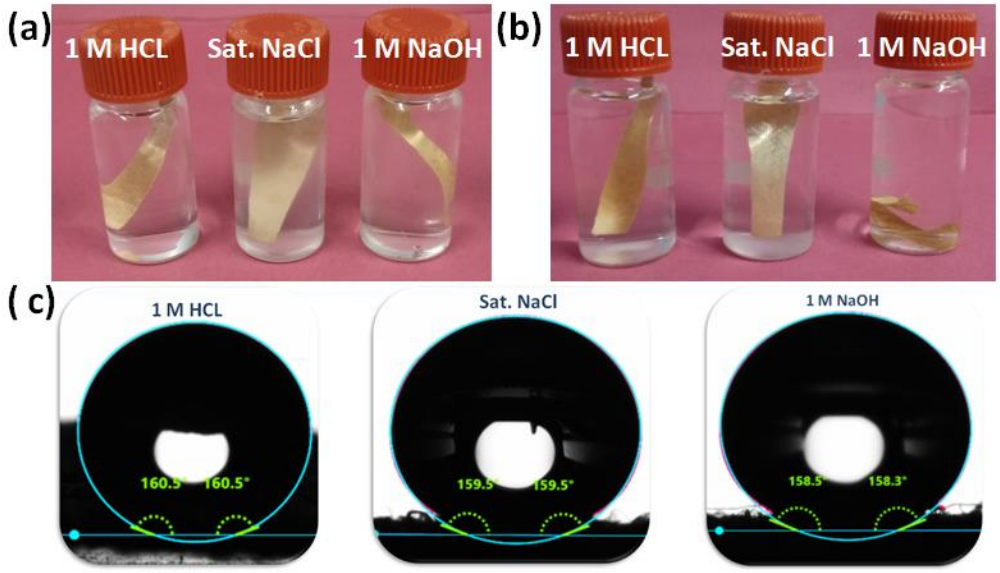

Fig. 4.8. Photographic images of the PWCA 5 coated textile membranes during immersion test. (a) first day of immersion, (b) after 1 week of immersion, and (c) corresponding contact angle measured after 1 week immersion

4.4.7 Oil-Water Separation Capability

The ability of the CNSL-Boehmite-Wax modified, superhydrophobic hybrid textile membranes to separate various kinds of oils from oil-water mixtures was tested using an experimental setup which is depicted in the **Fig. 4.8**. For that, textile membrane

having PWCA5 hybrid top-coat is firmly glued at the bottom of a glass separating funnel fitted on the top of the beaker**.** The experimental set up was first confirmed that it is free from water leakage. Water was poured into the membrane assembly and left for 30 minutes to check the leakage. After the confirmation, the oil-water separation process was conducted.

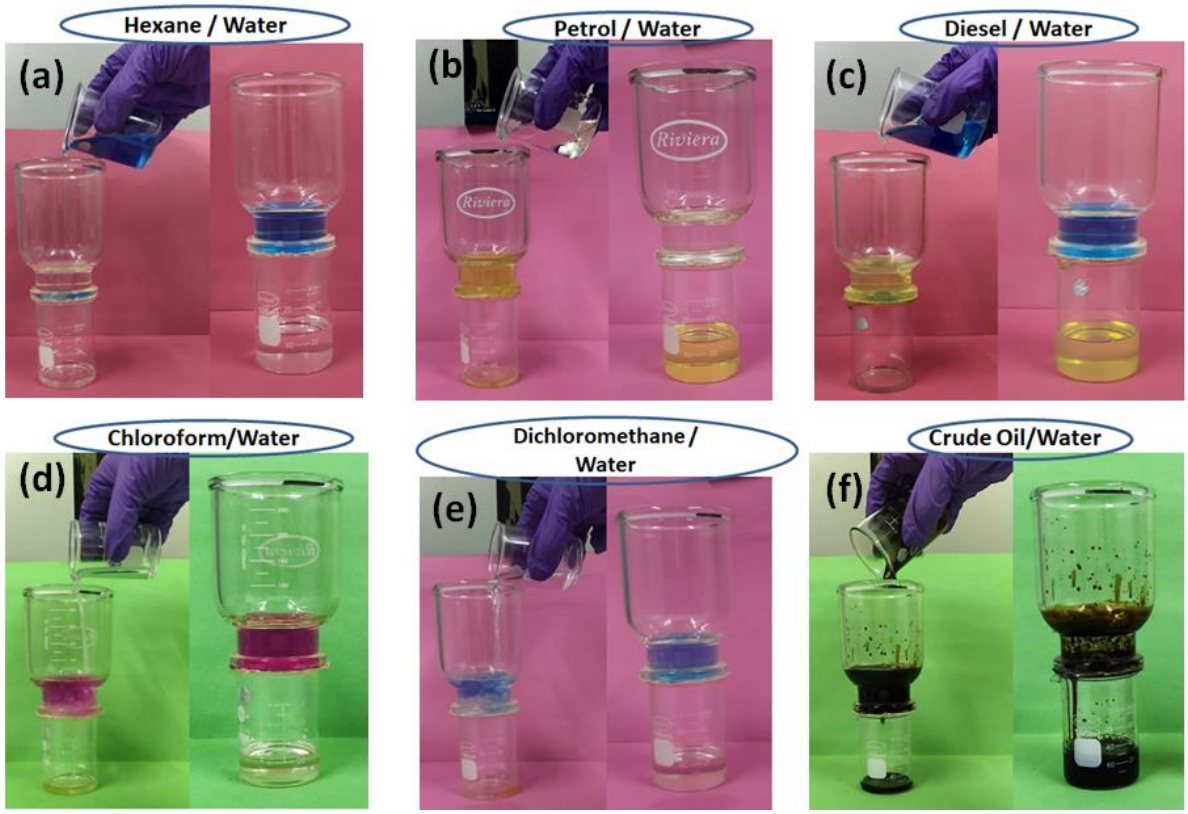

Fig. 4.9. Oil- water separation process by using PWCA5 coated hybrid sample (a) hexane, (b) petrol, (c) diesel, (d) chloroform, (e) dichloromethane, and crude oil

Fig. 4.9. depicts the results of gravity-driven oil-water separation using the textile membranes having PWCA5 hybrid coat. A 30 mL of hexane poured into the beaker quickly permeated the mesh and was collected in the beaker beneath the mesh, whereas the same amount of water poured into the beaker was retained in the beaker above the mesh. Except for crude oil, all oils (30 mL) permeated through the

superhydrophobic textile membranes in less than 3 minute, whereas crude oil took longer time for complete permeation.

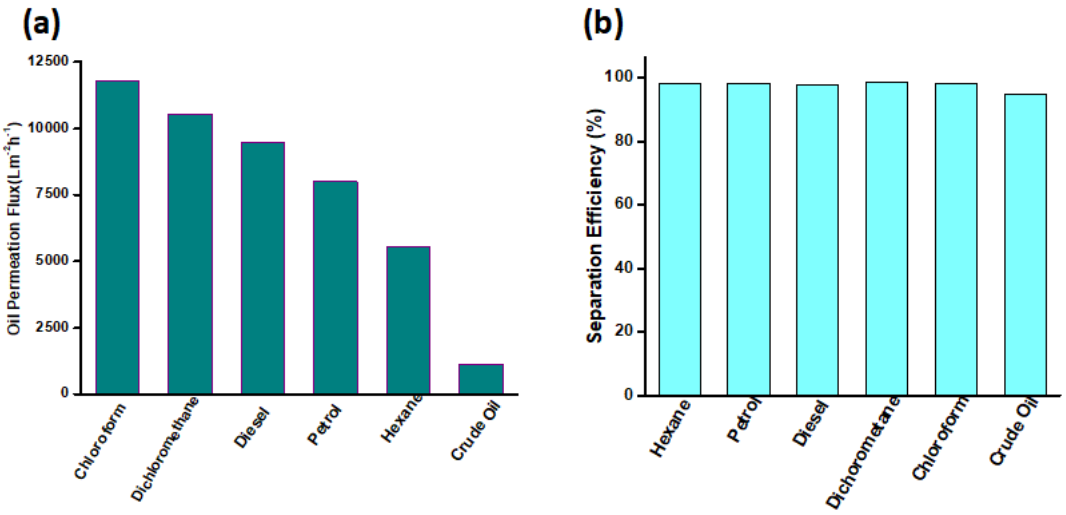

Fig. 4.10. Comparative data on oil-water separation efficiency of textile membrane fabricated in this work. (a) Oil permeation flux (b) Separation efficiency of PWCA5 hybrid modified textile membrane

The permeation flux is another important parameter to consider when exploring the oil- water separation capability of the materials. The oil permeation flux (J) was calculated by dividing the total volume of permeated oil (L) by the product of active area of the superhydrophobic leaf mesh (m^2) and total time (h) required for permeation. [42] At atmospheric pressure, we measured the permeation flux for 30 mL of oil with the fixed active area (4.15 cm^2) of the superhydrophobic cotton textile. **Fig.4.10. a.** depicts the separation fluxes of heavy oil and light oil, which differed due to their densities. The average permeates fluxes of chloroform and CH_2Cl_2during heavy oil separation could be as high as 12457±156 and 11765± 200 L/m^2h, respectively. The average permeates fluxes of diesel,petrol, hexane, and crude oil in water when separating the light oil could be as high as 9625 ± 271, 8114 ± 232, 6577 ± 78, and 1750 ± 261 L/m^2·h. The flux is strongly related to the pore size of the separation membrane materials. [43]The pore size of the CNSL-boehmite-Wax hybrid coated textile membrane is

comparatively larger than that of the other usual membrane materials, such as nylon membranes, PET textiles, and polyethersulfone membranes reported in the previous literature. The larger pores may enable high-flux separation without the application of any external pressure.[43]

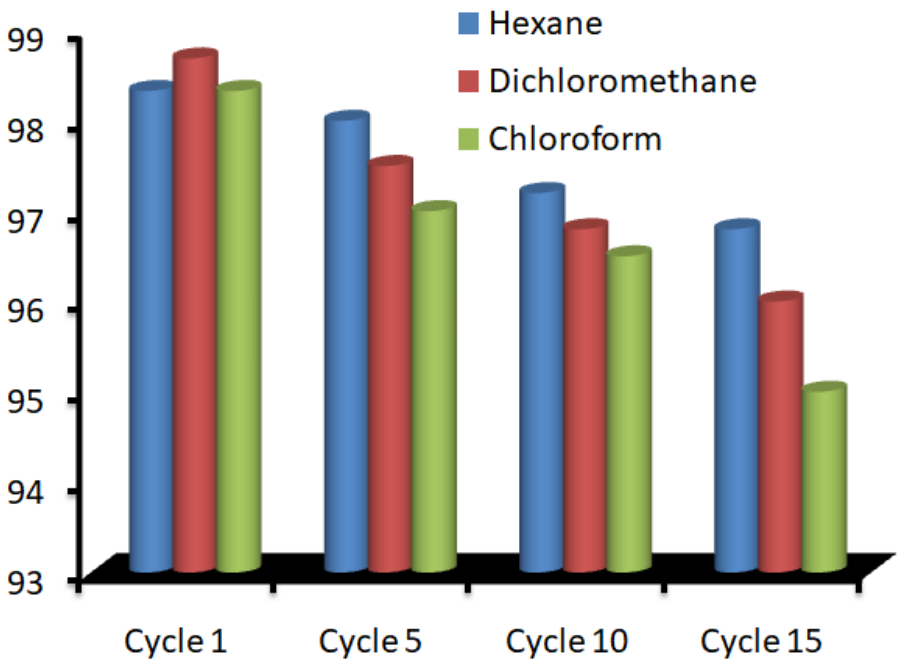

Fig. 4.11. Recyclability of PWCA5 hybrid coated textile

The separation efficiency of the superhydrophobic textile was calculated by comparing the oil's mass percentage ratio before and after the separation process.[44] Oils with low viscosity shows separation efficiency greater than 97% due to their fast permeation through the superhydrophobic textile membrane and maintained it for more than 15 separation cycles, as shown in **Fig. 4.10. b.** However, highly viscous crude oil partially clogs the membrane pores resulting in a reduced separation efficiency. In this case nearly 89% efficiency was noticed. Due to partial absorption into the textile, and fractional wetting of the containers, perfect separation efficiency during oil-water separation could not be achieved. However, after 15 cycles of oil-water separation, the separation efficiency gradually decreased. This may be due to the gradual degradation

or the erosion of the hybrid architecture which is expected during each time we conduct the separation experiment.

We have also studied the water rejection rate of superhydrophobic hybrid textile membranes.

The following equation was used.[45]

$$R(\%) = [1 - C_1/C_o] \times 100 \quad (4.2)$$

where R is rate of water rejection and C_o and C_1 are the concentration of water in initial and filtered oil, and the values are tabulated in **Table4.3.** Herein, the oil-water mixture was prepared by adding water in series of oils including hexane, petrol, diesel, chloroform, dichloromethane, and crude oil. The water-in-oil volume ratio was kept at 3:7, and the entire mixture was stirred for 30 minutes with a magnetic stirrer.

The superhydrophobic hybrid textile membrane demonstrated a higher water rejection rate for water/low viscous oil mixtures. The water rejection rate was comparatively lower for water/high viscous oil mixtures.

Table 3: Relative Permeation Flux, and Water Rejection Rate for Various Oil/Water Mixtures

	OILS					
	Hexane	**Petrol**	**Diesel**	**Chloroform**	**Dichloro-methane**	**Crude oil**
Permeation flux J [L/(m²·h)]	6577 ± 78	9625 ± 271	8114 ± 232	12457 ±156	11765± 200	1750 ± 261
Water rejection rate (%)	99.2	98.7	98.1	97.6	96.8	95

4.5. Conclusions

Anew inorganic-organic hybrid architecture consisting of boehmite gel, natural organic resin, CNSL and wax was designed that ultimately produced mechanically robust superhydrophobic top-coats on textile fabrics. It seems to be a facile strategy for making economically affordable, flexible superhydrophobic hybrid textile membranes. The CNSL-boehmite hybrid improved the hydrophobicity of wax modified textile surfaces. The entire Wax-Boehmite-CNSL hybrid system decides the transformation of the hydrophilic textile surface into more hydrophobic and also for achieving the significant level of superhydrophobicity.The hybrid modified textile membrane offers excellent water repellence with a WCA of 160°, as well as good self-cleaning ability. This superhydrophobic hybrid textile membrane was validated for separating the hexane, petrol, diesel, chloroform, dichloromethane and crude oil/water systems. The separation efficiency was >97% for more than 15 cycles. The hybrid textile membrane assembly results in high permeation fluxes toward oils with low viscosities. The CNSL-Boehmite-Wax based superhydrophobic hybrid coatings showed resistant to knife scratching and remained extremely stable even in harsh aqueous chemical conditions. This kind of inorganic-organic hybrid coatings on textiles appears to be promising for making cost effective, environmentally friendly, green membrane system for any oil-water separation applications.

4.6 References

1. Huang, L.; Deng, S.; Guan, J.; Chen, M.; Hua, W. Development of a novel high-efficiency dynamic hydrocyclone for oil–water separation. *Chem Eng Res Des.* ***2018****;130:266-273.*
2. Wu, Z; Luo, J.; Sun, L. Synthesis and performances for treating oily wastewater of polyether copolymers based on polyethyleneimine. *Polym Adv Technol.* ***2018****;29(2):814-819.*
3. Fraser, B.; Oil in the Forest. *Science* ***2016****, 353, 641–643.*

4. Shannon, M. A.; Bohn, P. W.; Elimelech, M.; Georgiadis, J. G.;Mariñas, B. J.; Mayes, A. M. Science and Technology for WaterPurification in the Coming Decades. *Nature **2008**, 452, 301–310.*
5. Jin, M. H.; Wang, J.; Yao, X.; Liao, M.; Zhao, Y.; Jiang, L. Underwater Oil Capture by a Three-Dimensional Network Architectured Organosilane Surface. *Adv. Mater. **2011**, 23, 2861–2864.*
6. Gupta, R. K.; Dunderdale, G. J.; England, M. W.; Hozumi, A. Oil/Water Separation Techniques: A Review of Recent Progresses andFuture Directions. *J. Mater. Chem. A **2017**, 5, 16025–16058.*
7. Ge, J.; Zhao, H. Y.; Zhu, H. W.; Huang, J.; Shi, L. A.; Yu, S. H.Advanced Sorbents for Oil-Spill Cleanup: Recent Advances and FuturePerspectives. *Adv. Mater. **2016**, 28, 10459–10490.*
8. Su, B.; Tian, Y.; Jiang, L. Bioinspired Interfaces with Superwettability: From Materials to Chemistry. *J. Am. Chem. Soc.**2016**, 138, 1727–1748.*
9. Wang, B.; Liang, W. X.; Guo, Z. G.; Liu, W. M. Biomimetic Super-Lyophobic and Super-Lyophilic Materials Applied for Oil/Water Separation: A New Strategy beyond Nature. *Chem. Soc. Rev. **2015**, 44, 336–361.*
10. Zhang, Y.; Wei, S.; Liu, F.; Du, Y.; Liu, S.; Ji, Y.; Yokoi, T.;Tatsumi, T.; Xiao, F. S. Superhydrophobic nanoporous polymers as efficient adsorbents for organic compounds. *Nano Today **2009**, 4,135–142.*
11. Ge, J.; Zhao, H. Y.; Zhu, H. W.; Huang, J.; Shi, L. A.; Yu, S. H. Advanced sorbents for Oil-Spill cleanup: Recent advances and future perspectives. *Adv. Mater.**2016**, 28, 10459–10490.*
12. Xue, Z.; Wang, S.; Lin, L.; Chen, L.; Liu, M.; Feng, L.; Jiang, L. A Novel Superhydrophilic and Underwater Superoleophobic Hydrogel-Coated Mesh for Oil/Water Separation. *Adv. Mater. **2011**, 23,4270–4273.*
13. Wang, Y.; Shi, Y.; Pan, L.; Yang, M.; Peng, L.; Zong, S.; Shi, Y.; Yu, G. Multifunctional superhydrophobic surfaces templated from innately microstructured hydrogel matrix, *Nano. Lett. **2014**, 14, pp.4803-9.*
14. Mishra, P.; Balasubramanian, K. Nanostructured microporous polymer composite imprinted with superhydrophobic camphor soot, for emphatic oil–water separation.*Rsc. Adv. 4 **2015**,53291-53296.*
15. Shi, H.;He, Y.; Pan, Y.; Di, H.; Zeng , G.; Zhang, L.; Zhang, C. A modified mussel-inspired method to fabricate TiO2 decorated superhydrophilic PVDF membrane for oil/water separation. *J. Membrane. Sci. **2016,** 506,60-70*
16. Zhu, H.; Guo, P.; Shang, Z.; Yu, X.; Zhang, Y. Fabrication of Underwater Superoleophobic Metallic Fiber Felts for Oil-Water Separation. *Appl. Surf. Sci. **2018,** 447, 72–77.*
17. Satapathy, M.; Varshney, P.; Nanda, D.; Panda, A.; Mohapatra, S.S; Kumar. Fabrication of superhydrophobic and superoleophilic polymer composite coatings on cellulosic filter paper for oil–water separation, *Cellulose. 24 **2017**, pp. 1-14.*
18. Cong, H.-P.; Ren, X.-C.; Wang, P.; Yu, S.-H. Macroscopic Multifunctional Graphene-based Hydrogels and Aerogels by a Metal Ion Induced Self-Assembly Process. *ACS Nano **2012**, 6, 2693–2703.*
19. Peng, S.; Yang, X.; Tian, D.; Deng, W. Chemically Stable and Mechanically Durable Superamphiphobic Aluminum Surface with a Micro/Nanoscale Binary Structure. *ACS Appl. Mater. Interfaces **2014**, 6, 15188–15197.*

20. Li, J.; Jing, Z.; Zha, F.; Yang, Y.; Wang, Q.; Lei, Z. Facile Spray- Coating Process for the Fabrication of Tunable Adhesive Superhydrophobic Surfaces with Heterogeneous Chemical Compositions Used for Selective Transportation of Microdroplets with Different Volumes. *ACS Appl. Mater. Interfaces* ***2014****, 6, 8868–8877.*
21. Zhang, W.; Zhu, Y.; Liu, X.; Wang, D.; Li, J.; Jiang, L.; Jin, J. Salt-Induced Fabrication of Superhydrophilic and Underwater Superoleophobic PAA-g-PVDF Membranes for Effective Separation of Oil In-Water Emulsions. *Angew. Chem., Int. Ed.* ***2014****, 53, 856–860.*
22. Guix, M.; Orozco, J.; García, M.; Gao, W.; Sattayasamitsathit,S.; Merkoçi, A.; Escarpa, A.; Wang, J. Superhydrophobic Alkanethiol-Coated Microsubmarines for Effective Removal of Oil. *ACS Nano* ***2012****, 6, 4445–4451.*
23. Hayase, G.; Kanamori, K.; Fukuchi, M.; Kaji, H.; Nakanishi, K. Facile Synthesis of Marshmallow-Like Macroporous Gels Usable Under Harsh Conditions for The Separation of Oil and Water. *Angew. Chem., Int. Ed.* ***2013****, 52, 1986–1989.*
24. Li, J.; Kang, R.; Tang, X.; She, H.; Yang, Y.; Zha, F. Superhydrophobic Meshes that Can Repel Hot Water and Strong Corrosive Liquids Used for Efficient Gravity-Driven Oil/Water Separation. *Nanoscale* ***2016****, 8, 7638–7645.*
25. Fan, J. B.; Song, Y.; Wang, S.; Meng, J.; Yang, G.; Guo, X.;Feng, L.; Jiang, L. Directly Coating Hydrogel on Filter Paper forEffective Oil–Water Separation in Highly Acidic, Alkaline, and Salty Environment. Adv. Funct. Mater. 2015, 25, 5368–5375.
26. Barthlott, W.; Neinhuis, C.; Purity of the sacred lotus, or escape from contamination in biological surfaces. *Planta* ***1997****;202:1–8.*
27. Feng, L.; Li, S.;, Li, Y.;, Li, H.;, Zhang, L.; Zhai, J.; Song, Y.; Liu, B.; Jiang, L.; Zhu, D. Super-hydrophobic surfaces: from natural to artificial. *Adv. Mater.* ***2002****;14:1857–1860.*
28. Ronggang Cai; Karine,G.; David De Smet; Myriam, V.; Nicolas Mannu; Benoît Kartheuser; Bernard Nysten; and Alain M. Jonas *ACS Applied Materials & Interfaces* ***2018*** *10 (18), 15346-15351*
29. Seo, K.; Kim, M.; & Kim, D. H. Candle-based process for creating a stable superhydrophobic surface. *Carbon,* ***2014****, 68,583–596. Doi:10.1016/J.carbon.****2013****.11.038*
30. Zeng, O.; Wang, X.; Yuan, Z;, Wang, M.; & Huang, J. Fabrication of a superhydrophobic surface on copper foil based on ammonium bicarbonate and paraffin wax coating. *Surface Topography: Metrology and Properties,* ***2015****, 3(3), 035001.*
31. Zhao, Y.; Liu, E.; Fan, J.; Chen, B.; Hu, X.; He, Y., & He, C. Superhydrophobic PDMS/wax coated polyester textiles with self-healing ability via inlaying method. *Progress in Organic Coatings,* ***2019*** *132, 100–107.*
32. Lomonaco, D.; Mele, G.; & Mazzetto, S. E.. Cashew Nutshell Liquid (CNSL): From an Agro-industrial Waste to a Sustainable Alternative to Petrochemical Resources. *Cashew Nut Shell Liquid,****2017*** *19–38.*
33. Sultania, M.; Rai, J. S. P.; & Srivastava, D. A study on the kinetics of condensation reaction of cardanol and formaldehyde, part I. *Int. J. Chem. Kinet.,* ***2009****, 41, 559–572.*
34. Devi, A.; & Srivastava, D. Enzymatic epoxidation and polymerization of cardanol obtained from a renewable resource and curing of epoxide-containing polycardanol. *J. Appl. Polym. Sci.,* ***2006****, 102, 2730–2737.*

35. Chuayjuljit, S.; Rattanametangkool, P.; & Potiyaraj, P. Preparation of cardanol–formaldehyde resins from cashew nut shell liquid for the reinforcement of natural rubber. *J. Appl. Polym. Sci., **2007**, 104, 1997–2002.*
36. Jian Huang; Chang Lou; Dong Xu; Xin Lu; Zhong Xin; Changlu Zhou; Cardanol-based polybenzoxazine superhydrophobic coating with improved corrosion resistance on mild steel. *Progress in Organic Coatings, Volume **2019**, 136, 105191, ISSN 0300-9440.*
37. Bai, W.; Lin, H.; Chen, K.; Xu, J.; Chen, J; Zhang, X.; Xu, Y. Eco-friendly stable cardanol-based benzoxazine modified superhydrophobic cotton fabrics for oil–water separation. *Separation and Purification Technology, **2020**, 117545.*
38. Fallahi, Elham & Barmar, Mohammad & Kish, Mohammad. Preparation of Phase-change Material Microcapsules with Paraffin or Camel Fat Cores: *Application to Fabrics. Iranian Polymer Journal (English Edition).2010,19.*
39. Das, P.; Sreelatha, T.; & Ganesh, A. Bio oil from pyrolysis of cashew nut shell-characterisation and related properties. *Biomass and Bioenergy, **2004,** 27(3), 265–275.*
40. Ai, Q.; Yang, D.; Zhu, Y.; Jiang, Z. Fabrication of Boehmite/Alginate Hybrid Beads for Efficient Enzyme Immobilization.*Ind. Eng. Chem. Res. **2013**, 52 , 14898-14905.*
41. Magdalena, A. G.; Silva, I. M. B.; Marques, R. F. C.; Pipi, A. R. F. Lisboa-Filho, P. N.; & Jafelicci, M. EDTA-functionalized Fe 3 O 4 nanoparticles. *Journal of Physics and Chemistry of Solids,**2018** 113, 5–10.*
42. Wei, C.; Dai, F.; Lin, L.; An, Z.; He, Y.; Chen, X.; Chen, L.; Zhao, Y. Simplified and Robust Adhesive-Free Superhydrophobic SiO2-Decorated PVDF Membranes for Efficient Oil/Water Separation.*J. Membr. Sci. **2018**, 555, 220–228.*
43. Abdelrasoul, A.; Doan, H.; Lohi, A.; & Cheng, C.H. Mass Transfer Mechanisms and Transport Resistances in Membrane Separation Process. Mass Transfer - Advancement in Process Modelling. ***2015.***
44. Zhang, Z.-h.; Wang, H.-j.; Liang, Y.-h.; Li, X.-j.; Ren, L.-q.; Cui,Z.-q.; Luo, C. One-Step Fabrication of Robust Superhydrophobic and Superoleophilic Surfaces with Self-Cleaning and Oil/Water Separation Function. *Sci. Rep. **2018**, 8, 3869.*
45. Tang, H.; Hao, L.; Chen, J.; Wang, F.; Zhang, H.; Guo, Y. Surface Modification to Fabricate Superhydrophobic and Superoleophilic Alumina Membranes for Oil/Water Separation. *Energy Fuels **2018**, 32, 3627–3636.*

CHAPTER – 5

Boehmite/Chitosan Hybrid Aerogel:- Study on Thermal Insulation and Flame Retardant Properties

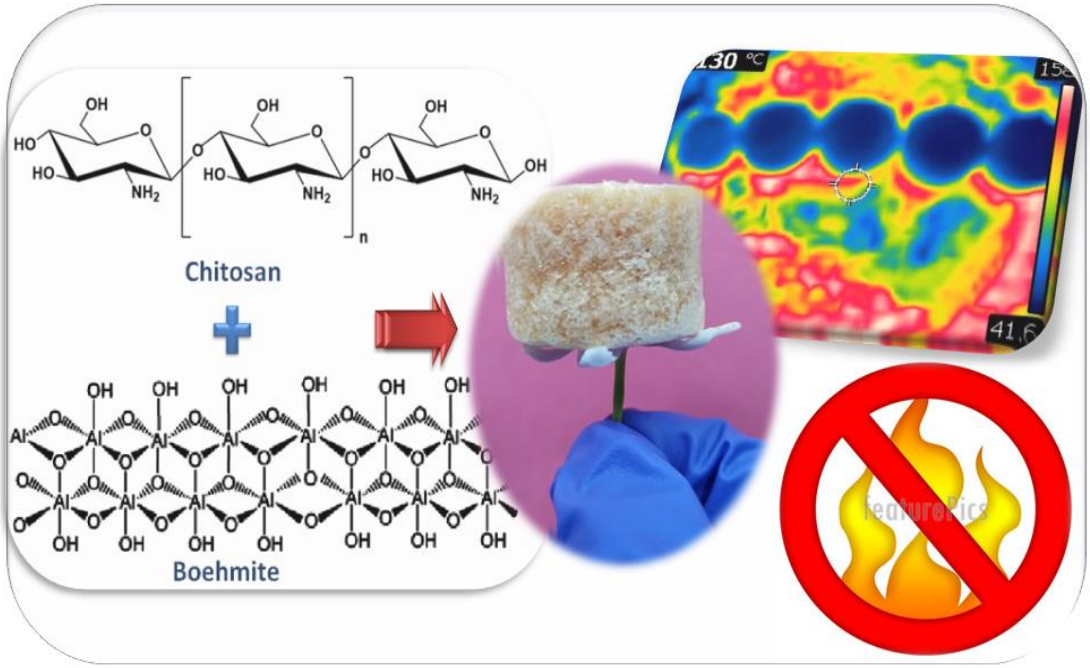

5.1. Abstract

This chapter describes processing of an inorganic-organic hybrid aerogel from boehmite and chitosan biopolymer. An investigation is made to study the beneficial properties of this boehmite-chitosan hybrid aerogel with respect to thermal insulation and flame propagation protection efficiency. Fabrication of boehmite/chitosan hybrid aerogel was achieved by sol-gel technique involving cross-linking of boehmite with chitosan biopolymer. The three dimensional porous aerogel body was obtained by gelation and freezing / drying technique. The resultant aerogel produced highly porous, lightweight, 3D networked solids. This porous hybrid aerogel was found to limit the heat transfer as well as to prevent the combustion of organic compounds. The structural as well as textural properties of the hybrid aerogel were characterized by FTIR, XPS, SEM, and N_2 adsorption-desorption analysis, and the results are discussed. This study demonstrates that the boehmite incorporated, chitosan based hybrid aerogel with porous 3D framework is a promising alternative to replace the non-biodegradable, easily flammable environmentally toxic, polymer based thermal insulation material [e.g styrene foams] in packing and construction fields.

5.2. Introduction

Thermally insulative, flame retardant packing materials are extremely important for the safe transportation of electronics, electrical and heat-sensitive objects. In recent years, an increased number of fire-accidents occur in high-rise buildings where the quick-spread of the fire as well as the hazardous dense, toxic fumes emanate from the conventional polymer based insulation packing material. Hence the use of polymer based, flammable thermal insulation packing needs an alternate technology. In this respect light weight, inorganic porous, flame protective, thermal insulation packing material preferably made up of composite or hybrid architecture is truly essential.

Aerogels are classical meso/micro porous solids having an inter-connected, three-dimensional nano-particulated networkedstructure.[1,2] Inorganic oxidic aerogels [e.g monoliths and composite designs] offer low density and high porosity. These characteristics make aerogel solids as the most promising flame retardant, thermal insulation materials.[3-5] Aerogel materials are usually made by well-known *supercritical drying* method. This production technology is well standardized and successfully employed for the processing of well-defined aerogels.[6, 7] However, super critical drying technique requires high pressure and temperature and needs special instrumentation. It is commonly said that the conventional super critical drying technique is energy-intensive and expensive process. Freeze-drying is emerged as an alternate technique and researchers reported processing of aerogel materials using metal oxides, carbon, cellulose, graphene, and clay through freezing and drying method.[8-12]

Hydrated alumina is a known and widely used inorganic flame retardant material. It has favorable non-toxic, non-volatile, fumeless and heat resistance properties.[13, 14] Similar to alumina hydrates, the mono hydroxy aluminium oxide, boehmite is also a candidate offering proven fire retardant properties. The fire retardant ability of boehmite could be explained by a dual suppression action that consists of releasing surface water at a lower decomposition temperature (223 ℃) and dissipating heat via an endothermic decomposition reaction with the formation of transition Al_2O_3 phases [e.g γ-alumina]at temperatures in the range 450-600 ℃.[15] However, freeze drying processing of phase-pure boehmite aerogels has an issue. At the time of aerogel preparation via freezing procedure, ice nucleates and the crystals of boehmite particles form ice-templated solids, resulting in fragile solids and therefore restricts their use in practical application.[16, 17]Incorporation of suitable macromolecules

may possibly increase the mechanical strength of such fragile aerogels, ultimately resulting in hybrid/composite aerogel architectures.[18, 19]

Researchers employed bio-polymers for forming structurally stable aerogels.[20, 21] Significant progress has been made in fabrication of bio polymer /aerogel hybrids and composite architectures.[22,23] In most of the reported works, such hybrid aerogel is explored for the drug immobilization and also for the controlled targeted delivery. Till date, varieties of oil-free, renewable biopolymer sources are considered. Sustainable biomass resources e.g., polysaccharides, proteins, and nucleic acids are used to form pure aerogel materials or their hybrids and composites by cross linking or using appropriate reinforcement phases such as silica and silsesquioxanes. Such inorganic-organic hybrid aerogel is reported to have lightweight and thermally super-insulating properties. [24, 25]

Chitosan, a deacetylated derivative of natural components in crustacean shells, is the second most abundant amino polysaccharide polymer.[26,27]It dissolves in acidic solutions to form three-dimensional networked colloidal mass, and its active amino groups react with various aldehydes to form a homogenous hydrogel.[28, 29] Previous research has shown that the multifunctional nature of chitosan, as well as its ready chemical compatibility with inorganic colloidal nano particulates, favours the design of micro/nano inorganic/organic hybrids. Yu et al. synthesized novel composite aerogel using chitosan as a sacrificial template to incorporate silica with phenol formaldehyde resin.[30] This outstanding three-dimensional nanostructure had exceptional low thermal conductivity and could with stand a temperature of 1300 °C. Furthermore, a series of biomimetic aerogels were created from chitosan, phenolic sol, along with various inorganic nanomaterials using a directional freezing method. Moreover, when low temperature polymer based solidification technique combined with freezing is

employed, the end-product not only demonstrated excellent thermal insulation properties but also sufficient mechanical strength comparable to the natural wood materials.[31] Chen and co-workers fabricated an ultrasensitive fire-warning chitosan/montmorillonite/carbonnanotube [CNT] composite aerogels and claimed that such material design showed considerable fire-resistance property. [32] Because of the hierarchical porous structure of the aerogel and the excellent barrier effect of the montmorillonite, the prepared composite could tolerate a high-temperature flame up to 1200 °C. Also, the chitosan hybrid aerogel found to effectively prevent the thermal radiation and maintained insulation in the non-exposed side. It is evident from the reported literature that chitosan-based aerogels have some remarkable properties like light weight, strong mechanical strength and good thermal insulation ability. Among many published works, processing of chitosan-based hybrid/composite aerogels using boehmite matrix is seldom reported. In particular, boehmite-chitosan hybrid aerogel for flame retardant and thermal insulation application is yet to be reported.

Hence in this working chapter, design of boehmite-chitosan inorganic-organic hybrid aerogel was attempted. Chitosan is a green, renewable biomaterial. Sol-gel derived colloidal boehmite is a layered, inorganic, heat-resistant material. Chitosan-boehmite hybrid is formed by chemical cross-linking *via* gluteraldehyde and a stable 3D aerogel is reached via freezing technology. The as-prepared hybrid monolith demonstrated a low density, high porosity, and unidirectional porous structure. The flame retardancy and self-extinguishing properties of the boehmite-chitosan aerogel was investigated and reported. Hybrid aerogels with different percentage of boehmite were also prepared and the thermal stability and flame retardant performance were compared with the percentage of boehmite loading. Owing to the high proportion of boehmite, the resulting aerogel demonstrated exceptional flame tolerance and could

withstand the temperature without collapsing indirectly indicating its flame resistance. This study demonstrates the multifunctional nature of the boehmite-chitosan hybrid aerogel.

5.3. Experimental Section

5.3.1. Materials

Aluminium isopropoxide (AIP, purity >98%), chitosan (medium molecular weight), and glutaraldehyde solution were purchased from Aldrich and used in as received condition. Nitric acid (HNO_3, purity 69-72%), and acetic acid were obtained from S.D. Fine-Chemicals Ltd. Double distilled water (DD) was used for the preparation of boehmite (AlOOH) sol and chitosan solution.

5.3.2. Preparation of chitosan aerogel

Chitosan was first dissolved in acetic acid solution (1.0 vol. %) and stirred at 60 °C to form an aqueous homogeneous chitosan solution (sample code: CH, chitosan amount 3.0 wt. %). This chitosan solution was chemically cross linked with 0.1 mL of glutaraldehyde solution. The resulting yellow solution was transferred to a Teflon mold and then cured at room temperature for 2 h to form a strong hydrogel. Subsequently, the hydrogel was placed at 4 °C to avoid macro fracture during the subsequent pre-freezing process.[33] Finally, the above hydrogel was frozen at -80 °C for 24 hours, and the resulting cryogel was transferred to a vacuum freeze-drying apparatus (Vir Tis Genesis 25L Piolot Lyophilizer) with a vacuum of below 5 Pa and a condenser temperature of -56 °C for 48 hours to obtain chitosan aerogel.

5.3.3. Preparation of cross linked boehmite/chitosan hybrid aerogel

The procedure described in section 2.3.2 of Chapter 2 was typically followed for synthesizing sol-gel derived boehmite. For making boehmite-chitosan bio-hybrid aerogel, the boehmite was used in the form of nano size boehmite gel powder. Once the

aqueous chitosan solution was prepared, different amounts of boehmite gel powder were added while stirring. The boehmite gel disperses readily in aqueous chitosan and forms a homogeneous boehmite-chitosan composite mix. With this the cross-linking agent glutaraldehyde was added to obtain chitosan-boehmite bio-hybrid aerogel. The same procedure was repeated to obtain hybrid aerogel with different loadings of boehmite. For comparison pure boehmite aerogel was also prepared. The hybrid aerogel and its counterparts were designated as CH Gel, AL Gel, CH-AL1, CH-AL2, CH-AL3, and CH-AL4. The AL 1-4 shows the loading of 1 to 4 wt.% loading of boehmite.

5.3.4. Characterizations

Infrared spectra were recorded using PerkinElmer Spectrum-Two FTIR spectrometers. The surface chemical nature of the hybrid aerogel was studied by PHI 5000 VersaProbe-II Focus X-ray photoelectron spectroscopy (XPS) (ULVAC-PHI Inc., USA) equipped with micro focused (200 μm, 15 KV) monochromatic Al-Kα X-Ray source (hν = 1486.6 eV). The morphologies of boehmite/chitosan hybrid aerogels were examined by scanning electron microscopy (SEM). SEM analysis was carried out using a Zeiss EVO 18 cryo-SEM operating at an accelerating voltage of 20 kV. SEM is equipped with an energy dispersive spectroscopy (EDS) attachment. Small pieces of hybrid aerogel were directly mounted on the SEM grids for the imaging. Differential scanning calorimetry (DSC) analysis was carried out with advanced research-grade modulated differential scanning calorimeter (DSC) TA Q2000 under flowing nitrogen gas. The heat flow and temperature were calibrated using a standard high purity indium. Samples were first heated to 200 °C at a rate of 10 °C/min, where it was isothermally kept for 2 min to delete the thermal history of samples and then cooled to room temperature at a rate of 10 °C/min. Samples were reheated at the rate of 10 °C/min to obtain melting temperature. Thermal stability of boehmite/chitosan hybrid aerogel was obtained by

thermo gravimetric analyzer TA Q50 (TGA) using the heating schedule. from room temperature to 800 °C at a rate of 10 °C/min under oxygen atmosphere.

5.3.5. Heat insulation and fire resistance analysis

The heat dissipation/diffusion across the CH-AL hybrid aerogel matrix was monitored using an infrared thermal imaging camera [Philips FLIR-C2]. The samples were placed on a flat plate heat source that was heated to 150 °C, and the upper surface temperature of the hybrid aerogel was recorded as a function of time. Meanwhile, the infrared thermal distribution image was captured under the thermal equilibrium state.

The flame tolerance and flame protection efficiency was ascertained using 'vertical burning test'. Since the standard instrument facility is not available to characterize the flame protection property, an indigenously designed set-up was used for understanding the flame-retardant performance. In a closed chamber candle flame was generated. The thermal structure of the stable, yellowish candle flame is complex and is characterized to have intense, short-distance, steep temperature gradients. Such thermal structures are reported to have an average temperature of 1000 ℃. The study reports on candle flame temperature indicate the luminous to non-luminous temperature in different zones vary from 600 to 1200^{o}C. In this study, the vertical candle flame test was carried out using the hybrid aerogels. The sample with a size of 5 cm × 1.5 cm × 2 cm was vertically exposed to a candle flame with a length of 2.5 cm. The distance between the bottom of the samples and the flame was approximately 1 cm. After being exposed to the flame for 10 seconds, each burning state of the sample was observed and recorded.

5.4. Results and Discussion

Fig. 5.1. provides a detailed schematic summary of the preparation of the CHAL hybrid aerogel; the steps involved are (1) preparation of aqueous chitosan solution,

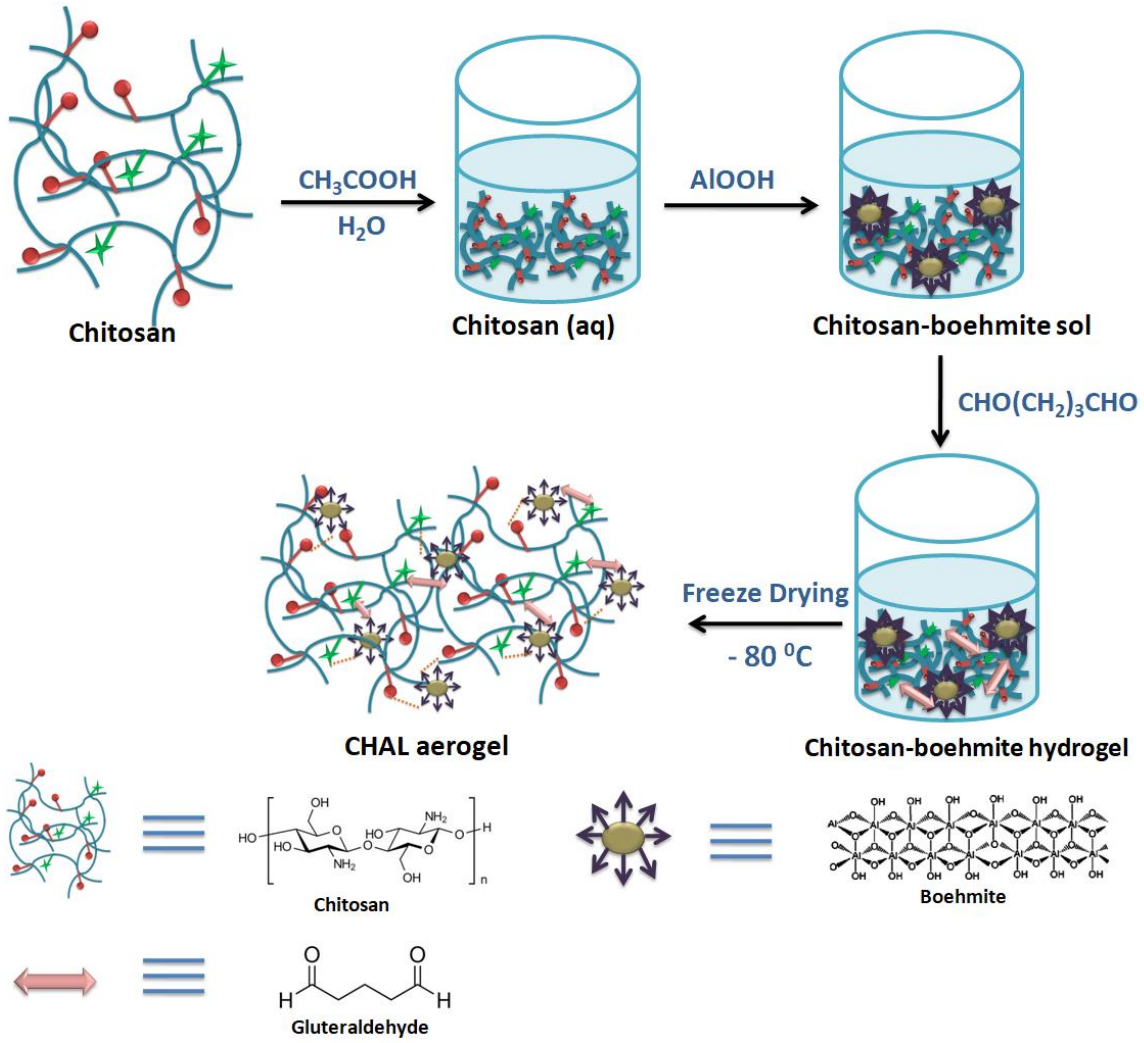

Fig. 5.1. Schematic illustration of the preparation of CHAL hybrid aerogel

(2) introducing boehmite gel powder and cross linking with glutaraldehyde [GA], and (3) freeze-drying of the CHAL hydrogel. An aqueous chitosan solution obtained in 1 vol.% acetic acid was used as a starting precursor in the preparation of CHAL hybrid aerogels. The -NH_2 group of chitosan is protonated during this process, resulting in the formation of a weak electrostatic interaction in the system.[34] The addition of boehmite gel powder followed by GA, the chemical cross linking readily takes place due to the presence of reactive surface hydroxyl groups and the construction of 3D hybrid structure is successfully formed. The aging/curing strengthens the 3D structure of the hybrid aerogel. The stronger electrostatic interaction is the driving force for gelation as

well as chemical cross linking between chitosan, boehmite, and GA. The photographic images of the prepared hybrid aerogel are depicted in the **Fig. 5.2.**

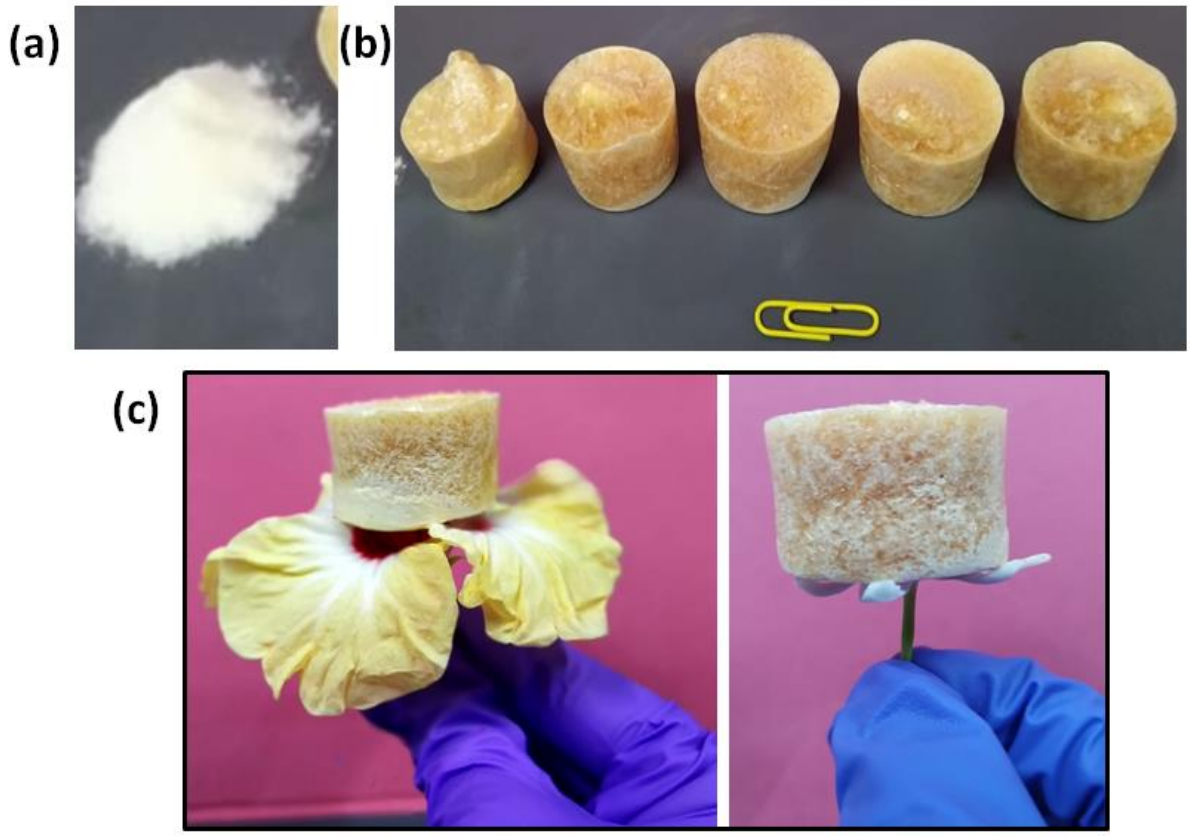

Fig.5.2. Photographic images of (a) AL Gel, (b) CHAL hybrids with varying concentration of boehmite, and (c) CHAL4 hybrid

5.4.1. Structural Characteristics of CHAL Hybrid Aerogel

Fourier transform infrared spectroscopy (FTIR) was used to analyse the functional groups of the chitosan (CH), boehmite gel(AL), and boehmite-chitosan hybrid aerogels (CHAL)to demonstrate the electrostatic interactions in the aerogel architecture. **Fig.5.3. a** depicts the FTIR spectra of CH and AL. The neat chitosan powder exhibits the characteristic absorption of glycosidic linkage at 896 cm^{-1}, as well as the absorption at 3371 cm^{-1} attributed to OH stretching vibration of hydroxyl groups and NH stretching vibration of amino-groups. Furthermore, the NH bending vibration of chitosan is clearly visible at 1589cm^{-1}.[35,36] In case of boehmite, the strong, broad band at 3274 cm^{-1} is

assigned to stretching vibration of OH group in the hydroxide structure as well as physically absorbed water. The intensive bands at 3069 cm^{-1} can be described to the symmetric stretching vibrations of (Al) O–H. The shoulder peak at 1597 cm^{-1} is taken for the bending mode of absorbed water. While the bands at1155$cm^{-1}$and 1066 $cm^{-1}$are believed to be asymmetric and symmetric stretching Al–O–H mode respectively. The band formed at 748 cm^{-1} belongs to theAlO_6 vibration mode. In addition, the peak at 1391 cm^{-1} indicates the presence of trace amount of the peptizing agent used.[37] In the FTIR spectra of CH gel and CHAL hybrid aerogel, a new peak is observed near 1651 cm^{-1} indicates the formation of imine bond with the crosslinking of GA.[38]

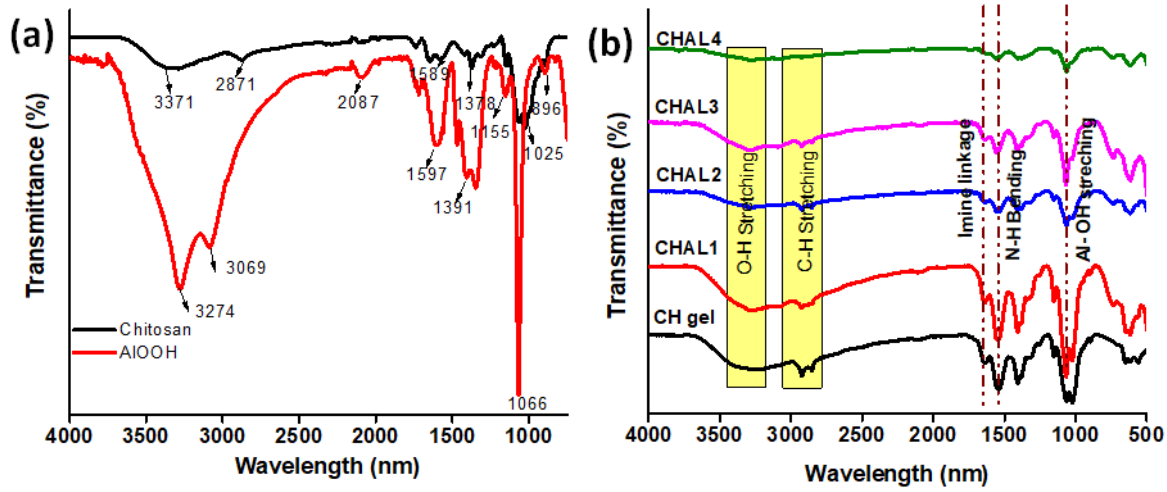

Fig.5.3. FTIR spectra of (a) boehmite(AlOOH), chitosan (b) chitosan aerogel and different concentration of AlOOH in CHAL hybrid aerogel

Meanwhile, there was no observed free aldehyde group (1710 cm^{-1}, derived from glutaraldehyde) in the aerogels, indicating that the completion of the Schiff base reaction. Moreover, the characteristic band of Al- OH shifts from 1155 cm^{-1} to 1070 cm^{-1}, which is attributed to the stronger interaction between chitosan, and boehmite through GA. The broadening of peaks around 3700-3200 cm^{-1}seen in aerogel can be due to the greater steric hindrance of a 3D gel network as well as the hydrogen bonding effect

which further provides evidence for the successful chemical-interaction of CH and AL in their hybrid aerogel.

The XPS studies of CHAL hybrid aerogel was performed to get an insight into the chemical interaction between chitosan and boehmite during cross linking with glutaraldehyde. The corresponding XPS spectra recorded for the hybrid aerogel are depicted in **Fig. 5.4.** The XPS survey scan shown in **Fig. 5.4. a.** clearly showed the presence of C, O, N, and Al elemental peaks in the aerogel hybrids. The deconvulated core level spectra of O1s **Fig. 5.4.b.** can be fitted into three individual peaks at 530.31, 531.86, and 533.53eV which represent the O-H, C-O-C, C-OH and Al-OH bonds respectively.[39] Moreover, the deconvoluted peaks for N 1s shown in **Fig. 5.4.c.** have peaks at 399.10 eV, 399.43 eV, 399.81,and 401.50 indicating the formation of C=N ,C-N, $C–NH_2$, and O= C-NH bonds respectively in the CHAL hybrid. This indicates that presence of amines chemically react with glutaraldehyde to form imines, which further verifies the completion of Schiff bases.[40]The XPS data clearly prove the reactants and are successfully cross linked to form a stable chitosan-boehmite hybrid aerogel. Again, the core level deconvoluted XPS spectrum for Al2p **Fig. 5.4.d.** displays two distinguished intense peaks at 73.71 eV, and 74.32 eV. The first peak indicates the characteristic peak for the Al-O-Al and the other peak for the Al-OH bonds in boehmite.[41]

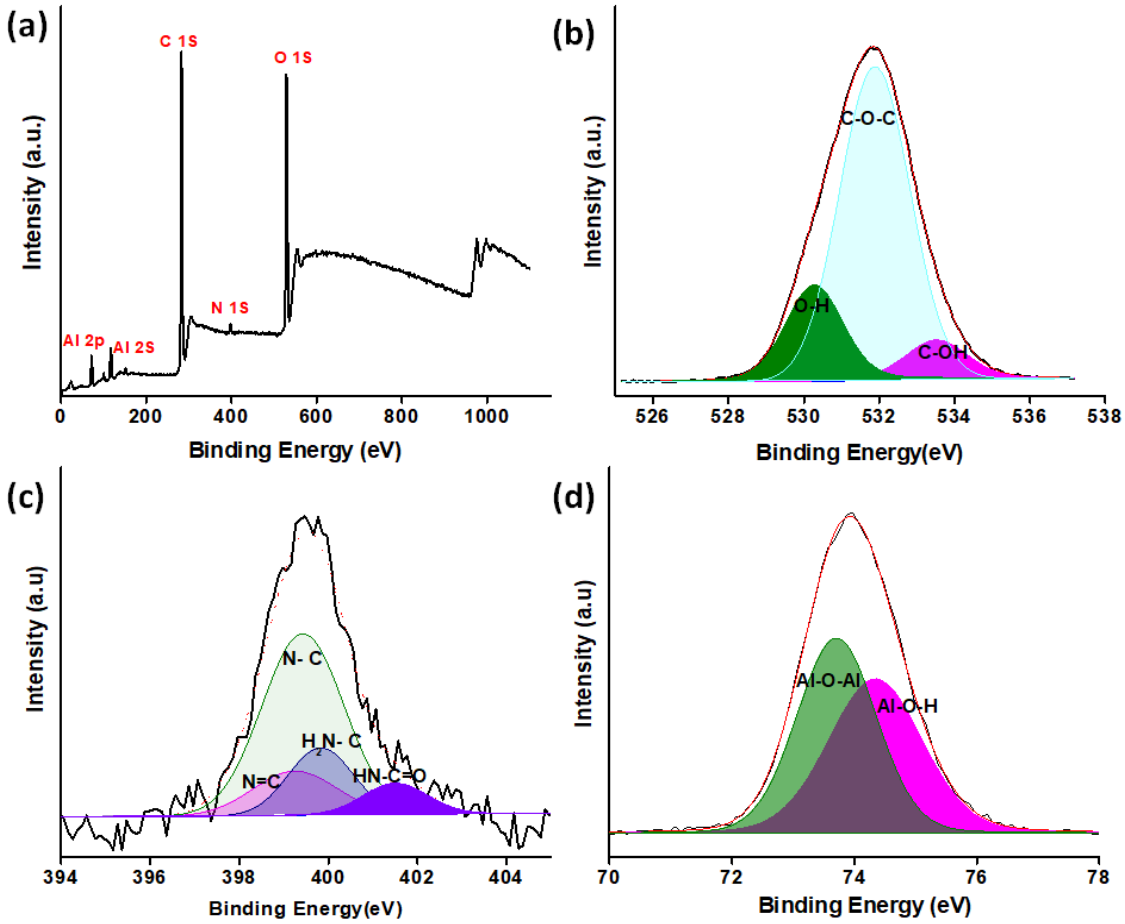

Fig.5.4. (a) XPS survey scan of CHAL4 hybrid aerogel and core-level XPS of (b) O 1s, (c) N 1s , and (d) Al 2p

5.4.2. Textural analysis

BET surface area measurements reveal the structural porous nature of the CHAL hybrid aerogels. The N_2 adsorption isotherms indicate the average pore diameter of the 3D porous aerogel. **Fig. 5.5.a.** depicts the adsorption and desorption isotherms of chitosan, boehmite, and CHAL hybrid aerogels. The pure chitosan aerogel exhibited a typical type III isotherm, which was attributed to the macro porous structure coming from the weak hydro-gel formation. In this case the BET surface area is extremely low and pure chitosan aerogel is found to have surface area only less than 2 m^2/gm. As it is evident from the **Fig. 5.5.b.,** boehmite aerogel have a type IV isotherm with a typical H_2 hysteresis loop, capillary condensation occurring at $p/p_0 > 0.5$ reflecting the

mesoporous characteristics.The boehmite aerogel found to have excessively high surface area. The physical properties such as BET surface area, pore diameter, and apparent density of pure chitosan aerogel and the hybrid aerogels are presented in **Table 5.1.** When boehmite gel was added to the chitosan skeleton, the specific surface area of the hybrid aerogel increased significantly than its counterpart, pure chitosan aerogel. Hybrid aerogel primarily displaying the mesoporous/macroporous adsorption/desorption hysteresis curve.As the boehmite content increases, the apparent density (〉) of hybrid aerogel is increased gradually. Among them, CHAL4 has the highest specific surface area (S_{BET} = 17.77 m^2 g^{-1}) and pore diameter (36.87 A^o). Therefore, addition of boehmite has a positive effect on the surface area, pore diameter, and microtopography of the chitosan skeleton, which is beneficial in inhibiting the gas-phase heat transfer of material.

Table 5.1. Physical parameters of CH Gel, AL Gel, and CHAL hybrid gels

Sample	BET Surface area (m^2/g)	Porediameter (A^o)	Density (g/cc)
CH Gel	1.21	NA	0.064
AL Gel	290.84	39.917	0.073
CHAL1	6.98	11.433	0.077
CHAL2	7.86	16.568	0.080
CHAL3	10.33	23.382	0.086
CHAL4	17.77	36.870	0.093

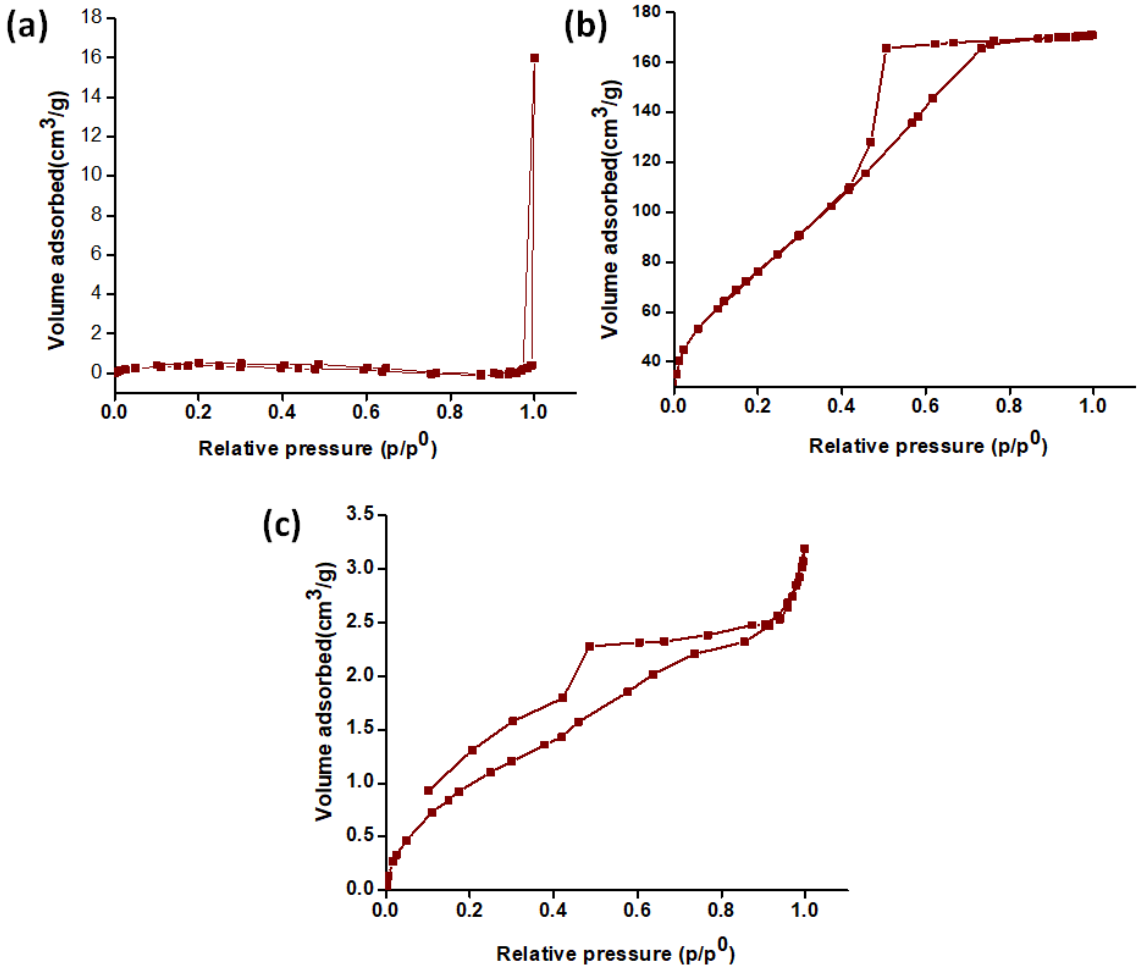

Fig. 5.5. Nitrogen adsorption- desorption isotherms of (a) CH Gel, (b) AL Gel, and (c) CHAL4 hybrid aerogel

5.4.3. Thermal stability of CHAL hybrid aerogel

TGA thermogram was used to investigate the thermal stability of CH Gel, AL Gel, and CHAL hybrid aerogels in an oxygen atmosphere. **Fig.5.6.a.** displays the typical TGA plots of CH, AL and CHAL hybrid aerogel samples. It can be seen that there is no discernible weight loss in the inorganic boehmite gel. However, the degradation of pure chitosan aerogel,CH showed three stage decomposition: (1) The weight loss observed below 100 °C was attributed to the dehydration of the biopolymer and water molecules present in the chitosan hydrogel; (2) The main weight loss of 63% occurred at 200-400 °C, and the weight loss is maximum at 274 °C, indicating the glycosidic bond decomposition and the

volatilization of organic compounds; and (3) A final weight loss at 550°C is due to the thermal degradation, followed by gradual stabilization, resulting in a carbon residue at 800°C.[42]The stage of thermal degradation for CHAL hybrid aerogels is similar to that of CH Gel, but with a variation in the peak temperature for the degradation of the hybrid structure. With increasing boehmite contents, the weight loss % of hybrid aerogels decreases gradually compared to pure CH Gel. Notably, the rate of thermal degradation is relatively mild and gradual when the boehmite % is gradually increased. It indicates that boehmite-chitosan hybrid aerogels have comparatively high thermal stability at elevated temperatures. Boehmite is a polymorphic material and the thermal degradation is associated with the formation of transition alumina. The transformation of boehmite into porous alumina possibly introduces thermal stability and decreases effective rate thermal degradation. In summary, the TGA study reveals, the inorganic boehmite can considerably improve the thermal stability of the chitosan-based aerogel, which is beneficial for the application of the thermal insulation applications.

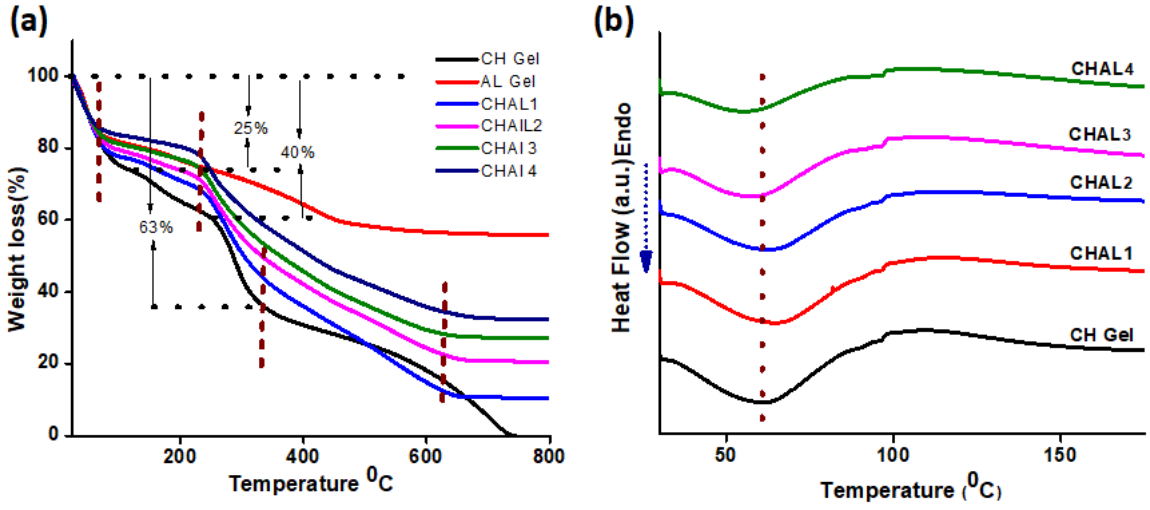

Fig.5.6. Thermal Stability of CH, AL and CHAL hybrid aerogels
(a) TGA plot of pure CH Gel, AL Gel, and CHAL hybrid aerogel and
(b) DSC plot of CH Gel and CHAL hybrid aerogels

DSC analysis provides useful information about the phase transitions within the aerogel materials. DSC data normally record the glass transition and softening (melting) temperatures of the material. Chitosan is a biopolymer whereas the boehmite gel is an inorganic polymeric material. DSC thermograms representing chitosan aerogel and CHAL hybrid aerogel were presented in**Fig.5.6.b.** The pure chitosan aerogel exhibits a broad endothermic peak at temperatures between 50 to 70^{o}C with the peak temperature of ~61°C. Since the amino groups present in the chitosan readily crosslink with the glutaraldehyde, there exists a limited amount of free-water as well as amino groups. Moreover, the availability of amino groups is also less to form hydrogen bonds with water molecules in the cross-linked aerogel. **Fig. 5.6.b.** shows shifting of the endothermic peak to a higher temperature in the case of boehmite–chitosan hybrid aerogel, indicating the hybrid retains relatively more water molecules. With the addition of boehmite, new hydrophilic centres are formed in CHAL hybrid aerogel, i.e. the terminal hydroxyl groups of boehmite bind a greater number of water molecules, increasing the bound water content. When the content of boehmite is further increased, the endothermic peak is shifted to a lower value, suggesting that, there is no possible site for bonding with water.

5.4.4. Morphological analysis

The structure and morphology of the CHAL hybrid aerogels were examined with scanning electron microscopy (SEM). The neat chitosan aerogel exhibited a porous structure with the pores of arbitrary shape and its randomly distributed pattern **(Fig. 5.7.a.).** The porous structure results from the sublimation of frozen water during the freeze- drying process. In contrast, as shown in **Fig. 5.7.b.** the boehmite aerogel shows the characteristic layered platy structure and comparatively dense nature. Fragments of

the layered boehmite are clearly seen. Once colloidal boehmite gel is introduced into the chitosan, the CHAL hybrid aerogels display significant porous structure.

In fact, as the boehmite content increases, the pore size of the aerogels becomes larger.In contrast, as shown in **Fig. 5.7(cf),** CHAL hybrid aerogels have an agglomerated coral-like pattern with porous structure rather than a homogeneous isolated porous nature with uneven meso/ macropores.

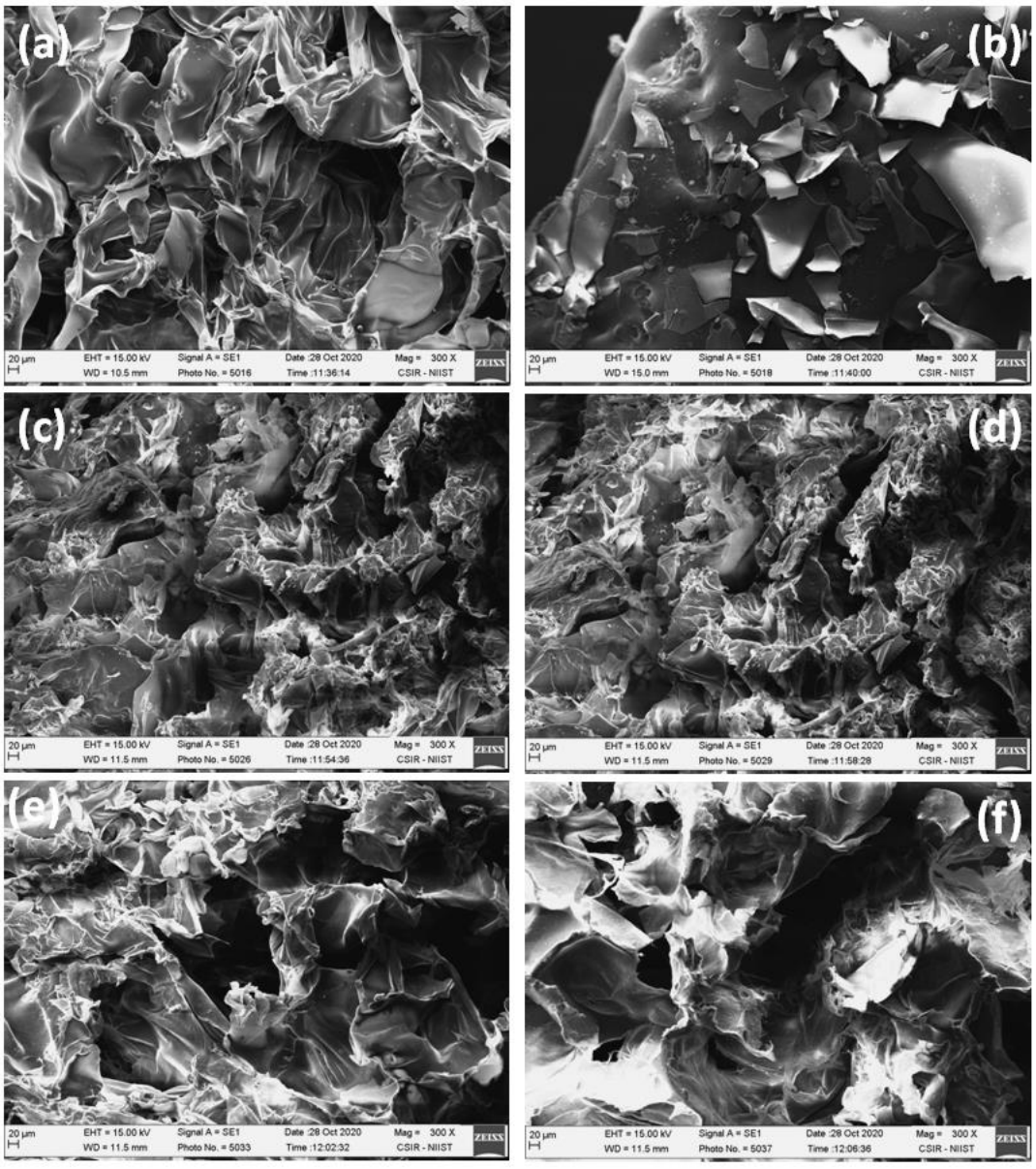

Fig. 5.7. SEM image of (a) CH Gel, (b) AL Gel, (c) CHAL1, (d) CHAL2, (e) CHAL3, and (f) CHAL4 hybrid aerogels

5.4.5. Flame test for fire protection applications

Vertical burning test was used to investigate the effect of boehmite on the combustion nature of the CHAL hybrid aerogel. A digital camera recorded the flame test and the flammability of the hybrid aerogel during vertical burning. The video snapshots at different time periods were made to explain the interaction of the aerogel object with the candle flame. The snapshots corresponding to the pure chitosan aerogel as well as for the CHAL hybrid aerogel are presented in **Fig.5.8**. It can be seen that the pure chitosan aerogel captures the fire within 6 seconds and shows the sign of burning when it comes in contact with the flame. In the case of hybrids, the aerogels show comparatively high degree of structural stability and it is evident that the addition of boehmite limits the flame to generate fire and also its propagation. Moreover, when the hybrid aerogel is moved away from the fire, the flame immediately extinguishes without any afterglow, indicating the auto-extinguishable feature of the hybrid material. In fact, once boehmite is added into the aerogel, no matter how much the boehmite content is, all the aerogels show significant stability under the flame. The flame test also showed a carbonized residue in the flame contact area but interestingly the carbon residue retains the original shape and dimension. No structural degradation is seen due to the flame. If the aerogel is ignited again, it begins to glow red without blaze, suggesting that the sample has turned into ceramized residue. Surprisingly, the prepared CHAL hybrid aerogel could not produce flame, and this self-extinguishing behavior could reduce the potential fire hazards. The boehmite present in the hybrid gets transformed to alumina ceramic body covered with the carbonaceous layer. The transformation boehmite to alumina imparts structural stability to the porous carbon. The formation of porous alumina and carbon restricts the flame propagation.

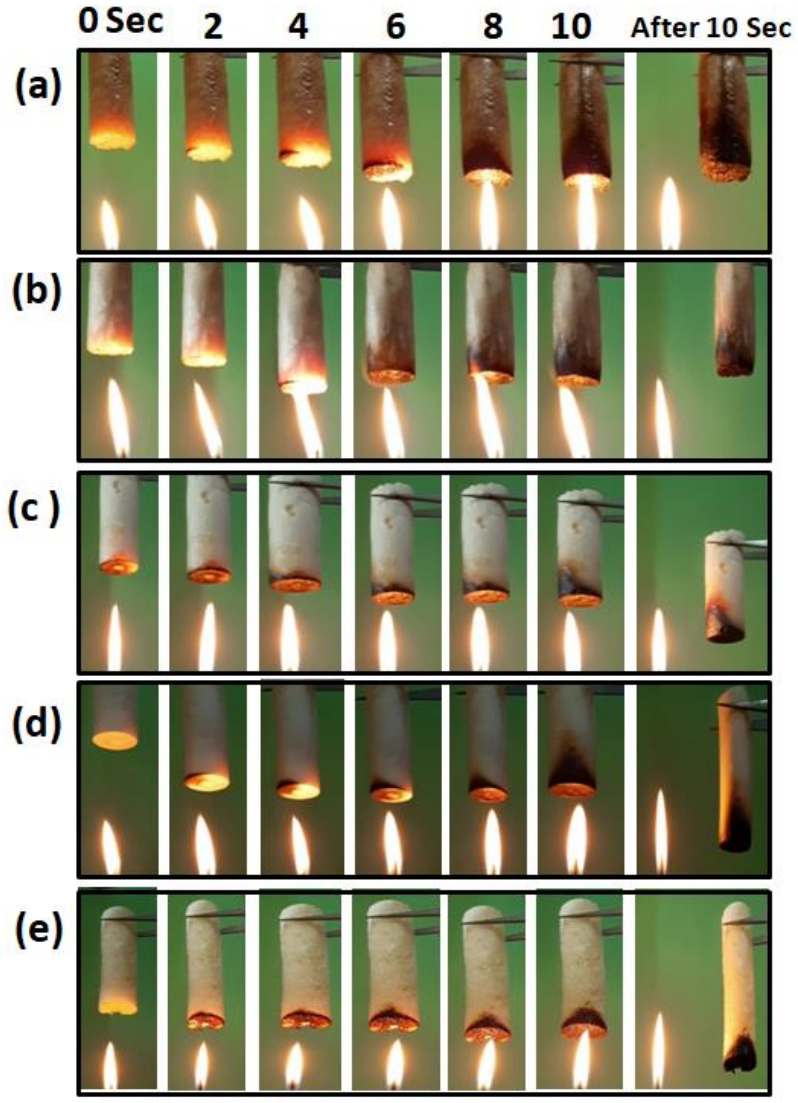

Fig.5.8. Photographs of pure CH Gel and its hybrid aerogels under vertical combustion process (a) CH Gel, (b) CHAL1,(c) CHAL2, (d) CHAL3, and (e) CHAL4

The thermal insulation or the heat diffusion/dissipation behavior of the prepared CHAL hybrid aerogel was examined through an indirect proof-of-concept. Here the time-dependent temperature of the CHAL hybrid aerogel was recorded using non-contact IR sensor at different set temperatures. The results are shown in **Fig. 5.9.** The chitosan aerogel as well as the CHAL hybrid aerogels were placed on a steel top heating platform with a set temperature of 150^{o}C. The heating platform was allowed to heat. During heating the dynamic temperature variation on the top surface the aerogel

as well as the heating platform was monitored using an infrared thermometer. Simultaneously the heat distribution was also recorded using a thermal imaging camera. Chitosan aerogel has low thermal conductivity. Its' hybrid design with boehmite is also expected to retain low thermal conductivity. It is noticed that the CHAL hybrid aerogel displayed more uniform internal temperature distribution and good infrared barrier properties.

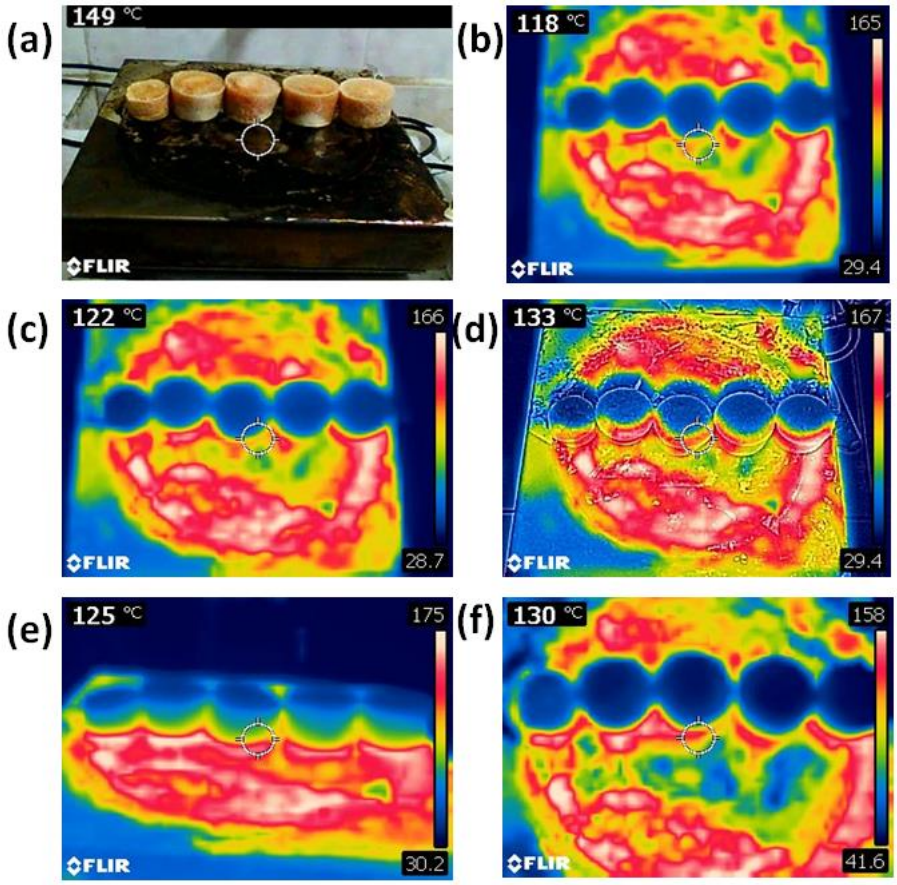

Fig. 5.9. photographic and infrared images of CH Gel and CHAL hybrid aerogels(a)Thermal insulation setup, at (b)0 min, (c) 15 min, (d) 30 min, (e) 45 min, and (f) 60 min

Further the change in the surface temperature of the CHAL hybrid aerogel was observed, when the temperature on the surface of the heating platform steadily rises and stabilizes at nearly 200 °C. In the case of CHAL4 hybrid aerogel, the surface temperature rises slowly and the thermal equilibrium temperatures on the top surface

increased to 41.6 °C after 60 min. In addition, the bottom of the pure chitosan aerogel sample, touching the heating platform, was black after the heat conduction experiment, indicating that the chitosan aerogel was partially carbonized. In comparison, no carbonization was observed for the CHAL hybrid aerogels. The excellent thermal barrier property in CHAL hybrid aerogel was owing to meso/macro porous nature of the hybrid aerogel.The results show that CHAL hybrid aerogel has good thermal stability and heat insulation performance. It can effectively avoid the heat loss to the ambient environment and also could be used as a thermal insulation material in daily life.

5.5. Conclusions

In this work, fabrication of eco-friendly bio based chitosan-boehmite inorganic-organic hybrid aerogel (CHAL) was demonstrated for possible fire-resistance, thermal insulation application. The hybrid aerogel was successfully prepared via sol-gel assisted freeze drying technique. The as-prepared hybrid aerogels offered highly porous 3D networked solid structure. The TGA study confirmed that the incorporation of boehmite into chitosan offers significant thermal stability. The results seen with the vertical burning test indirectly indicate the CHAL hybrid aerogel exhibited notable flame stability and resistance against fire-propagation. Owing to the hierarchical porous structure of the boehmite–chitosan hybrid aerogel, the heat dissipation across the aerogel geometry was significantly restricted. When the hybrid aerogel was subjected to the heating temperature of ~200 ^{o}C, a sign ofheat-barrier effect is realized. Due to the presence of boehmite, CHAL could withstand the temperature up to 200 °C and effectively prevent the thermal conduction towards the non-exposed side, proving the concept of thermal insulation. The study is significant because the packing industry needs alternate light weight, fire proof, thermal insulation materials. CHAL hybrid aerogel may have a promising future in this application.

5.6. References

1. Lyu, J.; Li, G.; Liu, M.; Zhang, X. Aerogel-directed energy-storage films with thermally stimulant multi responsiveness. *Langmuir* ***2019****,35, 943–949.*
2. Zhao, W.; Wang, T. P.; Wu, J. L.; Pan, R. P.; Liu, X. Y.; Liu, X. K.Monolithic covalent organic framework aerogels through framework crystallization induced self-assembly: heading towards framework materials synthesis over all length scales. *Chinese J.Polym. Sci.* ***2019****, 37, 1045–1052*
3. Baetens, R.; Jelle, B. P.; and A. Gustavsen, Aerogel insulation for building applications: a state-of-the-art review. *Energy and Buildings,* ***2011****, 43, 761–769,*
4. Schubert, U.;Silica-based and transition metal-based inorganic-organic hybrid materials a comparison, *Journal of Sol-Gel Science and Technology,* ***2003****, 26, 47–55,.*
5. Koebel, M. M.; Rigacci, A.; Achard, P.; Aerogels for Superinsulation: A Synoptic View. In Aerogels Handbook M. A. Aegerter; N. Leventis; Koebel, M. M., *Eds.* ***2011****, 607-633.*
6. Husing, N.; Schubert, U.; Aerogels Airy Materials: Chemistry, Structure, and Properties. *Angew. Chem. Int. Ed.* ***1998,*** *37, 22-45.*
7. Maleki, H.; Duraes, L.; A. Portugal, An overview on silica aerogels synthesis and different mechanical reinforcing strategies. *J. Non-Cryst. Solids* ***2014,*** *385, 55–74.*
8. Axel, F.; Sara, S.-P.; Suraj, N.; Natalja, W.; Massimo, C.;Giammarino, P.; Jan, P.; Cansunur, D.; Imme, K.; Detlef, W. B.; Peter,B.; Nadja, C. B. Versatile Aerogel Fabrication by Freezing and Subsequent Freeze-Drying of Colloidal Nanoparticle Solutions. *Angew.Chem., Int. Ed.* ***2016****, 55 1200–1203.*
9. Wang, C.; Pan, Z.-Z.; Lv, W.; Liu, B.-L.; Wei, J.; Lv, X.-H.; Luo, Y.; Nishihara, H.; Yang, Q.-H. A Directional Strain Sensor Based on Anisotropic Micro Honeycomb Cellulose Nanofiber-Carbon Nanotube Hybrid Aerogels Prepared by Unidirectional Freeze Drying. *Small* ***2019****, 15, 1805363.*
10. Ghannadpour, M.; Wicklein, B.; Carosio, F.; Wagberg, L. All Natural and highly flame-resistant freeze-cast foams based on phosphorylated cellulose nanofibrils. *Nanoscale* ***2018****, 10, 4085–4095.*
11. Wicklein, B.; Kocjan, D.; Carosio, F.; Camino, G.; Bergström, L. Tuning the Nanocellulose-Borate Interaction To Achieve Highly Flame Retardant Hybrid Materials. *Chem. Mater.* ***2016***, 28, 1985−1989.
12. Dove, C. A.; Bradley, F. F.; Patwardhan, S. V. A material characterisation and embodied energy study of novel Clay-Alginate Composite Aerogels. *Energy and Buildings* ***2019****, 184, 88–98.*
13. LUNDBERG, C. V; Hydrated Alumina as a Fire-Retardant Filler in Styrene Polyester Casting Compounds. *Fillers and Reinforcements for Plastics,* ***1974****. 184–194.*
14. Wypych, G.; FILLERS – ORIGIN, CHEMICAL COMPOSITION, PROPERTIES, AND MORPHOLOGY. *Handbook of Fillers,* ***2016,****13–266.*
15. Fan, B.; Chen, S.; Yao, Q.; Sun, Q.; & Jin, C.. Fabrication of Cellulose Nanofiber/AlOOH Aerogel for Flame Retardant and Thermal Insulation. *Materials,* ***2017,*** *10, 311.*
16. Huang, P.; Fan, M. Development of facture free clay-based aerogel: Formulation and architectural mechanisms. *Composites, Part B* ***2016****, 91, 169–175.*
17. Madyan, O. A.; Fan, M.; Feo, L.; Hui, D. Enhancing mechanical properties of clay aerogel composites: *An overview. Composites, Part B* ***2016****, 98, 314–329.*

18. Chen, H.-B.; Schiraldi, D. A. Flammability of Polymer/Clay Aerogel Composites: *An Overview. Polym. Rev.* ***2019****, 59 (1), 1–24.*
19. Chen, H.B.; Shen, P.; Chen, M.J.; Zhao, H.B.; Schiraldi, D. A. Highly Efficient Flame Retardant Polyurethane Foam with Alginate/ Clay Aerogel Coating. *ACS Appl. Mater. Interfaces* ***2016****, 8, 32557–32564.*
20. Druel, L.; Bardl, R.; Vorwerg, W.; Budtova, T. Starch aerogels: A member of the family of thermal superinsulating materials. *Biomacromolecules* ***2017****, 18, 4232–4239.*
21. Groult, S.; Budtova, T. Thermal conductivity/structure correlations in thermal super-insulating pectin aerogels. *Carbohydr. Polym.* ***2018****, 196, 73–81.*
22. Wang, Y.; Wu, K.; Xiao, M.; Riffat, S. B.; Su, Y.; Jiang, F. Thermal conductivity, structure and mechanical properties of konjac glucomannan/starch based aerogel strengthened by wheat straw. *Carbohydr. Polym.* ***2018****, 197, 284–291.*
23. Zhao, S.; Malfait, W. J.; Guerrero-Alburquerque, N.; Koebel, M.M.; Nyström, G. Biopolymer aerogels and foams: chemistry, properties, and applications. *Angew. Chem., Int. Ed.* ***2018****, 57, 7580–7608.*
24. Raman, S. P.; Gurikov, P.; Smirnova, I. Hybrid alginate based aerogels by carbon dioxide induced gelation: Novel technique for multiple applications. *J. Supercrit. Fluids* ***2015****, 106, 23–33.*
25. Zhu, G.; Xu, H.; Dufresne, A.; Lin, N. High-adsorption, self extinguishing thermal, and acoustic-resistance aerogels based on organic and inorganic waste valorization from cellulose nanocrystals and red mud. *ACS Sustainable Chem. Eng.* ***2018****, 6, 7168–7180.*
26. Baldino, L.; Cardea, S.; Reverchon, E. Nanostructured chitosan gelatin hybrid aerogels produced by supercritical gel drying. *Polym. Eng. Sci.* ***2018****, 58, 1494–1499.*
27. Shi, X.; Jiang, S.; Hu, Y.; Peng, X.; Yang, H.; Qian, X. Phosphorylated chitosan-cobalt complex: A novel green flame retardant for polylactic acid. *Polym. Adv. Technol.* ***2018****, 29, 860–866.*
28. Li, A.; Lin, R.; Lin, C.; He, B.; Zheng, T.; Lu, L.; Cao, Y. An environment-friendly and multi-functional absorbent from chitosan for organic pollutants and heavy metal ion. *Carbohydr. Polym.* ***2016****, 148, 272–280.*
29. Zhao, S.; Malfait, W. J.; Jeong, E.; Fischer, B.; Zhang, Y.; Xu, H.; Angelica, E.; Risen, W. M., Jr.; Suggs, J. W.; Koebel, M. M. Facile one-pot synthesis of mechanically robust biopolymer silica nanocomposite aerogel by cogelation of silicic Acid with chitosan in aqueous media. *ACS Sustainable Chem. Eng.* ***2016****, 4, 5674–5683.*
30. Yu, Z.L.; Yang, N.; Apostolopoulou-Kalkavoura, V.; Qin, B.; Ma, Z.-Y.; Xing, W.-Y.; Qiao, C.; Bergström, L.; Antonietti, M.; Yu, S.H. Fire-retardant and thermally insulating phenolic-silica aerogels. *Angew. Chem., Int. Ed.* ***2018****, 57, 4538–4542.*
31. Yu, Z.-L.; Yang, N.; Zhou, L.-C.; Ma, Z.-Y.; Zhu, Y.-B.; Lu, Y.- Y.; Qin, B.; Xing, W.-Y.; Ma, T.; Li, S.-C.; Gao, H.-L.; Wu, H.-A.; Yu, S.-H. Bioinspired polymeric woods. *Sci. Adv.* 2018, 4, No. 7223. Chen, J.; Jiang, S. D.; Huang, Z. Q.; Tang, G.; Hu, Y. Selfassembly of hydroxyapatite with polyelectrolyte as a green flame retardant for poly(vinyl alcohol). *J. Fire Sci.* **2017**, 35, 507–520.
32. Jundong Zhu, Renjie Xiong, Fuxing Zhao, Tangping Peng, Jiang Hu, Le Xie, Huasheng Xie, Kang Wang, and Chongwen Jiang *ACS Sustainable Chemistry & engineering* **2020** *8,* 71-83
33. Yang, J.Y.; Xia, Y.; Zhao, J; Yi, L.F.; Song, Y.J.; Wu, H.; Guo ,S.Y.; Zhao ,L.J.; Wu , J. R. Flame-retardant and Self-healing Biomass Aerogels Based on Electrostatic Assembly. *Chin J Polym Sci* ***2020****, 38, 1294–1304*

34. Ghosh, A.; Ali, M. A. Studies on physicochemical characteristics of chitosan derivatives with dicarboxylic acids. *J. Mater. Sci.* **2011**, *47*,1196–1204.
35. Orienti, I.; Cerchiara, T.; Luppi, B.; Bigucci, F.; Zuccari, G.; Zecchi, V Influence of different chitosan salts on the release of sodium diclofenac in colon-specific delivery. *Int. J. Pharm.* **2002**, *238*, 51–59.
36. Ai, Q.; Yang, D.; Zhu, Y.; Jiang, Z. Fabrication of Boehmite/Alginate Hybrid Beads for Efficient Enzyme Immobilization. *Ind. Eng. Chem. Res.* **2013**, *52* , 14898-14905.
37. Zhang, S.; Feng, J.; Feng, J.; Jiang, Y.; Li, L. Ultra-low shrinkage chitosan aerogels trussed with polyvinyl alcohol. *Mater. Des.* **2018**, 156, 398–406.
38. Lawrie, G., Keen, I., Drew, B., Chandler-Temple, A., Rintoul, L., Fredericks, P., & Grøndahl, L. Interactions between Alginate and Chitosan Biopolymers Characterized Using FTIR and XPS. *Biomacromolecules,* **2007**,*8(8), 2533–2541.*
39. Zhang, D.; Wang, L.; Zeng, H.; Yan, P.; Nie, J.; Sharm, V. K.; Wang, C. A three-dimensional macroporous network structured chitosan/cellulose biocomposite sponge for rapid and selective removal of mercury(II) ions from aqueous solution. *Chem. Eng. J.* **2019**, 363, 192–202.
40. Sahoo, N. G.; Cheng, H. K. F.; Li, L.; Chan, S. H.; Judeh, Z.; Zhao, Specific Functionalization of Carbon Nanotubes for Advanced Polymer Nanocomposites
J. Adv. *Funct. Mater*. **2009**, 19, 3962.
41. Hong,P.Z.;Li,S.D.; Ou, C.Y.; Li, C.P.; Yang, L.; & Zhang, C.H. Thermogravimetric analysis of chitosan. *Journal of Applied Polymer Science, **2007**,105(2), 547–551.*

CHAPTER –6

Conclusions, Contributions, and Future Directions

6.1. Research Summary

Inorganic-organic hybrid materials exhibiting high surface area with preferably hierarchical structured porous architectures have gained much attention as competitive materials to the expensive MOFs (metal organic frameworks) and COFs (covalent organic frameworks). The driving force behind the synthesis of such new-fangled materials is due to their exciting surface functional properties and enhanced performance for any multifunctional applications. Today hybrid porous materials find place in environmental remediation, energy storage, sensors, electronics, and health care.

In nanoscale inorganic metal oxides, *Boehmite* (monohydroxy aluminium oxide) a multifaceted material has attracted much interest due to its easy synthesis in colloidal particulates as well as in gel structure, significant chemical andthermal stability, surface OH groups, ready dispersion and chemical interaction with the active molecules, high surface area, favourable biocompatibility, tunable morphological features, and scope for tailoring the surface characteristics. These remarkable properties of boehmite offer endless possibilities for the design and synthesis of inorganic-organic hybrid materials that find impressive applications in fore-front areas of applied materials.

The thesis entitled*"**Investigations on Inorganic-Organic Hybrid Nanomaterials from Boehmite [AlOOH] Gels for Multifunctional Applications"*** has opened a new avenue in hybrid materials design. In this thesis work, the boehmite based inorganic-organic hybrid architectures were successfully designed by two strategies; (i) incorporation of a photocatalytic material, $CeO_2$and (ii) tailoring the functionality using an organic molecule derived from the Natural plant, Cashew Nut Shell Liquid [CNSL]. These two different hybrid materials weresystematically investigated for the niche areas of applications such as a photocatalytic-adsorbent for environmental remediation, electrochemical sensor, oil/water separation and flame tolerant, thermal insulation aerogels. In this chapter the highlights of

the salient research outcomes and scientific observations made in the thesis work are summarized.

At the beginning of the thesis work, focus was given to explore boehmite based hybridmaterial as a potential photocatalytic sorbent. Hybrid was obtained through nanocasting of sol gel derived boehmite chemically modified with the polyethyleneimine and dispersion of nano ceria. The gel monolith hybrids due to the presence of ceria /boehmite showed catalytic- sorbent properties. The synthesized boehmite-CeO_2hybrid were demonstrated for the adsorption and photo-degradation of lignin and organic dye in water. In addition, the antimicrobial propertyof the hybrid was also documented.

In another work module, a newelectrochemical sensor was designed using boehmite gelchemically modified with a natural organic molecule CNSL. Electrochemical sensing property towards neurotransmitter dopamine [DA] was studied. It was found that the sensor designed out of boehmite-CNSL hybrid material displays a higher electro-catalytic activity toward DA oxidation with a wider linear detection range of 50 µM to 450 µM and a lower detection limit of 23×10^{-9} m. Furthermore, the developed electrochemical biosensor also portrayed satisfactory level of selectivity, operational stability, and reproducibility.

Later, inorganic-organic hybrid coating design was considered. In this work, boehmite gel based hybrid formulation was prepared by combining the boehmite gel with the organic CNSL oil and paraffin wax. This hybrid formulation offered super hydrophobicityand resistance to water impact. This hybrid suspension was applied on pristine cotton textile. The hybrid coated cotton textile was used for the systematic study of oil/water separation including crude oil and other organic solvents.

Finally, lightweight, porous hybrid aerogel was prepared by cross-linking chitosan and boehmite with gluteraldehyde. Lyophilization method was employed for the preparation of hybrid aerogel. Flame tolerance property of the hybrid aerogel was investigated through

the vertical burning test.It was understood from the study that the boehmite-chitosan based porous hybrid aerogel is an environment-friendly, multifunctional packing material that can possibly replace the flammable polymer packing materials.

6.2. Contributions

In this thesis work, systematic research contributions were made to make three different kinds of new inorganic-organic hybrid materialsusing boehmite.

(i) Hybrid Nanocomposite material consisting of boehmite and photoactive, antimicrobial nano ceria

(ii) Boehmite-CNSL Inorganic-organic hybrid Electrochemical Sensor

(iii) Super hydrophobic hybrid coatings for functional membranes

(iv) Hybrid Aerogels

The hybrid materials processed out of boehmite is a notable contribution and the application studies conducted to validate the boehmite hybrids produced new scientific knowledge in the area of advanced functional materials

6.2.1. Boehmite Based Hybrid Photocatalytic Sorbent (CeO_2@AlOOH/PEI)

In this work package, a contribution is made to make a multifunctional photoactive, antimicrobial hybrid catalytic-sorbent. A facile strategy was proposed to obtain a mesoporous boehmite gel hybrid functionalized with anamine molecule and also engineered with nano CeO_2. At the end a new catalytic sorbent material namely CeO_2@AlOOH/PEI was designed.This hybrid catalyst is explored for the treatment of industrial waste water contaminated with lignin and organic dye. The adsorption efficiency of CeO_2@AlOOH/PEI hybrid nanocomposite for lignin wasanalysed. Photodegradation of lignin and methyl orange dye under sunlight and UVirradiation confirms that CeO_2@AlOOH/PEI hybrid nanocompositesis a dual functional material that offers both adsorption and photocatalytic degradation. Above all, the CeO_2@ AlOOH/PEI hybrid sorbent showed efficient antimicrobial activity against both gram positive and gram negative bacteria. These results

suggest that CeO_2@AlOOH/PEI hybrid is a suitable catalytic sorbent for the recovery of water resources that are contaminated with lignin as well as organic dye.The antimicrobial activity helps in combating bio-fouling.

6.2.2. Natural CNSL Oil -Boehmite Hybrid [PFAC] Green-Electrode asDopamine Sensor

In yet another study, we developed a biohybrid electrode architecture designed from boehmite gel and natural organic resin, CNSL(PFAC). This hybrid system was explored for the first time to perform as a catalyst for electrochemical detection of dopamine (DA). The suggested strategy was unique in its simplicity.The electrochemical measurements illustrate that the combination of CNSL oil and inorganic porous AlOOH has advantages like ability to improve current, fast electron transfer kinetics and increase in the electrochemically active surface area. It was found that the sensor displays a higher electrocatalytic activity toward DA oxidation with a wider linear detection range of 50 µM to 450 µM and a lower detection limit of 23×10^{-9} m. The prepared sensor is the most promising candidate for the determination of DA in real samples. The obtained results suggest that the PFAC hybrid offers a new promising platform for preparing an electrochemical DA sensor with high performance and can be used in pharmaceutical and clinical application.

6.2.3. CNSL Resin Modified Superhydrophobic Boehmite Gel Hybrids (PWCA) for Oil-Water Separation

In this work chapter, we could successfully synthesize a new inorganic-organic hybrid architecture consisting of boehmite gel, natural organic resin, CNSL and paraffin wax that ultimately produced mechanically robust superhydrophobic top-coats on textile fabrics. The entire Wax-Boehmite-CNSL hybrid system decides the transformation of the hydrophilic textile surface into more hydrophobic and also for achieving the significant level of superhydrophobicity. The hybrid modified textile membrane offers excellent water repellency

with a WCA of 160°, as well as good self-cleaning ability. This superhydrophobic hybrid textile membrane was validated for separating the hexane, petrol, diesel, chloroform, dichloromethane and crude oil/water systems. The separation efficiency was >97% for more than 15 cycles. The hybrid textile membrane assembly results in high permeation fluxes toward oils with low viscosities. The as prepared textiles exhibited satisfactory stability after knife scratching and under harsh chemical condition. Thus, it is concluded that the inorganic-organic hybrid superhydrophobic textile developed in this work is suitable for oil-water separation in real world application.

6.2.4.Boehmite/Chitosan Hybrid Aerogel(CHAL) on Thermal Insulation and Flame Retardant Applications

In this work, fabrication of a green, eco-friendly bio-based chitosan- boehmite hybrid aerogel (CHAL) is attempted. The hybrid aerogel was successfully prepared via sol-gel assisted freeze drying technique. The as-prepared hybrid aerogels offered highly porous 3D networked solid structure. The low thermal conductivity nature of porous boehmite-chitosan, a significant heat insulation performance is expected out of this hybrid system. The TGA study confirmed that the incorporation of boehmite into chitosan offers significant thermal stability. Moreover, CHAL hybrid aerogel exhibited satisfactory flame retardantproperty in the vertical burning test. Owing to the hierarchical porous structure of aerogel and the excellent barrier effect of boehmite, CHAL could resist a heat build-up and heat dissipation and effectively prevent the thermal diffusion towards the non-exposed side from increasing, indicating a sign of thermal insulation. The CHAL hybrid aerogel would have a promising future in the applicationof green packing material that can replace the flammable polymer packaging materials.

6.3. Recommendations and Future Directions

During the course of this thesis work, a variety of research attempts generated a number of ideas, which could not be experimentally proved due to time constrains and limitations in the experimental characterization facilities, and a few of them are suggested below:

- Variety of spectroscopic techniques like Si MAS NMR and Al MAS NMR can be used for the systematic investigation of chemical reaction involved in the boehmite-CNSL hybrids to obtain detailed information regarding the hybrid interface and mechanism involved in the sol-gel reaction.
- Fabrication of flexible and foldable sensor devicescan be considered in future
- Boehmite is a candidate with large surface hydroxyl groups. It can be explored to modify boehmite with other bio materials mainly starch for designing hybrid adhesives
- The superhydrophobic PWCA hybrid formulation prepared in this research work has a great potential as active components in paints and surface coatings. This can be explored further with materials like Mg, CeO_2 to prevent the surface corrosion, and moisture penetration for developing functional coatings.
- Bio-polymer modified boehmite hybrids can be electro-spinned for developing alumina fibres for thermal insulation as well as membrane filtration applications
- It is proposed to study the biodegradability and antimicrobial properties of chitosan-boehmite hybrid for food packaging kind of applications.
- Chitosan-boehmite gel hybrid can further be studied with CNSL and Nano Silica for designing Insulation paints and package to replace thermocol.
- Boehmite is well known as reinforcing fillers for polymers for tailoring mechanical stability. It will be worth investigating the chitosan-boehmite hybrids for scaffold fabrication and testing.

ABSTRACT

Name of the Student: **Shuhailath K.A.** Registration No.:10CC14J39009
Faculty of Study: Chemical Sciences Year of Submission: 2021
AcSIR academic centre/CSIR Lab: CSIR-National Institute for Interdisciplinary Science and Technology (CSIR-NIIST) Name of the Supervisor: Dr. S. Ananthakumar

Title of the thesis: **Investigations on Inorganic-Organic Hybrid Nanomaterials from Boehmite [AlOOH] Gels for Multifunctional Applications**

The integration of inorganic and organic active molecules in a single hybrid material has emerged as a very potent and promising class of materials in the field of research. Boehmite (monohydroxy aluminium oxide) a multifaceted material has attracted more interest due to its chemically and thermally stable properties, high specific surface area, favourable biocompatibility, tunable morphological features, and scope for tailoring the surface characteristics. These remarkable properties of boehmite offer endless possibilities for the design and synthesis of advanced functional materials that find impressive applications in energy, environment, biology, optics, and electronics, etc. **Chapter 1** gives the general introduction on inorganic organic hybrid materials, and sol-gel synthesis of hybrid gels to porous structures. This chapter highlights advantages of boehmite hybrids in different fields of science and technology. The specific objectives and outlook of the present work are also outlined in the introductory chapter.

In **Chapter 2**, we prepared hybrid multifunctional photoactive and antimicrobial catalytic-sorbent (CeO_2@AlOOH/PEI). This hybrid catalyst is explored for the treatment of industrial waste water contaminated with lignin and organic dye. Above all, the antibacterial property of CeO_2@ AlOOH/PEI sorbent was also studied against both gram positive and gram negative bacteria. This study has manifested resulted in the development of an eco-friendly, sustainable CeO_2@AlOOH/PEI sorbent for the recovery of water resources from the lignin and dye contaminated industrial effluent.

In **Chapter 3**, electrochemically active biohybrid sensor is designed from boehmite gel, natural organic resin, CNSL. The prepared hybrid sensor is utilized for detecting the neurotransmitter dopamine. Furthermore, the developed biosensor also portrayed favorable selectivity, operational stability, and reproducibility. Real sample analysis and interference studies demonstrate that the proposed modified electrode is a promising candidate in the pharmaceutical and medical fields.

In **Chapter 4,** we formulated hybrid coating suspension from organic CNSL oil, boehmite, and paraffin wax [PWCA] and demonstrated its super hydrophobicity and resistance to water impact. This hybrid suspension was used to modifying pristine cotton textile. The coated textiles possess excellent self-cleaning ability and could be used to selectively separate various kinds of oil-water mixture including crude oil-water mixture. More interestingly, the fabric can recover its super liquid-repellent property after drying at 120 °C in an oven, even after immersing in water for a week. The studies indicated that the PWAC coated textiles a promising candidate for oil-water separation in real world application.

Chapter 5 deals with the fabrication of high fire-resistance and low thermal conducting chitosan/boehmite hybrid aerogel (CHAL) via freeze-drying. Importantly, the aerogel exhibited excellent flame retardancy and self-extinguished in the vertical burning test. This work provides a facile, environmentally-friendly, and cost-effective approach to fabricating multifunctional fire-safe aerogel, showing promising applications in exterior wall insulation, vehicle interior, and fire fighting.

The summary of the entire thesis is provided in **Chapter6** which also accommodates the scope for future work**.** We hope that this thesis will provide insights to, scientist, researchers and entrepreneurs to assess boehmite based inorganic-organic hybrid materials from a different perspective and fortify the search for innovative products of technological importance.

List of Publication from the Thesis

Published

Shuhailath, K. A.; Linsha , V.; Nishanth Kumar, S.;. Babitha, K. B.; Peer Mohamed, A.; Ananthakumar, S. Photoactive, Antimicrobial CeO2 Decorated AlOOH/PEI Hybrid Nanocomposite: A Multifunctional Catalytic-sorbent for Lignin and Organic Dye. https://doi.org/10.1039/C6RA07836B 2.

Manuscript under Preparation

Shuhailath, K. A.; and Ananthakumar, S. CNSL Resin Modified Sol Gel Al2O3 Treated Superhydrophobic Textile Membrane for Selective Oil-Water Filtration (to be communicated)

Shuhailath, K. A.; Khan, A.; Viji, S.; and Ananthakumar, S. A Natural CNSL Oil Crosslinked Boehmite [AlOOH] Hybrids:- A New Effective Green-Electrode Design for Sensing Neurotransmitter Dopamine (to be communicated) 5. Shuhailath, K. A.; Peer Mohamed, A.; and Ananthakumar, S. A Light Weight Super flexible Chitosan/AlOOH Hybrid Aerogel for Thermal Insulation and Fire Retardancy.(Manuscript Under Preparation

List of Publication from other Related Work

Linsha , V.; Shuhailath, K. A.; Mahesh K.V.; Peer Mohamed, A.; Ananthakumar, S. Biocatalytic Conversion Efficiency of Steapsin Lipase Immobilized on Hierarchically Porous Biomorphic Aerogel Supports, ACS Sustainable Chemistry & Engineering, 2016, 4, 4692–4703. https://doi.org/10.1021/acssuschemeng.6b00821 3.

List of Conference Proceedings

K.A. Shuhailath, Linsha Vazhayal, Peer Mohamed, Ananthakumar S, Selective Adsorption and Degradation Studies of Lignin on Alumina Hybrid and Hybrid Nanocomposites, National Seminar On Hydrogen Energy And Other Renewable Energy Sources, **HEAM Scholar 2014**, Held on 17th November at Department of chemistry, University of Kerala.

K.A. Shuhailath, Linsha Vazhayal, Peer Mohamed, Ananthakumar S, Design and Synthesis of Boehmite Based Organic-Inorganic Hybrid Xerogel: An Efficient Adsorbent and Photocatalyst for Lignin in Effluents, NATIONAL SEMINAR ON NANOSCIENCE AND NANOTECHNOLOGY, Held on 19th March 2015 at Department of chemistry, University.

K.A. Shuhailath., Linsha Vazhayal, Nishanth Kumar S., A. Peer Mohamed and Ananthakumar S. A Multifunctional CeO_2 Decorated AlOOH/PEI Catalytic Sorbent for Efficient Removal of Organic and Microbial Contaminants, 2nd International Conference on Soft Materials (ICSM 2016), held at MNIT Jaipur from December 12-16, 2016

K. A. Shuhailath and S. Ananthakumar, CNSL Resin Modified Sol Gel Al_2O_3 Treated Hydrophobic Textile Membrane for Selective Oil-Water Filtration, International Conference on Nanotechnology: Ideas, Innovations & Initiatives-2017" **(ICN: 3I)**, held at IIT, Roorkee ,06-08 December 2017

RSC Advances

ROYAL SOCIETY OF CHEMISTRY

CORRECTION

View Article Online
View Journal | View Issue

Check for updates

Cite this: *RSC Adv.*, 2020, **10**, 44773

Correction: Photoactive, antimicrobial CeO_2 decorated AlOOH/PEI hybrid nanocomposite: a multifunctional catalytic-sorbent for lignin and organic dye

K. Aboo Shuhailath,[ab] Vazhayal Linsha,[b] Sasidharan Nishanth Kumar,[c] K. Babu Babitha,[b] Abdul Azeez Peer Mohamed[b] and Solaiappan Ananthakumar*[ab]

DOI: 10.1039/d0ra90136a

rsc.li/rsc-advances

Correction for 'Photoactive, antimicrobial CeO_2 decorated AlOOH/PEI hybrid nanocomposite: a multifunctional catalytic-sorbent for lignin and organic dye' by K. Aboo Shuhailath *et al.*, *RSC Adv.*, 2016, **6**, 54357–54370, DOI: 10.1039/C6RA07836B.

The authors regret that the one of the affiliations (affiliation *a*) was incorrectly shown in the original manuscript. The corrected list of affiliations is as shown above.

The Royal Society of Chemistry apologises for these errors and any consequent inconvenience to authors and readers.

[a]*Academy of Scientific and Innovative Research [AcSIR], Ghaziabad-201002, India*

[b]*Functional Materials Section, Materials Science and Technology Division (MSTD), National Institute for Interdisciplinary Science and Technology (CSIR-NIIST), Trivandrum-695 019, Kerala, India. E-mail: ananthakumar70@gmail.com; Tel: +91-471-2515289*

[c]*Agroprocessing and Natural Products Division, National Institute for Interdisciplinary Science and Technology (CSIR-NIIST), Trivandrum-695 019, Kerala, India*

Open Access Article. Published on 17 December 2020. Downloaded on 6/28/2021 12:26:30 PM.
This article is licensed under a Creative Commons Attribution 3.0 Unported Licence.

RSC Advances

PAPER

Cite this: *RSC Adv.*, 2016, **6**, 54357

Photoactive, antimicrobial CeO_2 decorated AlOOH/PEI hybrid nanocomposite: a multifunctional catalytic-sorbent for lignin and organic dye†

K. Aboo Shuhailath,‡[ab] Vazhayal Linsha,‡[b] Sasidharan Nishanth Kumar,[c] K. Babu Babitha,[b] Abdul Azeez Peer Mohamed[b] and Solaiappan Ananthakumar*[b]

In this study an amine functionalized, mesoporous monohydroxy aluminium oxide (AlOOH/PEI) hybrid is prepared and further catalytically engineered with nano-CeO_2 to make a multifunctional photoactive and antimicrobial catalytic-sorbent (CeO_2@AlOOH/PEI). Structural and physico-chemical properties of this catalytic-sorbent were characterized using powder XRD, FTIR, SEM, TEM, N_2 sorption analysis, TGA and zeta-potential measurements. This hybrid catalytic-sorbent is explored for the treatment of industrial waste water contaminated with lignin and organic dye. A comparative study was also done with other known conventional sorbents and the developed CeO_2@AlOOH/PEI catalytic-sorbent shows a better adsorption capacity towards lignin. Photodegradation of lignin and methyl orange dye using the CeO_2@AlOOH/PEI hybrid nanocomposite was also investigated under sunlight and UV irradiation. Both the pollutants show a better photodegradation under UV. Above all, the antibacterial properties of the CeO_2@AlOOH/PEI sorbent were also studied against both Gram-positive (*S. aureus*) and Gram-negative (*E. coli*, *K. pneumoniae*) bacteria and showed efficient antimicrobial activity against these tested bacteria. An eco-friendly, self-regenerative, sustainable CeO_2@AlOOH/PEI catalytic sorbent is designed and validated for the recovery of water resources from lignin and dye contaminated industrial effluent.

Received 25th March 2016
Accepted 29th May 2016

DOI: 10.1039/c6ra07836b

www.rsc.org/advances

Introduction

Adsorption and photodegradation are two highly connected, simple processes for the effective recovery of reusable water from industrial waste streams. Many known conventional sorbents and catalysts are not good enough to perform simultaneously both functions in a solo material. Nanostructured hybrid materials exhibiting multiple functions such as selective adsorption of hazardous pollutants, photocatalytic degradation of toxic elements, thermochemical stability, and resistance against microbial attack, have great potential as advanced functional materials. The design and development of such catalytically engineered high surface area, mesoporous hybrid adsorbents possessing self-regeneration capability to regain their catalytic efficiency by simple photoirradiation has become essential for sustainable waste water treatment technologies.

Paper mills, bio-fuel production plants and textile dye units require such catalytic sorbents for the treatment of voluminous industrial effluents. Processed water from these industries are usually contaminated with intensely coloured lignin and organic dyes.[1–3] Over 10 000 different dyes has been used by textile industry with an annual consumption of 7×10^5 tons and ultimately gushed into the natural water bodies.[3,4] A paper mill typically discharges 8700 gallons of lignin contaminated water per ton of paper produced.[5] It causes severe environmental pollution not only to the land mass fertility but also to the aquatic systems, and also increases the COD and BOD of the water bodies.[5,6] Despite of all these downsides; lignin an aromatic biopolymer is composed of phenyl propanoid units such as *p*-coumaryl alcohol, coniferyl alcohol and sinapyl alcohol linked through variety of C–C bonds and ether linkages.[7,8] These lignin derivatives have good industrial values and hence the removal of lignin in a safe manner is also considered to be a great concern in such industries.

For several years, wastewater treatment is being carried out *via* adsorption, coagulation, flotation, oxidation, biosorption, biodegradation, UV photodecomposition and ultrafiltration, but these methods are not cost-effective.[9,10] Adsorption is considered to be one of the most promising methods for

[a]*Academy of Scientific and Innovative Research (AcSIR), CSIR-National Institute for Interdisciplinary Science and Technology (CSIR-NIIST), Trivandrum-695019, India*

[b]*Functional Materials Section, Materials Science and Technology Division (MSTD), National Institute for Interdisciplinary Science and Technology (CSIR-NIIST), Trivandrum-695 019, Kerala, India. E-mail: ananthakumar70@gmail.com; Tel: +91-471-2515289; +91-9497271547*

[c]*Agroprocessing and Natural Products Division, National Institute for Interdisciplinary Science and Technology (CSIR-NIIST), Trivandrum-695 019, Kerala, India*

† Electronic supplementary information (ESI) available: FTIR, EDS, figure corresponding to the effect of concentration on % lignin removal, table summarizing N_2 sorption analysis data and parameters of kinetic fit for adsorption and photo catalysis. See DOI: 10.1039/c6ra07836b

‡ These authors contributed equally to this work.

effluent treatment due to its high efficiency, low cost and easy handling.[10,11] Several studies have been reported on adsorption of lignin using activated carbon from xylo-oligosaccharides, pre-hydrolysis kraft and waste water from mechanical pulping.[12–14] Similarly, photocatalytic methods also found to be a better technology for the decomposition of toxic wastes. The main advantage seen here is the complete degradation of organic pollutants to carbon dioxide and water.[15–17] For this purpose, use of nanostructured semiconducting TiO_2, CeO_2, ZnO, Fe_2O_3 photocatalytic metal oxides are being explored.[15] Kobayakawa *et al.* studied the complete mineralization of lignin using TiO_2 as photocatalyst.[18] Ohnishi *et al.* reported noble metal loaded TiO_2 and demonstrated extreme competence in decolourization of lignin effluent.[19]

However, in recent years integrated adsorption and degradation are emerging as a more efficient and simplest technology for waste water treatment. Hence, engineered hybrid catalytic-sorption technologies using catalytically modified carbon, mesoporous silica and alumina, as well as bio-polymeric catalytic-sorbents are recently explored.[20–22] Such synergetic effect was reported using powdered TiO_2 and activated carbon (AC) in the sorption and catalytic degradation of organic pollutants.[22] Cordero *et al.* studied the associative effects between TiO_2 and AC during the photodegradation of 4-chlorophenol using various kinds of AC.[23]

In this work, a catalytic-sorbent material CeO_2@AlOOH/PEI hybrid nanocomposite was designed out of inorganic and organic functional moieties having competent adsorptive and photocatalytic functions for single-stage cleaning technologies. Boehmite (AlOOH), a layered inorganic oxy hydroxide form of alumina is a thermally stable, inert medium, used as solid industrial inorganic adsorbent for the removal of toxic pollutants from effluents.[24,25] Sol–gel is a technique recognized for synthesizing porous metal-oxides with controlled pore architecture. Hence, the surface characteristics of sol–gel synthesised AlOOH was tailored by introducing organic polyethylene imine (PEI) functionality to further enhance the adsorption capacity. Additionally, CeO_2 is decorated over AlOOH/PEI hybrid gels to obtain CeO_2@AlOOH/PEI hybrid nanocomposite framework. CeO_2 is an n-type semiconductor, with a band gap of 2.9–3.2 eV, well known for non-toxicity, high thermal stability and recognized as a visible light driven photocatalyst.[26] Monolithic macrobeads of CeO_2@AlOOH/PEI porous supports were fabricated *via* sol–gel granulation technique, so that it can be easily packed in a reactor for the continuous operation. Effective performance of the CeO_2@AlOOH/PEI catalytic sorbent was then studied primarily for lignin adsorption as well as a model methyl orange dye with respect to various adsorption parameters and the results are discussed. The photocatalytic degradation of lignin and dye were also studied in presence of UV and sunlight to recover the water from contaminated source.

We have also explored the antibacterial ability of the proposed material. Nowadays, the need for functional materials with antimicrobial property in water treatment is more investigated. The designing of a material which can act as an adsorbent, photocatalyst and antimicrobial agent is still considered to be a challenge task. The antibacterial property of proposed hybrid material was assessed using Gram-negative *E. coli*, *K. pneumoniae* and Gram-positive *S. aureus* as model organisms and the results are discussed.

Experimental methods

Materials

All chemicals and reagents used were of analytical grade. Aluminium isopropoxide (AIP, purity > 98%), alkali kraft lignin, branched-polyethylene imine (PEI, MW ~ 25 000) and cerium dioxide (CeO_2, nanopowder, <25 nm particle size) were purchased from Sigma Aldrich and Methyl Orange (MO) from SD fine chemicals was used as model organic dye. *Staphylococcus aureus* MTCC 902 (*S. aureus*), *Escherichia coli* MTCC 2622 (*E. coli*) and *Klebsiella pneumonia* MTCC 109 (*K. pneumoniae*) were used as test bacterial pathogens for antimicrobial studies. All the test microorganisms were purchased from Microbial Type Culture collection Centre, IMTECH, Chandigarh, India. The test bacteria were maintained on nutrient agar slants.

Sol–gel synthesis of boehmite sol (AIP-sol)

A stable boehmite sol (AIP-sol) was prepared by the well-known Yoldas process, involving the hydrolysis and condensation of AIP.[27] The alkoxide precursor, AIP was first hydrolysed in 1000 mL distilled water at 80–85 °C, and after stirring for 1 h, the hydrolysed product, was peptized with 1 M HNO_3 until the pH become 3. The peptized AIP sol was then refluxed overnight at 90–95 °C. The resultant sol was gravimetrically estimated for the boehmite (AlOOH) content. The AlOOH concentration in the resultant AIP sol was 0.0675 g mL^{-1}.

Preparation of AlOOH/PEI hybrid and CeO_2@AlOOH/PEI hybrid nanocomposite gels and monoliths

In a typical process, 1 M AIP sol (50 mL) containing 3.37 g of AlOOH was mixed with 1.5 g of PEI, and stirred for 2 h. A rapid coagulation occurred and the sol transformed into a stiff gel. The gel was treated further with 1 M HNO_3 to control the pH in the range 2 to 3. At this stage, the thick gel collapsed and resulted in flowable gel mass to obtain AlOOH/PEI hybrid gel. For the preparation of catalytically engineered CeO_2@AlOOH/PEI hybrid nanocomposite gel, the same experiment was repeated as mentioned above. To the AlOOH/PEI hybrid gel, 0.8 g nano-CeO_2 was mechanically blended. The gel mixture was stirred for 3–5 h to obtain a well homogeneous CeO_2@AlOOH/PEI hybrid nanocomposite gel. The chemical interaction of AlOOH with PEI and CeO_2 modified AlOOH/PEI gels is illustrated in the Scheme 1.

The gels obtained were then moulded into cylindrical and spherical monolithic structures. The gels were aged in ammonia in cylindrical vials to obtain cylindrical monoliths and were subjected to spherical granulation process by an injector into the ammonia bath (pH = 8.5), prepared with a top-layer out of paraffin oil. The acidified gel when dropped into an ammonia bath, undergo immediate gelation and self-assembled to form highly uniform, spherical shape wet gel beads. The wet gel samples were evaporative dried in hot air oven to obtain xerogels samples.

 This journal is © The Royal Society of Chemistry 2016

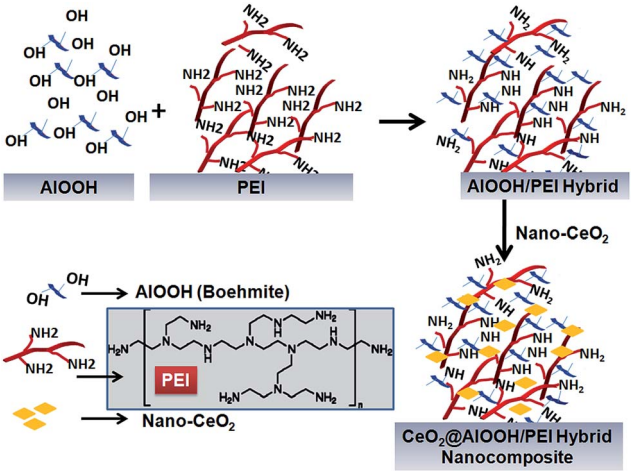

Scheme 1 Simplified scheme of synthetic steps involved in the formation of AlOOH/PEI hybrid and CeO_2@AlOOH/PEI hybrid nanocomposite.

Characterization

X-ray diffraction (XRD) patterns of the samples were obtained with a Philips X'pert Pro X-ray diffractometer in the 2θ range 10–80° using Cu Kα radiation ($\lambda = 1.54178$ Å) under a voltage of 40 kV and current of 40 mA. Fourier transform infrared (FTIR) analysis was performed using Shimadzu IR Prestige-21 spectrophotometer to understand the chemical interaction in the hybrid system. A standard KBr pellet technique was employed and the chemical structure of the hybrid was analysed in the wavelength range of 4000–400 cm^{-1} through transmission method. The thermal decomposition of AlOOH/PEI and CeO_2@AlOOH/PEI was investigated by Shimadzu TG-50 Thermo Gravimetric Analyser (TGA), between the temperature range 100–1000 °C at a constant heat flow of 10 °C min^{-1} in air atmosphere. The bulk micro-structural characteristics of the hybrid monoliths were examined using JEOL 5600 SL Scanning Electron Microscope (SEM). The morphological features of the hybrids were ascertained further by Tecnai G2, FEI Transmission Electron Microscope (TEM) operated at an accelerating voltage of 300 kV. Energy dispersive X-ray spectroscopy (EDS) was carried out in combination with TEM to investigate the chemical composition of the prepared hybrid nanocomposite. The surface charge analysis was carried out using 3000H Malvern Zetasizer Instrument. Surface area and porosity nature was studied by standard N_2 adsorption technique using Micromeritics Gemini 2375 surface area analyzer after degassing the samples at 200 °C for 2 h. Brunauer–Emmett–Teller (BET) model was utilized to calculate the specific surface areas. A desorption isotherm was used to determine the pore-size distribution using the Barrett–Joyner–Halenda (BJH) model. Shimadzu UV 240 IPC UV/Vis spectrophotometer was used to determine the concentration of lignin and organic dye MO in aqueous solution. The characteristics peaks at wavelengths 280 and 464 nm, was considered for the analysis of lignin and MO, respectively.

Application study for removal of lignin from aqueous sample

Adsorption studies. Adsorption capacities of AlOOH/PEI and CeO_2@AlOOH/PEI sorbents towards kraft lignin were investigated by batch experiment at room temperature. For the adsorption experiments, lignin stock solution was prepared with 10 g lignin in 1 L distilled water. From this stock solution, different concentrations of lignin solution (500, 1000, 2000, 2500, 3000, 4000, 6000, 8000 mg L^{-1}) were prepared. In a typical batch experiment, 0.5 g of sample was added to 25 mL of lignin solution. For analyzing the adsorption efficiency, 1 mL of the lignin solution was withdrawn from the bulk at definite time intervals. After centrifugation (8000 rpm, 10 min at room temperature), the concentration of the lignin in solution was determined by UV/Vis spectrophotometer and the amount of lignin adsorbed was calculated using eqn (1) and (2):

$$\% \text{ adsorption} = (C_0 - C_e)/C_0 \times 100 \quad (1)$$

$$Q_e = (C_0 - C_e) \times V/m \quad (2)$$

where Q_e (mg g^{-1}) is the amount of lignin adsorbed, C_0 (mg L^{-1}) is the initial lignin concentration, C_e (mg L^{-1}) is the lignin concentration at equilibrium, V (mL) is the volume of lignin solution, and m (g) is the amount of adsorbent added. The effect of pH and temperature on lignin adsorption process was studied over pH range 1 to 12 and temperature 30, 35, 45, 55 and 65 °C. The pH of the lignin solution was adjusted using 0.1 M NaOH and 0.1 M HNO_3. The rate of adsorption of lignin was studied at different time intervals that were as long as 700 min using different initial concentrations as mentioned above at pH 5 and 30 °C.

Photoactivity studies. Photocatalytic activity of the as prepared samples was evaluated by the photodecomposition of kraft lignin with the illumination of sunlight and UV. 0.5 g of the catalytic material was stirred with 75 mL of lignin (4000 mg L^{-1}) solution. Prior to any irradiation, the reactant solutions were magnetically stirred in the dark for 30 min to establish adsorption/desorption equilibrium between lignin and the catalyst surface. Later, the samples were exposed to UV/sunlight irradiation. About 5 mL of sample was collected at different time intervals and centrifuged for separating the residue. Degradation of lignin was analysed by the decrease in the absorption peak at λ_{max} 280 nm for lignin with the aid of UV/Vis spectrophotometer. The percentage of lignin degradation was calculated using the eqn (3):

$$\% \text{ degradation} = (C/C_0) \times 100 \quad (3)$$

where C_0 is the initial concentration and C is the concentration of the lignin at time t.

Application study for removal of organic dye from aqueous sample. Batch adsorption experiments were carried out by adding 0.5 g of the samples to 25 mL of 25 mg L^{-1} of organic dye MO in aqueous solution. The mixture was shaken vigorously at 30 °C for different lengths of time. The supernatant was then collected, centrifuged (8000 rpm, 10 min at room temperature) and was assayed in a spectrophotometer. The amount of adsorbed MO was calculated from the absorbance measured at

464 nm before and after adsorption. Similarly, photodegradation studies were also conducted by illumination with UV and sunlight. The percentage adsorption and degradation were calculated as mentioned above.

Bacterial resistance test

Antibacterial assay by disc diffusion method. The antibacterial activity of the test samples was determined by the disc diffusion method against the test bacteria on Muller–Hinton agar, according to the Clinical and Laboratory Standards Institute (CLSI). The media plates (MHA) were streaked with bacteria 2–3 times by rotating the plate at 60 °C for each streak to ensure the homogeneous distribution of the inoculums. After inoculation, discs (10 mm Hi-Media) loaded with 100 μg mL^{-1} of the test samples were placed on the bacteria-seeded plates using sterile forceps. The plates were then incubated at 37 °C for 24 h. The inhibition zone around the discs was measured and recorded. Ciprofloxacin (Hi-Media) was used as the positive controls to compare the efficacy of the test samples. The assays were carried out in duplicates (detailed procedure for bacterial culture preparation to demonstrate the killing efficiency of the hybrid material is provided in the ES1†).

Results and discussion

Structural and chemical analysis of synthesized hybrid nanocomposite

Fig. 1A shows the optical micrograph of monolithic structures fabricated from the functionally engineered AlOOH/PEI and CeO_2@AlOOH/PEI hybrid nanocomposite xerogels. Monolithic structures especially spherical shape for functional porous materials is more preferable in the case of specific adsorbent/catalytic support used in fluidized bed for separation and purification processes. This is because spheres can be uniformly suspended with higher packing density, can reduce breakage loss by collision and lower pressure drop. Herein, the as-prepared granules have a size of around 2–3 mm in diameter, which shrinks to 1 mm in diameter during drying which is suitable for use as an adsorbent/catalytic support. We have carried out all the further characterization and studies of this microspherical monolithic supports.

The powder XRD of the sol–gel AlOOH, and its hybrids AlOOH/PEI and CeO_2@AlOOH/PEI are shown in Fig. 1B. In the XRD pattern of the obtained boehmite (curve a), the diffraction peaks at 2θ values 14.2°, 27.8°, 38.3°, 49.1° and 64.1° can be indexed for the Bragg reflection planes (020), (120), (031), (200), and (231) of orthorhombic AlOOH crystals. These peaks are found to be closely matching with the standard reported for the AlOOH crystals (JCPDS card 21-1307).[28] Upon hybridization of organic moiety PEI and immobilization of nano-CeO_2, the crystalline peaks notably changed. In AlOOH/PEI system (curve b), the peak width is broadened and the intensity is decreased indicating the bulk effect of amine moieties. In comparison to the XRD patterns of AlOOH/PEI, CeO_2 decorated AlOOH/PEI hybrid nanocomposite (curve c), peaks correspond to nano crystalline CeO_2 is seen at $2\theta = 28.6°$, 33.1°, 47.5° and 56.3° which are attributed to the presence of (111), (200), (220), and (311) planes, respectively (JCPDS card 34-0394).[29] From these patterns it is obvious that the nano-CeO_2 is well distributed in the AlOOH/PEI hybrid gel network forming a nanocomposite hybrid system.

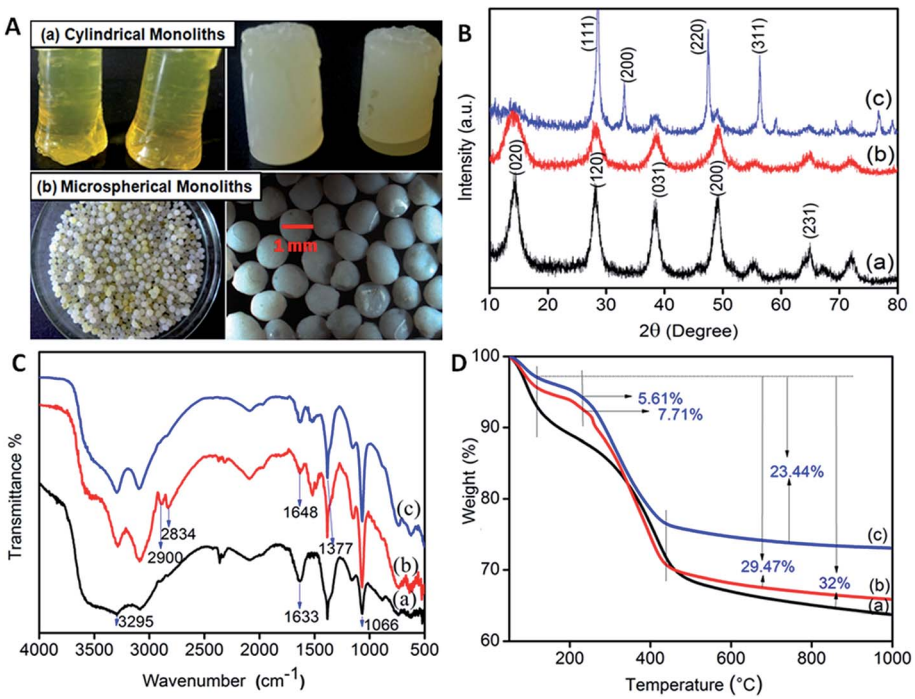

Fig. 1 (A) Optical images (B) powder XRD patterns and (C) FTIR spectra and (D) TGA graph of the synthesised material, in all the graphs (a) pure AlOOH (black line) (b) AlOOH/PEI (red line) and (c) CeO_2@AlOOH/PEI (blue line).

This journal is © The Royal Society of Chemistry 2016

The hybrid nature of the catalytically activated AlOOH/PEI sorbent was also confirmed from the FT-IR analysis. Alkoxide derived sol–gel AlOOH (curve a) exhibits the characteristic band for Al–O–Al stretching vibration at 1066 cm^{-1}.[30] The peaks at 3295, 1633, 1162 cm^{-1} can be assigned to stretching, bending mode of adsorbed water and deformation mode of –OH group, respectively. The hybrid formation was well confirmed by the presence of symmetric and asymmetric stretching vibration of functional groups C–H (–CH_2–), associated to the PEI organic component, at 2900–2834 cm^{-1} and the existence of N–H bending at 1633 cm^{-1} (curve b). Similarly, stretching vibration of N–H and C=N were also observed at 3295 cm^{-1} and 1648 cm^{-1} respectively.[25] While, in nano-CeO_2 decorated hybrid catalyst (curve c), the appearance of absorption band between 500 and 750 cm^{-1} is attributed to the characteristic stretching vibration mode of Ce–O. A vibration band at 1377 cm^{-1} appeared in CeO_2@AlOOH/PEI due to the presence of vibration overtone of surface hydroxyl group of nano-CeO_2 (this band is clearly visible in pure CeO_2 shown in Fig. S1†).

Thermal stability of synthesized hybrid material was assessed by TGA in comparison with the parent AlOOH and the corresponding thermogram is shown in Fig. 1C. All the three systems exhibit two stage weight losses; one at 100–150 °C due to dehydration of adsorbed water molecules and another between 450 and 1000 °C which is credited to the dehydroxylation in the phase transition from AlOOH to γAl_2O_3. The thermogram shows additional weight loss due to polymer degradation at temperatures 250–300 °C in AlOOH/PEI and CeO_2@AlOOH/PEI. The parent AlOOH exhibits a steep weight loss of 32% in the entire temperature range whereas AlOOH/PEI and CeO_2@AlOOH/PEI show a gradual total weight loss of 29.4 and 23.4%, respectively. The change in slope of the weight loss curves indicates better thermal stability in the AlOOH/PEI and CeO_2@AlOOH/PEI systems.

Microstructural analysis of synthesized hybrid nanocomposite

Fig. 2 depicts the SEM microstructures of bulk AlOOH/PEI and CeO_2@AlOOH/PEI granules. In case of AlOOH/PEI hybrid (Fig. 2a and b), the surface texture is very homogeneous and it appears that the hybrid gel spheres have random assemblage during wet gel granulation and the polymeric PEI has played a definite role as structure directing macromolecule. A sign of thermal-stress during drying is noticed here. Overall the image confirms the clustering of AlOOH nanolamellar during gelling and retained the agglomerated structure during drying.

Fig. 2c and d represent the SEM images of nano-CeO_2 modified AlOOH/PEI hybrid. The surface texture clearly indicates that nano-CeO_2 particles are uniformly distributed in the hybrid gel matrix. The microstructure reveals the relative smoothness of the surface and ordered gel assembly with minimal drying stress. Also, structurally modified hybrids possess porous texture.

The nanolamellar AlOOH particle and also the distribution of PEI and nano-CeO_2 in boehmite hybrid were further confirmed from the TEM images. The dispersion of pure AlOOH deposited on Cu-grid clearly shows the nano-dimensional, lamellar type AlOOH crystallites (Fig. 3a). In hybrid AlOOH/PEI (Fig. 3b and c) homogeneous distribution of lamellar boehmite crystallites on PEI polymer is observed. The TEM images (Fig. 3d) for pure CeO_2 shows nano-octahedron type morphology. Hence, in the bulk CeO_2@AlOOH/PEI hybrid nanocomposite, the presence of uniformly distributed nano-particulate octahedron CeO_2 is very well observed in AlOOH/PEI network. The elemental mapping was also conducted by EDS analysis on pure AlOOH, AlOOH/PEI and CeO_2@AlOOH/PEI. It is obvious that the pure AlOOH and AlOOH/PEI hybrid showed only the presence of major constituents such as aluminium and oxygen. Though, ceria decorated hybrid nanocomposite (CeO_2@AlOOH/PEI), showed clear peaks for Ce atom in addition to Al and O, thus confirming the uniform distribution of ceria over AlOOH/PEI hybrid network (Fig. S2†). Thus the SEM and TEM images confirmed that the hybrid gel mass is porous, catalytically modified and can be better exploited for the adsorption and photodegradation of organic contaminants.

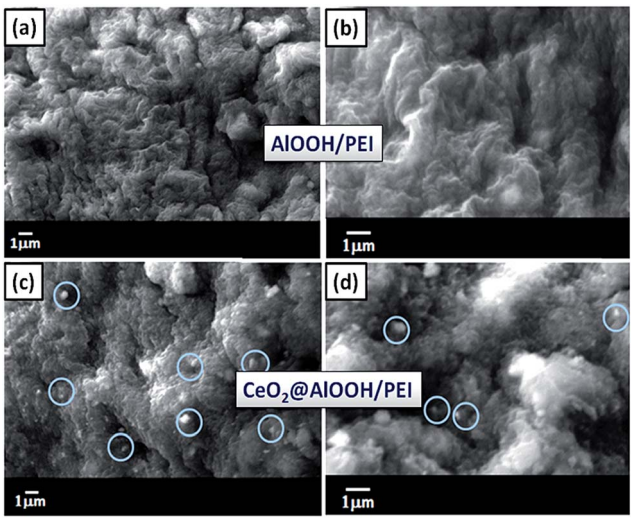

Fig. 2 SEM images: of (a) and (b) AlOOH/PEI (c) and (d) CeO_2@AlOOH/PEI at magnifications of 10k× and 20 k×, respectively.

Textural features and surface charge of synthesized hybrid nanocomposite

Surface area and the functional groups on the surface of the adsorbents are the two crucial factors influencing the adsorption process. The bulk surface area and associated pore feature of the catalytically modified AlOOH sorbent is analysed through N_2 sorption analysis. Fig. 4a shows the N_2 adsorption/desorption isotherm of parent AlOOH, AlOOH/PEI and CeO_2@AlOOH/PEI. All the three samples exhibits a typical type IV isotherm with steep hysteresis loop in the relative pressure range of 0.45–0.95, which suggests that the hybrids have mesoporous structures. The mesoporous AlOOH has high specific surface area of 311 m^2 g^{-1} and an average pore diameter of 4.8 nm. In aminated and nano-CeO_2 modified hybrids, the BET surface area is slightly decreased to 260 and 215 m^2 g^{-1} respectively inferring that the

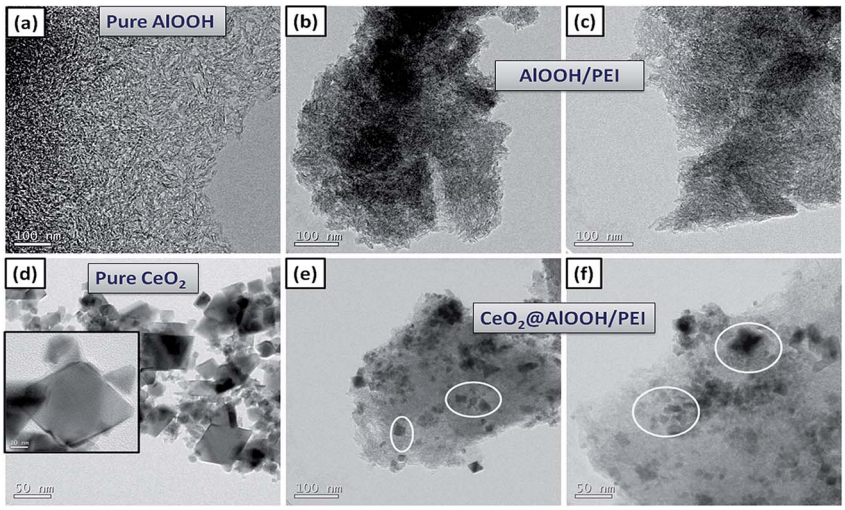

Fig. 3 TEM micrographs: (a) pure AlOOH, (b and c) AlOOH/PEI, (d) pure CeO_2 and (e and f) CeO_2@AlOOH/PEI.

organic functional group PEI and nano-CeO_2 are trapped in the mesopores considerably. Table S1† summarizes the BET surface area and pore feature evaluated for the boehmite and hybrids. Moreover, the pore size distribution (Fig. 4b) shows of AlOOH/PEI and CeO_2@AlOOH/PEI exhibits higher pore diameter 6.5 and 5.6 nm, respectively than the parent AlOOH. Therefore, the high surface area and porosity of the hybrid material can provide more active sites to improve its adsorption capability.

The susceptibility of the prepared samples towards adsorption can also be evaluated through the zeta potential measurements. This is measured to examine the surface charge of synthesised material at different pH range. The results are presented in Fig. 4c. The isoelectric point (IEP) of AlOOH/PEI and CeO_2@AlOOH/PEI hybrid were found to be 9.8 and 5.5, respectively indicating the adsorbents will be positively charged below this pH values and hence adsorption of anionic pollutant became more prominent.

Lignin adsorption and photocatalytic degradation studies

Adsorption studies. Lignin adsorption studies were conducted in batch process. Effect of very relevant influential factors such as concentration, contact time, pH and temperature was

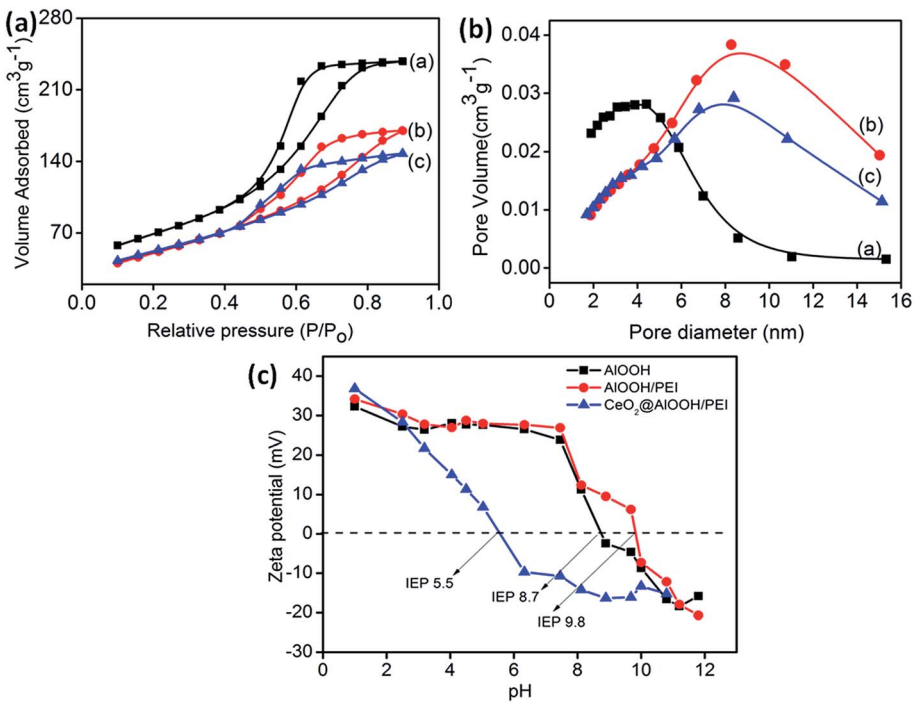

Fig. 4 (a) Nitrogen adsorption and desorption isotherms and (b) pore-size distribution curve (c) zeta potential analysis of pure AlOOH, AlOOH/PEI and CeO_2@AlOOH/PEI as a function of pH.

This journal is © The Royal Society of Chemistry 2016

systematically studied. The initial lignin concentration is an important driving force to overcome the mass transfer resistance of the lignin from the aqueous to the solid phase. The uptake of lignin by AlOOH/PEI and CeO_2@AlOOH/PEI hybrid sorbents were first determined with the initial lignin concentration in the range (5–100) $\times$ 10^2 mg L^{-1} at pH 5 (Fig. 5a). A pronounced increase in the lignin adsorption capacity by AlOOH/PEI and CeO_2@AlOOH/PEI hybrid is seen with an increase in lignin concentration. The maximum adsorption capacity estimated for AlOOH/PEI and CeO_2@AlOOH/PEI hybrids is 66.31 mg g^{-1} and 97.53 mg g^{-1} respectively at the initial concentration of 4000 mg L^{-1}. Similarly, % lignin removal for both the hybrid systems initially increases at lower concentration and gradually decreases at higher concentrations (Fig. S3†). This is because at higher lignin concentrations, the increased number of adsorbate ion can interact with the available binding site of the adsorbent and facilitate faster uptake of lignin. Hence, for the further studies a fixed initial concentration of 4000 mg L^{-1} was used.

For water treatment technology, a perfect adsorbent should possess faster uptake of pollutants and reach equilibrium in shorter time. Fig. 5b shows the effect of contact time on the adsorption efficiency of lignin using AlOOH/PEI and CeO_2@AlOOH/PEI by varying the time of contact from 0–150 min. It was observed that the uptake of lignin increases with increase in contact time and reaches equilibrium within 30 min, for both the sorbents.

The solution pH is another critical factor affecting the adsorption process. pH of the solution directly alters the solution chemistry and chemical interaction with the binding sites of the adsorbent surface. The adsorption of lignin onto the hybrid sorbents were assessed at pH values in the range 1–12 (Fig. 5c). The hybrids show a strong dependence of pH on the adsorption capacity of the lignin. As the pH of lignin solution increases from 1 to 5, the adsorption capacity of the hybrid sorbent increased due to the positively charged sorbent surface. Maximum adsorption of lignin by hybrid was seen at pH 5. Under acidic pH, the protonation of imine and amine functional groups present in the hybrid adsorbent occurs.[31] Thus, a strong electrostatic force of attraction between protonated adsorbent and negatively charged lignin can lead to better adsorption (Scheme 2a). When the pH increases above 5, the lignin adsorption tendency gradually declined. At this pH range, probably deprotonation of surface amino groups occurs and results in electrostatic repulsion with lesser uptake of lignin. Also, AlOOH/PEI shows maximum adsorption in broad range of pH when compared to CeO_2@AlOOH/PEI. Probably this is due to the variation in the IEP (AlOOH/PEI – 9.8 and CeO_2@AlOOH/PEI – 5.5). Hence, sorption kinetics and photodegradation studies were carried out at a fixed pH 5.

In addition to pH, the temperature effect is also studied for the lignin adsorption between temperature range 35 to 65 °C and the results are shown in Fig. 5d. It was found that, in both the adsorbents the lignin uptake increases with an increase in temperature. It is renowned that increase in temperature decreases the solution viscosity.[32] In such case it can enhances the mobility of lignin molecules and provides adequate energy to facilitate the interaction between lignin molecules and sorption sites at the surface of sorbents.

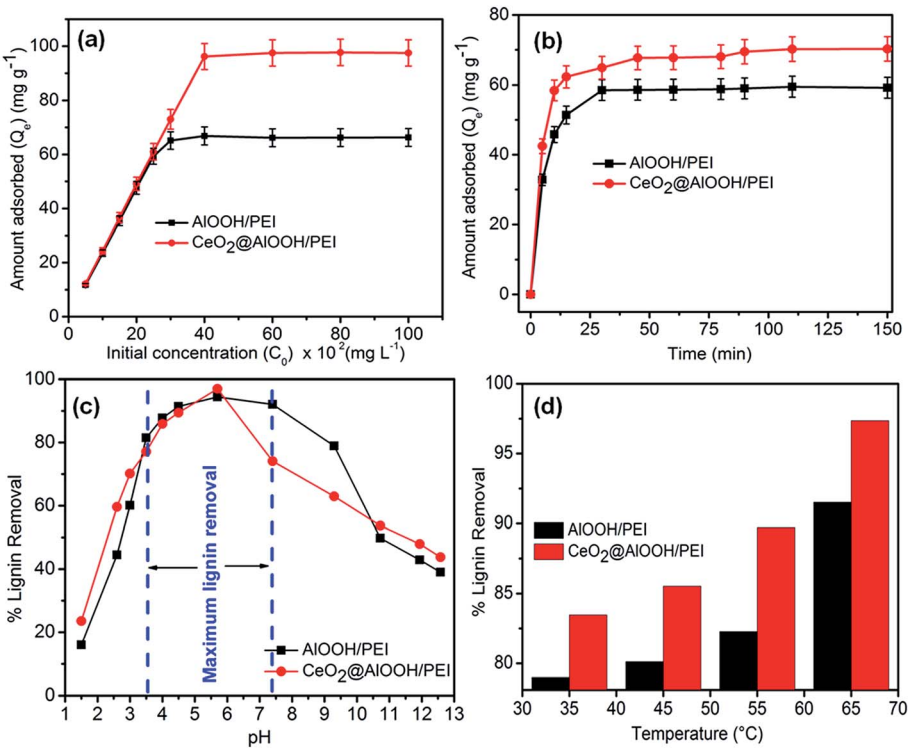

Fig. 5 Effect of (a) initial concentration (b) contact time (c) lignin solution pH, and (d) temperature on amount of lignin adsorbed by AlOOH/PEI and CeO_2@AlOOH/PEI hybrid sorbent.

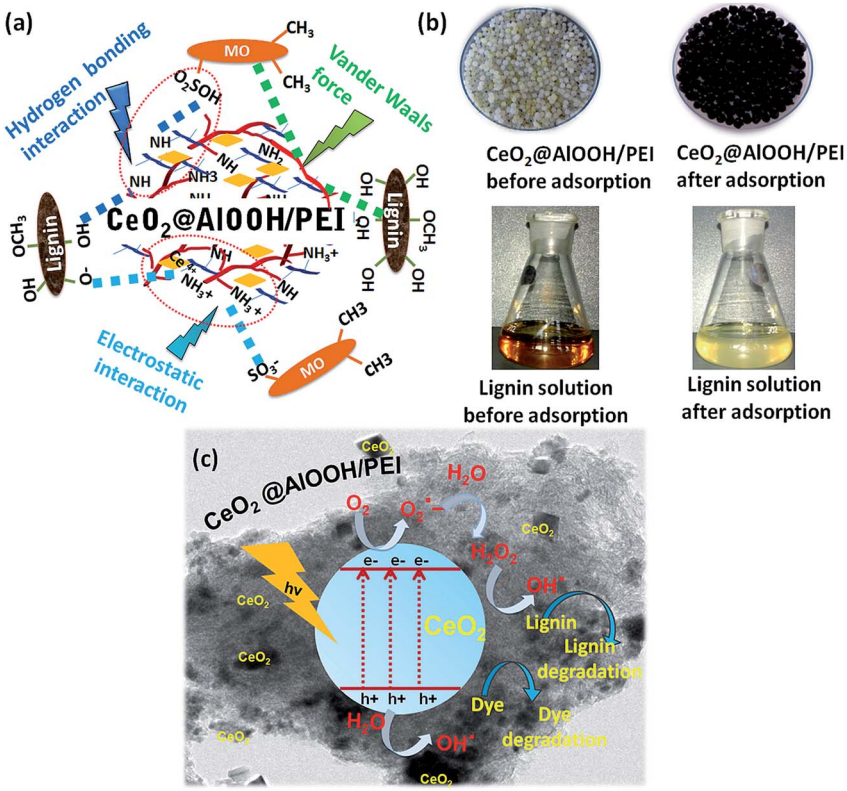

Scheme 2 Schematic illustration (a) of the possible interaction between CeO_2@AlOOH/PEI hybrid nanocomposite sorbent with lignin and MO dye molecule (b) photograph of CeO_2@AlOOH/PEI and lignin solution before and after adsorption (c) proposed mechanism for photocatalytic degradation of the organic pollutants under light irradiation.

It is observed from Fig. 6a and b, the adsorption proceed quickly in the initial stage of reaction and then becomes slow until the sorption process nearly reach equilibrium. The initial rapid adsorption of lignin by AlOOH/PEI and CeO_2@AlOOH/PEI is due to the presence of large number of adsorption sites (amine and imine group present in the polymer PEI) on the hybrid and nanocomposite. The subsequent slow step is attributed to the limited active adsorption sites on the surface of the adsorbent.[33] Lignin adsorbed on the surface would further hinder the diffusion of other lignin resulting in a long time to reach equilibrium. Based on the data obtained from experimental runs, pseudo-first-order model and pseudo-second-order model were used to simulate the kinetics adsorption of lignin on to both the AlOOH/PEI shown in Fig. 6c and d and CeO_2@AlOOH/PEI shown in Fig. 6e and f. The used kinetic model equations are given below:

$$\text{Pseudo-first-order: } \log(q_e - q_t) = \log q_e - (k_1/2.303)t \quad (4)$$

$$\text{Pseudo-second-order: } t/q_t = (1/k_2 q_e^2) + (1/q_e)t \quad (5)$$

where q_e and q_t are the amounts of lignin adsorbed on the adsorbents (mg g^{-1}) at equilibrium and at time t (min), respectively. k_1 (min^{-1}) and k_2 (g mg^{-1} min^{-1}) are the rate constants of the pseudo-first-order and pseudo-second-order adsorption, respectively. Kinetic data modelling was performed by a linear regression analysis and the results are shown in Table S2.†

The kinetic plot shows that the lignin adsorption process on AlOOH/PEI and CeO_2@AlOOH/PEI were found to fit better with pseudo-second-order with a high correlation coefficient (R^2 = 0.999) than pseudo-first-order (R^2 = 0.97). The best correlation of pseudo-second-order model with the experimental data reveals that the rate limiting step in adsorption process is controlled by chemisorption, which is a monolayer adsorption.[34] The rate of adsorption is one of the most important parameter in the kinetic study. From the Table S2,† it is evident that the values of k_2 decreases with increasing concentration. This may be due to the fact that, at higher concentration of lignin solution, lower is the possibility of lignin to get attached to the active site of the adsorbent surface. Similarly, the adsorption capacity of the prepared sorbents was compared with the known conventional sorbents and results are summarized in Table 1. It demonstrates that CeO_2@AlOOH/PEI hybrid sorbent possess remarkable adsorption capacity than some of the known conventional sorbents.

From the adsorption data it is understood that the most probable mechanism controlling the lignin adsorption is as follows; surface of the hybrid adsorbent possess large number of amino ($-NH_2$) group which get protonated. Thus the adsorption of anionic organic pollutant takes place by electrostatic interaction with protonated amino group on the surface (Scheme 2a). In addition to the $-NH_2$ group, AlOOH nanoparticles have large number of surface hydroxyl group that may

 This journal is © The Royal Society of Chemistry 2016

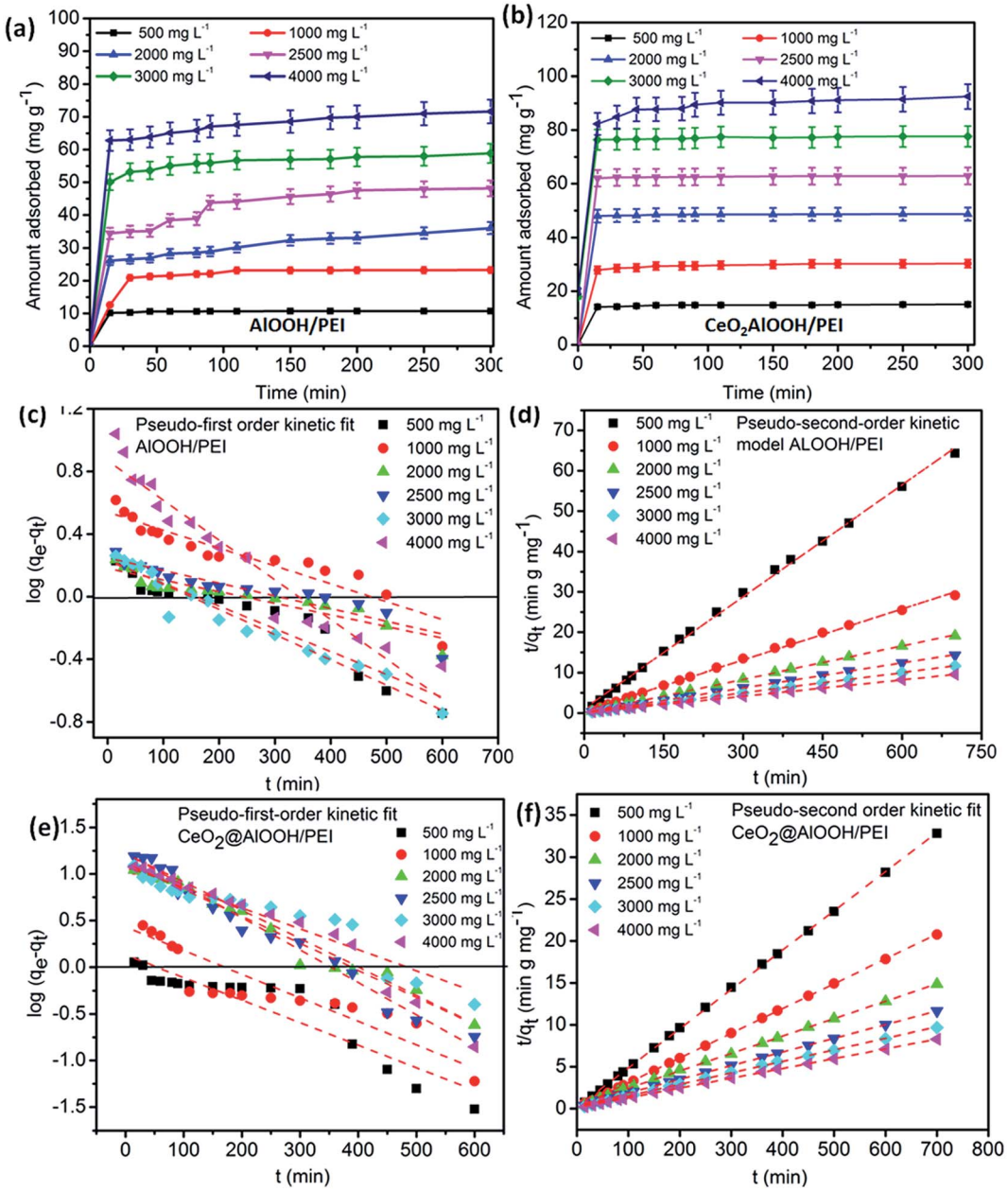

Fig. 6 Adsorption kinetics study of (a) AlOOH/PEI and (b) CeO_2@AlOOH/PEI with lignin conc. 500–4000 mg L^{-1}, equilibration time $t = 600$ min (graph shown only up to 300 min), kinetic model fit for pseudo-first-order and pseudo-second-order adsorption (c and d) AlOOH/PEI and (e and f) CeO_2@AlOOH/PEI.

also uptake anionic pollutants by hydrogen bonding and van der Waals interaction (Scheme 2a). Hence, a complete decolorization of lignin was observed within the adsorption equilibrium.

Photocatalytic degradation studies. The photocatalytic activity of the developed material towards lignin under sunlight and UV irradiation after the dark adsorption is shown in Fig. 7. From the Fig. 7a and b, it can be clearly observed that CeO_2@AlOOH/PEI possesses higher photoactivity compared to both AlOOH and AlOOH/PEI under UV and sunlight. Fig. 7a indicates that after 100 min of UV irradiation, 98% of lignin was degraded with CeO_2@AlOOH/PEI. But for AlOOH and AlOOH/PEI, the % of degradation was 34% and 72%, respectively. To quantitatively assess the photocatalytic efficiency of the catalyst, kinetic data are fitted to apparent first of rate equation,

$$\ln(C_0/C) = k \times t \quad (6)$$

where, C_0 and C are the initial and the final concentrations of lignin at time $t = 0$ and at t respectively; k is the apparent rate constant (min^{-1}). From the experimental results the apparent rate constant for the photo degradation of CeO_2@AlOOH/PEI under UV irradiation is found to be 0.03941 min^{-1}. It is almost *ca.* 3 times higher than the rate constant of AlOOH/PEI.

Table 1 Comparison of results obtained in this study with other adsorbents

Adsorbents	Adsorption parameters		Adsorption capacity (mg g^{-1})
	pH	Temp (°C)	
Bentonite	5	30	25.54 (present study)
Nano-silica	5	30	27.51 (present study)
Nano-alumina	5	30	71.28 (present study)
Zeolite	5	30	27.93 (present study)
AlOOH/PEI	5	30	66.31 (present study)
CeO_2@AlOOH/PEI	5	30	97.53 (present study)
Activated charcoal	6.8	—	213.0 (ref. 14)
Fly-ash	6.8	—	13.0 (ref. 14)
Eggshell	7		63.46 (ref. 6)

The same trend was observed for the photodegradation of AlOOH, AlOOH/PEI and CeO_2@AlOOH/PEI under sunlight exposure. The % of photoactive degradation for CeO_2@AlOOH/PEI under sunlight exposure is 96%, with an apparent rate constant of 0.0318 min^{-1} which gets reduced to 30 and 68% for AlOOH and AlOOH/PEI, respectively. The kinetic parameters are summarised and are shown in Table S3.†

For the photodecomposition of lignin, the adsorption efficiency of the catalyst plays a key role, since the photocatalytic reaction generally occurs at the surface of the catalyst than in the bulk. In CeO_2@AlOOH/PEI, the surface active groups as well as the porous nature of AlOOH/PEI helps in the enhanced adsorption of the lignin molecules. At the same time, AlOOH/PEI acts as a good supports for the uniform distribution of nano-CeO_2 and this results in the good absorption of UV/sunlight. Hence, the developed CeO_2@AlOOH/PEI hybrid nanocomposite is found to be effective in the complete removal (~96–98%) of lignin *via* simultaneous adsorption and photodegradation from 4000 mg L^{-1} aqueous solution. The pictorial representation of the UV/sunlight active degradation mechanism of uniformly distributed nano CeO_2 in CeO_2@AlOOH/PEI hybrid nanocomposite is shown in the Scheme 2c.

Removal of organic dyes from environmental aqueous samples

Anionic dye MO was selected as a model pollutant for the adsorption studies of the proposed material. Fig. 8a and b shows the % removal of MO at different time interval. As expected, the removal efficiency of CeO_2@AlOOH/PEI for MO was 95% within 30–40 min, which was remarkably greater than that of the original materials, AlOOH (34%) and AlOOH/PEI (67%) respectively. This phenomenon can be explained by electrostatic interaction between the positively charged sorbent and negatively charged MO molecule (through its sulfonate group) as described in Scheme 2a.

The evaluation of photocatalytic activity of the prepared sample was also carried out using MO. Fig. 8c and d illustrates the photocatalytic activity of the catalytic sorbent under both the sunlight and UV light irradiation. It was noticed that about 90% of MO was degraded within 120 min under UV and 85% under

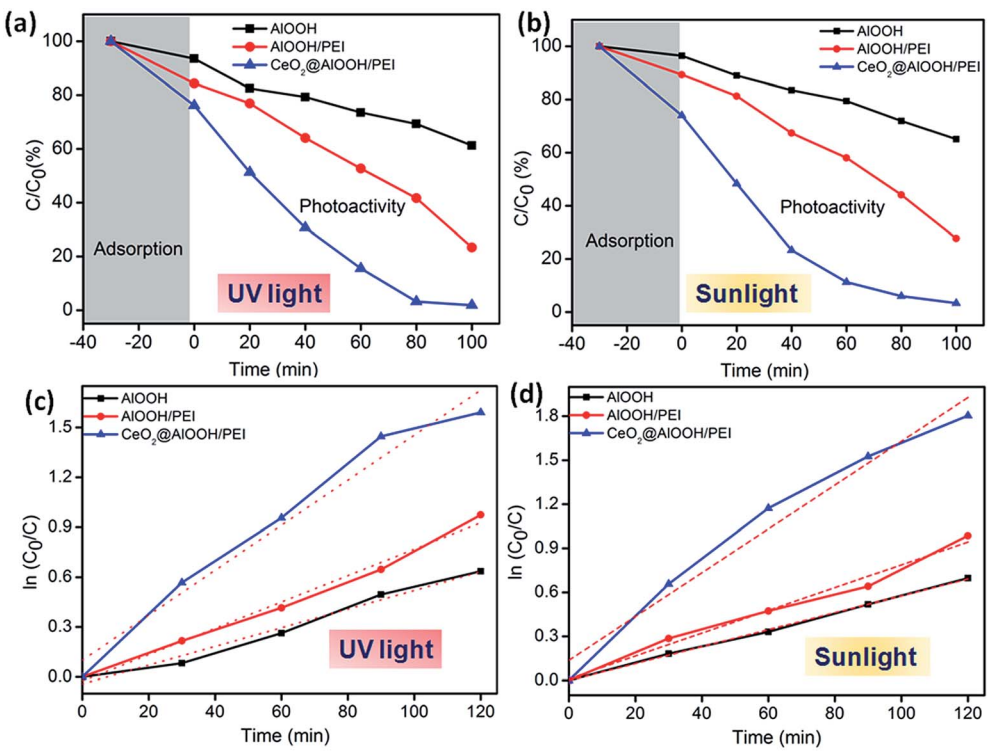

Fig. 7 Photocatalytic degradation and corresponding regression curves of $\ln(C_0/C)$ *versus* irradiation time of lignin on AlOOH, AlOOH/PEI and CeO_2@AlOOH/PEI under UV (a and c) and sunlight (b and d), respectively.

This journal is © The Royal Society of Chemistry 2016

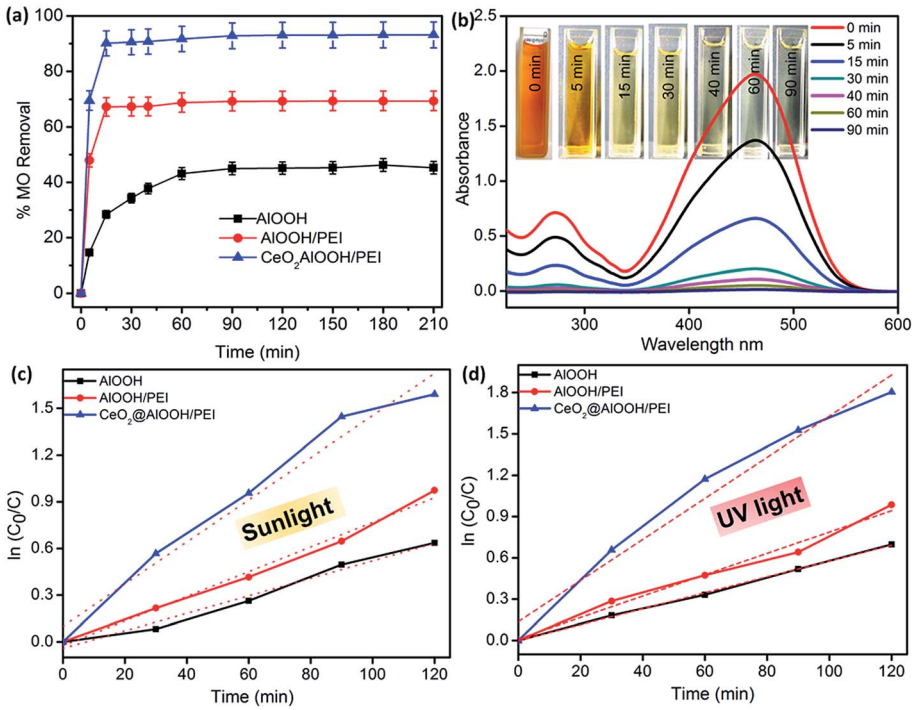

Fig. 8 (a and b) Adsorption curves of MO from aqueous solution at various time intervals (c and d) regression curves of $\ln(C_0/C)$ *versus* irradiation time of MO on AlOOH, AlOOH/PEI and CeO_2@AlOOH/PEI under sunlight and UV.

sunlight with CeO_2@AlOOH/PEI. In contrast, the photocatalytic activity of AlOOH and AlOOH/PEI were extremely lower than that of CeO_2@AlOOH/PEI, which indicates that removal has only occurred due to adsorption. The kinetics of the photodegradation of MO was assessed using the first order reaction. The rate constant k determined for CeO_2@AlOOH/PEI was 0.0135 and 0.0164 min^{-1} under sunlight and UV, respectively (Table S4†).

Antibacterial activity of the proposed materials

The antibacterial property of the prepared hybrid material was assessed using Gram-negative (*E. coli*, *K. pneumonia*) and Gram-positive (*S. aureus*) bacteria as model microorganisms by the disc diffusion method. These bacteria were selected for the investigation of antibacterial efficacy, because they are usually associated with water distribution systems which cause infections. Fig. 9 shows the results obtained for disc diffusion assay of AlOOH, AlOOH/PEI and CeO_2@AlOOH/PEI. We observed that both aminated and CeO_2 decorated hybrid system shows the clear zone of inhibition around the samples after 24 h of incubation when compared to pure AlOOH. Among the three tested bacteria, *K. pneumonia* shows larger zone of inhibition of around 13 mm radius and *E. coli* and *S. aureus* have comparatively smaller zone of inhibition of 10 and 11 mm radius, respectively (Fig. 9).

From the earlier reports, it was observed that quaternary ammonium compounds causes lysis of the bacterial cell walls by binding with cell components and further causing the seepage of cytoplasm.[35] Similarly, PEI was demonstrated to have a broad spectrum of antimicrobial activity against large number of Gram-positive and Gram-negative bacteria.[35,36] A strong antibacterial effect against all tested bacteria was observed in PEI modified AlOOH hybrid material. The acidified AlOOH/PEI gel results in the formation of quaternary ammonium in the gel framework, which strongly interacts with bacterial cell walls and disrupts negatively charged bacterial cell membrane.

Furthermore, CeO_2 itself has antibacterial effect. The formation of oxygen species and reactive oxide species (ROS) in CeO_2 can be utilized for the bacterial toxicity effect.[37] The most prominent ROS responsible for the bactericidal effect are hydroxyl, super-oxide radicals and H_2O_2 formation.[37,38] When bacteria come in contact with CeO_2, it interrupts the transport of electron, protein oxidation and also causes the membrane potential collapse. Hence, the coupled oxidation by the dissolved oxygen bonded to the surface of CeO_2, production of ROS from H_2O_2, and the basic exciton formation owing to the semiconducting nature are the major reason for efficient antibacterial activity exhibited by the developed hybrid material.

Antibacterial activity of CeO_2@AlOOH/PEI against *E. coli*, *K. pneumonia* and *S. aureus* was further investigated using SEM microscopy. The CeO_2@AlOOH/PEI porous microbead was incubated with bacterial solution at room temperature for 1 h. It was found that large number of bacteria was attached and killed all through the time of contact with the bacterial solution (Fig. 10). Slow disruption of bacterial cell wall was also clearly noticed form SEM (Fig. 10d–f). Among the three tested bacteria, larger number of *K. pneumoniae* is adhered on the surface of the

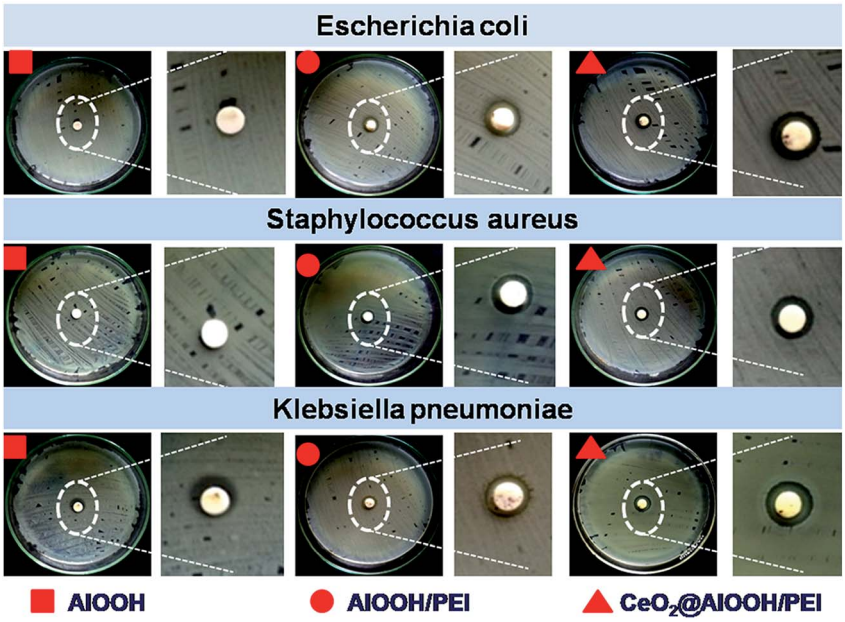

Fig. 9 Photographs of the antibacterial test of ■AlOOH, ●AlOOH/PEI and ▲CeO_2@AlOOH/PEI against Gram-negative *Escherichia coli*, *Klebsiella pneumoniae* and Gram-positive *Staphylococcus aureus* as model microorganisms.

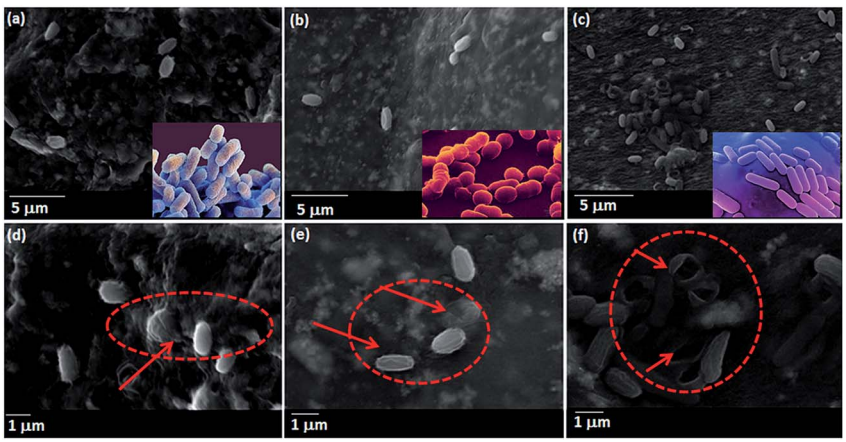

Fig. 10 SEM images CeO_2@AlOOH/PEI hybrid material after 10 minutes incubation with (a) *S. aureus* (b) *E. coli* (c) *K. pneumoniae*. Optical images of the used bacteria for the experiment are shown in the inset corresponding SEM images. High magnification images showing the disruption of cell walls of the bacteria (d) *S. aureus* (e) *E. coli* (f) *K. pneumonia* as a result of antibacterial efficiency of the material.

hybrid sorbent when compared to other two test bacteria. Probably the reason for this is *K. pneumonia* cell surface consist of filaments with thin hair-like extension, as a result large number of it get adhered on the material surface. Hence, all these results indicates that it a promising material in removal of bacterial pathogens from water.

Conclusions

Here in, we have prepared mesoporous hybrid nanocomposite (CeO_2@AlOOH/PEI) *via* the simple sol–gel synthesis route by using polyethylene imine (PEI), CeO_2 nanoparticle and boehmite (AlOOH) as precursors and exploited for the adsorption and photodegradation of lignin and MO. The detailed investigation of the adsorption behaviour of the hybrid nanocomposite revealed that the adsorption performance was mainly due to electrostatic, hydrogen bonding and van der Waals interaction between the surface of the sorbent and the organic pollutants. We also found that the pseudo-second-order equation (R^2 = 0.99) gave the better correlation for the adsorption kinetics of lignin than the pseudo-first-order equation (R^2 = 0.97). The hybrid nanocomposite shows better photodegradation of lignin and MO under UV than sunlight. The prepared hybrid nanocomposite CeO_2@AlOOH/PEI also showed an excellent antibacterial efficiency towards *E. coli*, *K. pneumonia* and *S. aureus* bacteria. Thus, the present study discloses a new class of hybrid material with the potential to use as an adsorbent, catalyst and antimicrobial agent.

This journal is © The Royal Society of Chemistry 2016

Acknowledgements

The authors thank Director A. Ajayaghosh, National Institute for Interdisciplinary Science and Technology, CSIR-NIIST, Trivandrum for providing laboratory facilities for the work. Authors K. A. S. and L. V. is grateful to Council of Scientific and Industrial Research (CSIR) and University Grants Commission (UGC), Government of India for providing Research Fellowship to carry out this work. Dr N. K. S. thanks KSCSTE for providing post doc fellowship. Mr Kiran and Mrs S. Soumya are acknowledged for TEM and SEM analysis respectively. All the members of Materials Science and Technology Division are acknowledged for providing general support.

References

1 S. P. Zhao, F. Zhou, L. Y. Li, M. J. Cao, D. Y. Zuo and H. T. Liu, Removal of anionic dyes from aqueous solutions by adsorption of chitosan-based semi-IPN hydrogel composites, *Composites, Part B*, 2012, **43**, 1570–1578.

2 F. M. Amaral, M. T. Kato, L. Florencio and S. Gavazza, Color, matter and sulfate removal from textile effluents by anaerobic and aerobic processes, *Bioresour. Technol.*, 2014, **163**, 364–369.

3 A. L. Colin, H. Johannes, C. Peter and C. Michael, Photocatalytic active coatings for lignin degradation in a continuous packed bed reactor, *Int. J. Photoenergy*, 2014, **1**, 1–6.

4 S. X. Zhang, Y. Y. Zhang, G. M. Bi, J. S. Liu, Z. G. Wang, Q. Xu, H. Xu and X. Y. Li, Mussel – inspired polydopamine biopolymer decorated with magnetic nanoparticles for multiple pollutants removal, *J. Hazard. Mater.*, 2014, **270**, 27–34.

5 D. Andrew and A. L. Lucian, Titanium Dioxide Catalyzed Photodegradation of Lignin in Industrial Effluents, *Ind. Eng. Chem. Res.*, 2004, **43**, 7996–8000.

6 M. A. Zulfikar, E. D. Mariske and D. D. Samitha, Adsorption of lignosulfonate compounds using powdered eggshell, *Songklanakarin J. Sci. Technol.*, 2012, **34**, 309–316.

7 D. N. John, S. M. Bryan and R. J. S. Corey, A photochemical strategy for lignin degradation at room temperature, *J. Am. Chem. Soc.*, 2014, **136**, 1218–1221.

8 D. L. Dhrubojyoti, P. T. Melvin, C. Xiao wen, L. H. Gregory and Y. Bin, Noble-metal catalyzed hydro deoxygenation of biomass-derived lignin to aromatic hydrocarbons, *Green Chem.*, 2014, **16**, 897–910.

9 B. Shi, G. Li, D. Wang, C. Feng and H. Tang, Removal of direct dyes by coagulation: the performance of preformed polymeric aluminium species, *J. Hazard. Mater.*, 2007, **143**, 567–574.

10 B. Chen, Z. Zhu, S. Liu, J. Hong, J. Ma, Y. Qiu and J. Chen, Facile hydrothermal synthesis of nanostructured hollow iron-cerium alkoxides and their superior arsenic adsorption performance, *ACS Appl. Mater. Interfaces*, 2014, **6**, 14016–14025.

11 X. D. Zhu, Y. C. Liu, C. Zhou, S. C. Zhang and J. M. Chen, Novel and high-performance magnetic carbon composite prepared from waste hydrochar for dye removal, *ACS Sustainable Chem. Eng.*, 2014, **2**, 969–977.

12 M. Daniel, N. Debora, M. Anna, T. F. Vanessa and F. Vanessa, Removal of Lignin and Associated Impurities from Xylo-Oligosaccharides by Activated Carbon Adsorption, *Ind. Eng. Chem. Res.*, 2006, **45**, 2294–2302.

13 S. G. Jenny and S. Herbert, Regeneration of Spent Activated Charcoals Used for Lignin Removal from Pre Hydrolysis-Kraft Pre Hydrolyzates, *Ind. Eng. Chem. Res.*, 2012, **51**, 8624–8630.

14 I. A. Kerstin, E. Marie and N. Magnus, Removal of Lignin from Wastewater Generated by Mechanical Pulping Using Activated Charcoal and Fly Ash: Adsorption Kinetics, *Ind. Eng. Chem. Res.*, 2011, **50**, 7733–7739.

15 D. Zhao, C. Chen, Y. Wang, W. Ma, J. Zhao, T. Rajh and L. Zang, Enhanced Photocatalytic Degradation of Dye Pollutants under Visible Irradiation on Al(III)-Modified TiO_2: Structure, Interaction, and Interfacial Electron Transfer, *Environ. Sci. Technol.*, 2008, **42**, 308–314.

16 K. Amit, S. Gaurav, M. Naushad, S. Pardeep and K. Susheel, Polyacrylamide/$Ni_{0.02}$ $ZnO_{0.98}$ Nanocomposite with High Solar Light Photocatalytic Activity and Efficient Adsorption Capacity for Toxic Dye Removal, *Ind. Eng. Chem. Res.*, 2014, **53**, 15549–15560.

17 Q. Wang, C. Chen, D. Zhao, W. Ma and J. Zhao, Change of Adsorption Modes of Dyes on Fluorinated TiO_2 and Its Effect on Photocatalytic Degradation of Dyes under Visible Irradiation, *Langmuir*, 2008, **24**, 7338–7345.

18 K. Kobayakawa, Y. Sato, S. Nakamura and A. Fujishima, Photodecomposition of kraft lignin catalized by titanium dioxide, *Bull. Chem. Soc. Jpn.*, 1989, **62**, 3433–3436.

19 H. Ohnishi, M. Matsumura, H. Tsubomura and M. Iwasaki, Bleaching of lignin solution by a photocatalyzed reaction on semiconductor photocatalysts, *Ind. Eng. Chem. Res.*, 1989, **28**, 719–724.

20 C. P. Amaresh, K. M. Parida and N. Binita, Enhanced photocatalytic and adsorptive degradation of organic dyes by mesoporous Cu/Al_2O_3–MCM-41: intra-particle mesoporosity, electron transfer and OH radical generation under visible light, *Dalton Trans.*, 2011, **40**, 7348–7356.

21 M. H. Farzana and S. Meenakshi, Synergistic Effect of Chitosan and Titanium Dioxide on the Removal of Toxic Dyes by the Photodegradation Technique, *Ind. Eng. Chem. Res.*, 2014, **53**, 55–63.

22 B. Katie, D. Yael and S. Isam, Synergetic effect between photocatalytic degradation and adsorption processes on the removal of phenolic compounds from olive mill wastewater, *Water Res.*, 2012, **46**, 789–798.

23 T. Cordero, J. M. Chovelon, C. Duchamp, C. Ferronato and J. Matos, Surface nano-aggregation and photocatalytic activity of TiO_2 on H-type activated carbons, *Appl. Catal., B*, 2007, **73**, 227–235.

24 R. A. Anthony, R. Warwick, C. A. Philip, V. Nafty, C. J. Peter, S. Leone, N. Daniel and M. P. Jennifer, Functionalised pseudo-boehmite nanoparticles as an excellent adsorbent material for anionic dyes, *J. Mater. Chem.*, 2008, **18**, 2466–2474.

25 V. Linsha, P. S. Suchithra, A. P. Mohamed and S. Ananthakumar, Amine-grafted alumino–siloxane hybrid porous granular media: a potential sol–gel sorbent for treating hazardous Cr(VI) in aqueous environment, *Chem. Eng. J.*, 2013, **220**, 244–253.

26 Z. R. Tang, Y. Zhang and Y. J. Xu, A facile and high-yield approach to synthesize one-dimensional CeO_2 nanotubes with well-shaped hollow interior as a photocatalyst for degradation of toxic pollutants, *RSC Adv.*, 2011, **1**, 1772–1777.

27 F. L. Wong and A. A. Azi, Development of crack-free alumina sol–gel/poly(vinyl alcohol) membranes for glucose oxidase immobilization, *Asia-Pac. J. Chem. Eng.*, 2007, **7**, 61–67.

28 Z. G. Zhao, N. Nagai, T. Kodaira, Y. Hukuta, K. Bando, H. Takashima and F. Mizukami, Surface treatment- and calcination temperature-dependent adsorption of methyl orange molecules in wastewater on self-standing alumina nanofiber films, *J. Mater. Chem.*, 2011, **21**, 14984–14989.

29 N. Zhang, X. Fu and Y.-J. Xu, A facile and green approach to synthesize Pt@CeO_2 nanocomposite with tunable core–shell and yolk–shell structure and its application as a visible light photocatalyst, *J. Mater. Chem.*, 2011, **21**, 8152–8158.

30 Q. Ai, D. Yang, Y. Zhu and Z. Jiang, Fabrication of Boehmite/Alginate Hybrid Beads for Efficient Enzyme Immobilization, *Ind. Eng. Chem. Res.*, 2013, **52**, 14898–14905.

31 N. Sana, K. Katrin, F. Aleeza, D. Hatice, O. Zehra, T. Eylul, Y. Basit, R. Saadia and H. R. Tariq, Design and Fabrication of Branched Polyamine Functionalized Mesoporous Silica: An Efficient Absorbent for Water Remediation, *ACS Appl. Mater. Interfaces*, 2014, **64**, 408–4417.

32 H. Xiaoyun, B. M. Keith, N. N. Pavel, B. Dermot, P. Brett and H. T. L. John, Adsorption and Desorption of Methylene Blue on Porous Carbon Monoliths and Nanocrystalline Cellulose, *ACS Appl. Mater. Interfaces*, 2013, **5**, 8796–8804.

33 Y. X. Zhang, X. Y. Yu, Z. Jin, Y. Jia, W. H. Xu, T. Luo, B. J. Zhu, J.-H. Liu and X.-J. Huang, Ultra high adsorption capacity of fried egg jelly fish-like γ-AlOOH(Boehmite)@SiO_2/Fe_3O_4 porous magnetic microspheres for aqueous Pb(II) removal, *J. Mater. Chem.*, 2011, **21**, 16550–16557.

34 L. Liu, Z. Y. Gao, X. P. Su, X. Chen, L. Jiang and J. M. Yao, Adsorption Removal of Dyes from Single and Binary Solutions Using a Cellulose-based Bioadsorbent, *ACS Sustainable Chem. Eng.*, 2015, **3**, 432–442.

35 N. Kawabata and M. Nishiguchi, Antibacterial activity of soluble pyridinium-type polymers, *Appl. Environ. Microbiol.*, 1988, **54**, 2532–2535.

36 N. Beyth, Y. Houri-Haddad, L. Baraness-Hadar, I. Yudovin-Farber, A. J. Domb and E. I. Weiss, Surface antimicrobial activity and biocompatibility of incorporated polyethylenimine nanoparticles, *Biomaterials*, 2008, **29**, 4157–4163.

37 D. A. Pelletier, A. K. Suresh, G. A. Holton, C. K. McKeown, W. Wang, B. Gu, N. P. Mortensen, D. P. Allison, D. C. Joy, M. R. Allison, S. D. Brown, T. J. Phelps and M. J. Doktycz, Effects of Engineered Cerium Oxide Nanoparticles on Bacterial Growth and Viability, *Appl. Environ. Microbiol.*, 2010, **76**, 7981–7989.

38 E. M. Dumas, V. Ozenne, R. E. Mielke and J. L. Nadeau, Toxicity of CdTe quantum dots in bacterial strains, *IEEE Transactions on NanoBioscience*, 2009, **8**, 58–64.

 This journal is © The Royal Society of Chemistry 2016